Decoding calcium signals in *Medicago truncatula*

Maria Angeles Contreras Delgado

Doctor of Philosophy

University of East Anglia

April 2020

Abstract

Calcium is an intracellular second messenger involved in the regulation of many processes in eukaryotes. In plants, changes in intracellular calcium concentration occur in response to biotic and abiotic stimuli. These specific changes in calcium concentration are called calcium signatures and are sensed by calcium decoders that contain two specific protein motifs: the EF-hand motif which binds a calcium ion, and the calmodulin binding domain that binds calmodulin which itself contains four EF-hand motifs.

Plant symbiosis is one of the best studied models of plant Ca^{2+} signalling. About 80% of plants establish a beneficial association with arbuscular mycorrhizal (AM) fungi species, but only legumes such as *Medicago truncatula*, are able to establish a symbiosis with both AM fungi and nitrogen fixing rhizobial bacteria. The calcium and calmodulin dependent protein kinase (CCaMK) is a calcium decoder considered as the central regulator of the common symbiotic signalling pathway in plants.

Using a synthetic biology approach, the calcium binding properties of the EF-hand motifs will be studied using CCaMK as the model protein during symbiosis. Ultimately, these studies would provide the possibility of designing novel hybrid proteins that could be used in other calcium signalling pathways of other species.

List of Contents

List of Tables

List of Figures

Acknowledgments

I am very grateful to many people who have been part of this experience since I started my PhD in 2016. Foremost, I would like to express my gratitude to Ben for his continuous support during my PhD research and for teaching me that “sometimes less is more”. His patience, enthusiasm and expertise have been a real inspiration to me, and I could not imagine a better supervisor for my or anyone’s PhD.

I would also like to thank my secondary supervisor Prof. Richard Morris for his insightful comments, encouragement and positive attitude that kept me motivated and stimulated even further my passion for my research.

During the course of my PhD research, I had the opportunity to work with other members of the Miller’s and Dalmay’s lab who provided me with very enjoyable moments during these past 3 years. I would especially like to thank Connor Tansley for being always so supportive and fun to work alongside.

I am also very thankful to the Eastern Arc and University of East Anglia for funding my PhD as this work would not have been possible without their financial support.

Lastly but very importantly, I am deeply grateful to my family and friends outside the lab for all their love and unconditional support throughout my PhD. I could not be more grateful to my partner Juan Pulido and my best friends Estela Perez, Leticia Sanchez, Leticia Romero, Ana Munoz, Natalia Sanchez and Isabel Calatrava for their guidance and making me feel amazingly loved and inspired in the pursuit of my research.

Chapter One - General introduction

1. Calcium signalling in eukaryotes

Intracellular free calcium (Ca^{2+}) functions as a ubiquitous second messenger responsible for controlling many cellular processes in eukaryotes. Controlled changes in intracellular Ca^{2+} concentration occur in response to different environmental and developmental stimuli and are perceived as 'signals' that activate specific physiological responses.

In animals, calcium signals occur during fertilisation, cell differentiation, cancer and many other physiological processes. During fertilisation, the generation of transient calcium release events called "spikes" with a defined spatiotemporal pattern results in a nuclear envelope breakdown and cell cleavage (Chang and Meng, 1995; Kono et al., 1996). In cell differentiation, calcium spikes also regulate the development of neural and muscle cells (Buonanno and Fields, 1999), as for example, calcium transients are involved in axon extension and specific connections (Gomez and Spitzer, 1999). Moreover, calcium also plays important roles in cancer, in which drug-induced blockage of Ca^{2+} entry has a retarding effect on the growth of certain tumours (Benzaquen et al., 1995; Nie et al., 1996; Haverstick et al., 2000). In all these processes, calcium is encoding stimulus-specific signalling information through the generation of calcium signatures with very different spatial and temporal dynamics (Berridge et al., 2003).

In plants, calcium signals of specific frequency, duration, amplitude and spatial distribution named as calcium signatures are induced in response to biotic and abiotic stimuli such as light, temperature, drought, touch, pathogens, and symbionts (Sanders et al., 1999). In the model plant *Arabidopsis thaliana*, cytosolic Ca^{2+} is involved in a dual mechanism of stomatal closure regulation in response to certain stimuli such as the stress hormone abscisic acid (ABA), cold and atmospheric CO_2 (Allen et al., 2001; Young et al., 2006). Rapid stomatal closure is induced upon elevation of cytosolic Ca^{2+} concentration, while Ca^{2+} oscillations of a defined duration, amplitude and frequency prevents a programmed stomatal reopening process (Allen et al., 2001; Sanders et al.,

2002). In addition, cytosolic Ca^{2+} oscillations are also part of a Ca^{2+} gradient essential for tip-growth of pollen tubes, which is maintained by specific calcium channels (Sanders et al., 1999; Peter K. Hepler et al., 2001; Dutta and Robinson, 2004). This shows that differences in the dynamics of Ca^{2+} signals can potentially encode information in response to specific stimuli (Figure 1.1).

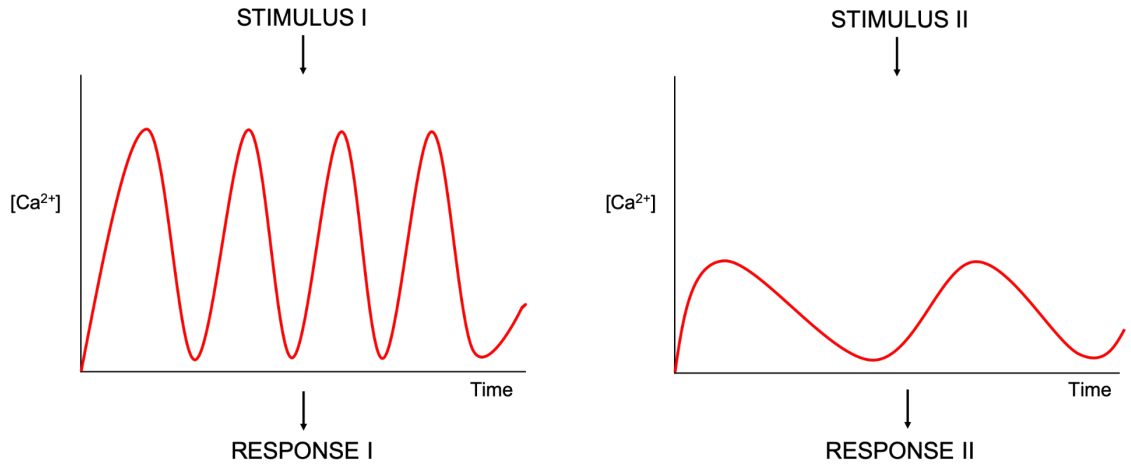

Figure 1. 1. Ca^{2+} oscillation patterns in response to different stimuli and that induce specific responses.

Different biotic and abiotic stimuli result in the activation of specific channels and pumps for the generation of Ca^{2+} signatures of distinct patterns (frequency, duration, amplitude and spatial distribution). For example, in this figure stimulus I induces a high frequency and high amplitude signal that results in response I as opposed to stimulus II which is of lower amplitude and frequency and induces response II. As a result, different signalling pathways specific to the stimulus are activated in order to induce an adequate biological response.

In eukaryotes, the Ca^{2+} levels in the extracellular space correspond to ~10^{-3} M, 10^4 times higher than in the cytoplasm, nuclear matrix and mitochondrial matrix (~10^{-7} M). Since Ca^{2+} controls many aspects of cellular function, maintaining the basal levels of free Ca^{2+} is crucial for survival of the cell. Uncontrolled and sustained increases of cytosolic Ca^{2+} concentrations ($[Ca^{2+}]_c$) over 10^{-4} M, can cause severe damage to membranes and organelles due to nucleic acid and protein aggregation and precipitation of phosphates, ultimately leading to cytotoxicity, cell injury and cell death (Sanders et al., 1999).

The eukaryotic cell contains different mechanisms to control these changes in ($[Ca^{2+}]_c$) and avoid toxicity. The cell maintains Ca^{2+} at low levels in the cytosol by the export of Ca^{2+} across the plasma membrane to the extracellular space or by storing it in various intracellular compartments. There are different cellular organelles that function as Ca^{2+} stores and contribute to maintain intracellular Ca^{2+} homeostasis. The main internal Ca^{2+} store is the endoplasmic reticulum (ER), followed by the mitochondrion and the Golgi apparatus. In plants, the vacuole and chloroplast are also important Ca^{2+} stores (Costa et al., 2018). In addition to internal Ca^{2+} stores, the cell also possesses cytosolic proteins that act as buffers capturing most of the Ca^{2+} that enters the cell from the extracellular matrix or the internal stores. These Ca^{2+} buffers control the spread of free Ca^{2+} ions by diffusion and aid the cell to resist small fluctuations in intracellular Ca^{2+} concentrations. However, a small amount is rendered as free Ca^{2+} for binding to effector proteins responsible for activating Ca^{2+}- dependent signalling processes (Berridge et al., 2003).

External and internal stimuli of different intensity and identity induce oscillations in intracellular Ca^{2+} concentration with a defined duration, amplitude, frequency and spatial distribution. These specific elevations of Ca^{2+} concentration are perceived as signals and due to their defined characteristics, these signals are designated as “calcium signatures” (Webb et al., 1996; McAinsh and Hetherington, 1998). Animal and plant systems possess different channels, pumps and exchangers that act in concert to generate these specific calcium signatures. There are many commonalities between animals and plants in their encoding and decoding of calcium signals, but this chapter will be mostly focused on the plant mechanisms as they are most relevant to this thesis.

2. Encoding of the calcium signal in plants

The generation of Ca^{2+} signals involves the influx of Ca^{2+} into the cytoplasm or other organelles including the nucleus, mitochondria and chloroplast, from the external medium or the internal stores. This is mediated by the action of specific ion channels located at the plasma membrane or endomembranes such as the ER and the vacuole. Subsequently, the Ca^{2+} influx is reversed by the inactivation

of these channels and the activation of pumps and exchangers located at different cellular membranes, in order to reduce the Ca^{2+} concentration back to the resting level and to refill the Ca^{2+} stores.

2.1. Ca^{2+} influx

The stimulus-induced influx of Ca^{2+} into cells is mediated by the action of ion channels that are permeable but nonselective to Ca^{2+} in plants (Schroeder and Hagiwara, 1990) and Ca^{2+} selective in the case of animal cells (Zou et al., 2002). Nonselective cation channels (NSCCs) are classified based on their mechanism of activation: mechanical, voltage-dependent and ligand-dependent (White et al., 2002).

Voltage-dependent Ca^{2+}-permeable channels can be activated by a membrane depolarization or hyperpolarization in response to a wide variety of stimuli (White et al., 2002). For instance, environmental stresses such as osmotic pressure or microbes induce depolarization of the plasma membrane resulting in the increase of cytoplasmic Ca^{2+} concentration, which suggests a possible role for depolarization-activated Ca^{2+} channels (DACC) (Lhuissier et al., 2001; Okazaki et al., 2002). Moreover, hyperpolarization-activated Ca^{2+}-permeable channels (HACCs) contribute to the cytoplasmic Ca^{2+} influx in response to many stimuli including abscisic acid (ABA) and reactive oxygen species (ROS) in guard cells and root hairs (Pei et al., 2000; Ward et al., 2009; Murata et al., 2001; Demidchik et al., 2018).

Mechanosensitive Ca^{2+} channels (MCCs) have been reported to be involved in the response to the Ca^{2+} increase caused by mechanical stimuli including wind and touch in plants (Braam, 2005). These channels are present in the plasma membrane of plant cells (Sanders et al., 2002) including guard cells, mesophyll cells and pollen grain protoplasts (Cosgrove and Hedrich, 1991; Dutta and Robinson, 2004; Qi et al., 2004). Different mechanical stimuli originate a distinct pattern of Ca^{2+} concentration elevations. This was observed in *Arabidopsis thaliana* roots where the MCCs may be involved in the monophasic or biphasic cytosolic Ca^{2+} elevation elicited in response to touch or bending respectively (Edel et al., 2017; Monshausen et al., 2007, 2009).

In addition, the reduced hyperosmolarity-induced $[Ca^{2+}]_{cyt}$ increase channels (OSCAs) were recently identified as a well-conserved protein family in eukaryotes involved in Ca^{2+} influx (Edel and Kudla, 2015). Two OSCAs, the OSCA1.1 and OSCA1.2 have been identified so far in *Arabidopsis* and experimentally confirmed their ability to transport Ca^{2+} (Hou et al., 2014; Yuan et al., 2014). Both OSCA1.1 and OSCA1.2 have been suggested to be responsible for the change in $[Ca^{2+}]_{cyt}$ which occurs in response to osmotic stress (Hou et al., 2014). Therefore, the OSCAs constitute further components of the Ca^{2+} machinery.

There are also Ca^{2+}-permeable channels that can be activated by specific ligands. There are two main classes of ligand-dependent channels with a possible role in shaping Ca^{2+} signatures. Cyclic nucleotide-gated channels (CNGCs) constitute one of them, being encoded by 20 CNGC genes in *Arabidopsis thaliana* (Mäser et al., 2001), involved in many physiological processes in plants. CNGC2 is a well characterised channel whose absence in *Arabidopsis thaliana* results in an impaired response to the pathogenic attack by *Pseudomonas syringae*, suggesting the role of this channel in pathogen resistance (Clough et al., 2000). Furthermore, CNGC15a, CNGC15b and CNGC15c play an important role in the generation of nuclear calcium oscillations during plant-microbe symbiosis (Charpentier et al., 2016). In addition to CNGC involvement in plant-microorganism interactions, these channels participate in other processes. It has been reported the role of *Arabidopsis thaliana* CNGC18 in pollen tube growth which is characterised by a tip-focused Ca^{2+} gradient and consistent with CNGC18 being preferentially localized at the growing tip (Frietsch et al., 2007).

Similarly, Ca^{2+} influx is also regulated by glutamate receptor-like channels (GLRs). There are 20 genes encoding for GLRs in *Arabidopsis thaliana* (Chiu et al., 2002; Qi et al., 2006; Stephens et al., 2008). These genes may be responsible for the increase in cytoplasmic Ca^{2+} concentration and membrane depolarization induced by glutamate in many physiological processes in which a Ca^{2+} influx is essential, including root elongation, root branching, cell division, differentiation and resistance to pathogens (Sivaguru et al., 2003; Li et al., 2006; Seock et al., 2006; Walch-Liu et al., 2006). Moreover, it has recently been found that GLRs

can be activated not only by glutamate but instead, by a broad spectrum of amino acids allowing to act as sensors in a wide variety of biological processes such as plant defence (Forde and Roberts, 2014). Consistently, glutamate as well as other amino acids were demonstrated to induce membrane depolarisation and GLR-mediated Ca^{2+} influx in planta (reviewed by Price et al. (2012).

2.2. Ca^{2+} efflux

In order to be a representative signal, the generation of calcium signatures requires the extrusion of the Ca^{2+} release induced by the specific stimulus. This is achieved by the concerted action of P-type Ca^{2+}-ATPases and cation exchangers.

The Ca^{2+} exchangers (CAX) are low affinity high capacity antiporter proton antiporters that transport Ca^{2+} from the cytosol in a counter exchange of another ion. There are six genes in *Arabidopsis thaliana* encoding for H^+/Ca^{2+} exchangers (Cai and Lytton, 2004; Shigaki et al., 2006) whose gene products have different localizations, including the plasma membrane, vacuole and tonoplast where these exchangers act to maintain the Ca^{2+} homeostasis (Schumaker and Sze, 1985; Kasai and Muto, 1990; Hirschi et al., 1996; Ueoka-Nakanishi et al., 2000). Unlike Ca^{2+} exchangers, P-type Ca^{2+}ATPases pump Ca^{2+} with a high affinity low turnover, which allows the maintenance of the low resting Ca^{2+} concentration. P-type Ca^{2+} ATPases are a subgroup of P_2-ATPases. These P_2-ATPases can be classified in two types, the P_{2A}-ATPases including the plant ER-type Ca^{2+} ATPases (ECAs) and the P_{2B}-ATPases, including the plant autoinhibited Ca^{2+}-ATPases (ACAs) (Baxter et al., 2003). The latter ATPase owes its name to the autoinhibitory region at its N-terminal domain that allows the Ca^{2+}-dependent activation of the pump. However, the role of the ECAs needs to be further investigated although have been observed at organelle membranes, such as the ER and the Golgi, which can serve as the local Ca^{2+} stores for the spatial specificity of the Ca^{2+} signals (Liang et al., 1997; Mills et al., 2008).

3. Calcium signatures are decoded by different Ca^{2+} binding proteins

Ca^{2+} signals induced by specific stimuli are decoded by an array of proteins named Ca^{2+} sensors of distinct calcium binding affinities, expression patterns and

subcellular localizations (McAinsh and Hetherington, 1998). Most of the Ca^{2+} sensors perceive changes in the Ca^{2+} concentration by binding this ion through a Helix-Loop-Helix (HLH) motif termed as "EF-hand motif". The binding of calcium causes the protein to undergo a conformational change that allows its interaction with other proteins or modifies its activity in order to activate the specific response to the stimulus. In addition, phosphorylation is an important function of many of the Ca^{2+} sensors to decode Ca^{2+} signatures into downstream signalling responses (Harmon et al., 2000; Batistic and Kudla, 2004).

Ca^{2+} sensors are classified in two groups according to their mode of action. The first group comprises the sensor relays such as calmodulin (CaM) and calcineurin B-like (CBLs) proteins (Figure 1.2) which sense the change in Ca^{2+} concentrations but lack any intrinsic activity and therefore, their function is the transmission of the information to target proteins. The second group corresponds to the sensor protein kinases including calcium-dependent protein kinases (CDPKs) and Ca^{2+}/CaM-dependent protein kinases (CCaMKs) (Figure 1.2) whose kinase domains enable them to directly respond to Ca^{2+} and transmit the signal downstream (see Sections 1.3.2, 1.3.3, 1.3.4, 1.3.5 and 1.3.6).

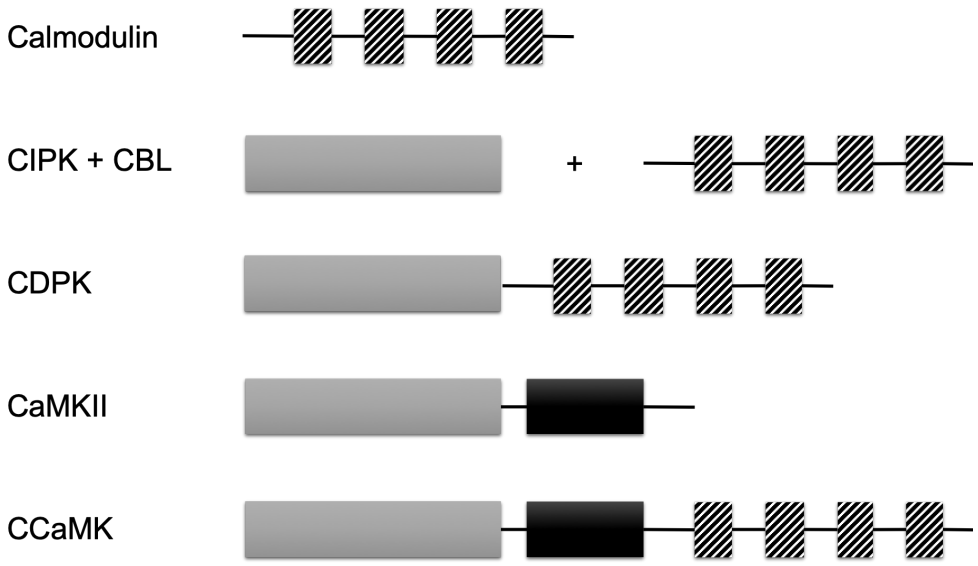

Figure 1. 2. Domain organisation of the best studied Ca^{2+} binding proteins.

The figure shows the main structural domains for calmodulin, calcineurin B-like protein (CBL) and its interacting partner CBL-interacting protein kinase (CIPK), calcium

dependent protein kinase (CDPK), calcium/calmodulin dependent protein kinase II (CaMKII) and calcium and calcium/calmodulin dependent protein kinase (CCaMK). The kinase domain is shaded in grey, calmodulin binding domain (CaMBD) is shaded in black, and the EF-hand motifs are shaded with diagonal lines.

3.1. The EF-hand motif

The EF-hand motif consists of two α-helices, the N-terminal and C-terminal helices, linked by a turn-loop, creating a common helix-loop-helix (HLH) secondary structure (Kretsinger and Nockolds, 1973). The canonical EF-hand loop contains nine residues which provide five out of the seven ligands for Ca^{2+} coordination, while the other two ligands are provided by a single residue located three residues away from the C-terminus of the loop. Besides not being a structural part of the loop, this residue is considered the twelfth residue (Strynadka and James, 1989).

The ligands are named according to two different criteria, numerically based on their linear position from the N-terminus to the C-terminus, and alphabetically based on their three-dimensional structure adopted upon Ca^{2+} binding: 1(+X), 3(+Y), 5(+Z), 7(-Y), 9(-X), 12(-Z) (Kretsinger and Nockolds, 1973). The Ca^{2+} bound pair of ligands Y and Z, 3(+Y), 5(+Z), 7(-Y), 12(-Z), constitute the vertices of an approximately planar pentagon while the X pair of ligands, 1(+X) and 9(-X), are positioned perpendicularly and in opposite sides of the pentagonal plane (Figure 1.3) (Herzberg and James, 1985). This arrangement creates a pentagonal bipyramid which characterises how Ca^{2+} binds to EF-hand motifs of calcium binding proteins such as CCaMK.

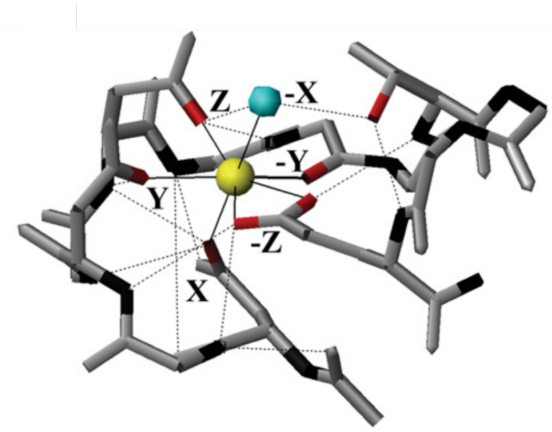

Figure 1. 3. The EF-hand loop coordination sphere.

The figure shows the pentagonal bipyramidal conformation acquired upon binding of a Ca^{2+} ion by the six Ca^{2+}-coordinating ligands of the EF-hand loop. Figure adapted from Gifford et al., (2007).

Oxygen is the coordinating atom of choice for Ca^{2+} chelation by the EF-hand motifs. Four of the oxygen ligands are provided by the side-chain carboxy groups of the first, third, fifth and twelfth ligands, which correspond to the negatively charged amino acids glutamic acid and aspartic acid. Another oxygen ligand comes from the backbone carbonyl group of the seventh loop residue and finally, a water molecule bound to the ninth loop residue completes the coordination sphere (Strynadka and James, 1989; Kawasaki et al., 1998; Nelson and Chazin, 1998a; Lewit-Bentley and Réty, 2000). The EF-loop is rich in negatively charged amino acids glutamic acid and aspartic acid, with a preference for carboxylate ligands provided by aspartates (D) which originates a DxDxDGxxExxE pattern (Figure 1.4) (Rigden and Galperin, 2004).

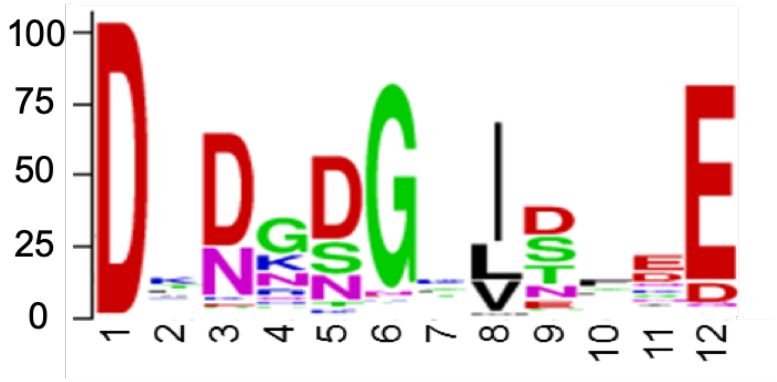

Figure 1. 4. A sequence logo of the EF-hand loop.

The figure shows the most common amino acids found at each position of the 12-residue EF-hand loop. The likelihood of each amino acid is represented by the size of the residue-indicating letter and the percentage of conservation is showed in the Y-axis (0, 25, 50, 75 and 100%). Figure adapted from Rigden and Galperin (2004).

Each ligand of the loop has an important role in the coordination and stabilization of the structure with some of them highly conserved among the EF-hand motifs. The first residue of the loop, 1(+X) ligand is an invariant aspartate essential for the arrangement of the loop through its several hydrogen bonds with other loop residues (Figure 1.4). Position six of the loop corresponds to a glycine that is also hydrogen-bonded to several residues of the loop, particularly, to the aspartate residue at position 1(+X) originating a 90º turn of the loop that help to place the remaining ligands in their coordinating positions. The residue at position eight is a hydrophobic amino acid hydrogen-bonded to the corresponding eighth residue of a second EF-hand creating a short β-sheet in which the seventh and ninth residues are also involved. This β-sheet allows the pairing of two EF-hand motifs (see below). The ninth residue is the last residue of the loop and the first of the C-terminal helix (the exiting helix) and usually coordinates Ca^{2+} via a water molecule. Finally, the twelfth residue is most of the times a glutamate that constitutes a bidentate ligand as it coordinates Ca^{2+} through the two oxygen atoms of its carboxylate group. The structure of the EF-hand motif is further stabilized through a combination of hydrogen bonds between chelating as well as non-chelating residues (Figure 1.3) (Strynadka and James, 1989).

Many factors are responsible for the Ca^{2+} binding properties of the EF-hand motifs. Firstly, the nature and position of the ligands and non-coordinating residues of the loop are important in determining the Ca^{2+} binding affinity of the EF-hand. For instance, the presence of glutamate residues instead of aspartates are thought to increase the affinity due to a higher length of the side chain of glutamines or glutamic acid residues (Gifford et al., 2007). This has especially been observed in position ninth of the loop, where a residue of a shorter side chain would need a bridging water molecule in order to coordinate the Ca^{2+} ion, but a glutamine residue would be able to chelate the Ca^{2+} ion directly. The incorporation of a water molecule into the coordination sphere results in a decrease in entropy that makes the Ca^{2+} chelation less favourable and thus, reduces the affinity for Ca^{2+} (Drake and Falke, 1996). In many cases, position twelve is also occupied by an aspartic acid instead of glutamic acid and a water molecule is required for completion of the Ca^{2+} coordination sphere since the side chain of aspartic acid is not long enough for both oxygen atoms to chelate the Ca^{2+} ion (Gentry et al., 2005). Additionally, non-ligand residues of the loop have also been found important due to their concerted role with the ligands in balancing the electrostatic repulsion occurred in both the unbound and Ca^{2+}-bound forms (Shaw et al., 1991). However, the loop residues are not the sole responsible for the Ca^{2+} binding affinity of the EF-hand as the helices are also found to play a role. In fact, higher hydrophobicity of both the incoming and exiting helices was found to provide a more stable protein core that results in an increased Ca^{2+} affinity (Kragelund et al., 1998). Furthermore, interactions between the helices also occur. These interactions are stronger during the Ca^{2+}-unbound state due to their antiparallel arrangement (Gifford et al., 2007).

The EF-hand motifs almost always occur in pairs (Figure 1.5) and therefore, the two members of the pair can influence each other's Ca^{2+} binding properties. The pair structure is maintained through the short β-sheet that connects the calcium binding loops of both EF-hands but also through the hydrophobic interactions among the four α-helices (Strynadka and James, 1989; Nelson and Chazin, 1998b). The EF-hand motif helices are amphipathic and stack against one another with the hydrophobic faces inward creating a hydrophobic core, and their hydrophilic face outward, interacting with the solvent (Figure 1.5).

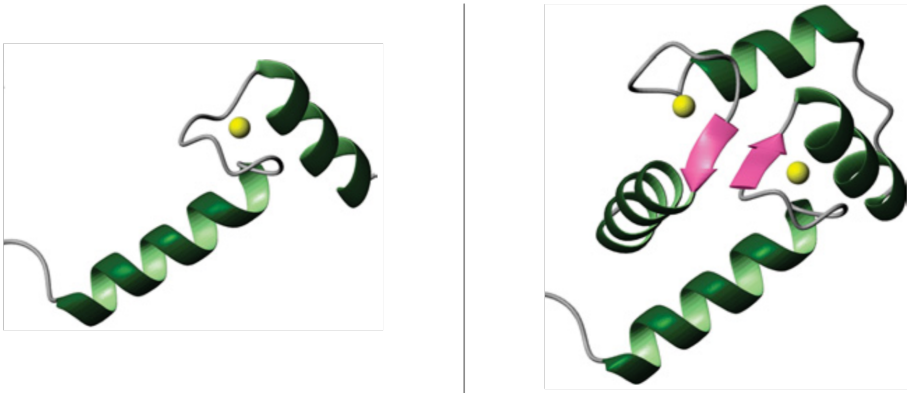

Figure 1. 5. Structures of a single EF-hand motif and the EF-hand pair.

Representation of a single EF-hand motif with a helix-loop-helix structure from which the loop is responsible for binding of the Ca^{2+} ion. The EF-hand motifs arrange in pairs through interaction between the loops of the two EF-hand motifs. Figure adapted from Gifford et al., (2007).

The EF-hand pairing enables cooperativity of ligand binding in many cases. Many EF-hands interact with their paired partner and the binding of Ca^{2+} to one of them increases the affinity of the second for this ion. This is the case of CaM, one of the most studied calcium sensors (see section .Introduction to CaM) in which the binding of Ca^{2+} to the site I at the N-terminal EF-hand pair induces a tenfold increase in the affinity of site II for Ca^{2+} (Beccia et al., 2015). However, there are EF-hand containing proteins that do not bind Ca^{2+} in a positively cooperative manner. CCaMK is an example of non-EF-hand cooperativity as the three functional EF-hands bind Ca^{2+} independently (Swainsbury et al., 2012) (Section 1.5.1).

The two EF-hands in the pair are related by an approximate 2-fold symmetry axis. However, EF-hand pairs are preferentially composed of two different EF-hand motifs (heterodimers) rather than two identical EF-hand motifs (homodimers). The two different EF-hand motifs of the heterodimer allow a higher packing of the core structure and results in a higher Ca^{2+} affinity than in homodimers (Gifford et al., 2007). This is the case of CCaMK that contains a non-functional EF-hand motif in its structure, the EF-hand 1, in which the substitutions of the 5(+Z) ligand

and the highly conserved glycine at position six could be responsible for the loss of this EF-hand Ca^{2+} binding capability (Swainsbury et al., 2012).

The binding of Ca^{2+} via EF-hand motifs causes EF-hand proteins to undergo a conformational change that enables them to transduce the increased Ca^{2+} concentration. Members of the CaM subfamily, including CCaMK, bind Ca^{2+} in a two steps mechanism: firstly, the N-terminal part of the loop corresponding to the first, third, fifth and seventh ligands, 'extend' their side chains to bind the Ca^{2+} ion facilitated by the flexible nature of this region (Kobayashi and Takada, 2006). Subsequently, the exiting helix (C-terminal helix) reorients in order to locate the C-terminal ligands close enough to complete the coordination sphere. The repositioning of the exiting helix causes a conformational change in which the helices of the paired EF-hand motifs switch from an approximately antiparallel interhelical arrangement to an approximately perpendicular orientation (Figure 1.5) (Nelson and Chazin, 1998c; Yap et al., 1999).

Although much information is available about the characteristics of EF-hand motifs, it still remains unclear whether the primary sequence of EF-hand motifs and/or their tertiary structure adopted upon Ca^{2+} binding are the factors which determine how these Ca^{2+} sensors respond to Ca^{2+} signals.

3.2. Calmodulin

Calmodulin (CaM) is a highly conserved ubiquitous protein with an approximate 70% identity between animal and plant cells (Yang and Poovaiah, 2003). CaM expresses in both the cytoplasm and nucleus and due to its size, CaM is able to diffuse from the cytosol to the nucleus (Chin and Means, 2000). In *Arabidopsis thaliana*, there are seven genes encoding four isoforms of CaM with a highly similar amino acid composition (McCormack and Braam, 2003). In spite of the high level of sequence identity, CaMs possess a high target specificity as a different Ca^{2+} sensitivity is observed depending on the CaM isoform and their target protein (Lee et al., 2000; Luoni et al., 2006). CaM participates in many cellular processes due to its ability to bind and regulate a wide variety of target proteins including the plant ACAs, CNGCs and kinases such as CCaMK (DeFalco et al., 2010).

CaM structure consists of four Ca^{2+} binding EF-hand motifs arranged in two pairs, one pair at the N-terminal domain (N-lobe) and the other pair at the C-terminal domain (C-lobe), both connected by a flexible central linker region (Meador et al., 1992, 1993). The two pairs of EF-hand motifs have different calcium binding capabilities as the EF-hands of the C-lobe show higher Ca^{2+} binding capabilities than the N-lobe EF-hand motifs (Andersson et al., 1983). Moreover, CaM is able to respond to Ca^{2+} concentrations ranging from 10^{-12} M to 10^{-6} M, which makes CaM a very versatile Ca^{2+} sensor (Chin and Means, 2000).

The function of CaM is the regulation of its target proteins in a Ca^{2+} dependent manner. This is achieved through the binding of Ca^{2+} to its four EF-hand motifs which induces a conformational change of the protein and leads to the exposure of hydrophobic surfaces located within the N- and C-lobes, which are the interaction sites with CaM target proteins (Yun et al., 2004). Additional conformational changes within the linker region can occur, especially the unwinding of the α-helix located at this region to various extends that allows different degrees of structural rearrangements, ranging from compact to fully extended conformations. This structural flexibility further allows CaM to interact with a wide array of target proteins (Ishida and Vogel, 2006; Halling et al., 2005). Binding of CaM to the target protein results in the activation or inhibition of the protein activity for the translation of the Ca^{2+} signal into a biochemical response.

3.3. Introduction to Calcineurin B-like proteins

In addition to CaMs, Calcineurin B-like proteins (CBLs) also belong to the subgroup of Ca^{2+} sensor relays, with 10 *CBL* genes in *Arabidopsis thaliana* as well as rice (Kolukisaoglu et al., 2004). CBLs are composed of two domains, harbouring two EF-hand motifs each, connected by a short linker (Figure 1.2) (Nagae et al., 2003).

Similar to CaM, the CBLs are able to bind Ca^{2+} through their EF-hand motifs in response to changes in intracellular Ca^{2+} concentrations triggered upon stimuli perception. Ca^{2+} binding induces CBLs to undergo a conformational change that expose a hydrophobic surface responsible for facilitating the interaction with target proteins (Sánchez-Barrena et al., 2005). Unlike the highly conserved EF-

hand motifs of CaMs, the CBLs exhibit different degrees of EF-hand motif conservation compared with the canonical EF-hand sequence (Nagae et al., 2003). For instance, EF-hand 1 of *AtCBL2* lacks the conserved Asp at position 1 of the EF-hand loop but has three residues inserted between position X and Y, resulting in a 14 amino acid EF-hand loop rather than the canonical 12-amino acid (Nagae et al., 2003). This variety of EF-hand motif sequences in the CBLs is thought to contribute to the Ca^{2+} response specificity.

Unlike CaMs, the CBLs have only one specific group of target proteins which are designated as the CBL-interacting protein kinases (CIPKs) (Shi et al., 1999). There are 26 genes encoding for CIPKs in *Arabidopsis thaliana* and 30 genes in rice. The interaction between CBLs and CBL-interacting protein kinase allows the transmission of information into downstream responses. The variation in the EF-hand sequences may be responsible for the different specific responses to calcium signalling by the calcium sensors and in this case, another layer of specificity is provided by the possible interaction combinations between the CBLs and the CIPKs. For instance, CBL1 and CBL9 are both involved in responses to salt, drought, salinity and ABA but with antagonist roles. CBL1 and CBL9 target an overlapping set of CIPKs resulting in their competition for the same target in response to specific stimuli. This is observed in that CIPK1 interacts with CBL9 in order to function in ABA signalling, but the interaction with CBL1 results in the opposite effect as it leads to the ABA-independent signalling (Pandey et al., 2004). In addition, CBL1 and CBL9 have been reported to decrease the kinase activity of CIPK9 in *Arabidopsis thaliana*, while the CIPK9 kinase activity is enhanced by CBL2 and CBL3 (Yadav et al., 2018).

3.4. Introduction to Ca^{2+}-dependent protein kinases

In plants, several Ca^{2+}-dependent protein kinases decode Ca^{2+} signals via phosphorylation such as a family of Ca^{2+}-dependent and CaM-independent protein kinases (CDPKs). *Arabidopsis thaliana* contains 34 genes encoding for CDPKs with a highly conserved structure (Cheng et al., 2002). The CDPKs structure consists of an N-terminal variable domain, a serine/threonine protein kinase domain and a CDPK activation domain (CAD; Figure 1c). The CAD compresses an autoinhibitory domain and calmodulin-like domain (CLD)

composed of four EF-hand motifs arranged in pairs (Chandran et al., 2006). The two pairs of EF-hand motifs have different affinities for Ca^{2+}, with the N-terminal pair containing the low affinity EF-hand motifs, and the C-terminal pair containing the high affinity EF-hands (Rutschmann et al., 2002; Christodoulou et al., 2004; Dixit and Jayabaskaran, 2015). In the inactive state, the C-terminal EF-hand pair is bound to Ca^{2+} which stabilizes the interaction between the autoinhibitory domain and the kinase domain, maintaining the protein in the inactive state. However, when Ca^{2+} concentrations change upon stimuli perception, Ca^{2+} binds to the N-terminal EF-hand motifs resulting in a dramatic conformational change of the CDPK. This conformational change causes a rearrangement in which the kinase domain is relieved from autoinhibition and is able to phosphorylate its substrate as observed by Wernimont et al., (2010) in the CDPK from the apicomplexan parasites *Toxoplasma gondii* and *Cryptosporidium parvum*. Finally, substrate specificity is provided by the N-terminal variable domain which is involved in substrate binding (Ito et al., 2010). Interestingly, several CDPKs have been suggested to interact with CaM despite no CaM-binding domain (CaMBD) found in their structure via in-silico predictions (Popescu et al., 2007). Recently, CPK28 was in fact shown to interact with CaM with high affinity in a Ca^{2+}-dependent manner, which adds another layer of regulation by Ca^{2+} to CDPK activity (Bender et al., 2017). Additionally, CDPKs have been shown to autophosphorylate on Ser, Thr and Tyr residues resulting in either activation or inhibition depending on the CDPK (Oh et al., 2012; Swatek et al., 2014; Chaudhuri et al., 1999; Saha and Singh, 1995). However, the physiological consequences of CDPK autophosphorylation is still unclear.

CDPKs are implicated in many plant biological processes including biotic and abiotic stresses, immune responses, hormone-dependent developmental processes, among others (reviewed in Harper et al., 2004; Ludwig et al., 2004). For example, *CPK3* and *CPK6* encoding for two different CDPKs in *Arabidopsis thaliana* have been reported to be involved in stomatal closure by guard cells. Ca^{2+} concentration regulates stomatal closure through two different mechanisms: a rapid stomatal closure induced by an increase in Ca^{2+} concentration, and a long-lasting stomatal closure induced by Ca^{2+} oscillations of a defined pattern. In *Arabidopsis thaliana*, *cpk3-cpk6* double mutants are defective in the rapid

stomatal closure due to impairment in the activation of slow-type ion channel. However, this double mutant is not impaired in the long lasting stomatal closure indicating the specificity in the perception of the Ca^{2+} signals by the CDPKs (Mori et al., 2006).

3.5. Introduction to CaM-dependent protein kinases

CaM-dependent protein kinases (CaMK) are only present in animals and their characteristics are relevant to this thesis due to their high homology to CCaMK. CaMKs comprise a family of protein isoforms involved in many cellular functions in response to Ca^{2+} signals. CaMKII constitutes one of the most abundant proteins in neural tissues, where Ca^{2+} oscillations of a defined amplitude and frequency occur upon stimuli perception (Erondu and Kennedy, 1985; Sjöström and Nelson, 2002). In addition, CaMKII has been reported to have an important function in learning and memory (Hudmon and Schulman, 2002a).

CaMKII is a multi-subunit holoenzyme of 8-12 subunits derived from four closely related genes designated as α, β, γ and δ, generating a family of isoforms that differ in the ratio of the four subunits present in the complex (Bennett et al., 1983; Okuno et al., 1994). The CaMKII canonical subunit consists of a catalytic domain containing ATP and substrate binding sites, an autoregulatory region compressing an autoinhibitory domain contiguous with a Ca^{2+}/CaM binding domain, and an association domain (Figure 1d) (Hudmon and Schulman, 2002b).

In the inactive state, the autoinhibitory domain acts as a pseudosubstrate that covers both the ATP and protein substrate binding sites of CaMKII, blocking the kinase activity (Hudmon and Schulman, 2002a, b; Rosenberg et al., 2005). Ca^{2+} concentration changes upon stimuli perception induces the binding of Ca^{2+} to CaM and therefore CaM activation. Consequently, the Ca^{2+}/CaM complex exposes hydrophobic surfaces for interaction with the hydrophobic residues at the CaM binding domain of CaMKII. This hydrophobic interaction leads to the wrapping of Ca^{2+}/CaM around the target sequence with the C-terminal lobe of CaM interacting with the N-terminal part of the CaMB sequence of CaMKII (Meador et al., 1993). Binding of Ca^{2+}/CaM results in the release of the ATP and substrate binding sites from the autoinhibition and in the exposure of an

autophosphorylation site, Thr-286, located at the catalytic domain. Thr-286 autophosphorylation is intra-holoenzyme and this trans-autophosphorylation occurs between the kinase domains of adjacent subunits of the holoenzyme upon binding to the Ca^{2+}/CaM complex (Rich and Schulman, 1998; Rosenberg et al., 2005). Thr-286 autophosphorylation results in a 3-fold increase in the affinity for CaM allowing the retention of CaM bound to CaMKII after the Ca^{2+} spike has ended, an event designated as CaM-trapping (Putkey and Waxham, 1996). In addition, Thr-286 autophosphorylation also results in a 10-fold decrease in autoinhibition capability rendering CaMKII with a 70% activity after CaM dissociation (Colbran et al., 1989). Dissociation of CaM expose two additional autophosphorylation residues, Thr-305 and Thr-306, both located at the CaMB domain whose autophosphorylation blocks the rebinding of CaM (CaM-capping) (Mukherji and Soderling, 1994) and thus, CaMKII is inactivated.

3.6. Introduction to Ca^{2+} and CaM-dependent protein kinase

Ca^{2+} and CaM-dependent protein kinase (CCaMK) was first identified from lily (*Lilium longiflorum*) as a protein of 520 amino acids and a structure composed of a kinase domain, a CaMBD and three EF-hand motifs (a more detailed explanation of CCaMK structure and mechanism of activation will be given in Section 1.5) (Patil et al., 1995). CCaMK is found in most plants species such as in legumes (Levy, 2004; Mitra, 2004), rice (*Oryza sativa*) (Godfroy et al., 2006), mosses, liverworts and hornworts but it is absent in members of the *Brassicaceae* (Levy, 2004; Wang et al., 2010).

The first proposed role for CCaMK was in the perception of Ca^{2+} oscillations during anther development and pollen tube formation. CCaMK expression was observed in pollen mother cells and increased during meiosis in *Nicotiana tobacum* (Poovaiah et al., 1999). In addition, CCaMK was also reported to be involved in abiotic stress responses. PsCCaMK from pea (*Pisum sativum*) was found to be specifically upregulated in roots in the presence of salt and at low temperatures in a Ca^{2+} dependent manner (Pandey et al., 2002). Furthermore, the activity of PsCCaMK in response to low temperatures was found to be mediated via both Ca^{2+} and CaM whereas the salinity response was only mediated by Ca^{2+}. Ca^{2+}/CaM appeared to stimulate PsCCaMK kinase activity in

vitro resulting in the phosphorylation of a protein called p40 which always coeluted with PsCCaMK. The p40 protein has DNA binding capability and is involved in the negative regulation of the promoter of *CaM5* from *Arabidopsis thaliana* (*pAtCaM5*). Phosphorylation of p40 by PsCCaMK has been proposed to release p40 from the *pAtCaM5* allowing other proteins to bind in order to activate the specific stress signalling response (Pandey et al., 2002).

The second case of CCaMK involvement in abiotic stresses corresponds to wheat CCaMK. The wheat CCaMK gene *TaCCaMK* is expressed in roots of wheat seedlings and was downregulated by the phytohormone abscisic acid (ABA), high-salinity (NaCl) and water deficit induced by polyethylene glycol (PEG). ABA plays an essential role during many different abiotic stresses as for instance, ABA accumulates during high-salinity conditions and inhibits seed germination as well as confers salt tolerance during seedling growth (Zhu, 2002). *TaCCaMK* was found to negatively regulate ABA signalling during stress responses as overexpression of *TaCCaMK* in the heterologous system *Arabidopsis thaliana* under salt treatments resulted in increased seed germination rates compared to wild-type (WT) controls (Yang et al., 2011).

In contrast, the closely related maize (*Zea mays*) *ZmCCaMK* expression and the encoded protein activity were upregulated during nitric oxide (NO)-induced ABA signalling in maize leaves (Ma et al., 2012). NO has been found to participate both upstream and downstream of Ca^{2+} and CaM during the antioxidant defence response induced by ABA (Zhang et al., 2007; Sang et al., 2008; Aboul-Soud et al., 2009). Indeed, ABA-induced expression of *ZmCCaMK* in maize protoplasts was found to increase the activity of ZmCCaMK and also antioxidant enzymes such as the superoxide dismutase (SOD) and ascorbate peroxidase (APX), demonstrating the requirement of ZmCCaMK for ABA-induced antioxidant defence. Moreover, ABA-induced activation of ZmCCaMK also required H_2O_2 in addition to NO in leaves of maize plants, further supporting the role of ZmCCaMK in antioxidant defence (Ma et al., 2012). During ABA-induced antioxidant defence in response to drought stress, ZmCCaMK functions in conjunction with its interacting partner ZmNAC84, a transcription factor found to physically interact with and be phosphorylated by ZmCCaMK (Zhu et al., 2016a).

In analogy to ZmCCaMK, the rice (*Oryza sativa*) *OsCCaMK* expression levels increased in response to ABA treatment along with OsCCaMK activity in rice plant leaves. This was also observed in rice protoplasts where antioxidant enzymes SOD and catalase (CAT) activity levels were also enhanced in response to ABA in an OsCCaMK-dependent manner. Furthermore, the role of OsCCaMK in antioxidant defence in rice plant leaves was found to be dependent on Ca^{2+} and CaM (Shi et al., 2012). The mitogen-activated protein kinase (MAPK) cascade has also been shown to be involved in plant abiotic stresses as for instance, OsMPK1 is known to be involved in ABA-induced antioxidant defence (Zhang et al., 2012). In fact, a link between OsCCaMK and OsMPK1 was demonstrated in which OsCCaMK functions upstream and regulates the activity of OsMPK1 that in turn leads to the regulation of the activity of antioxidant enzymes and H_2O_2 production (Shi et al., 2014).

In rice, CCaMK has also been found to directly interact with the type 2C protein phosphatase PP45 which is an important regulator of ABA signalling (Ni et al., 2019). In the absence of ABA, PP45 dephosphorylates Thr263 of CCaMK which results in CCaMK inactivation. In contrast, the expression of *PP45* is inhibited in the presence of ABA-induced H_2O_2 and Cys350 and Cys428 of PP45 are oxidised which results in the formation of PP45 intermolecular homodimers. As a consequence, the interaction between PP45 and CCaMK is blocked and CCaMK remains active (Ni et al., 2019). Therefore, these results further demonstrate the role of CCaMK during ABA-induced stress responses.

However, the key role of CCaMK is the decoding of nuclear Ca^{2+} oscillations during plant-microbe symbioses consistent with CCaMK is expressed in roots and nodules (Levy, 2004; Mitra, 2004). A mutant of *Medicago truncatula* named *dmi3* (does not make infection 3) was identified by Catoira (2000) as defective in root nodule formation during symbiosis with nitrogen-fixing bacteria (rhizobia; more information about symbiosis can be found in Section 1.4). Four years after the discovery of *dmi3*, the gene *DMI3* was identified to encode a CCaMK (Levy, 2004; Mitra, 2004). During symbiotic signalling, the unique ability of CCaMK to perceive Ca^{2+} signals directly via EF-hand motifs and indirectly via CaM places it

as the central regulator of endosymbiosis. The perception of symbiotic Ca^{2+} spiking activates CCaMK for phosphorylation of its main interacting partner CYCLOPS in *L. japonicus* (IPD3 in *M. truncatula*), a coiled-coil protein that is essential in both mycorrhizal and rhizobial symbioses (Messinese et al., 2007; Yano et al., 2008; Horváth et al., 2011; Ovchinnikova et al., 2011; Singh et al., 2014). Additionally, CCaMK is also able to interact with CIP73, a protein of yet unknown function. The silencing of *CIP73* resulted in a decreased nodulation phenotype during rhizobial symbiosis but no apparent phenotype during AM-symbiosis was found. Therefore, despite CIP73 was demonstrated to be an interactor partner of CCaMK, CIP73 is not considered a member of the common symbiotic signalling pathway (CSSP) shared between the two symbiotic interactions (Kang et al., 2011).

Plant symbiosis and CCaMK is one of the best characterised models for study of plant Ca^{2+} signalling and was chosen as the system of study for this thesis.

4. Plant-microbe symbiosis

Nutrients are essential for the metabolism of cells and their limited availability compromises cell growth, development and productivity. Nitrogen (N) and phosphorous (P) are essential nutrients for plant metabolism but their presence in available forms in the soil is very limited (Marschner, 1995). In addition to the direct capture of these essential nutrients from the soil, plants have developed an indirect form of nutrient capture by interactions with microorganisms in the rhizosphere. Symbiosis is a mutually beneficial relationship between plants and microorganisms. The microorganisms are able to provide nutrients that limit the plant growth in exchange for a carbon source required by the microorganism for its metabolism. However, not all plants are able to establish these beneficial symbiotic interactions, such as the case of the members of *Brassicaceae* (which includes the model plant *Arabidopsis thaliana*).

About 80% of land plants are able to establish symbiotic interactions with Arbuscular mycorrhiza fungi (AMF) (Smith & Read, 2008). The evolution of AM-symbiotic interactions dates to approximately 460 million years ago with the first fossil evidence of the current morphology dating to 400 million years ago

(Brundrett, 2002). However, legumes are unique in their additional ability to interact with nitrogen-fixing bacteria, named rhizobia, an interaction that evolved much later as the first fossil evidence dates to approximately 65 millions ago (Kistner and Parniske, 2002). AMF mycelium (a branching filamentous structure) captures nutrients, mostly phosphate, and water from the soil (Kistner and Parniske, 2002) while rhizobia are able to take the atmospheric nitrogen (N_2) and convert it into ammonia (nitrogen fixation), the available form of nitrogen for the plant. Legumes, such as *Medicago truncatula* and *Lotus japonicus*, can establish both symbiotic interactions which enable them to satisfy their needs of both nitrogen and phosphorous, among other nutrients and water. In return, both AMF and rhizobia acquire a continuous supply of carbohydrates from the plant necessary for the microbial metabolism. In spite of AMF being a fungus and *Rhizobium* a bacterium, both microorganisms have a very similar mode of infection.

The symbiotic interaction starts with the release of specific compounds from the host plant to the rhizosphere, flavonoids and strigolactones, that are perceived by rhizobia and AMF, respectively (Long and Staskawicz; Akiyama et al., 2005; Besserer et al., 2006; Gomez-Roldan et al., 2008). In response, rhizobia and AMF produce and release diffusible signals, called Nod and Myc factors that are recognized by the host plant. This dialog constitutes the first stage of the signalling process for the establishment of symbiosis (Denarie et al., 1996; Chabaud et al., 2002; Kosuta et al., 2003; Oláh et al., 2005; Kosuta et al., 2008; Maillet et al., 2011). The result of the symbiotic signalling pathway is the generation of specialized structures, nodules in case of rhizobia, and arbuscules in case of mycorrhiza, where the nutrient exchange takes place.

4.1. Legume-rhizobial symbiosis

Nodulation is the symbiotic interaction between legumes and rhizobia. Ammonia is the biologically active form of nitrogen required for plant metabolism but ammonia presence in the soil is very limited. Rhizobia are capable of nitrogen fixation which consists of the conversion of nitrogen gas (N_2) into ammonia. Therefore, the rhizobia-legume interaction provides the plant with a continuous source of biologically active nitrogen in form of ammonia. The result of this

interaction is the formation of a symbiotic organ, the root nodule, where the nitrogen fixation takes place. The formation of nodules requires the spatio-temporal coordination of two developmental processes, nodule organogenesis and bacterial infection (Oldroyd and Downie, 2008). All the arrangements for the accommodation of rhizobia within a nodule are guided by a common signalling pathway shared with the AMF symbiosis.

The first step of the legume-rhizobial interaction establishment is the plant release of flavonoids which diffuse across the bacterial membrane and activate the rhizobial production of Nod factors. In addition, flavonoids also act as a chemotactic attractant to bacteria and promote their movement towards the plant root hairs, where they release Nod factors among other components including polysaccharides (Downie, 2010). Nod factors are lipochitooligosaccaharides (LCOs) whose structure consists of a chitin backbone formed by three to five β1-4 linked N-acetylglucosamine residues. The β1-4 N-acetylglucosamine backbone constitutes the core of the Nod factor structure and can be decorated with different substituents such as acyl, methyl and sulphate groups as well as other sugars, providing host specificity to these signals (Lerouge et al., 1990; Perret et al., 2000). Perception of the Nod factors upon bacterial attachment at the extracellular region of a growing root hair tip at the root epidermis induces tip swelling and an outgrowth (Figure 1.6) (Esseling et al., 2003). In addition, Nod factor perception also induces the division of cortical cells for the generation of the nodules, suggesting the presence of a diffusible signal between the epidermis and the cortex (Truchet et al., 1991).
In order for the bacteria to enter the plant root and ultimately the nodules, the root hair tip outgrowth enables the root hair to bend back upon itself resulting in a curling that entraps bacteria into a sealed two cell wall space called the infection pocket (Geurts et al., 2005).

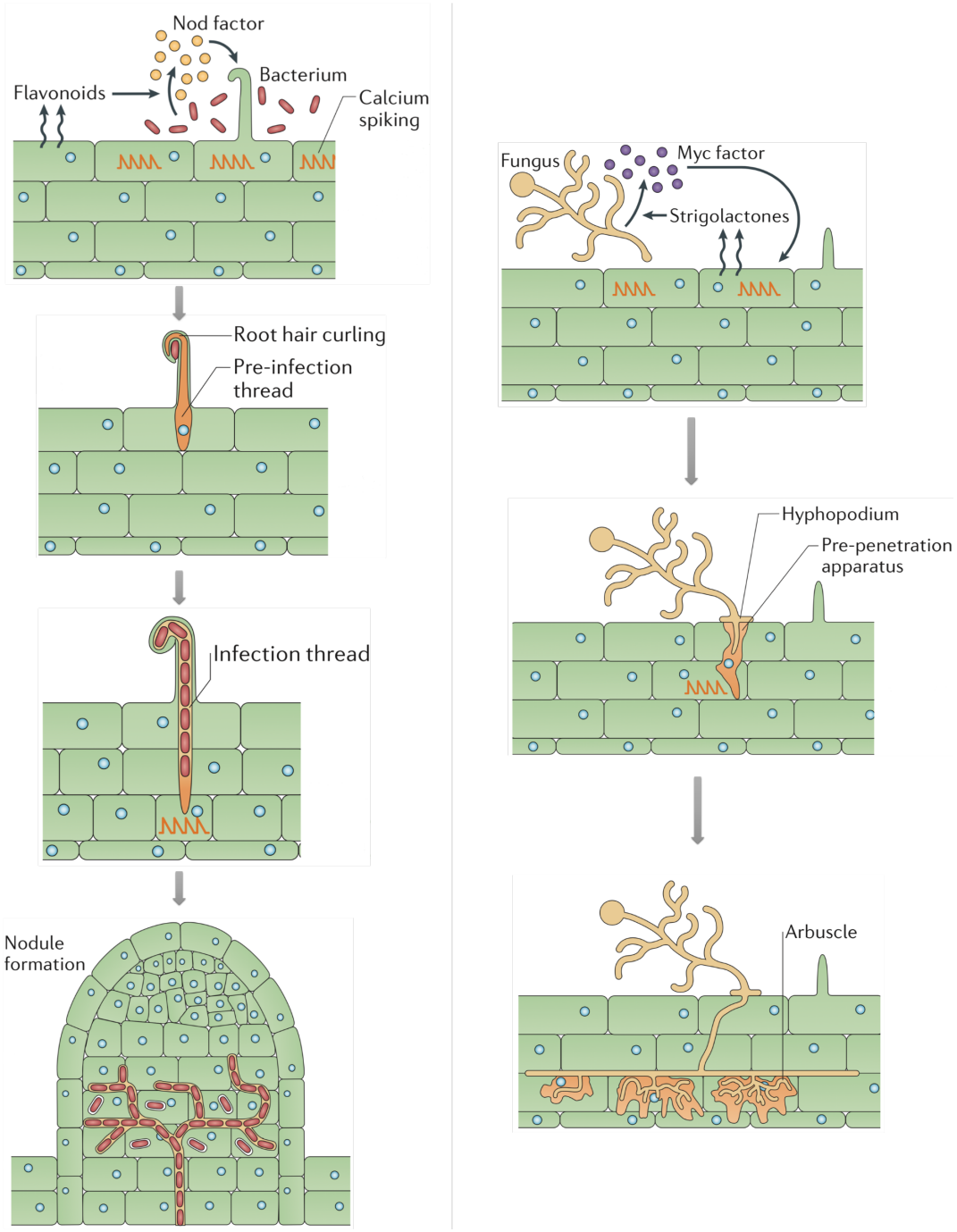

Figure 1. 6. Infection processes during plant-microbe symbioses.

Mechanism of infection during legume-rhizobial symbiosis is shown in left-hand side panel. AMF-symbiosis is shown in right-hand side panel. Both symbiotic interactions start with an exchange of diffusible signals that lead to the plant recognition of Nod and Myc factors, triggering the mechanisms responsible for the formation of the structures required in the accommodation of the symbiont. Figure adapted from Oldroyd (2013) Nature Reviews Microbiology.

The infection pocket is required for the localized degradation of the root hair cell wall, which constitutes the start point for the formation of a tube-like structure called the Infection Thread (IT) which will allow the bacteria to cross the different root cell layers and finally enter the nodules (Ridge and Rolfe, 1985; Turgeon and Bauer, 1985). The IT lumen constitutes the path in which entrapped bacteria divide as they move across the different cell layers. The cells situated immediately underneath the cell that is being infected, develop low frequency nuclear Ca^{2+} oscillation similar to that observed during infection of the previous cell (Sieberer et al., 2012). In addition, the cell wall of the underlying cortical cell is degraded to enable the formation of a new IT from the site where the epidermal IT ended (van Brussel et al., 1992). During the growing of the IT, the root hair cell switches from low to high frequency nuclear Ca^{2+} oscillations leading to its irreversible commitment to infection (Sieberer et al., 2012). This process continues to take place in the successive cortical cell layers until the IT reaches the developing nodule cells. As the IT progress through the different root cell layers, rhizobia continue to grow in the IT lumen, which is topologically outside of the root hair cell (Brewin, 2004; Gage, 2004), while bacterial surface polysaccharides act as a molecular signal to the host plant (Figure 1.6) (Gibson et al., 2008). Degradation of the root hair cell wall is necessary for rhizobial entry and it could be mediated by both plant and bacterial enzymes, such as the plant polygalacturonases (Muñoz et al., 1998; Rodríguez-Llorente et al., 2004) and bacterial cellulase (Laus et al., 2005; Robledo et al., 2008). Once a cell has been infected and the IT has progressed to the subsequent cell, the Ca^{2+} oscillations no longer occur (Sieberer et al., 2012)

In the infection pocket, rhizobia divide to form colonies that constitute the infection foci. After rhizobia entrapment, there is a reorientation of the polar growth that results in an inward growing invagination of the root hair cell (Miwa et al., 2006). The root hair cell nucleus moves closer to the infection focus and the cytoskeleton reorients creating a cytosolic bridge or pre-IT (PIT) structure that guides the inward growth across the root hair cell (Figure 1.6). In addition, Nod factor perception also induces the cytoskeleton reorientation and nucleus relocation to the centre of the cortical cells in a way that all are aligned (van Brussel et al., 1992; Timmers et al., 1999).

When the IT reaches the nodules, the final stage of the infection process is the release of bacteria into them. The formation of the symbiotic organ, the nodule, constitutes the key event for the establishment of symbiosis as nodules provide the suitable environment for the bacterial nitrogen fixation. The endocytosis of rhizobia at the tip of the IT creates an organelle-like structure in the nodule, the symbiosome, in which bacteria are in direct contact with the host plasma membrane allowing the nutrient exchange to take place (Figure) (Brewin, 2004).

4.2. Arbuscular mycorrhizal symbiosis

Most families of terrestrial plants can establish a symbiotic interaction with Arbuscular mycorrhiza fungi (AMF) which belong to the phylum *Glomerycota* (Harrison, 2012).

The first step in the development of the AM symbiosis is the fungal perception of plant diffusible signals, strigolactones which induce germination and hyphal branching (Akiyama et al., 2005). During hyphae growth toward the host root, arbuscular mycorrhiza fungi (AMF) release diffusible compounds, Myc factors, that allow the plant to recognize the fungus and trigger plant symbiotic signalling pathway (Kosuta et al., 2003; Kuhn et al., 2010; Maillet et al., 2011).

Similar to Nod factors, Myc factors are also lipochitooligosaccaharides (LCOs) composed of a tetrameric or pentameric chitin backbone that can be sulphated on the reducing terminus. There are two LCOs produced by the fungus *Rhizophagus irregularis* that present differences in their structures including an unsaturated C18:1 acyl chain in one of them while the other contains a saturated C16 acyl chain (Maillet et al., 2011). In addition, short-chain chitin oligomers (COs) such as the tetra-acetyl chitotetraose (CO4) were also found in arbuscular mycorrhizal (AM) germinated spore exudates (GSEs) and are able to activate the CSSP (Genre et al., 2013; Sun et al., 2015a). While both Myc-LCOs and COs induce calcium oscillations in legumes such as *Medicago truncatula*, calcium oscillations are only induced by COs (but not LCOs) in non-legumes such as rice (Sun et al., 2015a). These differences in the composition of the Myc factors and

in the structure of the LCOs and COs might allow the interaction with a wide variety of host plants.

When the hyphae reaches the root surface, the fungus forms a hyphopodium in a process that requires cutin monomers provided by the plant (Wang et al., 2012). The plant cell contacted by the newly formed hyphopodium forms a tube-like structure similar to the PIT in the rhizobial symbiosis, the pre-penetration apparatus (PPA) (Genre et al., 2005). In analogy to the formation of the PIT, the PPA formation is initiated by the positioning of the plant cell nucleus below the hyphopodium contact site and subsequently, the nucleus migrates to transverse the plant cell vacuole. In turn, this creates an intracellular accommodation structure that guides the fungal progression through the different cell layers (Genre et al., 2005).

As the fungal hypha grows within the PPA across the cell, high frequency nuclear Ca^{2+} oscillation occur. In addition, the cells situated immediately below the cell which the hyphae is traversing, present low frequency Ca^{2+} spiking that, similarly to rhizobial symbiosis, precedes the infection (Sieberer et al., 2012). The hyphae continues its growth through the different cell layers guided by the PPA and once the fungal hyphae reaches the cortical cells, it branches and progresses through the apoplast where it forms the arbuscules (Genre et al., 2008; Harrison, 2012). The arbuscules are branched tree-like structures formed by the AMF inside the root cortex cells and where the nutrient exchange takes place during symbiosis. Arbuscule formation involves changes in the cytoskeleton (Genre and Bonfante, 1998; Blancaflor et al., 2001) in which actin filaments and microtubules acquire a basket like structure that surrounds the arbuscule, in addition to changes in the vacuole and nucleus position (Figure 1.6) (Fester et al., 2001; Lohse et al., 2005; Pumplin and Harrison, 2009).

Although there is an intracellular accommodation of the arbuscules in the cortex, the hyphae are not in direct contact with the plant cytosol but they are separated by the so-called the periarbuscular membrane (PAM). The PAM is a plant derived membrane contiguous with the plant plasma membrane that constitutes an envelope around the arbuscules branches. This requires a large extension of the

plasma membrane that increases the surface for nutrient exchange as a space, the periarbuscular space, is created between the PAM and the fungal membrane. In spite of the PAM being derived from the plasma membrane, it has a different composition specific for the symbiotic process (Pumplin and Harrison, 2009).

Finally, the nutrient exchange takes place according to the plant nutritional needs. The fungus acquires the nutrients including inorganic phosphorous (Pi), nitrogen, water and other micronutrients from the soil by the extraradical hyphae. These are then transported to the intraradical hyphae including the arbuscules, where they are transferred to the plant cytoplasm by crossing the fungal and periarbuscular membranes. In turn, the fungus obtains a carbon source in form of hexoses from the plant cytoplasm that are converted into their transportable forms the long distance between the arbuscules and the extraradical hyphae (Smith and Read, 2008).

4.3. AM and rhizobial symbioses share a Common Symbiotic Signalling Pathway (CSSP)

The diffusible Nod and Myc factor signals released by rhizobia and AMF respectively, are recognized at the plasma membrane of root hair cells by the Lysin Motif (LysM) domain of receptors-like kinases. Two LysM-receptor like kinases have been found to contain docking sites for Nod factor recognition at their LysM domains: LysM receptor kinase 3 (LYK3) (Smit et al., 2007) of *M. truncatula* (NFR1 in *L. japonicus*) and Nod Factor Perception (NFP) of *M. truncatula* (NFR5 in *L. japonicus*). NFR1 autophosphorylates and transphosphorylates NFR5, whose kinase domain has been reported to be non-functional (Radutoiu et al., 2003; Madsen et al., 2011). This transphosphorylation suggests that NFR1 and NFR5 function as a heterocomplex in which Nod factor recognition is carried out by both receptors of the complex but only NFR5 has an additional role in the downstream signalling pathway. The identity of the Myc factor receptors is not yet known but some studies suggest that both LYK3 and NFP could be also involved in Myc factor perception (Maillet et al., 2011; Czaja et al., 2012; Zhang et al., 2015). Symbiosis receptor like kinase (SYMRK) of *L. japonicus* and its ortholog Does not make infection 2 (DMI2) of *M. truncatula*

interact with the LysM receptor complex in the recognition of Nod and Myc factors (Figure 1.7) (Endre et al., 2002; Stracke et al., 2002; Gherbi et al., 2008).

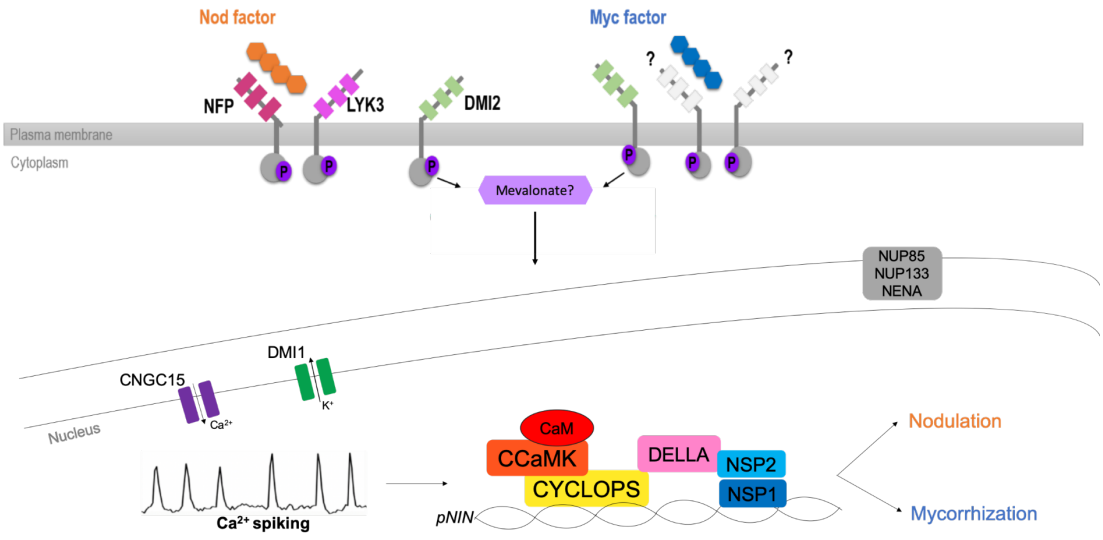

Figure 1. 7. The common symbiosis signalling pathway (CSSP). Perception of Nod and Myc factors occurs at the plasma membrane of the root hair cells.

Nod factors are perceived by two Lys-M receptor like kinases LYK3 and NFP in conjunction with the co-receptor DMI2 which also participates in Myc factor perception. The identity of the Myc factor receptors remains yet to be clarified but LYK3 and NFP have also been suggested to be involved in Myc factor perception. After Nod and Myc factor perception, a second messenger of unclear identity is activated, with mevalonate as a possible candidate, and drives the signal to the nucleus where the Ca^{2+} spiking is generated. The cyclic-nucleotide-gated Ca^{2+} channel CNGC15, the voltage-gated ion channel with a preference for potassium ions DMI1 and the ATPase MCA8 participate in the generation of the Ca^{2+} spiking. The nucleoporins NUP85, NUP133 and NENA are also required for the Ca^{2+} spiking generation. The Ca^{2+} spiking is decoded by CCaMK that interacts with and phosphorylates the transcription factor CYCLOPS. The CCaMK-CYCLOPs complex is bridged to the NSP1-NSP2 complex through DELLA which allows the activation of specific transcription factors required for the establishment of symbiosis.

Recognition of Nod and Myc factors at the plasma membrane and internalisation of the signal within the cell triggers oscillation of nuclear calcium concentration, denoted as calcium spiking which constitutes one of the earliest measurable

responses (Ehrhardt et al., 1996; Kosuta et al., 2008). Therefore, in order for the signal to be transmitted from the plasma membrane to the nucleus, a secondary messenger whose identity remains unclear is required. SYMRK/DMI2 was also found to interact with 3-hydroxy-3-methylgluratyl-CoA reductase (HMGR), an enzyme involved in mevalonate synthesis, suggesting a role for mevalonate as a second messenger that drives the signal from the plasma membrane to the nucleus. RNA interference silencing of *HMGR* showed a sharp decrease in root infection and number of nodules obtained (Kevei et al., 2007). In addition, mevalonate exogenous application triggered nuclear calcium oscillations in root epidermal cells (Venkateshwaran et al., 2015). All these results together suggest that DMI2 activation might induce activation of HMGR bound to DMI2, which catalyses the production of mevalonate and then, mevalonate (or a chemical derivative) is translocated into the nucleus where it induces calcium spiking by the activation of calcium channels.

Generation of nuclear Ca^{2+} oscillations requires a calcium channel(s) that allows the movement of calcium ions from the store into the nucleoplasm, a cation channel that enables the efflux of a counter-ion and a calcium pump(s) that enables the transport of calcium back into the store. Most of these components were found on the nuclear membrane suggesting that the ER is the symbiotic calcium store, as it is contiguous with the nuclear envelope (Sieberer et al., 2009; Capoen et al., 2011). These channels and pumps need to be transported into the nucleus and three nucleoporines, NUP85, NUP133 and NENA, might be involved in this, as it was shown that they are essential for the calcium spiking generation (Figure 1.7) (Kanamori et al., 2006; Saito et al., 2007; Groth et al., 2010). A voltage-gated ion channel, DMI1 of *M. truncatula* (CASTOR and POLLUX of *L. japonicus*) has been identified (Ané et al., 2004; Imaizumi-Anraku et al., 2005; Riely et al., 2007; Charpentier et al., 2008; Capoen et al., 2011) with a preference for potassium ions (Figure 1.7) (Charpentier et al., 2008). It has been hypothesized that the function of DMI1 could be the efflux of potassium from the nucleoplasm to restore the membrane charge balance after the depolarization produced by the calcium influx, or that it could induce the hyperpolarization of the nuclear membrane potential resulting in the opening of a voltage-gated calcium channel (Charpentier et al., 2013). Three cyclic-nucleotide gated channels,

CNGC15a, CNGC15b, and CNGC15c from *M. truncatula* were discovered to be required for the generation of Ca^{2+} oscillations in both mycorrhizal and rhizobial symbioses. The channels CNGC15a, CNGC15b, and CNGC15c located at the nuclear envelope are Ca^{2+} permeable and physically interact with DMI1 (Figure 1.7). Therefore, it has been proposed that interaction of CNGC15a, CNGC15b, and CNGC15c act to coordinate the Ca^{2+} mobilisation from the ER (continuous with the nuclear envelope) Ca^{2+} store to the nucleus and the potassium efflux for the generation of the Ca^{2+} spiking (Charpentier et al., 2016). Finally, MCA8 was found as a calcium ATPase in the SERCA-type family whose role is the pumping of calcium ions back into the store by using the energy of the ATP hydrolysis (Figure 1.7) (Capoen et al., 2011).

4.4. Symbiotic Ca^{2+} spiking

During nodulation, the Ca^{2+} spiking is induced after 10 min of the application of either Nod factors or rhizobia and occurs within the nucleus of the root hair cell (Sieberer et al., 2009; Ehrhardt et al., 1996a). Regular Ca^{2+} oscillations originate from the perinuclear region with periodicities varying between 50 and 150 s, corresponding to 90 s in *Medicago truncatula* (Kosuta et al., 2008) and asymmetrical nature as the up-phase (increasing Ca^{2+}) of the spike was observed to last less than the down-phase (decreasing Ca^{2+}; Figure 1.8) (Ehrhardt et al., 1996a). The spiking was shown to have a cell-autonomous nature (Miwa et al., 2006; Sieberer et al., 2009), which was further demonstrated by the switch in the Ca^{2+} spiking frequency between the cells that are being infected and the adjacent cells that are not being infected yet (Sieberer et al., 2012). These changes in Ca^{2+} concentration occur within the physiological range, between 150 – 800 nM (Ehrhardt et al., 1996a) and have been demonstrated to activate gene expression as for instance, 36 spikes were sufficient to induce the expression of the early symbiotic marker gene *ENOD11* (Miwa et al., 2006).

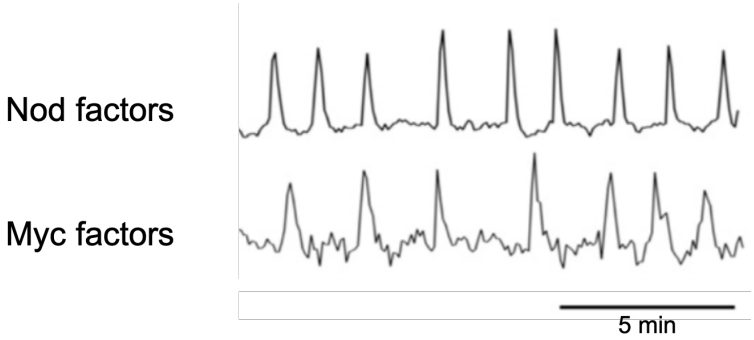

Figure 1. 8. The nuclear Ca^{2+} spiking in response to Nod and Myc factors.

The figure allows to visualize the differences in the Ca^{2+} signature patterns generated upon perception of Nod or Myc factors. Figure adapted from Sun et al., (2015).

Nuclear Ca^{2+} oscillations were also observed in response to either Myc factors or AM-fungi (Figure 1.8) (Kosuta et al., 2008; Chabaud et al., 2011). The periodicity in these signals was initially observed to be 30 s which is significantly shorter than that observed upon Nod factor application (90 s) (Kosuta et al., 2008). Additionally, both Nod factor and Myc factor induced Ca^{2+} spiking showed a chaotic nature despite their periodicity and since both types of diffusible signals can activate the same signalling components and yet induce very different responses, this allows flexibility in the response to both symbionts (Kosuta et al., 2008). These differences in the Ca^{2+} spiking pattern between the rhizobia and AM symbiosis could then be responsible for activating the specific signalling components leading to the required developmental processes for the establishment of each symbiosis. A more recent study demonstrated that the Ca^{2+} spiking induced by both symbionts were highly similar, with no differences in periodicity (period between 50 and 100 s) but small differences in frequency could still be observed. Moreover, Myc factors were also shown to be specifically recognised by the plant and activate different symbiotic gene expression than Nod factors (Sun et al., 2015a).

4.5. Downstream of Ca^{2+} spiking

Immediately downstream of the calcium spiking CCaMK acts as the Ca^{2+} signal decoder (Levy, 2004; Mitra, 2004). Nuclear calcium oscillations activate CCaMK which phosphorylates and forms a complex with CYCLOPS. The CCaMK-CYCLOPS complex activates a suite of transcription factors that differ depending

on the rhizobial or mycorrhizal symbiotic interaction (Figure 1.7). In addition to CCaMK, CYCLOPS was found to be essential for the establishment of symbiosis. This is consistent with the gain-of-function mutation of CYCLOPS which induce the activation of nodule organogenesis in the absence of rhizobia. This gain-of-function mutation correspond to a phosphomimetic version of CYCLOPS (CYCLOPS-DD). The spontaneous nodulation induced by phosphomimetic CYCLOPS was observed in *ccamk* mutant backgrounds and demonstrates that CYCLOPS phosphorylation is essential for the activation of downstream signalling components (Singh et al., 2014). Despite both symbiotic interactions sharing many signalling components of the CSSP, the symbiotic signalling pathway for each interaction will be explained separately for better clarity.

4.5.1. Rhizobial symbiosis signalling pathway downstream of CCaMK-CYCLOPS

CCaMK-phosphorylated CYCLOPS induces the transcriptional activation of *Nodule Inception* (*NIN*), a putative transcription factor essential for nodulation (Schauser et al., 1999; Borisov et al., 2003; Marsh et al., 2007), by direct binding to a region of the promoter of *NIN* (*pNIN*), the CYC-box, in a sequence specific manner (Singh et al., 2014). However, the CCaMK-CYCLOPS complex also associates with DELLA proteins (named after a highly conserved DELLA amino acid motif in their N-terminal domains) which have been shown to be involved in nodule organogenesis and infection thread formation in *Medicago truncatula* (Jin et al., 2016). This association with the DELLAs further promotes the CCaMK-CYCLOPS complex formation, increases phosphorylation levels of CYCLOPS and allows DELLAs to act as a bridge between the CCaMK-CYCLOPS complex and two GRAS (Gibberelic acid insensitive, Repressor of gai, Scarecrow) domain transcription factors, Nodulation Signalling Pathway 1 (NSP1) and NSP2 (Jin et al., 2016). NSP1 and NSP2 are required for nodulation and Nod factor signalling and promote the transcription of Nod factor (NF)-inducible genes (Catoira, 2000; Kalo, 2005; Smit, 2005). However, although only NSP1 (and not NSP2) contains a DNA-binding domain, the formation of a heterodimer between NSP1 and NSP2 has been shown to be necessary for NSP1 DNA binding to the NF-inducible promoters. The NSP1-NSP2 heterocomplex promotes the expression of different genes that regulate separate stages of the symbiotic process (Hirsch et al., 2009;

Cerri et al., 2012). *NIN* is one of these genes as *NIN* expression was abolished in *nsp1* or *nsp2* mutants (Hirsch et al., 2009). The *pNIN* also has a binding site for NSP1, the NRE-box, that is in close proximity with the CYC-box which allows the CCaMK-CYCLOPS and NSP1-NSP2 complexes bridged by DELLAs to activate the expression of downstream NF-inducible genes (Figure 1.7) (Jin et al., 2016).

After perception of NF, the NSP1/NSP2 heterocomplex also binds to the promoters of the *Ethylene Response Factor (ERF) Required for Nodulation 1 (ERN1)* and a second related ERF transcription factor, ERN2, in epidermal cells by binding to a promoter regulatory region called NF-box (Andriankaja et al., 2007). ERN1 is a transcription factor responsible for the induction of *Early Nodulin 11* (*ENOD11). ENOD11* encodes for a cell-wall-repetitive (hydroxyl)proline rich protein (RPRP) (Journet, 2001) which is well established as one of the earliest marker genes induced after NF-perception in the root epidermis (Journet, 2001; Charron et al., 2004). *ENOD11* is also associated with the rhizobial infection process as it is expressed in root hairs and cortical cells (Journet, 2001). The NSP1/NSP2 heterocomplex is involved in the regulation of *ENOD11* during subsequent stages of rhizobial infection through the binding of NSP1 to the -257 *ENOD11* promoter region that requires the presence of rhizobia (Boisson-Dernier et al., 2005; Cerri et al., 2012). The NIN transcription factor also has a role in the regulation of *ENOD11* expression. When NF-treatment was applied to wild-type and *nin-1* mutant plants transformed with a *pENOD11-GUS* construct, differences could be seen in the spatial and temporal pattern of expression. While wild-type mutant plants showed a restricted expression of *ENOD11* to the IT containing cells and infected cells, the *nin-1* mutant plants showed an expanded expression towards the root tip (Marsh et al., 2007). Moreover, it was reported that binding of NIN to the NF-box of the *pENOD11* occurs to the same region where ERN1 also binds (Vernié et al., 2015), suggesting a possible negative regulation of epidermal *ENOD11* expression through the NIN-mediated inhibition of ERN1 action (Liu et al., 2019).

NIN expression is also associated with cytokinin signalling, a hormone involved in nodule organogenesis. A cytokinin receptor in *Medicago truncatula* (MtCRE1)

is essential for nodule formation (Murray et al., 2007; Tirichine et al., 2007; Plet et al., 2011). NF application induces *CRE1* expression in the root cortex and this expression is dependent on *NIN*. In addition, NIN was found to associate with the *CRE1* promoter (Vernié et al., 2015). As epidermal *NIN* expression is sufficient for cytokinin signalling in the cortex, it has been suggested the existence of a mobile signal from the epidermal to cortical cells (Hayashi et al., 2014; Held et al., 2014). Finally, cytokinin signalling induces the expression of *NIN* in the cortex which activates nodule organogenesis (Gonzalez-Rizzo et al., 2006; Heckmann et al., 2011; Plet et al., 2011). This is an example of the role that hormones play in symbiosis. Plant hormones have an important role in organogenesis and therefore, during nodulation. Many plant hormones, including cytokinin, auxin, ethylene, gibberellins, strigolactones, abscisic acid, are involved in nodulation to tightly coordinate every step of the infection process through their different spatiotemporal mode of action (reviewed in Desbrosses and Stougaard, 2011; Mukherjee and Ané, 2011; Murray, 2011; Ferguson and Mathesius, 2014; Foo et al., 2014).

4.5.2. AM-symbiosis signalling pathway downstream of CCaMK-CYCLOPS

In addition to its requirement in the nodulation process, CCaMK-CYCLOPS complex is also required for arbuscule initiation (Kistner et al., 2005; Yano et al., 2008). CCaMK-CYCLOPS complex also interacts with DELLA proteins during AM-symbiosis, (Pimprikar et al., 2016) which are usually found to interact with DNA-binding transcription factors to regulate promoter activation (Fukazawa et al., 2014; Yoshida et al., 2014). DELLA is a repressor of the plant hormone gibberellin (Davière and Achard, 2013) which has been reported as an inhibitor of arbuscule formation (Floss et al., 2013; Foo et al., 2013; Yu et al., 2014). Subsequently, CCaMK-CYCLOPS-DELLA complex was shown to directly interacts with the promoter of *Required for Arbuscular Mycorrhization 1* (*RAM1*) (Pimprikar et al., 2016) which encodes a GRAS transcription factor necessary for hyphopodia formation, arbuscule branching and induction of arbuscule development marker genes (Park et al., 2015; Rich et al., 2015; Xue et al., 2015). This interaction is established through the direct binding of CYCLOPS to a specific region of the promoter of *RAM1* (*pRAM1*) which in turn, activates *RAM1*

expression (Gobbato et al., 2012; Pimprikar et al., 2016). RAM1 binds to the promoter of *RAM2* (*pRAM2*) in vivo. RAM2 encodes a Glycerol-3-Phosphate Acyl Transferase (GPAT) which has a role in the synthesis of cutin monomers required in the formation of hyphopodia (Wang et al., 2012) and arbuscule development (Gobbato et al., 2013). Therefore, RAM1 and RAM2 play important roles in the early stages of the symbiotic interaction promoting the formation of structures that facilitate the fungus invasion.

NSP1 and NSP2 also have a role in mycorrhization in addition to their function in nodulation (Maillet et al., 2011; Delaux et al., 2013). NSP1 and NSP2 were found to be involved in the induction of strigolactone production (Liu et al., 2011). Strigolactones, as explained in Section 1.4.2, are the initial signals released from the plant to the fungus to establish the symbiosis. As a result, NSP1 and NSP2 induce the plant to continue the production of strigolactones and the signalling to the fungus that results in hyphal branching and fungal progression (Akiyama et al., 2005).

In addition to NSP1, RAM1 also binds to NSP2 (Gobbato et al., 2012). The interplay among RAM1, NSP1 and NSP2 at the different stages of the infection process contributes to the regulation of different target gene expression: when NSP1 binds to NSP2, the production of strigolactones required for hyphal branching is promoted (Liu et al., 2011). However, the binding of NSP2 to RAM1 and subsequently, RAM1 activation of *RAM2* expression induces the production of cutin monomers required for hyphopodia and arbuscule formation.

During mycorrhization, NSP1, NSP2 and RAM1 activate the expression of different marker genes such as *ENOD11* (Kosuta et al., 2003), which is also present in nodulation, and *Membrane Steroid Binding Protein 1* (*MSBP1*) (Kuhn et al., 2010). The activation of *ENOD11* expression as an early response in both rhizobial and mycorrhizal symbioses demonstrate that both processes are coordinated by common symbiotic signalling components. Indeed, NIN was also reported to be involved in the AM-symbiosis, specifically in the control of fungal colonisation with no apparent role in arbuscule morphogenesis (Guillotin et al., 2016). NIN was found to have a similar role in the regulation of gene expression between nodulation and mycorrhization as for instance, NIN was required for

induction of CRE1 expression during mycorrhization (Guillotin et al., 2016), a cytokinin receptor also involved in nodule organogenesis. Furthermore, *ENOD11* was down-regulated by NIN during mycorrhization like in nodulation, suggesting the potential role of NIN in the signalling regulation of the initial steps of fungal invasion (Guillotin et al., 2016).

Both *ENOD11* and *MSBP1* marker genes are induced at early stages of the symbiotic association, upon Myc factor recognition and this induction is dependent on CCaMK (Sun et al., 2015). In addition, both *MSBP1* and *ENOD11* expression coincides in some root areas, such as appresorium-enriched areas and underneath branched hyphae (Kosuta et al., 2003; Kuhn et al., 2010).

The similarity in the infection processes as well as the sharing of symbiotic signalling components with Ca^{2+} spiking as a central element is consistent with a common origin of both interactions, with AM symbiosis as the evolutionary ancient association (Markmann and Parniske, 2009).

5. CCaMK, the central regulator of root endosymbiosis.

Nuclear Ca^{2+} spiking occurs upon Nod and Myc factors recognition and is considered the central element in both AM and rhizobial symbioses where CCaMK is responsible for the decoding of the symbiotic Ca^{2+} signal.

5.1. Domain structure and biochemical properties of MtCCaMK

In *Medicago truncatula*, CCaMK is a protein of 523 amino acids and 58.6 kDa encoded by a single gene (Levy, 2004; Patil et al., 1995). The structure of CCaMK consists of four functional domains: a catalytic domain with Ser/Thr kinase activity, an autoinhibitory domain which overlaps with a CaMB domain, and four EF-hand motifs (Figure 1.9) (Ramachandiran et al., 1997).

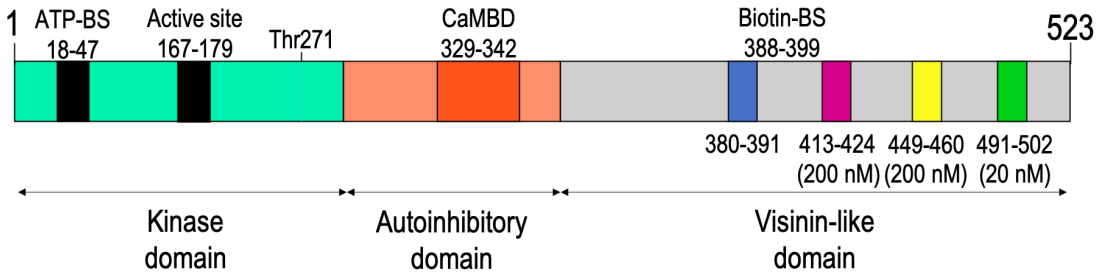

Figure 1. 9. Outline of the domain organisation of CCaMK.

The serine/threonine kinase domain is shaded in turquoise with the ATP binding site (ATP-BS) and kinase active site shaded in black as indicated. The autoinhibitory domain is shaded in orange with the calmodulin binding domain (CaMBD) shaded in dark orange. The visinin-like domain is shaded in grey, with the loops of EF-hands 1, 2, 3 and 4 shaded in blue, pink, yellow and green respectively. The values for the Ca^{2+} dissociation constant (Kd) of each EF-hand motif are indicated underneath the corresponding EF-hand. Labels denote residue numbers for the identified domains and features of CCaMK, which were identified in *M. truncatula.*

The kinase domain of CCaMK is placed at the N-terminus between residues 1 and 322 where all 11 major conserved sub-domains typically found in the catalytic domain of Ser/Thr kinases are also observed (Figure 1.9) (Hanks et al., 1988; Patil et al., 1995; Takezawa et al., 1996). The ATP binding site is predicted to be placed between residues 18-47 and the mutation K47E (K44E in *Lotus japonicus*) was shown to abolish kinase activity (Patil et al., 1995; Takezawa et al., 1996; Shimoda et al., 2012; Yano et al., 2008). CCaMK kinase activity is required for the transmission of the signal downstream during the Ca^{2+} decoding process via phosphorylation of protein targets. Indeed, the kinase-dead CCaMK mutant K44E in *Lotus japonicus* (K47E in MtCCaMK) was unable to interact with CYCLOPS, the interacting partner of CCaMK during symbiosis (Yano et al., 2008). In addition, CCaMK regulates its own kinase activity via autophosphorylation (Sathyanarayanan et al., 2000). The residue Thr271 located at the 10^{th} sub-domain of the kinase domain of *Medicago truncatula* CCaMK (MtCCaMK) (Thr267 in *L. japonicus*) has been reported to be conserved across monocotyledonous and dicotyledonous and to be the main autophosphorylation site of CCaMK (Sathyanarayanan et al., 2001). Thr271 autophosphorylation is Ca^{2+}-dependent as a 3.4 fold increase in the autophosphorylation levels of

CCaMK was observed in the presence of Ca^{2+} (Takezawa et al., 1996). This autophosphorylation on Thr271 constitutes a molecular brake that keeps the kinase inactive due to the interaction between the phosphate residue at phosphorylated Thr271 with other residues at the CaMBD (Sathyanarayanan et al., 2001; Miller et al., 2013; Routray et al., 2013). Similar to CaMKII, autophosphorylation at Thr271 increases the affinity of CCaMK for CaM (Patil et al., 1995; Sathyanarayanan et al., 2001), but unlike CaMKII, this autophosphorylation is Ca^{2+}-dependent/CaM-independent and does not activate CCaMK. Conversely, Thr271 autophosphorylation primes the protein for activation as an 8-fold increase in the affinity for Ca^{2+}-bound CaM was observed upon Thr271 autophosphorylation which in turn, increases the kinase activity by 5-fold compared to unphosphorylated CCaMK (Takezawa et al., 1996). A lack of Thr271 autophosphorylation still allows CaM binding but does not result in stimulation of the kinase activity (Sathyanarayanan et al., 2001).

The CaMBD has 79% homology to the α-subunit of the mammalian CaMKII (CaMKIIα) and constitutes a single binding site for CaM that overlaps with an autoinhibitory (AI) domain (Ramachandiran et al., 1997; Patil et al., 1995; Takezawa et al., 1996). The AI/CaMBD comprises amino acid residues 323-349 from which region 325-338 adopts a basic amphiphilic α-helix conformation similar to CaMKIIα and typical of CaMB domains (Takezawa et al., 1996; Patil et al., 1995; Swainsbury et al., 2012). Two important residues for CCaMK regulation, Ser322 and Arg323, are located at the CaMBD and were predicted to be part of a hydrogen network with phosphorylated Thr271 that links the AI/CAMBD and the kinase domain of CCaMK and keeps the protein inactive (Miller et al., 2013). The corresponding residues in LjCCaMK were also predicted by Shimoda et al. (2012). At either side of these two residues, Glu319 and Leu324 were found to be essential for CaM binding to CCaMK as their substitution to alanine resulted in a significant decrease in Thr271 autophosphorylation and reduction of nodulation and mycorrhization levels compared to WT-CCaMK (Miller et al., 2013). In addition to Thr271 located within the kinase domain, CCaMK possesses further phosphorylation sites. Ser337 in LjCCaMK (Ser343 in MtCCaMK) located in the CaMBD was reported to be an additional autophosphorylation site and important for the negative regulation of CCaMK

activity as the phosphomimetic mutation S337D resulted in the loss of Ca^{2+}/CaM binding ability (Liao et al., 2012). Lastly, Ser344 is another autophosphorylation site of MtCCaMK located at the CaMBD also implicated in the negative regulation of CCaMK, that is conserved across legumes and non-legumes, monocotyledonous and dicotyledonous plants but not in the OsCCaMK. Ser344 autophosphorylation was shown to impair CaM binding to CCaMK, CCaMK interaction with CYCLOPS as well as reduced CCaMK kinase activity levels (Routray et al., 2013). Moreover, the inhibition of CaM binding by both phosphorylated Ser343 and Ser344 residues was shown to require their intramolecular interaction with Ser277 located at the kinase domain as deletion of Ser277 restored CaM binding to CCaMK with phosphorylated Ser343 and Ser344 (Jauregui et al., 2017).

Downstream of the CaMBD, a region termed as the neural visinin-like domain (VLD) can be found comprising residues 350-523 with high homology to the visinin-like Ca^{2+} binding proteins found in neural tissue. The homology of CCaMK to both CaMKII and neural visinin-like Ca^{2+} binding proteins is responsible for the designation of CCaMK as being encoded by a chimeric gene. The VLD is composed of four EF-hand motifs arranged in two pairs, the N-terminal pair and the C-terminal pair, that have different Ca^{2+} binding capabilities (Swainsbury et al., 2012; Shimoda et al., 2012). From this point forward, these four EF-hand motifs are assigned numbers 1 to 4 from the N-terminus to C-terminus. EF-hand motif 1 is a non-functional Ca^{2+} binding site due to the presence of two specific substitutions within the EF-hand loop, Gly at position 6 and the -Z ligand, that severely impair the ability of this EF-hand motif to bind Ca^{2+} (Swainsbury et al., 2012). In contrast, EF-hand motif 2 has the ability to bind one Ca^{2+} ion and is the second member of the N-terminal EF-hand pair of CCaMK (Swainsbury et al., 2012). It was demonstrated that specific residues located in the β-sheets of EF-hand motifs 1 and 2, 7^{th} position of the EF-hand 1 loop and 8^{th} position of the EF-hand 2 loop, interact which allows both EF-hand motifs to constitute an EF-hand domain (Shimoda et al., 2012). Furthermore, within the VLD and more specifically, between EF hand 1 and 2 loops, a putative biotin-binding site of sequence LKAMKMNSLI was identified in lily CCaMK (LlCCaMK) comprising residues 389-399 by Patil et al. (1995). In MtCCaMK, the equivalent sequence is

LKAMNMLSLI and spans residues 393-402. The role of this putative biotin-binding site is not yet known but could potentially add another layer of regulation to CCaMK activity. Lastly, the C-terminal EF-hand domain is composed of EF-hand motifs 3 and 4.

The Ca^{2+} binding affinity values of the EF-hand motifs of CCaMK correspond to a dissociation constant (K_d) of 200 nM for EF-hands 2 and 3, and ≤20 nM for EF-hand 4, which indicates the Ca^{2+} sensing ability of the EF-hands in addition to their contribution to the protein structure. This is consistent with the values of the Ca^{2+} concentration at the basal state and during the spiking. In a *Medicago sativa* root hair, the basal intracellular calcium concentration ranges between 125 and 150 nM (Felle et al., 1999) whereas the peak at the Ca^{2+} spiking varies between 625 and 800 nM (Ehrhardt et al., 1996). EF-hand 4 is the EF-hand with the highest affinity for Ca^{2+} in CCaMK which suggests its occupancy at basal Ca^{2+} concentrations. On the other hand, EF-hands 2 and 3 have a much lower affinity and require a higher Ca^{2+} level, the Ca^{2+} spike, to be occupied. Therefore, according to this, only EF-hands 2 and 3 would be involved in the Ca^{2+} spiking response (Miller et al., 2013; Swainsbury et al., 2012). This constitutes a mechanism for CCaMK discrimination between basal concentrations and those during calcium spiking.

Ca^{2+} binding to the EF-hand motifs within the VLD of CCaMK induces a conformational change (Takezawa et al., 1996) that results in the exposure of a hydrophobic surface within the VLD, consistent with other EF-hand proteins (Grabarek, 2006; Gifford et al., 2007). The exposure of the hydrophobic surface in CCaMK has been shown not to be for intramolecular interactions between the VLD and the AI/CAMBD or the kinase domain (Ramachandiran et al., 1997; Swainsbury et al., 2012). Therefore, the purpose of the hydrophobic surface exposure is very likely to be the interaction with the CCaMK phosphorylation target CYCLOPS (Singh et al., 2014). In addition, Ca^{2+} binding has an effect in CCaMK tertiary structure as a change in the environment of the autoinhibitory/calmodulin binding domain upon Ca^{2+} binding was reported, consistent with the model of activation proposed for this protein (Swainsbury et al., 2012; Miller et al., 2013).

The presence of a CaMB domain and four EF-hand motifs makes CCaMK an exceptional Ca^{2+} signal decoder able to discriminate between basal Ca^{2+} concentrations and Ca^{2+} oscillations, by the direct sensing of Ca^{2+} through the EF-hand motif or indirect sensing via CaM (Patil et al., 1995). In analogy to the CDPKs and mammalian CaMKII, CCaMK is able to transmit the Ca^{2+} signals to downstream signalling components via phosphorylation.

5.2. Gain-of-function mutants of CCaMK

The discovery of gain-of-function (GOF) mutants was key for elucidating the mechanism of activation and the role of CCaMK during the symbiotic signalling pathway. GOF mutants of CCaMK are considered those which are able to induce the formation of nodules in the absence of the natural stimulus, rhizobia or Nod Factor (Figure 1.11).

The substitution of the main autophosphorylation site Thr271 for an alanine (T271A) or for an aspartate (T271D) in MtCCaMK (further explanation of these mutants in Section 1.5.3) was able to induce the expression of *ENOD11* in the absence of Nod factor, formation of spontaneous nodules and allowed the complementation of the *dmi3-1* (*ccamk*) phenotype as fully mature (infected) nodules were observed at similar levels than those produced by WT-CCaMK (Miller et al., 2013; Gleason et al., 2006). This is consistent with the equivalent mutant T265I of LjCCaMK which was also able to induce the formation of spontaneous nodules in the absence of the rhizobia (Tirichine et al., 2006). This demonstrated the importance of Thr271 for the negative regulation of CCaMK as the removal of autophosphorylation at this residue via substitution resulted in a fully active protein able to activate the symbiotic signalling pathway in the presence but also in the absence of rhizobia. Moreover, the LjCCaMK T265D mutant was also found to complement loss-of-function mutants of *symrk*, *castor*, *pollux* and *nup85* which are known to be key elements of the CSSP upstream of the Ca^{2+} spiking, further highlighting the central role of CCaMK during symbiosis (Hayashi et al., 2010).

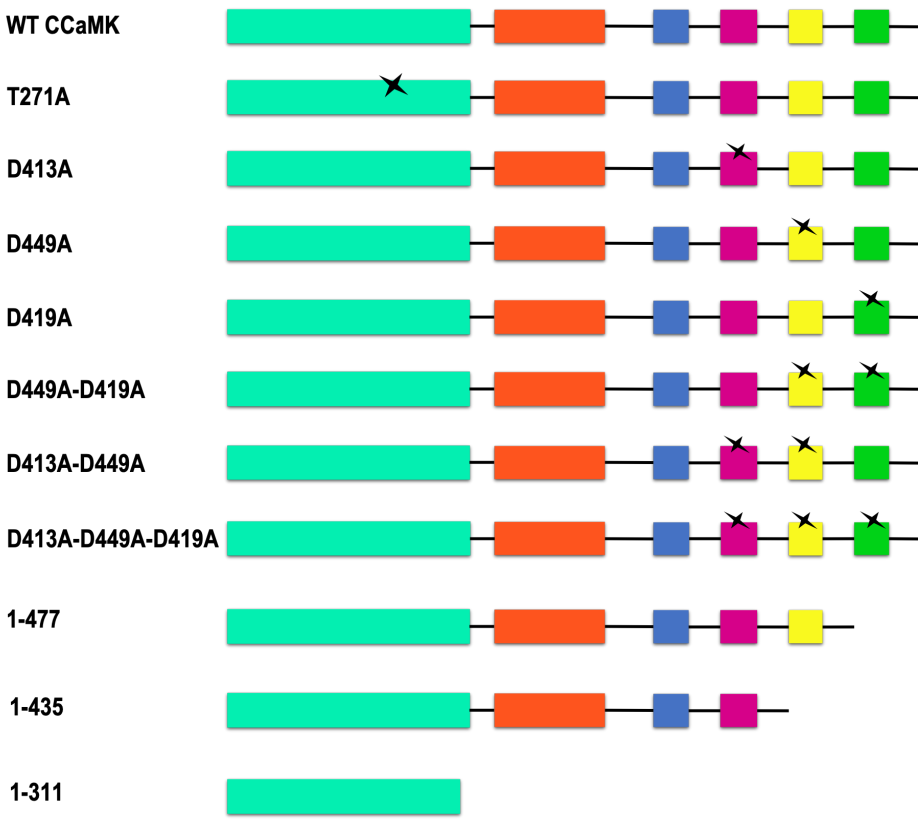

Figure 1. 10. Gain-of-function mutations of CCaMK.

The figure shows the CCaMK wild type and CCaMK mutant variants deregulated by the loss of autoinhibition either by the impairment of Ca^{2+} binding through mutation or deletion of any of the EF-hands, or by the mutation of the autophosphorylation site. The kinase domain is shaded in turquoise, the calmodulin binding domain (CaMBD) shaded in orange, EF-hands 1, 2, 3 and 4 shaded in blue, pink, yellow and green respectively. Mutation in any of these domains is indicated by a black cross.

The point mutation of the highly conserved aspartate (Asp) located at position 1 of an EF-hand loop to an alanine (Ala) impairs Ca^{2+} binding to the EF-hand motif (Putkey et al., 1989). When the Asp-to-Ala substitution was made in any of CCaMK EF-hand motifs, impairment of Ca^{2+} binding was observed in the mutated EF-hand motif (Swainsbury et al., 2012). The Asp-to-Ala substitution in either one, two or the three EF-hand motifs of CCaMK EF-hand motifs resulted in the formation of spontaneous nodules (Miller et al., 2013). Therefore, the single, double and triple EF-hand point mutants of CCaMK constitute further GOF mutants of CCaMK. In addition, the deletion mutants 1-477 and 1-435 lacking either EF-hand 4 and EF-hand 3 and 4 respectively, also showed GOF activity

and ability to induce spontaneous nodulation in the absence of rhizobia (Miller et al., 2013). However, deletion of the entire VLD rendering the kinase and CaMB domains of CCaMK (mutant 1-346) did not result in GOF activity as spontaneous nodule formation was not observed (Gleason et al., 2006; Miller et al., 2013). These data show the role that the EF-hand motifs play in the tight regulation of CCaMK activity during symbiosis.

When both the VLD and CaMBD were deleted, the kinase-only versions of CCaMK 1-311 and 1-322 both also gave rise to spontaneous nodulation in the absence of rhizobia or Nod Factor but did not show any ability to complement the *ccamk* mutant phenotype (Miller et al., 2013; Gleason et al., 2006). In contrast, the kinase-only CCaMK variants were able to complement the defective AM-symbiosis phenotype in *ccamk* in *Lotus japonicus*, highlighting the potential different CCaMK domain requirements for the rhizobial and AM symbioses (Takeda et al., 2012). This further shows that the CaMBD also plays an important role in the regulation of CCaMK activity. In fact, deletion of only the CaMBD (mutant ∆328-355) also displayed GOF activity (Miller et al., 2013; Gleason et al., 2006).

5.3. CCaMK possesses a two step-mechanism of regulation

Despite much effort by several research groups, the crystal structure of CCaMK has not yet been resolved. A crystal structure for CCaMK would allow better understanding of the role played by each structural domain within the mechanism of activation of CCaMK by Ca^{2+}. Therefore, based on the GOF mutants of CCaMK and the Ca^{2+} binding affinities of the EF-hands of CCaMK, a homology model of CCaMK mechanism of activation was developed using CDPK structure scaffold in the presence and absence of Ca^{2+} (Miller et al., 2013).

At basal Ca^{2+} concentrations, CCaMK is bound to Ca^{2+} through at least one of the three functional EF-hands, most likely EF-hand 4 because of its high Ca^{2+} affinity (Swainsbury et al., 2012). Ca^{2+} binding to EF-hand 4 promotes the autophosphorylation of Thr271 and induces a conformational change in which the hydrogen bond network between the kinase and CaMB domains is established (Figure 1.10) (Swainsbury et al., 2012; Miller et al., 2013). In the hydrogen bond network, autophosphorylated Thr271 is hydrogen bonded to

residues Arg323 and Ser322 located at the CaMBD which maintains CCaMK inactive (Miller et al., 2013). This is considered the default state of CCaMK consistent with that both phosphoablative and phosphomimetic mutations of Thr271 disrupt the hydrogen network and autoactivates the protein which results in spontaneous nodule formation in the absence of rhizobia (Gleason et al., 2006; Tirichine et al., 2006).

During Ca^{2+} spiking, Ca^{2+} binds to CCaMK EF-hands and induces the protein to undergo a conformational change that enables the Ca^{2+}/CaM complex to bind to the CaMBD. Binding of CaM causes the disruption of the hydrogen bond network, releasing the kinase domain from autoinhibition and CCaMK is now active for target phosphorylation. In addition, the conformational change also induces the exposure of a hydrophobic surface from the VLD which constitutes the binding region of CCaMK target protein, CYCLOPS (Figure 1.10) (Takezawa et al., 1996; Gleason et al., 2006; Tirichine et al., 2006; Shimoda et al., 2012; Miller et al., 2013). When the Ca^{2+} concentration decreases during the downward-phase of the spike, Ca^{2+} dissociates from both CaM and CCaMK as well as CaM dissociates from CCaMK (Swainsbury et al., 2012). Phosphorylation of both Ser343 and Ser344 inhibits further CaM binding (Liao et al., 2012; Routray et al., 2013) which constitutes the off-switch of CCaMK and another similarity to the mechanism of regulation of CaMKII (Section 1.3.5).

The different Ca^{2+} binding properties of CCaMK EF-hand motifs (Swainsbury et al., 2012) and the GOF activity of CCaMK EF-hand mutants (Miller et al., 2013) suggest that each of the EF-hand motifs of CCaMK play an essential role in regulating CCaMK activity during symbiosis. However, the factors that determine the behaviour of each EF-hand motif are not known.

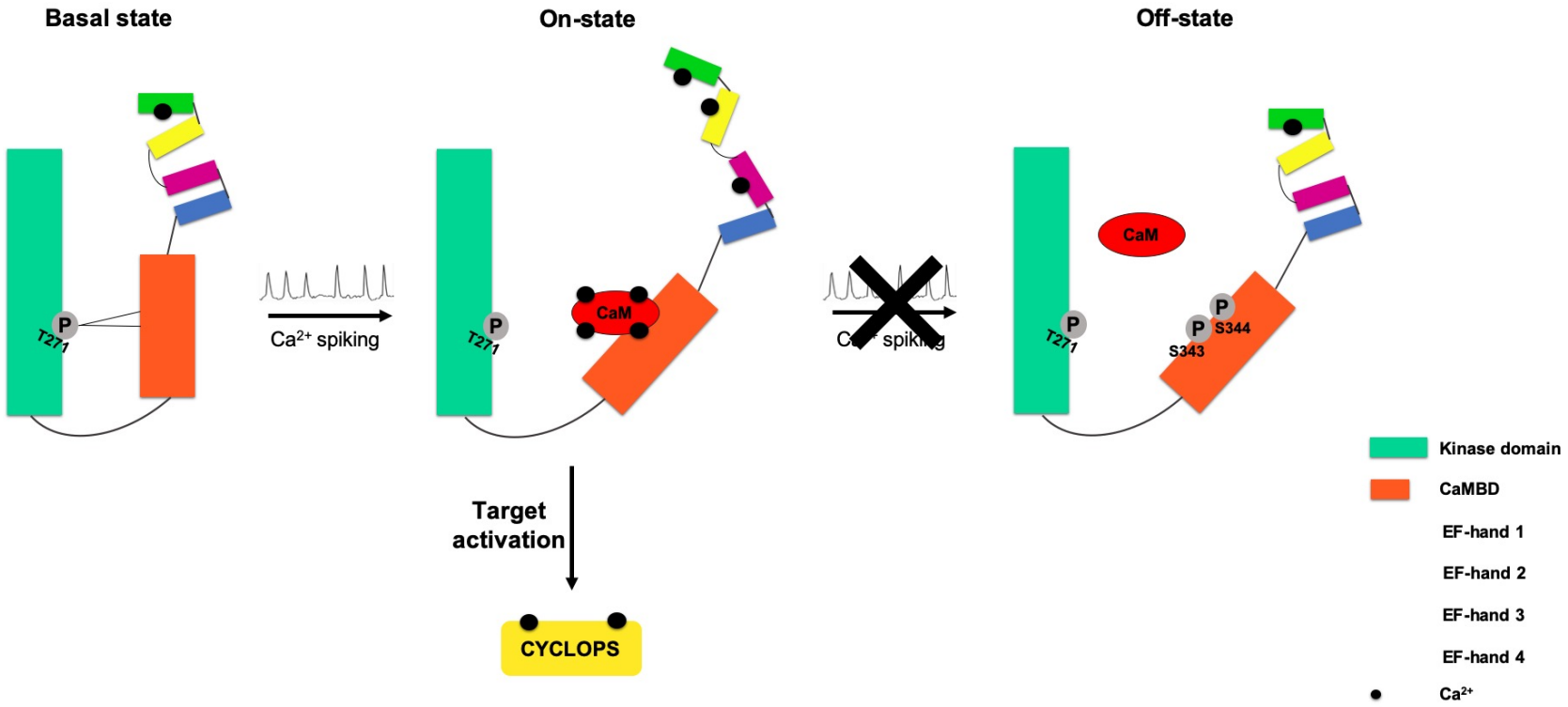

Figure 1. 11. Mechanism of activation of CCaMK during Ca^{2+} spiking decoding.

At basal [Ca^{2+}], CCaMK EF-hand 4 is very likely to be bound to Ca^{2+} due to its high affinity for Ca^{2+}, resulting in Thr271 autophosphorylation that allows formation of a hydrogen network between the kinase and CaMBD, rendering CCaMK inactive (Basal state). During the increasing [Ca^{2+}] phase of the Ca^{2+} spiking, CCaMK EF-hand motifs 2 and 3 also bind Ca^{2+} which induces a conformational change allowing the interaction of Ca^{2+}-bound CaM and releases the kinase domain from autoinhibition (On-state). CCaMK is then able to interact with and phosphorylate CYCLOPS for the decoding of Ca^{2+} spiking. During the down phase of the Ca^{2+} spiking ([Ca^{2+}] decreases), the EF-hand motifs 2 and 3 release the Ca^{2+} and CCaMK

autophosphorylates on Ser343 and Ser344 which blocks CaM binding (Off-state). Upon Ca^{2+} spiking termination, CCaMK returns to its basal state. The kinase domain is shaded in turquoise, the calmodulin binding domain (CaMBD) shaded in orange, EF-hands 1, 2, 3 and 4 shaded in blue, pink, yellow and green respectively. Phosphorylated residues are indicated by a P enclosed in a grey circle. Ca^{2+} ions are indicated by small black circles. CaM is shaded in red

6. Aims and objectives of this project

Ca^{2+} plays an important role in many eukaryotic signalling pathways as changes in Ca^{2+} concentration as well as specific Ca^{2+} signatures are associated with many physiological processes in both animal and plant systems. Plant symbiosis is a well-studied model of Ca^{2+} signalling, characterised by a nuclear calcium spiking developed after symbiont recognition. CCaMK is a calcium sensor considered the central regulator of the symbiotic signalling pathway due to its unique ability to discriminate between the basal Ca^{2+} concentrations and those during the nuclear Ca^{2+} spiking. In addition to symbiosis, there are many other plant and animal signalling pathways in which Ca^{2+} changes in concentration and calcium oscillations are present and that are decoded by different Ca^{2+} sensors. This decoding is carried out by the action of the EF-hand motifs present in the structure of the calcium relays and sensors. However, although the structure of the EF-hand motifs is well conserved, the binding of Ca^{2+} through each different EF-hand motif results in distinct responses from these calcium sensors. Therefore, we can infer that the EF-hand motif is responsible for this specificity in their response to the specific calcium signal originated by a particular stimulus. This raises the question of what it is exactly in the EF-hand motif that makes one particular Ca^{2+} sensor to respond to one specific signature and not to others.

The aim of this project was to study the Ca^{2+} binding properties of the EF-hand motifs using the model protein CCaMK during symbiosis in *Medicago truncatula*. The main approach was to alter the structure of the native EF-hand motifs of CCaMK by placing each CCaMK EF-hand loop in between each pair of EF-hand motif helices. This approach allowed the creation of new helix-loop-helix combinations within the CCaMK structural scaffold. These CCaMK mutants were then tested in planta for their ability to induce gene expression and allow nodulation (Chapter Three). If the primary sequence of the EF-hand motif was the main factor determining its Ca^{2+} binding capability, these mutants would show a different phenotype from WT-CCaMK. In contrast, if the tertiary structure of the EF-hand motif is the main factor responsible for Ca^{2+} binding ability, then no phenotype differences from CCaMK-WT would be observed. Since EF-hand 1 of CCaMK has no Ca^{2+} binding ability, a structural role for this EF-hand motif might be possible and would be confirmed with these mutants. In addition, these

mutants would have a different ability to bind Ca^{2+} that would likely impact on CCaMK autophosphoprylation and CaM-binding abilities (Chapter Four). Lastly, since Ca^{2+} signals of many different patterns (different amplitude, duration, frequency and spatial distribution) occur in nature and the EF-hand motif allows the Ca^{2+} sensor proteins to specifically respond to them, the ability of CCaMK to respond to a different Ca^{2+} signal than the symbiotic was interrogated. A detailed gene expression analysis was carried out to identified whether CCaMK had ability to respond to the Ca^{2+} signals during salt stress along with other genes of the symbiotic signalling pathway (Chapter Five).

CCaMK possesses four EF-hand motifs of different Ca^{2+} binding capability and this is important for its role as the central decoder of the Ca^{2+} spiking during symbiosis. However, the role played by each EF-hand motif within the activation mechanism of CCaMK and more specifically, what factors determine how each EF-hand motif functions, remains unclear. These experiments would help to answer these questions and ultimately, could lead to the possibility of designing novel hybrid calcium decoder proteins that are functional for the symbiotic signalling pathway or even for other signalling pathways.

Chapter Two - Materials and Methods

1. Bacterial strains

Escherichia coli strain DH5α (Invitrogen, catalogue number:18265017) was used for Golden Gate cloning (GGC) and propagation of level 0 and level 1 plasmids and *E. coli* DH10B (Invitrogen, catalogue number: 18297010) was used for level 2 plasmids. *E. coli* strains BL21 DE3 (New England Biolabs; NEB) and BL21 DE3-VR2-pACYC-LamP (Wernimont et al., 2010) were used for expression of pMaLc2x and GGC plasmids and purification of proteins. *Agrobacterium rhizogenes* strain AR1193 (Stougaard et al., 1987) was used for hairy root transformation of *Medicago truncatula*. *Agrobacterium tumefaciens* strain GV3101 (Larebeke et al., 1974) was used for transient expression of GGC plasmids in *Nicotiana benthamiana* leaves.

2. Media, buffers and antibiotics

The composition of bacterial and plant media is described in Table 2.1. All reagents were ordered from Sigma.

Table 2. 1. Composition of bacterial and plant growth media used in this thesis.

Medium	Recipe (1L)
Lysogeny broth (LB)	LB Broth Miller 25 g
LB Agar	LB Broth Miller with Agar 40g
Super opitmal broth (SOC)	SOC Broth 31.5 g
Distilled water agar (DWA)	Agar 15 g

Buffered nodulation medium (BNM)	MES buffer 390 mg, $CaSO_4(2H_2O)$ 344 mg, KH_2PO_4 0.125 g, $MgSO_4(7H2O)$ 122 mg, Na_2 EDTA 18.65 mg, $FeSO4(7H_2O)$ 13.9 mg, $ZnSO_4(7H_2O)$ 4.6 mg, H_3BO_3 3.1 mg, $MnSO_4(H_2O)$ 8.45 mg, $Na_2MoO_4(2H_2O)$ 0.25 mg, $CuSO_4(5H_2O)$ 0.016 mg, $CoCl_2(6H_2O)$ 0.025 mg, pH 6.0 For solid medium add: Agar 11.5 g
Modified FP	$CaCl_2(2H_2O)$ 0.1 g, $MgSO_4$ 0.12 g, $KHPO_4$ 0.01 g, $Na_2HPO_4(12H_2O)$ 0.150 g, ferric citrate 5 mg, H_3BO_3 2.86 g, $MnSO_4$ 2.03 g, $ZnSO_4(7H_2O)$ 0.22 g, $CuSO_4(5H_2O)$ 0.08 g, $H_2MoO_4(4H_2O)$ 0.08 g, NH_4NO_3 0.5 mM, Agar 8 g, pH 6.0

Appropriate antibiotics were 0.2 μm filter-sterilised and used for growth selections of *E. coli*, *A. rhizogenes* and *A. tumefaciens* (Table 2.2). The following antibiotics were ordered from Sigma.

Table 2. 2. Antibiotics used for bacterial selection in this thesis.

Antiobiotic	**Solvent**	**Final concentration in liquid culture (μg/ml)**	**Final concentration in solid culture (μg/ml)**
Ampicillin	dH_2O	100	100
Carbenicillin	dH_2O	50	50
Chloramphenicol	dH_2O	10	10
Gentamycin	dH_2O	40	40
Kanamycin	dH_2O	25	25
Rifampicin	DMSO	50	50
Spectinomycin	dH_2O	400	200

The composition of the buffers used for protein work is listed in Table 2.3. The following reagents were ordered from Sigma.

Table 2. 3. Composition of buffers used during protein studies.

Buffer	Recipe (1L)
SDS-PAGE Running Buffer	Tris 3.28 g, Glycine 14.42 g, 10% SDS 10 ml
LAEMMLI Buffer (Sample Buffer)	For 20 ml: 0.5M Tris pH 6.8 5ml, 10% SDS 0.8 ml, Glycerol 4ml, Bromphenol blue 0.004 g, 1M Dithiothreitol (DTT) 4ml, up to 20ml with dH_2O
SDS-PAGE Resolving gel	For 10%, 2 gels: 1.5M Tris pH 8.8 5 ml, dH_2O 7.9 ml, 10% SDS 0.2 ml, 30% Acrylamide/Bis solution 6.7 ml, Tetramethylethylenediamine (TEMED) 10 μl, 10% APS 200 μl
SDS-PAGE Stacking gel	For 5%, 2 gels: 0.5M Tris pH 6.8 1.5 ml, dH_2O 3.3 ml, 10% SDS 60 μl, 30% Acrylamide/Bis solution 1.005 ml, Tetramethylethylenediamine (TEMED) 6 μl, 10% APS 60 μl
Transfer Buffer	Tris 4.66 g, Glycine 2.34 g, 10% SDS 1 ml, Ethanol 200 ml, pH 9.2
Tris-Buffered Saline (TBS)	1M Tris-HCl 10 ml, 5M NaCl 30 ml, pH 7.5
TBS-Tween (TBST)	1M Tris-HCl 10 ml, 5M NaCl 30 ml, Tween20 1ml, pH 7.5
Blocking Buffer	For 20 ml: Tween20 20 μl, Bovine serum albumin (BSA) 1 g, up to 20 ml with TBS, pH 7.5

3. Construct generation

3.1. Generating the CCaMK truncations and point mutants

Truncations of CCaMK were generated in the GGC plasmids by polymerase chain reaction (PCR) using the Phusion high-fidelity DNA polymerase (Thermo Fisher). The PCR mix was prepared as follows: 4 μl of 5x HF Phusion Buffer, 1.6 μl of 2.5 mM dNTPs, 1 μl of 20 μM forward primer, 1 μl of 20 μM reverse primer, 0.5 μl of 20-100 ng/μl template DNA, 0.2 μl of Phusion high-fidelity DNA polymerase and dH_2O up to 20 μl. The PCR cycling conditions were as follows: 30 s at 98°C followed by 30 cycles of 10s at 98°C, 20 s at 53°C and 1 min per 1000 base pairs of DNA fragment at 72°C. After the 30 cycles, a last step of 5 min at 72°C was performed before cooling down to 10°C. The PCR products were separated by Tris-Acetate-EDTA gel electrophoresis (Section 3.5). The PCR products of the correct size were extracted and purified using the QIAquick gel extraction kit (Qiagen) according to the manufacturer's instructions. The purified DNA product was inserted into the GGC plasmid vectors following the instructions in section 3.2.

The generation of point mutations in CCaMK was performed by overlap extension PCR (Ho et al., 1989). Two sets of primers were designed for amplification from the 5' end to the point mutation and from the point mutation to the 3' end of the gene of interest and were used in Phusion PCR as described in the previous paragraph. After the desired DNA fragments required for overlap extension PCR were obtained by Phusion PCR, following the instructions described above, an overlap extension PCR reaction was performed overnight. The composition of the overlap PCR reaction mix consisted of the following: 8 μl of 5x HF Phusion Buffer, 3.2 μl of 2.5 mM dNTPs, 1 μl of 100 μM forward primer, 1 μl of 100 μM reverse primer, 5 μl of template DNA (2.5 μl of each PCR fragment), 0.3 μl of Phusion high-fidelity DNA polymerase and dH_2O up to 40 μl. The overlap PCR cycling conditions were as follows: 98°C for 30 s followed by 40 cycles of 98°C for 15 s, 45°C for 5 min and 72°C for 7 min. After the 40 cycles, a final step of 72°C was performed for 10 min followed by cooling down to 10°C. The PCR products were then run in an agarose gel electrophoresis as explained in section 3.5.

3.2. Golden Gate Cloning

Golden gate cloning (GGC) constitutes the method for genetic construct building used in this thesis (Weber et al., 2011). GGC is based on type IIS restriction enzymes that cleave outside the recognition site and allow the creation of compatible fusion sites flanking the DNA insert. The use of compatible fusion sites enables performing the restriction digestion and DNA ligation during the same reaction, which results in correct assembly of the DNA fragments after cleavage with the appropriate restriction enzymes. This cloning method comprises three levels of constructs:

- Level 0 modules are composed of a single genetic element, either a promoter, coding sequence or terminator. This genetic element is inserted into a vector based on the pUC19 backbone, which confers spectinomycin resistance (SpR). Level 0 modules contain BpiI and BsaI restriction sites positioned in an inverted orientation flanking a *LacZα* fragment that allows the blue/white selection of positively transformed bacteria. BsaI is the restriction enzyme used for cloning the insert from level 0 modules into a level 1 vector backbone.
- Level 1 modules contain an entire eukaryotic transcriptional unit formed by a promoter, coding sequence and terminator. Level 1 vectors confer ampicillin resistance and also contain a LacZα fragment flanked by BsaI and BpiI restriction sites, but in this case, BpiI is the restriction enzyme used for cloning the insert (transcriptional unit) from level 1 modules into a level 2 vector backbone.
- Level 2 modules are formed by a group of transcriptional units which are inserted in a level 2 destination vector. The level 2 vector contains a red colour selectable marker (CRed) responsible for canthaxanthin biosynthesis and a kanamycin resistance gene. The CRed marker is flanked by two BpiI sites positioned in an inverted orientation from each other. Building of the level 2 modules requires the level 1 modules containing the inserts and a level 1 module containing the appropriate end-linker. After building of the final level 2 modules through BpiI-based cloning, no type-IIS restriction sites are left, the backbone is “closed”, and no insertion of additional genes is possible. However, a different type of end-linker containing additional BsaI sites can be used in order to produce

a level 2-1 module which can be reopen for the insertion of additional genes.

3.3. Construct building and positive colony selection

The GGC restriction-ligation reactions were prepared by adding to one tube approximately 100 ng of DNA of each DNA component which consisted of either a PCR amplified product or plasmid, 10 U of the appropriate restriction enzymes (BpiI or BsaI) depending on whether level 0, 1 or 2 constructs were being built and 10 U of T4 DNA ligase in T4 ligase buffer with added bovine serum albumin (BSA) in a final reaction volume of 15 μl (see Table 2.4 for detailed composition of the GGC reactions). A list of all the level 2 constructs created in this thesis can be found in Appendix 1. The necessary level 0 and 1 constructs to make those level 2 constructs were also created by not included in Appendix 1.

Table 2. 3. Reaction mix components for construct building by GGC.

Component	Volume (μl)
1 mg/ml Bovine serum albumin (BSA)_	1.5
10x T4 ligase buffer (NEB)	1.5
400000 U/ml T4 Ligase enzyme	1
10 U/μl BpiI or BsaI	1
100 ng/μl Vector backbone (DNA plasmid)	1
DNA insert (PCR product or plasmid)	1
dH_2O	Up to 15 μl

The GGC reaction was incubated in a thermocycler for 25 cycles of 3 min at 37°C and 4 min at 16°C. After the 25 cycles, the reaction was incubated for 5 min at 50°C and 5 min at 80°C and then cooled down to 10°C. *E. coli* competent cells were transformed with 1 μl of GGC product as described in section 3.4.

3.4. Transformation of *E. coli* competent cells and colony PCR

After the GGC reaction, 1 μl of the reaction mix was added to 20 μl of chemically competent *E. coli* DH5α in the case of level 0 and level 1 constructs or *E. coli* DH10B in the case of level 2 constructs and incubated on ice for 20 min. The *E. coli* DH5α or DH10B cells were then transformed by heat shock at 42°C for 30 s. After the heat shock, cells were recovered on ice for 1 min and then 500 μl of SOC (Table 2.1) was added to the cells and incubated for 1 hour at 37°C with shaking at 300 rpm. The transformed *E. coli* cells were then plated on LB Agar plates (Table 2.1) with the appropriate antibiotic (Spectinomycin, Ampicillin or Kanamycin; Table 2.2), the gene expression inducer isopropyl β-D-1-thiogalactopyranoside (IPTG) at a final concentration of 100 μg/ml and X-gal (substrate for *LacZ* encoded β-galactosidase enzyme responsible for blue colour production) at a final concentration of 40 μg/ml. The plated cells were left to incubate overnight at 37°C. The positive colonies were selected by their white colour and tested by standard colony PCR.

The colony PCR reaction was set up by adding 5 μl of GoTaq® G2 Green Master mix (Promega), 1 μl each of the forward and reverse primers at a stock concentration of 20 μM, the bacterial colony and dH_2O up to 10 μl. The colony PCR reaction started with a 10 min incubation at 98 °C and followed by 30 cycles of 10 s at 98°C, 20 s at 52°C and depending on the size of the DNA fragment, 1 min per 1000 base pairs (bp). After the 30 cycles, there was an additional incubation step of 5 min at 72°C followed by a cooling down step to 10°C. The colony PCR products were then subjected to electrophoresis for visual confirmation of positively transformed bacterial colonies (Section 3.5). Single colonies containing the plasmid of interest were grown overnight in LB medium with the appropriate antibiotics at 37°C with shaking at 200 rpm. Cells were harvested by centrifugation at 4000 rpm for 2 min and the cell pellet was used for plasmid DNA isolation.

3.5. Agarose gel electrophoresis for DNA

The PCR products were loaded into wells of a 1% agarose gel (1 g of Agarose boiled in 100 ml of 1x Tris-acetate-EDTA, TAE) and the 1 kb Plus DNA ladder

(NEB) was used for fragment size identification. A potential of 100V was applied for 45 min and the agarose gel was incubated in a 0.5 μg/ml ethidium bromide bath for 10 min before the DNA was visualised by exposure to UV light at a wavelength of 365 nm.

3.6. Plasmid DNA isolation

Plasmid DNA was purified using the Wizard® Plus SV Minipreps DNA purification System (Promega) according to the manufacturer's instructions. The concentration of the purified plasmid DNA was measured using a NanoDrop (Thermo Scientific) and diluted to 100 ng/μl for convenience. Purified plasmid DNA was stored a -20°C.

3.7. Sanger sequencing

In order to identify correctly assembled clones and whether mutagenesis was successful, sequencing of plasmid DNA was performed by submission to Eurofins for analysis. The samples for sequencing were prepared by adding 8 μl of the 100 ng/μl DNA, 1 μl of a 20 μM gene specific primer and 8 μl of dH_2O (final volume of 17 μl). The sequencing results were visualised with the Ape Plasmid Editor (created by Wayne Davis) and were compared to the correct gene sequence through Basic Local Alignment Search Tool (BLAST) alignments.

4. Plant material, seed sterilisation and plant growth conditions

4.1. Plant material

Medicago truncatula ecotype Jemalong A17 (Barker et al., 1990) was used as wild type. The null mutants of *Medicago truncatula* A17 used in the experimental work of this thesis are summarised in Table 2.5.

Table 2. 4. Null mutants of *Medicago truncatula* Jemalong A17 used in this thesis.

Gene	Mutant allele	Reference
CCaMK	*dmi3-1*	Levy, 2004
IPD3	*ipd3-1*	Horváth et al., 2011
DMI1	*dmi1-1*	Ané et al., 2004
DMI2	*dmi2-1*	Limpens et al., 2005
NSP1	*nsp1-2*	Smit, 2005
NSP2	*nsp2-2*	Kalo, 2005
NFP	*nfp-1*	Arrighi et al., 2006
NIN	*nin-1*	Marsh et al., 2007

4.2. Seed sterilisation

M. truncatula seeds were scarified with sandpaper and surface-sterilised in a 10% sodium hypochlorite solution for 2-3 min followed by 5 washes with sterile dH_2O. The surface-sterilised seeds were then left to imbibe in sterile dH_2O for at least 2 hours, before being plated on DWA plates (Table 2.1). The plated seeds were placed at 4°C for at least 3 days for stratification. After stratification seeds were germinated overnight at room temperature for either transplantation into soil for gene expression experiments (Section 8), nodulation complementation tests (Section 6) and assessment of root growth in the presence of salt (Chapter Five), or onto different medium plates for spontaneous gene expression (Section 7) and root growth measurements in the presence of salt (Chapter Five).

4.3. Plant growth conditions

M. truncatula seedlings were grown on plates at 23°C (16 h photoperiod) or in soil in controlled environment growth rooms at 20°C light and 21°C darkness (16 h photoperiod).

For the assessment of nodulation (Section 6), seedlings were grown in a 1:1 mix of terragreen:sand. The seedlings were covered with transparent plastic lids during the immediate days after planting in soil and the lids were removed as the

plants developed, typically after 5-7 days. Plants were watered with BNM (a medium low in nitrogen).

The same growth conditions described in the previous paragraph were also employed for the assessment of root growth in the presence of different concentrations of NaCl (Chapter Five). However, seedlings were transplanted in multi-purpose compost (J. Arthur Bower's). Plantlets were watered with BNM for the first 5 days after transplantation followed by watering with BNM containing the appropriate [NaCl] for 14 days.

After overnight germination, *M. truncatula* seedlings were placed on BNM plates with different concentrations of salt (Table 2.6) for the assessment of root growth. It was important to transfer the seedlings from DWA to BNM plates under sterile conditions with sterile forceps without breaking the roots and to ensure that the root tips were placed in contact with the solid medium. The total volume of medium added to 245 x 245 mm squared plates (Table 2.6) was kept constant at 200 ml and each plate contained 14-16 seedlings. Plates were sealed with micropore tape and placed vertically in controlled environment growth cabinets or rooms (20°C light and 21°C darkness, 16 h photoperiod) for 8 days.

Table 2. 5. Composition of BNM plates with different concentrations of NaCl.

Final [NaCl] mM	BNM (ml)	dH_2O (ml)	5M NaCl (ml)
0	188	12	-
100	188	8	4
150	188	6	6
175	188	5	7
200	188	4	8
300	188	-	12

5. Plant transformation

5.1. Transformation of *Agrobacterium*

In order to prepare chemically competent cells of *Agrobacterium*, single colonies streaked from a glycerol were cultured in 10 ml of LB broth with the appropriate concentrations of rifampicin and carbenicillin (Table 2.2) and grown overnight at 28°C at 180 rpm. After overnight growth, 50 ml LB broth with appropriate antibiotics contained in a 250 ml flask was inoculated with 0.5 ml of the overnight culture and grown at 28°C with gentle shaking until an OD600 between 0.5 and 1 was reached. After measuring the OD600 with a spectrophotometer, the bacterial growth was interrupted by placing the culture on ice for 10 min. The bacterial cultures were then centrifuged at 3000 rpm for 5 min at 4°C in pre-chilled sterile 50 ml centrifuge tubes. The bacterial pellet was resuspended in 1 ml of ice cold 20 mM $CaCl_2$. These cells were now competent for DNA transformation. One μg of plasmid DNA was added to 100 μl of resuspended *Agrobacterium* cells and mixed by tapping. The tubes were frozen in liquid nitrogen and then thawed at 37°C for 5 min, followed by the addition of 500 μl of SOC and incubation at 28°C with shaking at 300 rpm for 2 hours. The transformed *Agrobacterium* cells were then plated on LB plates with the appropriate antibiotics for selection and incubated at 28°C for 2-3 days. Positive colonies were identified by colony PCR as described in Section 3.4.

5.2. Hairy root transformation of *Medicago truncatula*

The *A. rhizogenes* strain AR1193 was used for transformation of germinated *M. truncatula* seedlings as previously described (Boisson-Dernier, 2001). A single colony of positively transformed *A. rhizogenes* was cultured in 10 ml of LB with Rifampicin, Carbenicillin and Kanamycin (Table 2.2) and grown at 28°C at 180 rpm for 2 days. An aliquot of 1 ml of the *A. rhizogenes* grown culture was then spun down at 13000 rpm for 30 s and the pellet was resuspended in 200 μl of LB without antibiotics. The root tip (approximately 3 mm) of germinated *M. truncatula* seedlings was removed by cutting with a sterile scalpel. Subsequently, the plant was dipped into the resuspended *A. rhizogenes* culture and placed on to sterile Modified FP (ModFP; Table 2.1) 100 x 100 mM square plates sealed with micropore tape. The ModFP plates containing 6-8 transformed seedlings were

placed vertically in controlled environment growth cabinets at 23°C (16 h photoperiod) for three weeks. The plantlets were then screened for positive dsRED fluorescence as the transformed constructs contained the reporter gene encoding Red Fluorescent protein from *Discosoma sp*. Successfully transformed plants were harvested for spontaneous gene expression analysis (Section 7) or transferred to soil for nodulation complementation (Section 6).

5.3. *A. tumefaciens*-mediated transient transformation of *Nicotiana benthamiana* leaves

The *A. tumefaciens* strain GV3101 was used for transformation of 4-week old *N. benthamiana* leaves. N. benthamiana plants were grown in a controlled environment growth room 20°C light and 21°C darkness, 16 h photoperiod. A single colony of positively transformed *A. tumefaciens* was cultured in 10 ml of LB with Rifampicin, Gentamycin and Kanamycin (Table 2.2.) and grown overnight at 28°C with shaking at 180 rpm. The 10 ml *A. tumefaciens* culture was then centrifuged at 4000 rpm for 5 min and the bacterial pellet was resuspended in the appropriate amount of dH_2O to reach an OD600 of 0.3-0.4. Subsequently, the bacterial virulence inducer acetosyringone was added to a final concentration of 200 μM. The *A. tumefaciens* cells were left to incubate with acetosyringone for 2 hours at room temperature in the dark and were then infiltrated with a syringe in to 2-3 *N. benthamiana* leaves per construct. After 48 h, transformed material was harvested using a leaf punch and assessed for gene expression via histochemical staining (Section 7.1).

6. Nodulation complementation assays

Hairy root transformed *M. truncatula* plants (Section 4.3) were inoculated with *Sinorhizobium meliloti* strain 1021 (rhizobia) by dipping their roots in to a rhizobial culture of OD600 between 0.02 and 0.03 and then transferred to a 1:1 terragreen:sand mix in a controlled environment growth room at 20°C light and 21°C darkness (16 h photoperiod). Plants were watered with BNM for three weeks, after which the nodule number was assessed. Images of the nodules were taken using a stereoscope (Leica MZ16F, Leica DFC300 FX Digital Colour Camera).

7. Assessment of spontaneous gene expression ability of the CCaMK mutants

7.1. Histochemical staining

The histochemical technique termed as β-glucuronidase (GUS)-staining was employed for assessment of spontaneous expression of the nodulation marker *ENOD11* induced by the different CCaMK mutants. Hairy root transformed *M. truncatula* plants (Section 4.3) or *N. benthamiana* leaves with constructs containing both the *CCaMK* mutants and the *GUS* gene placed under the control of the *ENOD11* promoter (Section 3.) were harvested and in the case of *M. truncatula* plants, the shoots were removed. The transformed *M. truncatula* roots and the *N. benthamiana* leaf discs were submerged in 3 or 1 ml of GUS buffer, respectively, with added 5-Bromo-4-chloro-3-indolyl-ß-D-glucuronic acid (X-GlcA) dissolved in dimethylformamide (DMF) to a final concentration of 2.5 mM (Table 2.7) and gentle vacuum was applied until leaves were saturated. The plants were then left to incubate at 37°C overnight. The gene expression induction was visualised through the blue colour obtained. The stained plants were incubated with a A 70% ethanol solution overnight for removal of the chlorophyll, facilitating the visualisation of the staining.

Table 2. 6. Composition of the buffers used for GUS staining.

Solution	Composition
GUS buffer	0.5 M NaH_2PO_4 39 ml, 0.5 M Na_2HPO_4 61 ml, 0.5 M EDTA 0.8 ml, x100 Triton 0.4 ml, dH_2O up to 400 ml
X-GlcA	X-GlcA 0.032 g, DMF 125 μl

7.2. Fluorimetric GUS Assay (MUG assay)

M. truncatula hairy roots were excised and frozen in liquid nitrogen. Frozen tissue was homogenised with a pestle and mortar, resuspended in 500 μl of Passive Lysis Buffer (Table 2.8) and incubated on ice for at least 10 min followed

centrifugation at 4°C, 13000 rpm for 10 min. The supernatant was then transferred to a clean tube. An aliquot of 40 μl of sample was mixed with 100 μl of MUG Assay Buffer (Table 2.8) and 20 μl of the mixture was immediately added to 180 μl of Stop Buffer (Table 2.8) for the zero start point measurement of GUS activity. An aliquot of 20 μl of mixture was added to 180 μl of stop buffer after 30 min of incubation at 37°C for measurement. The assay was performed on 96-well black plates and samples were measured for GUS activity in a 2103 Envision™ Multilabel Plate Reader at 365 nm excitation and 465 nm emission.

Table 2. 7. Composition of the buffers used for the MUG assay.

Solution	Composition
Passive Lysis Buffer (20 ml)	Passive lysis buffer (Promega Dual-Luciferase Reporter Assay E1910) 4 ml, dH_2O 16 ml, cOmplete Mini EDTA-free protease inhibitor (Roche) 1 tablet
MUG Assay Buffer (2.94 ml)	0.5 M NaH_2PO_4 pH 7 2ml, 0.5 M EDTA 400 μl, 100% Triton 20 μl, 20% Sodium lauryl sarcosine 100 μl, β-mercaptoethanol 14 μl, MUG (4-methylumbelliferyl beta-D-glucuronide) 28 mg disolved in 280 μl of DMSO
Stop Buffer (20 ml)	Na_2CO_3 0.424 g in 20 ml of dH_2O

7.3. Dual-Luciferase reporter assay

M. truncatula root material was prepared following the protocol described in section 7.2 until the transfer of the supernatant to a clean tube. Measurement of *Firefly* and *Renilla* activities was performed using the Promega Dual-Luciferase Reporter Assay E1910 according to the manufacturer's instructions. Briefly, a volume of 20 μl of resuspended root material in Passive Lysis Buffer (PLB) was added to 100 μl of Luciferase Assay Reagent II (LAR II) in to wells of a 96-well

white plate and the *Firefly* luciferase activity was measured three times with a 2103 Envision™ Multilabel Plate Reader. After measurement of the *Firefly* activity, 100 μl of Stop & Glo® Reagent was added to the sample and the *Renilla* luciferase activity was measured using the default settings on the machine.

8. Gene expression analysis during salt stress in *Medicago truncatula*

8.1. RNA extraction and cDNA preparation

M. truncatula seedlings were grown for 8 days on BNM plates with different [NaCl] or treated with different [NaCl] in soil for 2 weeks (Section 4.3). The roots of these plants were harvested and ground in liquid nitrogen. Total RNA was extracted from this root material using the RNeasy® Plant Mini Kit (Qiagen) according to the manufacturer's instructions. The purified RNA was then treated with Turbo DNAse (Ambion) following the manufacturer's instructions. In order to test the absence of contaminating genomic DNA, a PCR reaction was performed with specific primers for the housekeeping gene *Elongation Factor-1α* (*EF1α*) (Table 2.10) using the GoTaq® G2 Green Master mix (Promega) as explained in section 3.4. The PCR cycling conditions were the following: 30 s at 98°C followed by 30 cycles of 10s at 98°C, 20 s at 53°C and 45 s at 72°C. Genomic DNA from A17 plants was used as a positive control. The absence of contaminating genomic DNA was confirmed by the lack of a band of 222 bp when the PCR product was run by Tris-Acetate-EDTA gel electrophoresis and visualised after staining in an ethidium bromide solution (Section 3.5).

The extracted RNA (RNA 1 μl + Blue loading dye (NEB) 1 μl + 4 μl dH_2O) was run by Tris-Acetate-EDTA gel electrophoresis and stained in ethidium bromide as described in section 3.5. The quality of the RNA extracted was confirmed by the presence of two bands corresponding to the 18S and 28S rRNA species. RNA was further quantified using a NanoDrop and a 1 μg total RNA was used for cDNA synthesis. The 1 μg of total RNA was mixed with 28 μl of RNase free water and added to 2.5 μl of 50 μM oligo(dT)17 to a final volume of 30.5 μl which was denatured at 65°C for 15 min followed by incubation on ice for a least 2 min. Then, 2.5 μl of 10 mM dNTPs, 5 μl of 0.1 M DTT, 10 μl of 5x strand buffer, 1 μl RNasin ribonuclease inhibitor (Promega) and 1 μl of Superscript™ II reverse

transcriptase (Invitrogen) were added to a final volume of 50 μl. This was incubated at 42°C for 1 h for the cDNA synthesis.

8.2. Reverse transcription polymerase chain reaction (RT-PCR)

The reverse transcription polymerase chain reaction (RT-PCR) was performed using a 1:15 (v/v) dilution of cDNA (in dH_2O) (Section 8.1), gene specific primers and the GoTaq® G2 Green Master mix (Promega). The reaction mix was prepared as shown in Table 2.9. The PCR cycling conditions were the following: 30 s at 98°C followed by 30 cycles of 10s at 98°C, 20 s at 53°C and 1 min at 72°C. After the 30 cycles, a last step of 5 min at 72°C was performed before cooling down to 10°C.The RT-PCR products were then run on an agarose gel electrophoresis and visualised as described in 3.5.

Table 2. 8. Preparation of the PCR reaction mix using cDNA as DNA template.

Component	Volume (μl)
GoTaq® G2 Green Master mix (Promega)	12
10 μM Forward primer	1
10 μM Reverse primer	1
1:15 cDNA	1
dH_2O	5

8.3. Quantitative real-time polymerase chain reaction (qRT-PCR)

Quantitative real-time polymerase chain reaction (qRT-PCR) was performed using an AriaMx Real-time PCR System G8830A (Agilent Technologies) and the accompanying software. The reactions were performed on 96-well plates with 5 μl of SYBR Green JumpStart Taq REadyMix without $MgCl_2$ (Sigma-Aldrich), 2.6 μl of 25 mM $MgCl_2$, 0.2 μl 10 nM gene-specific forward primer, 0.2 μl 10 nM gene-specific reverse primer and 2 μl of 1:15 (v/v) cDNA:dH_2O, with a final volume of 10 μl per well. The PCR cycling conditions were as follows: 95°C for 4 min followed by 40 cycles of 30 s at 94°C, 30 s at 55°C and 30 s at 72°C. The reading was performed at the 30 s 72°C step.

Table 2. 9. Primers used for qRT-PCR.

Gene	Forward primer	Reverse primer
EF1α	CTTTGCTTGGTGCTGTTTAGATGG	ATTCCAAAGGCGGCTGCATA
bZIP46	GGAATGGTTGGTTTGGCACC	CCTTTCCTCCCTCGCATACC
ABI5-7	CGGGAAGTAAAATGTCGCCG	TGACCTCGCAGCTGATTCTC
bZIP11	GAAAGCAATCGAACCGCGAA	AGTTCACACATTTGAGCCCTT
DMI1	TGGTGGTAGCATGGCTGAAG	ATGCCACCCGCACTAATTGA
DMI2	CCTGAGCGATTGGAGTTCGT	CTTGGACCCTCCAGCCAAAA
DMI3	GGCCTAGTGCTCTTGAGCTT	GCAGCTGCACGAAGTTTACG
IPD3	ACGAATGACAAGAAGCCGGT	TGTGCCCTTTTGGCTTGGTA
NSP2	CGACACACTTGCTGCTTTCC	TGTGGACCGTTGTTGTTGGA
NFP	GCCATGGATGTTGCAATCGG	AGAACCACCCCAAAAGCGAA
NIN	GCAATGTGGGGATTTAGAGATT	GGAAGATTGAGAGGGGAAGCTT

The efficiency of the primer pairs was tested and confirmed by the analysis of serial dilutions, 10^{-1}-10^{-5} ng/µl of each gene-specific PCR product. Each gene-specific PCR reaction was performed for three technical and biological replicates. The results of each PCR reaction were expressed as threshold cycle (CT) values. The CT values for each gene were averaged across the three technical replicates for each biological sample and the CT values for the housekeeping gene *EF1α* were used as a control. The primer efficiency of the PCR reaction was calculated by creating a standard curve with the CT values obtained from the serial dilutions where 100% efficiency was considered to be equivalent to the doubling of PCR product per cycle. The primer efficiency for each primer pair was used for the calculation of the fold induction of each gene. The fold induction of each biological replicate was calculated for NaCl-treated samples relative to untreated samples and the average fold induction was calculated form this.

9. Protein studies

9.1. Method 1 for expression and purification of CCaMK developed by Akira Miyahara

The *E. coli* BL21 DE3 cells were transformed with either the pL2V-CCaMK or pMaLc2x-CCaMK plasmids (Chapter Four) as described in Section 3.4. A single colony of freshly transformed *E. coli* BL21 DE3 cells was grown overnight in 50 ml of LB with kanamycin in the case of the pL2V-CCaMK and without kanamycin in the case of the pMaLc2x-CCaMK (Table 2.2) at 37°C with shaking (200 rpm). After the overnight incubation, 5 ml of the fully-grown culture of *E. coli* BL21 DE3 cells were added to 500 ml of LB with kanamycin and 2.5 ml of 20% glucose and cultured at 37°C with shaking (200 rpm). When an OD600 of 0.5-0.6 was reached, the cells were left at room temperature for 10 min, followed by the addition of the gene expression inducer isopropyl β-D-1-thiogalactopyranoside (IPTG) to a final concentration of 0.5 mM and left to incubate for 2 hours at 28°C and 180 rpm. After gene expression induction, the cells were centrifuged for 20 min at 4°C and 4000 rpm. The cell pellet was then resuspended in 25 ml of cold Lysis Buffer (Table 2.11) at 4°C and frozen overnight at -20°C. The resuspended cells were then thawed in cold water and lysed using a French Press Cell Disrupter (1500 psi; Thermo Electron Corporation). The insoluble material was removed by centrifugation of the lysed cells for 30 min at 4°C and 9000 rpm, and the supernatant was incubated with equilibrated Amylose resin (New England Biolabs E8021S) for 1 h in a shaker at 4°C. After three washes with 10 ml of Washing Buffer (Table 2.11), the protein-bound Amylose resin was transferred to a column and washed with 10 ml of Buffer 1 (Table 2.11) followed by the addition of 1 ml of Elution buffer (Table 2.11) and incubation for 5 min at 4°C. The eluate was then collected, and the concentration of protein was determined by Bradford assay using bovine serum albumin (BSA) as a standard and a spectrophotometer. Proteins were then diluted to 300-500 ng/μl with Buffer 1. Purity was assessed by SDS-PAGE and staining with Coomassie Brilliant Blue (Section). Protein aliquots of 50 μl were frozen in liquid nitrogen and stored at -80°C.

Table 2. 10. Composition of the buffers used during purification of CCaMK following Akira's protocol.

Buffer	Composition
Buffer 1	1M Tris-HCl pH 7.4 20 ml, NaCl 11.7g, dH_2O up to 1 L
Lysis Buffer	1M Tris-HCl pH 7.4 20 ml, NaCl 11.7g, 0.5 M EDTA 2 ml, 1M DTT 1 ml, dH_2O up to 1 L
Washing Buffer	1M Tris-HCl pH 7.4 20 ml, NaCl 11.7g, 0.5 M EDTA 2 ml, dH_2O up to 1 L
Elution Buffer	Maltose monohydrate 0.072 g, Buffer 1 20 ml, 0.45 μM filter sterilised

9.2. Method 2 for expression and purification of CCaMK

The *E. coli* BL21(DE3)-VR2-pACYC-LamP (Wernimont et al., 2010) cells were transformed with either the pL2V-CCaMK or pMaLc2x-CCaMK plasmids (Chapter Four) as described in section 3.4. A single colony of freshly transformed *E. coli* BL21(DE3)-VR2-pACYC-LamP cells was grown overnight in 50 ml of LB with or without kanamycin for the pL2V and pMaLc2x plasmids, respectively and Chloramphenicol (Table 2.2) at 37 °C with shaking (200 rpm). After overnight incubation, 5 ml of the fully-grown culture of *E. coli* BL21 DE3 cells were added to 500 ml of LB with kanamycin and 2.5 ml of 20% glucose and cultured at 37°C with shaking (200 rpm). When an OD600 of 0.5-0.6 was reached, the cells were left at room temperature for 10 min followed by the addition of the gene expression inducer isopropyl β-D-1-thiogalactopyranoside (IPTG) to a final concentration of 0.5 mM and left to incubate overnight at 18°C and 180 rpm. After gene expression induction, the cells were centrifuged for 20 min at 4 °C and 4000 rpm. The cell pellet was then resuspended at 4°C in 25 ml of cold Lysis Buffer (Table 2.11) with two tablets of cOmplete Mini EDTA-free protease inhibitor (Roche) added. The cells were then incubated with Lysozyme (Thermo Scientific Catalogue number 89833) added to a final concentration of 250 μg/ml for 20 min in a shaker (150 rpm) at room temperature and were then frozen in liquid nitrogen

(left for at least 3 min in the liquid nitrogen). The frozen resuspended cells were thawed in cold water and 50 U of Benzonase Nuclease (Sigma E1014) was added. Immediately after the addition of Benzonase nuclease, the cells were lysed using a French Press Cell Disrupter (Thermo Electron Corporation). The insoluble material was removed by centrifugation of the lysed cells for 30 min at 4 °C and 9000 rpm, and the supernatant was incubated with equilibrated Amylose resin (New England Biolabs E8021S) for 1 h on a rotator disk at 4°C. After three washes with 10 ml of Washing Buffer (Table 2.11), the protein-bound Amylose resin was transferred to a column and washed with 10 ml of Buffer 1 (Table 2.11) followed by the addition of 1 ml of Elution buffer (Table 2.11) and incubation for 5 min at 4°C. The eluate was then collected, and the concentration of protein was determined as described in Section 9.1. Proteins were frozen in liquid nitrogen and stored at -80°C.

Table 2. 11. Modified composition of the buffers used during purification of CCaMK.

Buffer	**Composition**
Buffer 1	1M Tris-HCl pH 7.4 20 ml, NaCl 11.7g, dH_2O up to 1 L
Lysis Buffer	1M Tris-HCl pH 7.4 20 ml, NaCl 11.7g, 0.5 M EDTA pH 8.0 10 ml, 0.5M EGTA pH 8.0 2 ml, 1M DTT 1 ml, dH_2O up to 1 L
Washing Buffer	1M Tris-HCl pH 7.4 20 ml, NaCl 11.7g, 0.5 M EDTA pH 8.0 10 ml, 0.5M EGTA pH 8.0 2 ml, dH_2O up to 1 L
Elution Buffer	Maltose monohydrate 0.072 g, Buffer 1 20 ml, 0.45 μM filter-sterilised

9.3. Sodium dodecyl sulfate polyacrylamide gel electrophoresis (SDS-PAGE)

SDS-PAGE gels at 10% (1.5 mm thickness, 15 wells) were used for separation of proteins and their composition can be found in Table 2.3. The samples were prepared by the addition of sample buffer (Table 2.3) and were heated for 5 min at 95°C before loading. Each well was loaded with 20 µl of sample and 5 µl of protein ladder was added to one well. The samples were run in Tris-Glycine SDS-PAGE Running Buffer (Table 2.3) for 1.5-2 h at 130 V. Gels were stained in Instant Blue protein stain (Expedeon) or used for western blotting (Sections 9.5 and 9.6).

9.4. Kinase assays

Kinase assays were performed for 30 min at 30°C in a total reaction volume of 20 µl, containing approximately 1-2 µg of protein with same amount of protein per reaction. The kinase assay reaction mixture for the negative control (without Ca^{2+}) was composed of 1x Kinase Buffer (recipe described below), 5 mM EGTA, 1 mM ATP, 1-2 µg of MBP-CCaMK, and super distilled water (SDW) up to 20 µl. For the Ca^{2+}-induced reaction mixtures, appropriate volumes of $CaCl_2$ were added depending on the final concentration of Ca^{2+} desired and the volume of SDW was adjusted to a total of 20 µl. The [Ca^{2+}] tested were 0.2, 0.4, 0.6, 2 and 10 mM. When the presence of calmodulin (CaM) was desired, bovine CaM was added to a final concentration of 0.5 µM and the volume of SDW was readjusted. As an additional negative control, a sample composed of SDW and MBP-CCaMK was also included and termed as “none”. The 10x Kinase Buffer was composed of 1 M HEPES-KOH pH 7.5, 1 M DTT and 200 mM of 99.995% $MgCl_2$*$6H_2O$ (Sigma-Aldrich Catalogue number 255777). After the kinase reaction, 7 µl of sample buffer was added to the 20 µl of kinase assay reaction mixture and boiled for 5 min at 95°C before subsequent SDS-PAGE (Section 9.3) and western blotting (Sections 9.5 and 9.6).

9.5. Detection of Ca^{2+}-induced Thr-autophosphorylation by western blotting using the Anti-Phosphothreonine-Horseradish Peroxidase conjugated antibody

The protein samples from the kinase assays were separated by SDS-PAGE and transferred to a polyvinylidene difluoride membrane (PVDF) previously activated with 99% ethanol for 15 min, washed with dH_2O for 5 min and incubated in 1x Transfer buffer (Table 2.3) for a further 15 min. The transfer of proteins from the SDS-PAGE gel to the PVDF membrane was performed for 1 h at 100 V at 4°C. The Anti-Phosphothreonine-Horseradish Peroxidase (α-PThr-HRP) conjugated primary antibody from Sigma-Aldrich (SAB5200088) was used for immunodetection of Ca^{2+}-induced autophosphorylation of CCaMK. A 1:500 (v/v) dilution of the α-PThr-HRP was used for immunodetection. A chemiluminescent signal was generated by Amersham ECL™ Prime Western Blotting Detection Reagent (GE Healthcare Life Sciences) according to the manufacturer's instructions and detected with a G:Box (Syngene).

The PVDF membrane was incubated in approximately 20 ml of PonceauS stain solution (Sigma-Aldrich) with agitation and de-stained with dH_2O for protein staining visualisation (as a loading control) with a G:Box (Syngene).

9.6. Detection of Ca^{2+}-induced Thr-autophosphorylation by western blotting using the pIMAGO reagent

The transfer of proteins run in a 10% SDS-PAGE gel to a PVDF membrane was performed as described in section 9.5. The detection of the Ca^{2+}-induced autophosphorylation levels of CCaMK was performed using the pIMAGO reagent (Expedeon), which has a high affinity for phosphate groups on any residue (Ser, Thr or Tyr). The pIMAGO reagent was used as previously described (Iliuk and Tao, 2015). A second PVDF membrane was included before the gel during the transfer step to decrease background signal, as suggested in the protocol, and each of the membrane washes were extended from 5 min to 10 min. The chemiluminescent signal generation and visualisation was performed as described in section 9.5.

Chapter Three - Assessing the effect of interchanging the native CCaMK EF-loops in nodulation

1. Introduction

Legumes can establish symbiosis with both nitrogen-fixing bacteria and arbuscular mycorrhizal fungi (AMF) species. Symbiosis signalling starts with an exchange of diffusible signals between the host plant and the microorganism that triggers nuclear Ca^{2+} oscillations. These calcium oscillations are called calcium spiking and are considered central in the common symbiosis signalling pathway (CSSP) (Ehrhardt et al., 1996; Oldroyd and Downie, 2006; Singh and Parniske, 2012). CCaMK is considered the central regulator of the symbiotic signalling pathway due to its unique ability to discriminate between basal Ca^{2+} concentrations and those during the nuclear Ca^{2+} spiking. This ability is conferred by CCaMK structure that consists of: a visinin-like domain (VLD) which contains four EF-hand motifs of different calcium binding capabilities, a calmodulin binding domain (CAMBD) that provides a second mode of regulation by calcium, and a kinase domain responsible for transmitting the signal downstream (Patil et al., 1995). CCaMK is positioned immediately downstream of the Ca^{2+} spiking with its interacting partner CYCLOPS and the NSP2-NSP1 transcription factor complex (Levy, 2004; Kalo, 2005; Smit, 2005; Heckmann et al., 2006; Yano et al., 2008). Both CCaMK-CYCLOPS and NSP2-NSP1 protein complexes are bridged by DELLA proteins to act in concert and regulate the expression of early genes of the CSSP (Jin et al., 2016). *NIN* constitutes one of these early genes (Schauser et al., 1999; Marsh et al., 2007; Madsen et al., 2010), whose expression is activated by CYCLOPS and NSP1 through direct binding to different regions of its promoter (Hirsch et al., 2009; Singh et al., 2014). Additionally, NSP1 also binds to the promoter of *ENOD11* (Hirsch et al., 2009), a widely recognised early marker gene of symbiosis (Chabaud et al., 2002; Charron et al., 2004; Journet, 2001; Kosuta et al., 2003). It has also been reported that CYCLOPS binds to the promoter and activates the expression of *RAM1* (Pimprikar et al., 2016) which forms a complex with NSP2 (Gobbato et al., 2012). RAM1 has been shown to have a role in early stages of AM symbiosis since it induces expression of *RAM2* that is involved in the formation of structures required for fungal invasion (Gobbato et al., 2013). In addition to RAM1, *MSBP1* is also considered an early

marker gene of AM symbiosis as its expression is rapidly induced upon Myc factor recognition and this induction is dependent on CCaMK (Kuhn et al., 2010; Sun et al., 2015a).

The aim of the CSSP is to induce the formation of specialised structures, nodules and arbuscules, where the symbiotic interaction occurs with rhizobial and AM species, respectively.

The essential role of CCaMK EF-hand motifs during symbiosis is demonstrated by gain-of-function (GOF) mutations of CCaMK. Deletion of either one or two EF-hand motifs, or both the entire VLD and CaMBD, 1-435, 1-477 and 1-311 respectively, result in deregulated mutants able to induce formation of nodules in the absence of rhizobia. These nodules are not able to accommodate rhizobia and the symbiotic interaction cannot be established (Gleason et al., 2006; Tirichine et al., 2007; Miller et al., 2013).

Substitution of the Aspartate in position 1 of the EF-hand loop for an Alanine (D to A) impairs calcium binding through the EF-hand motif in CCaMK (Swainsbury et al., 2012). When this mutation is made in either EF-hand 2, 3 or 4 of CCaMK, this results in an GOF variant able to induce spontaneous nodulation. Additionally, these mutants are also able to partially complement the *ccamk* mutant phenotype which means that these nodules can accommodate rhizobia, allowing symbiosis in reduced levels compared to WT (Shimoda et al., 2012; Miller et al., 2013). However, D to A mutation of two EF-hand motifs resulted in spontaneous nodule formation (Miller et al., 2013) but no rhizobial infection was allowed in all these mutants. The fact that the impairment of calcium binding to both EF-hands 2 and 3 allowed formation of fully mature nodules, but this was not the case for the other EF-hand double mutants (Shimoda et al., 2012), suggests that CCaMK EF-hand motifs have different roles within the protein. Additionally, the triple CCaMK EF-hand mutant did not induce mature nodule formation either (Shimoda et al., 2012), also demonstrating calcium sensing through CCaMK EF-hand motifs is an absolute requirement for symbiosis.

An additional proof of the importance of CCaMK EF-hand motifs during symbiosis can also be observed in GOF mutant T271A. It was previously shown that Thr271 autophosphorylation is calcium dependent (Sathyanarayanan et al., 2001) and keeps CCaMK inactive (Miller et al., 2013). However, Thr271 autophosphorylation also increases affinity for CaM and primes CCaMK for activation (Swainsbury et al., 2012). Mutation of Thr271 to Alanine removes the ability of CCaMK to be autophosphorylated at this site and results in formation of spontaneous nodules in the absence of rhizobia. Nonetheless, T271A mutant also allows formation of fully mature nodules at the same levels as WT (Shimoda et al., 2012; Miller et al., 2013). This shows the important role of calcium sensing through CCaMK EF-hands also during basal calcium concentrations for regulation of the protein's activity.

In order to better understand the link between the EF-hand motif primary sequence and CCaMK function, a synthetic biology approach was carried out. This approach consisted of placing each CCaMK EF-hand loop in between each possible pair of helices and in each EF-hand position within the CCaMK structure. Interchanging the native EF-loops of CCaMK was intended to modify the EF-hand motif's primary sequence with minimal effects on tertiary structure. As a result, a total of 23 CCaMK mutant variants, named CCaMK swaps, were created and tested for their abilities to allow nodulation and/or induce spontaneous gene expression in *Medicago truncatula*.

This chapter describes the experimental procedure followed in order to assess the effect of interchanging CCaMK EF-hand loops. Due to the high number of CCaMK mutants to test, it was first necessary to develop a fast plant transformation system for screening the different mutants. Additionally, *ENOD11* was selected as the symbiotic transcriptional marker for assessing the spontaneous gene induction capability of CCaMK mutants. A Dual-Luciferase reporter assay was developed to test whether the CCaMK swaps possess GOF activity through their ability to induce *ENOD11* gene expression in the absence of rhizobia. Furthermore, CCaMK swaps were tested in planta under native conditions in order to understand whether these mutants retain full, partial or have lost their capability to complement the *ccamk* mutant.

2. Results

2.1. Process for generation of CCaMK variants and construct building following the Golden Gate Cloning technique

Golden gate cloning (GGC) takes advantage of the ability of type IIS restriction enzymes to cleave outside the recognition site, creating compatible fusion sites that flank the DNA insert and allows the correct assembly of DNA fragments in a single reaction (see Chapter Two, Section 3.2; Weber et al., 2011). The cloning strategy followed in this thesis was based on the publication of Weber et al. (2011) and an example is summarised below to provide a better understanding of the executed procedure.

The CCaMK mutant variants including both CCaMK swaps as well as CCaMK EF-hand deletions and point mutants to be used as controls, were generated by standard overlap PCR and/or DNA synthesis (see Chapter Two, section 3). However, the *CCaMK* WT gene available in the lab was inserted in a plasmid vector suitable for traditional cloning rather than a GGC-compatible vector. Therefore, it was necessary to "transfer" the CCaMK gene variants into GGC-compatible vectors. This process required insertion of GGC compatible restriction sites flanking the CCaMK gene variants and the corresponding creation of suitable fusion sites for insertion in GGC-compatible vectors.

The aim of adding GGC restriction sites and create the fusion sites flanking *CCaMK* sequence was the insertion of the gene into the GGC level 0 vector, which can only contain a single genetic element. This then would allow the subsequent building of more complex constructs, of level 1 that include various genetic elements to form a single transcriptional unit, and level 2 comprised of various transcriptional units (see Chapter Two, section 3.2 for further detail into GGC vectors).

The first step of this process was the design of a suitable forward and a reverse PCR primer containing the appropriate recognition site for the type IIs enzyme to be used in the level 0 of the GGC reaction. Upon PCR amplification with these primers, *CCaMK* sequence would then be flanked with GGC restriction sites. However, the recognition site of the forward and reverse primers needed to be

designed in a manner that the two restriction sites, one upstream and one downstream of *CCaMK*, are positioned in reverse orientation from each other for the correct amplification of the gene sequence. Therefore, the sequence of the forward primer needed to be comprised of the following elements in the order shown:

1. Since the polymerase enzyme does not start to read from the first nucleotide of the sequence, at least three random nucleotides were added upstream of the restriction site. These nucleotides can be randomly assigned and starting either with G or C was thought beneficial to take advantage of the three hydrogen bonds that these nucleotides can form rather than the two that A or T form.
2. The three random nucleotides were followed by the restriction site sequence suitable for the type IIS restriction enzyme used in the corresponding level of GGC cloning. The restriction site sequence then was followed by two more randomly assigned nucleotides. This is because the type IIs enzymes cut two nucleotides away from their recognition site.
3. Following the two random nucleotides, a fusion site comprised of 4 nucleotides needed to be added, compatible with the fusion site of the suitable GGC destination vector.
4. Lastly, the primer sequence would contain the start codon followed by at least 6-10 nucleotides of the gene sequence of *CCaMK* starting from the 5' end.

The reverse primer consists of the same elements than the forward primer but the sequences must be reverse complement orientation as follows:

1. As for the forward primer, the reverse primer should start with at least three random nucleotides preferably G or C.
2. The recognition site should be in reverse orientation (3' – 5') for the polymerase enzyme to amplify towards the gene sequence instead of towards the plasmid vector that the gene is inserted in. In addition, the sequence should also be complementary to the 5' – 3' sequence of the suitable restriction site that is intended to be incorporated.
3. As for the forward primer, two random nucleotides should follow the reverse complement sequence of the restriction site and then followed by

a fusion site of choice according to the GGC level 0 destination vector to be used.

4. Lastly, the reverse complement sequence to 6-10 nucleotides of the *CCaMK* would follow the fusion site starting from the 3' end of the 5' – 3' gene.

Once the correctly designed primers are created following the above-mentioned process, a standard PCR is performed with this set of primers resulting in amplification of the *CCaMK* gene flanked by the appropriate type IIS restriction sites and the fusion sites that allow insertion into the corresponding level 0 GGC destination vector (Figure 3.1 panel A).

When the PCR amplification product was obtained, in this case the GGC compatible *CCaMK* gene, a GGC cloning reaction could then be performed. The type IIS restriction enzyme for which appropriate recognition sites were flanking the *CCaMK* gene, was added to the GGC reaction mix along with the compatible level 0 vector backbone for a reaction consisting of subsequent cycles of restriction digestion and DNA ligation (see Chapter Two, section 3 for further detail into the GGC reaction).

While in this case a genetic coding sequence (CDS), the *CCaMK* gene, was chosen as an example, the same process would follow for other genetic elements such as a promoter or a terminator. However, the level 0 destination vectors suitable for insertion of a promoter or a terminator are different from the CDS vector and therefore, the promoter or terminator vectors have their own different fusion sites. Therefore, when designing the forward and reverse primers, the corresponding fusion sites would have to be incorporated into their sequences accordingly if cloning of either a promoter or terminator is desired.

In order to create a transcriptional unit, at least a promoter, gene and terminator were needed. Once each of these elements are inserted into their corresponding level 0 destination vectors as explained above, a subsequent GGC cloning reaction, designated as of level 1, was performed in order to fuse them into one single construct. This is possible because the level 0 destination vector already contains the restriction sites of the corresponding type IIS restriction enzymes

suitable for level 1 GGC, flanking the genetic element. Therefore, it is important to highlight that primer design and PCR reaction was only required to insert each genetic element into appropriate level 0 vectors. The level 1 GGC reaction makes use of a different type IIS restriction enzyme from the one used in the level 0 reaction, making each level of cloning unique. Finally, the level 1 reaction results in a construct that contains an entire transcriptional unit made of at least a promoter, gene and terminator (Figure 3.1 panel B).

In order to create multigene constructs which were required for the experimental work on this thesis, level 2 GGC reactions were conducted in a similar manner as explained above for the level 1 construct building. The difference is that, in this case, multiple level 1 constructs were used in order to fuse several transcriptional units into a single plasmid vector, requiring a different type IIS restriction enzyme from the one used in the level 1 GGC reaction. One key aspect of the level 2 GGC reaction is that the multiple transcriptional units to be fused into one single construct are not assembled in a random order. Instead, the fusion site located downstream of the terminator sequence of one transcriptional unit must be compatible with the fusion site positioned upstream of the promoter sequence of the following transcriptional unit (Figure 3.1 panel C). Therefore, planning the genetic content as well as their order of the final level 2 constructs is recommended from the primer design step.

Lastly, the order of the transcriptional units to be fused into the level 2 constructs used in this thesis was an important aspect. The level 2 constructs were desired to be used for *Agrobacterium*-mediated plant transformation and it was known that *Agrobacterium* starts the DNA insertion into the plant genome from the right-border of the plasmid. Therefore, the position of each of the transcriptional units was carefully planned to ensure that key transcriptional units such as the *CCaMK* unit were inserted first into the plant genome.

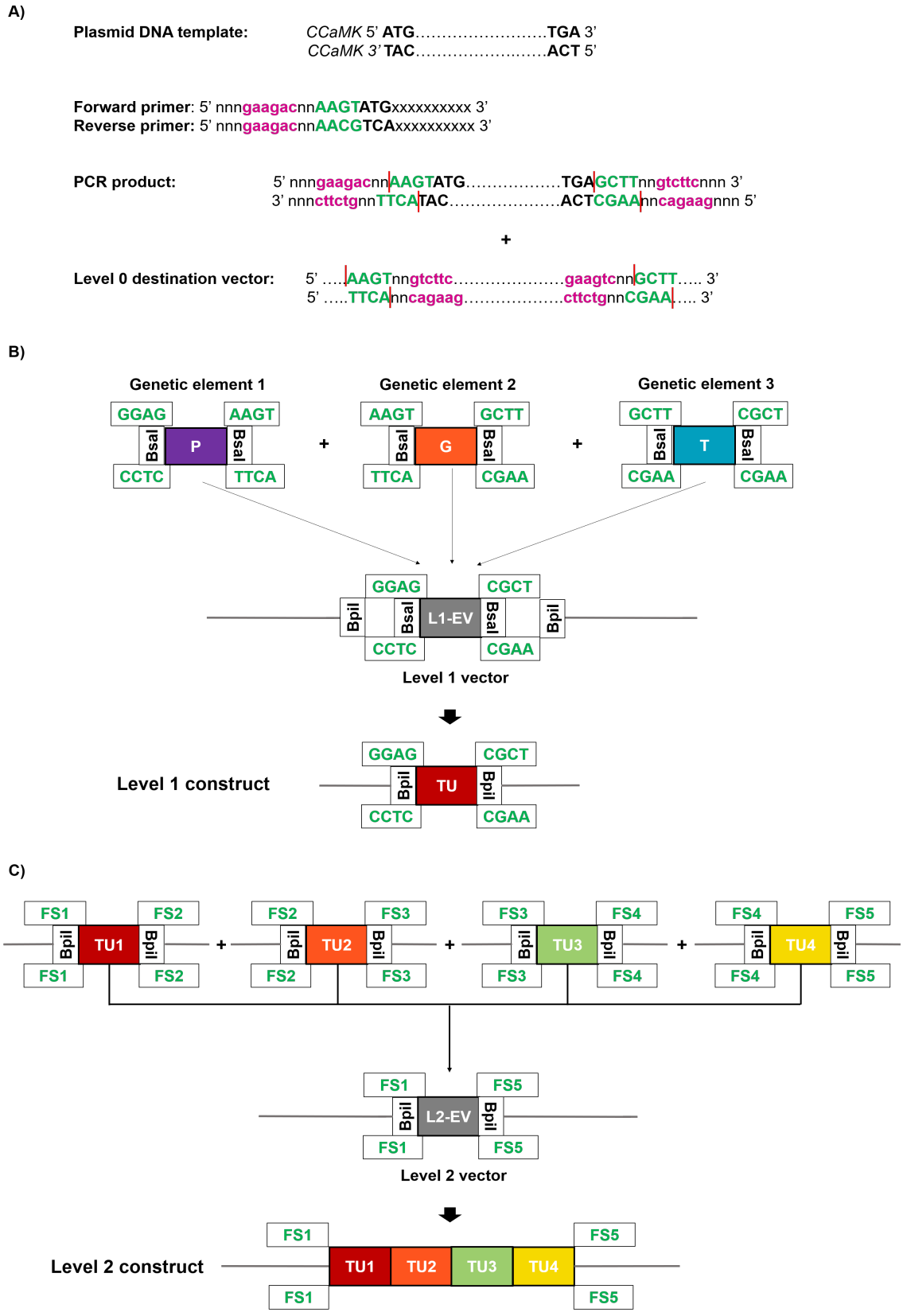

Figure 3. 1. Description of the procedure followed for GGC in this thesis.

Panel A) describes the PCR primer design process for insertion of type IIS restriction sites and a fusion site flanking the genetic element of interest. This facilitates the cloning

of the genetic element into the GGC-compatible level 0 vector of interest. The *CCaMK* gene has been chosen as an example to describe this process (see Chapter Three section 2.1 for further detail). The restriction site sequence is represented in pink font while the fusion site is represented in pink font. Panel B) describes the process of level 1 construct building based on the use of the restriction enzyme BsaI to fuse three genetic elements into one transcriptional unit. P, G and T denote promoter, gene and terminator, respectively. Panel C) describes the building of a multigene level 2 construct by fusing multiple transcriptional units. Fusion sites are represented in dark green font; BsaI and BpiI are two type IIS restriction enzymes widely used in GGC. TU denotes transcriptional unit; FS denotes fusion site. Different transcriptional units are represented in boxes of different colour. L1 and L2 denote level 1 and level 2 respectively. EV denotes empty vector to indicate that a genetic element is not yet present in the destination vector. Empty vectors are represented by grey boxes. This figure and the process described are based on the work of Weber et al. 2011.

2.2. Attempt of Fast Agro-mediated Seedling Transformation in *Medicago truncatula* seedlings

In order to test the high number of CCaMK control and EF-hand swap variants for their ability to induce nodulation or/and spontaneous nodulation in *Medicago truncatula*, a fast and efficient plant transformation method was required. To date, *Agrobacterium rhizogenes*-mediated hairy root transformation is the most widely used method of transient transformation in *Medicago truncatula (Boisson-Dernier, 2001)*. However, this method requires a three-week co-cultivation period and a faster method was desired. The development of Fast Agro-mediated Seedling Transformation (FAST) by Li et al. (2009) consisting of a transient transformation of *Arabidopsis thaliana* seedlings mediated by *Agrobacterium tumefaciens*, represented an interesting approach that would significantly shorten the transformation time and enable a faster obtaining of results. Therefore, different versions of the FAST method were attempted in *Medicago truncatula* seedlings to identify suitable conditions. In order to test the FAST transformation system, the β-glucorinidase (GUS) reporter gene system was used for the quick visualisation of plant transformation. Therefore, a construct containing the constitutive GUS reporter gene under the control of the constitutive *Arabidopsis thaliana* ubiquitin-10 promoter was built by GGC (Chapter Two, Section 3.3).

Plants successfully transformed with this construct would be visually identified by performing the histochemical GUS-staining technique. Two different strains of *Agrobacterium tumefaciens*, AGL1 and GV3101, were transformed with this construct followed by transformation of the *Medicago truncatula* seedlings. Moreover, different ages of the seedling, concentrations of the surfactant Silwett L-77, bacterial density of *Agrobacterium tumefaciens* cultures and co-cultivation periods of bacteria-seedlings were tested in *Medicago truncatula* (Table 3.1) as tested during the development of the FAST technique by Li et al. (2009). Although different combinations of the conditions presented in Table 3.1 were tested in order to identify the best conditions for *Medicago truncatula* seedlings, high efficiency of transformation could not be obtained as very low amounts of blue staining could be observed (Figure 3.1). Small patches of blue staining could be obtained under the condition combinations presented in Figure 3.2 in both shoots and roots, but these represented low efficiency of transformation. As a result, the high efficiency of transformation obtained for Li et al. (2009) in *Arabidopsis thaliana* seedlings could not be obtained for *Medicago truncatula*. Therefore, the FAST method was ruled out as an efficient transformation technique for *Medicago truncatula* seedlings, particularly since high levels of transformation efficiency were required for the screening of the CCaMK EF-hand swaps. As a result, *Agrobacterium rhizogenes*-mediated hairy root transformation was chosen for the CCaMK EF-hand swap screening (Boisson-Dernier, 2001).

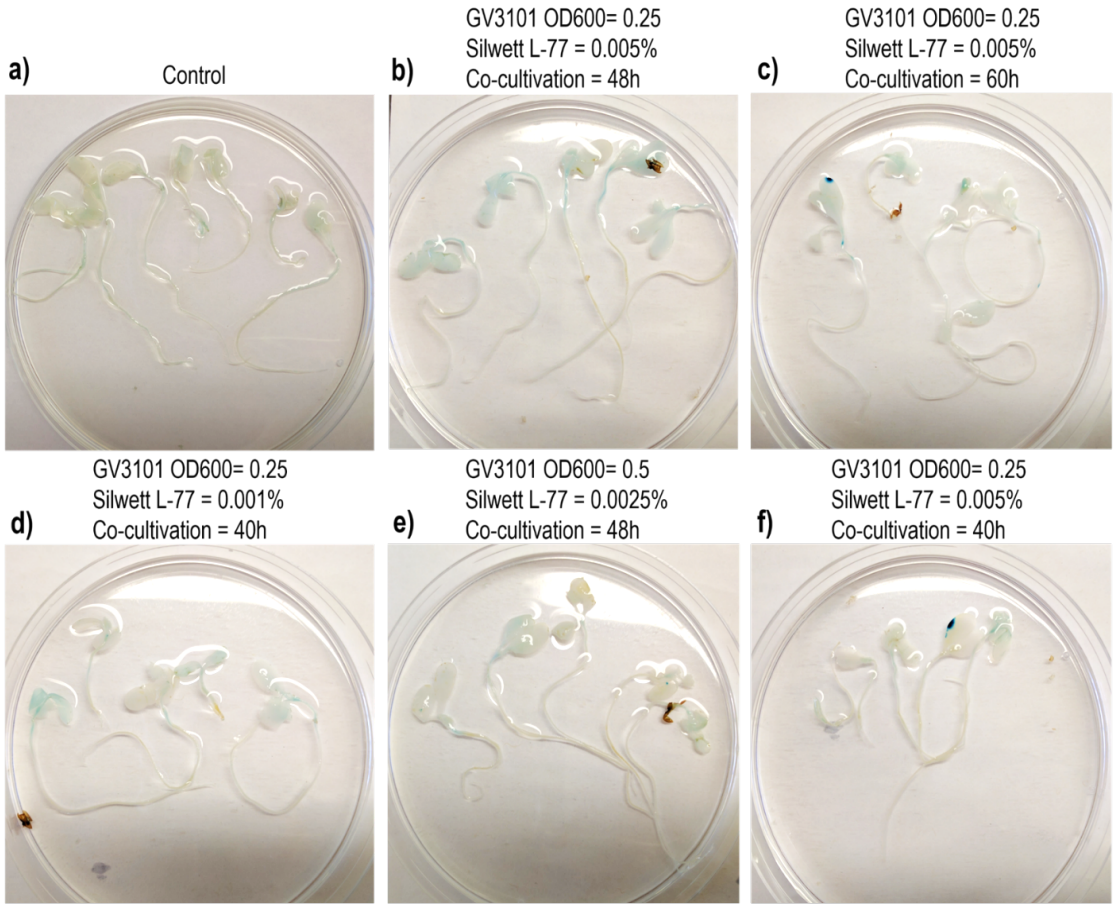

Figure 3. 2. Representative results obtained from the GUS-staining of Agrobacterium tumefaciens-mediated transformed Medicago truncatula seedlings.

Medicago truncatula seedlings were transformed following the FAST technique developed by Li et al. (2009) and GUS staining was performed subsequently. Plants were incubated overnight with 70% ethanol for chlorophyll removal. Different combinations of the conditions showed in Table 3.1 were tested. Only the conditions represented in this figure gave any levels of GUS staining. As a conclusion, the FAST technique was not suitable for the efficient transformation of *Medicago truncatula* under the conditions tested.

2.3. Selection of a symbiotic transcriptional marker for testing CCaMK mutants' gene induction ability

In order to assess whether the EF-hand swaps were able to induce spontaneous symbiotic gene expression (in the absence of the symbiotic stimulus), different transcriptional marker genes of symbiosis could be used. Gleason et al. (2006)

demonstrated that the gain-of-function 1-311, a kinase-only version of CCaMK, was sufficient to induce the expression of *ENOD11* and formation of spontaneous nodules in the absence of *Sinorrhizobium meliloti* in *Medicago truncatula.* Similarly, *CCaMK* was shown to be required for *NIN* expression in an *ENOD11* independent manner and *NIN* was also found essential during the auto-active 1-311 induced spontaneous nodule formation (Marsh et al., 2007; Schauser et al., 1999). However, in spite of *NIN* being known to be important during many stages of the nodulation process (Marsh et al., 2007; Schauser et al., 1999; Soyano et al., 2013; Vernié et al., 2015), *NIN* involvement in AM symbiosis (Guillotin et al., 2016) was still unclear at the time of these experiments and could only serve as a transcriptional marker of rhizobial symbiosis. On the contrary, *ENOD11* is a well stablished transcriptional marker for both rhizobial and AM symbioses (Chabaud et al., 2002; Charron et al., 2004; Journet, 2001; Kosuta et al., 2003) and therefore, a suitable candidate for testing CCaMK swaps' ability to induce both rhizobial and AM symbiotic signalling pathways. Despite having a potential transcriptional marker candidate suitable for both symbioses, an AM symbiosis specific transcriptional marker was also desired. RAM1 is a GRAS-type transcriptional factor shown to be specifically involved in AM signalling pathway, with no apparent role in Nod factor signalling, and whose expression is also dependent on CCaMK (Pimprikar et al., 2016). Alternatively, AM fungal signals released from branched hyphae have been shown to early induce the expression of *MSBP1* in *Medicago truncatula* (Kuhn et al., 2010), also dependent on *CCaMK* (Sun et al., 2015a).

In order to select which symbiotic marker gene to use for the EF-hand swap screening, an experiment was designed based on the β-glucuronidase (GUS) reporter gene system. The GUS reporter gene system allows the visualisation of the activity of a certain promoter in terms of the expression of the gene under that promoter through histochemical staining. Therefore, a series of constructs were built containing the β-glucuronidase encoding GUS reporter gene under the control of either *NIN*, *ENOD11*, *RAM1* and *MSBP1* promoters along with either *CCaMK-WT* or gain-of-function *CCaMK-T271A* variants for hairy root transformation of *Medicago truncatula dmi3-1* seedlings (Figure 3.3).

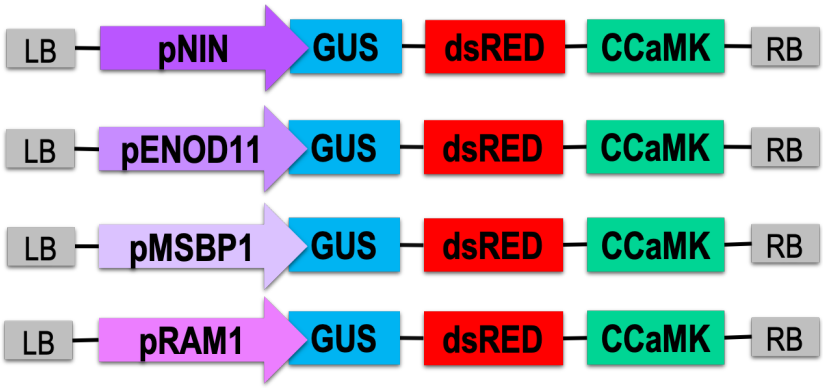

Figure 3. 3. Schematic representation of insert composition of genetic constructs used in the selection of symbiotic transcriptional markers via GUS staining of hairy-root transformed *Medicago truncatula* roots.

All constructs contained *dsRED* for positively transformed plant selection, CCaMK (different variants tested) and *GUS* gene under the control of the promoters of either *NIN, ENOD11, MSBP1* and *RAM1* which were the transcriptional marker candidates. In order to ensure its integration within the plant genome, *CCaMK* was placed at the right border (RB) as T-DNA insertion starts at this border and ends at the left border (LB).

In addition, dsRED was shown to be a suitable plant gene expression reporter (Jach et al., 2001) and was also included in these constructs as a plant selection marker to ensure only positively transformed plants were selected for further study. Therefore, positively transformed plants were selected through screening for dsRED fluorescence for GUS-staining on the roots of these plants in the absence of rhizobia or Nod factor. As previously shown (Gleason et al., 2006), reporter gene induction should only result in blue staining of the roots in the presence of Nod factor, rhizobia or GOF CCaMK variants (i.e. the auto-active T271A does not require the symbiotic stimulus for symbiotic gene induction). Therefore, it would be expected that CCaMK WT is unable to induce expression of either *NIN, ENOD11, MSBP1* or *RAM1* in these roots when in the absence of rhizobia or AM, and no blue staining should be obtained. Conversely, it was expected that CCaMK T271A, which is an auto active variant, would be able to induce the expression of these genes in the absence of rhizobia that would result in blue staining of the roots. Surprisingly, the results obtained from the GUS-staining showed that both CCaMK WT and T271A was able to induce the

expression of *NIN*, *ENOD11* and *MSBP1* as most of the plants showed blue roots, with no visual differences in the intensity of the staining or the number of plants stained (Figure 3.4). However, *RAM1* was not induced by either CCaMK WT or T271A as no blue staining of the roots was observed in any of the transformed plants (Figure 3.4). It has previously been observed by Tirichine et al. (2007) that particular CCaMK allelic mutant versions, such as *ccamk-1* in *Lotus japonicus*, show certain levels of leakiness. This leakiness can be observed in the *L. japonicus ccamk-1* loss-of-function mutant which contains a 299 bp duplication and is considered to have a non-nodulating phenotype, despite retaining certain ability to nodulate (Tirichine et al., 2006). Similarly, the *M. truncatula dmi3-1* (*ccamk-1*) might also have a certain degree of leakiness that results in enough induction of *NIN, ENOD11* and *MSBP1* to allow staining of the roots in the absence of rhizobia, although this has never been reported before. However, it is also possible that same levels of transient gene expression induction by WT and T271A CCaMK variants cannot be assumed from these results. It was expected that no induction would correspond to the lack of staining while gene induction would correspond to blue staining, but this was not the case (Figure 3.4). In contrast, it is possible that different shades of blue were obtained corresponding to different levels of gene expression and that, gene induction differences were obtained for CCaMK WT and T271A (Figure 3.4). However, these differences cannot visually be discriminated or quantified and as a result, this technique was concluded to be unsuitable for the desired purpose.

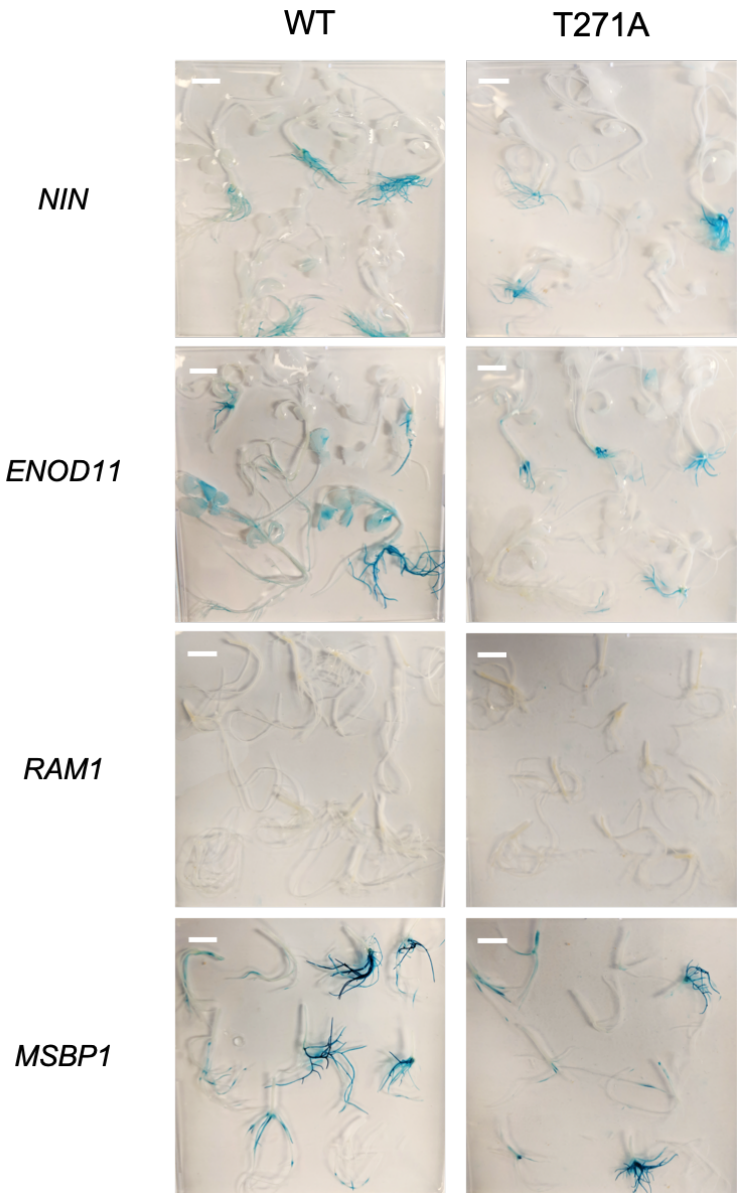

Figure 3. 4. GUS staining of hairy roots for assessment of spontaneous gene expression induction by WT and T271A CCaMK variants in Medicago truncatula.

NIN, ENOD11 and *RAM1* gene expression levels were induced by both CCaMK WT and T271A as visually detectable by the blue staining of the roots. In contrast, *RAM1* expression was not induced by either CCaMK WT or T271A as no blue staining was observed from transformed roots. Blue staining of the leaves was also obtained in some plants such as in the case of the plants transformed with construct containing pENOD11-GUS, but leaves were removed for ease of viewing and as this was not the tissue of interest.

An alternative to the histochemical GUS-staining technique for visualization of transient gene expression in the plant root tissue is the quantitative fluorometric GUS assay (MUG assay) (Jefferson et al., 1987). However, apart from quantification of the transcriptional activity of the four gene candidates mentioned above, quantification of plant transformation levels was also required for minimisation of experimental variability and normalisation of the differences in expression levels potentially caused by transformation efficiency and insert copy number variabilities. Bioluminescence assays based on luciferase enzymes have been wildly used in higher plants for reporting of gene expression (Millar et al., 1992; Luehrsen et al., 1992; Ow et al., 1986), including the use of a second luciferase enzyme for experimental normalisation (Sherf et al., 1996). The combination of the MUG assay with the Dual-Luciferase reporter assay seemed the best option in order to meet the need for quantification of plant transformation levels and assess transient expression levels of genes specific to two symbiotic signalling pathways. In addition to CCaMK WT and T271A variants, the GOF CCaMK 1-311 truncation (Chapter One, Section 5.2) and the kinase-dead CCaMK K47E (Carrera et al., 1993) were also included in this experiment. Therefore, genetic constructs were built that contained GUS under the control of a constitutive promoter, *Firefly* and *Renilla* luciferase genes driven by symbiotic gene promoters and different variants of CCaMK for hairy root transformation (Figure 3.5). The results obtained showed that the GOF CCaMK 1-311 variant was able to induce the expression of *ENOD11* and *RAM1* to statistically significant levels compared to CCaMK WT (Figure 3.6). However, although the expression levels of *NIN* were more highly induced by CCaMK 1-311 than by CCaMK WT, this induction was not statistically significant. In contrast, the CCaMK 1-311 caused the levels of expression of *MSBP1* to be statistically significantly lower than those induced by CCaMK WT. In contrast to CCaMK 1-311, the CCaMK T271A which also possesses GOF activity, was able to induce the expression of all *NIN*, *ENOD11*, *RAM1* and *MSBP1* to statistically significant levels (except for *NIN*) compared to CCaMK WT (Figure 3.6). Lastly, the kinase-dead CCaMK K47E was not able to induce the expression of either *NIN, ENOD11, RAM1* or *MSBP1* to statistically significant higher levels than CCaMK WT. Following these results, since *ENOD11* is considered a marker gene for rhizobial and AM symbioses and was also highly induced by CCaMK GOFs in

the MUG-Dual Luciferase assay (Figure 3.6), EF-hand swaps were decided to be tested for their ability to induce spontaneous *ENOD11* expression.

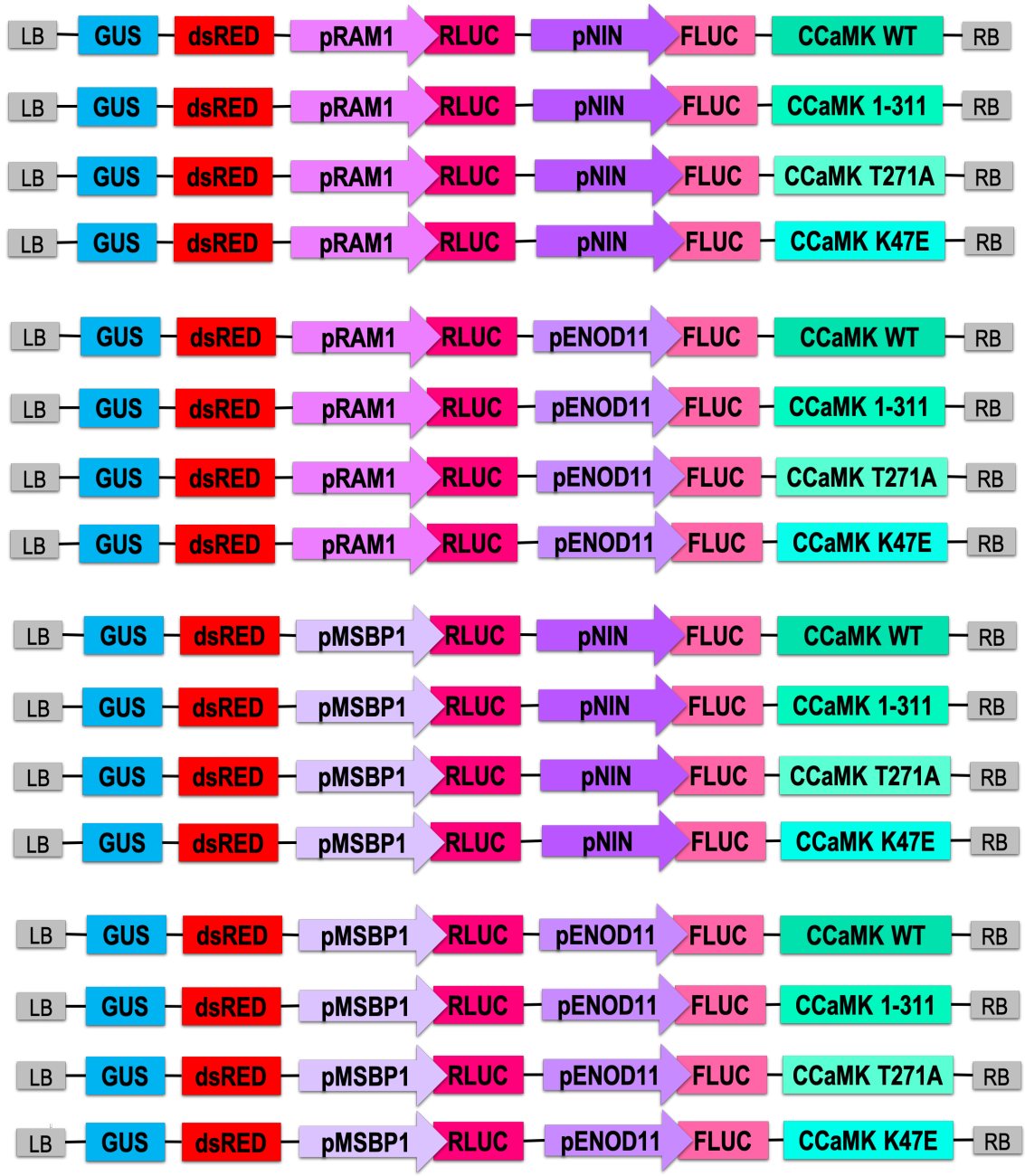

Figure 3. 5. Schematic representation of insert composition of genetic constructs used in the MUG-Dual Luciferase assay performed from hairy root transformed *Medicago truncatula* roots.

All constructs contained: *GUS* for quantification of plant transformation levels which allow minimisation of experimental variability and normalisation of the differences in expression levels; *dsRED* for positively transformed plant selection; *Renilla* luciferase gene under the control of *MSBP1* and *RAM1* promoters desired to be tested for their potential use as AM-symbiosis transcriptional markers; *Luciferase* gene under the

control of *NIN* and *ENOD11* promoters desired to be tested for their potential use as rhizobial-symbiosis transcriptional markers; and *CCaMK* (different variants tested). In order to ensure its integration within the plant genome, *CCaMK* was placed at the right border (RB) as T-DNA insertion starts at this border and ends at the left border (LB).

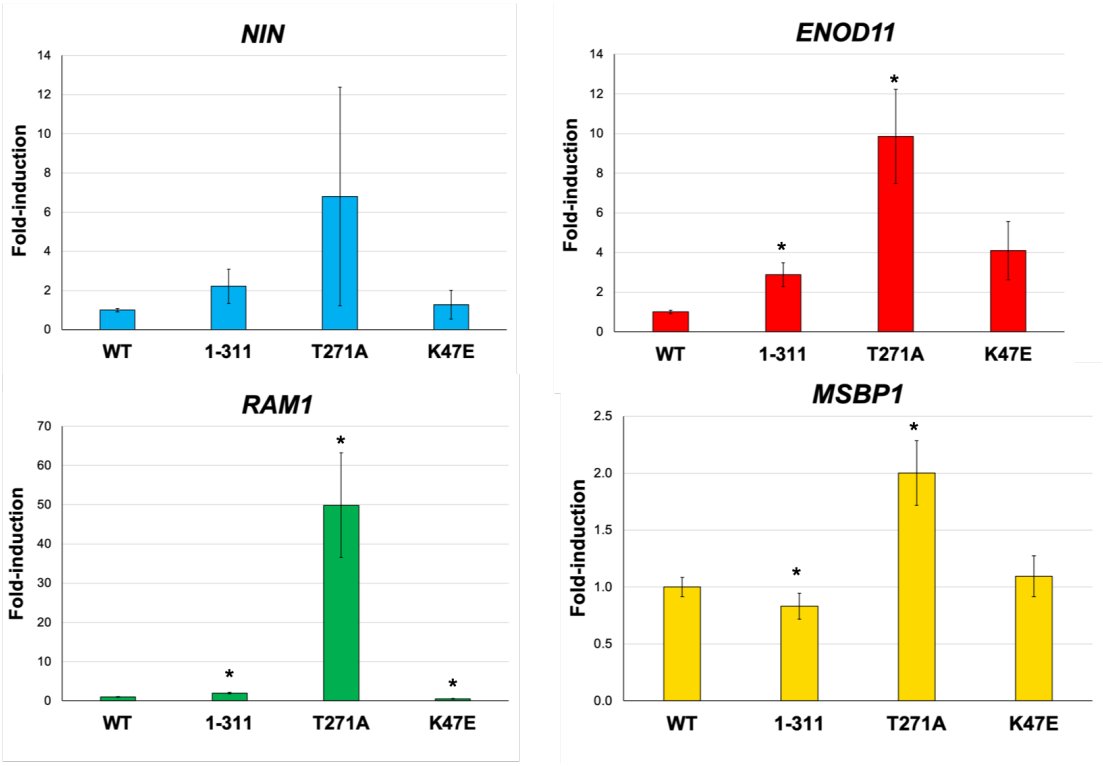

Figure 3. 6. Fold change of relative expression of symbiotic transcriptional markers by CCaMK mutants compared to WT assessed by MUG-Dual Luciferase assay.

NIN gene expression was not spontaneously induced by either CCaMK WT, 1-311, T271A or K47E. Both *ENOD11* and *RAM1* gene expression levels were induced 1-311 and T271A but not by CCaMK WT. CCaMK K47E (kinase-dead) induced the expression of *RAM1* but not *ENOD11. MSBP1* gene expression levels were induced by CCaMK T271A, reduced by CCaMK 1-311 and not changed by either CCaMK WT or K47E. Asterisk denote statistically significant increase or decrease of gene expression levels by either CCaMK 1-311, T271A or K47E compared to CCaMK WT gene expression induction levels in a pairwaise two-tailed test ($p<0.05$). Bars represent average

expression of three biological replicates (each with three technical replicates) with each biological replicate comprising roots from 3-6 plants. Error bars represent S.E.

2.4. Testing CCaMK swaps' ability to induce spontaneous *ENOD11* expression

The Dual-Luciferase reporter assay was developed to provide higher sensitivity than other reporter assays such as the chloramphenicol acetyltransferase (CAT) or GUS assays (Matsuo et al., 2001; Sherf et al., 1996; Töpfer et al., 1988). Therefore, this assay was the chosen method to assess whether CCaMK swaps are auto-active variants that activate the symbiotic signalling pathway in the absence of symbiotic stimuli. A series of new genetic constructs were built containing two different luciferase genes and *CCaMK* mutants (Figure 3.7) for hairy root transformation of *Medicago truncatula* seedlings under sterile conditions.

Figure 3. 7. Schematic representation of insert composition of the constructs used in the Dual-Luciferase assay performed from hairy root transformed *Medicago truncatula* roots.

All constructs contained: *dsRED* for positively transformed plant selection; Renilla luciferase gene under the control of p35S constitutive promoter; Luciferase gene under the control of *ENOD11* promoter used as a rhizobial-symbiosis transcriptional marker; and CCaMK (different variants tested). In order to ensure its integration within the plant genome, CCaMK was placed at the right border as T-DNA insertion starts at this border.

While gene order within the DNA construct has been shown to have no effect on gene expression levels, it is known that *Agrobacterium* T-DNA insertion starts at the right border (Aydın Akbudak and Srivastava, 2017). Therefore, CCaMK mutants were placed at the right border to ensure their integration into the genome. CCaMK was followed by two luciferase gene reporters, *Firefly* luciferase gene under the control of *ENOD11* promoter and *Renilla* luciferase gene under

the control of the constitutive p35S promoter for experimental normalisation. The fact that both reporter genes were placed in the same genetic construct allowed their insertion in the same region of the plant's genome and minimised gene expression variability due to genetic location, producing more reliable results. Lastly, *dsRED* was also included in these constructs for positively transformed plant selection (Figure 3.7).

Since *ENOD11* expression is induced at very early stages of symbiosis and CCaMK autoactive variants are responsible for spontaneous nodule formation, spontaneous *ENOD11* expression could be used as a proxy for spontaneous nodulation. Consequently, a wide range of CCaMK mutant variants with different symbiotic capabilities were chosen as controls for the CCaMK swap screening. T271A was included as a control due to its ability to fully complement ccamk mutant but also induce spontaneous nodulation in the absence of rhizobia. The single, double and triple EF-hand CCaMK point mutants (Figure 3.9) were also included for their spontaneous nodulation ability but reduced ability or total inability to accommodate rhizobia (Shimoda et al., 2012; Miller et al., 2013). Since their different phenotypes are due to different degrees of calcium binding ability, these EF-hand point mutants would be ideal for comparison against the CCaMK swap resulting phenotypes. In addition, truncated versions of CCaMK, 1-311, 1-435 and 1-477, were also included as they were previously shown to not fully complement *ccamk* but induce spontaneous nodulation (Miller et al., 2013). Assessment of the role of EF-hand 1 was also desired as it constitutes a non-Ca^{2+} binding site (Swainsbury et al., 2012) and its function remains yet unclear. The removal of the entire VLD in 1-346 resulted in no complementation of *ccamk* and no spontaneous nodulation in the absence of rhizobia (Miller et al., 2013). However, the removal of EF-hands 3 and 4 but the retaining of EF-hand 2, which corresponds to CCaMK 1-435, results in spontaneous gene expression and spontaneous nodulation in the absence of rhizobia (Miller et al., 2013). Since EF-hand 1 does not bind Ca^{2+} due to mutation of two essential residues for Ca^{2+} binding, the removal of EF-hands 2, 3 and 4 from CCaMK structure but keeping only the non-Ca^{2+} binding EF hand 1, would result in a mutant predicted to have a similar phenotype as 1-346. Therefore, the new truncated version CCaMK 1-402 was created which has the EF-hands 2, 3 and 4 removed. In addition, a putative biotin binding domain has previously been predicted in the exiting helix

of EF-hand 1 (Patil et al., 1995). In order to study whether this region has a role during CCaMK activation, the 1-391 truncation was also created lacking EF-hands 2, 3 and 4 and the exiting helix of EF-hand 1 but retaining the EF-hand 1 loop and incoming helix. 1-346 which showed no nodule formation or *ccamk* complementation, and the 1-402 and 1-391 variants which were expected to have a similar phenotype to 1-346, were included as negative controls as all three mutants lack calcium-binding EF-hand motifs but preserve the CaMB and kinase domains. As an additional negative control, the kinase-dead mutant K47E was also included (Carrera et al., 1993).

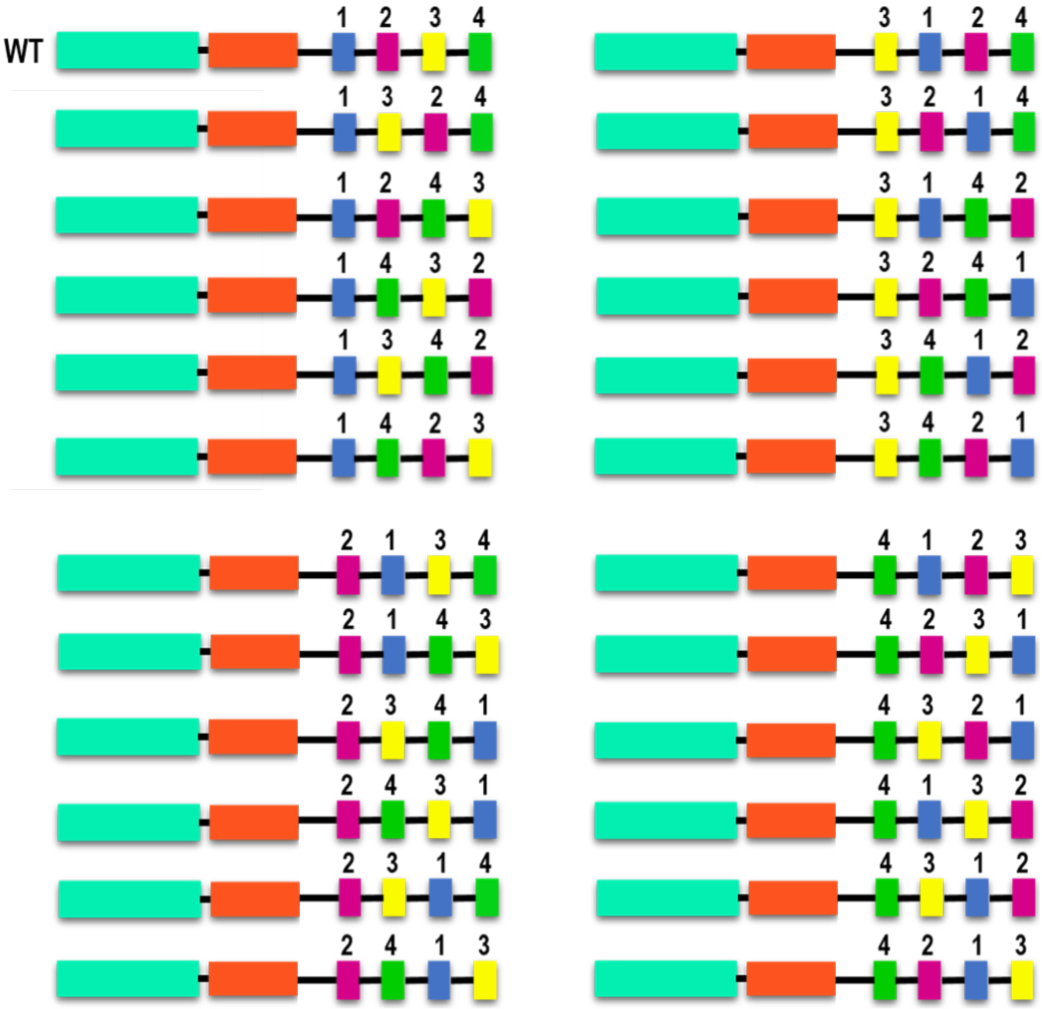

Figure 3. 8. Schematic representation of the 24 different CCaMK EF-hand swaps.

The kinase domain is presented in turquoise, CaMBD in orange, EF-hand 1 in blue, EF-hand 2 in pink, EF-hand 3 in yellow, EF-hand 4 in green. CCaMK WT is indicated as WT.

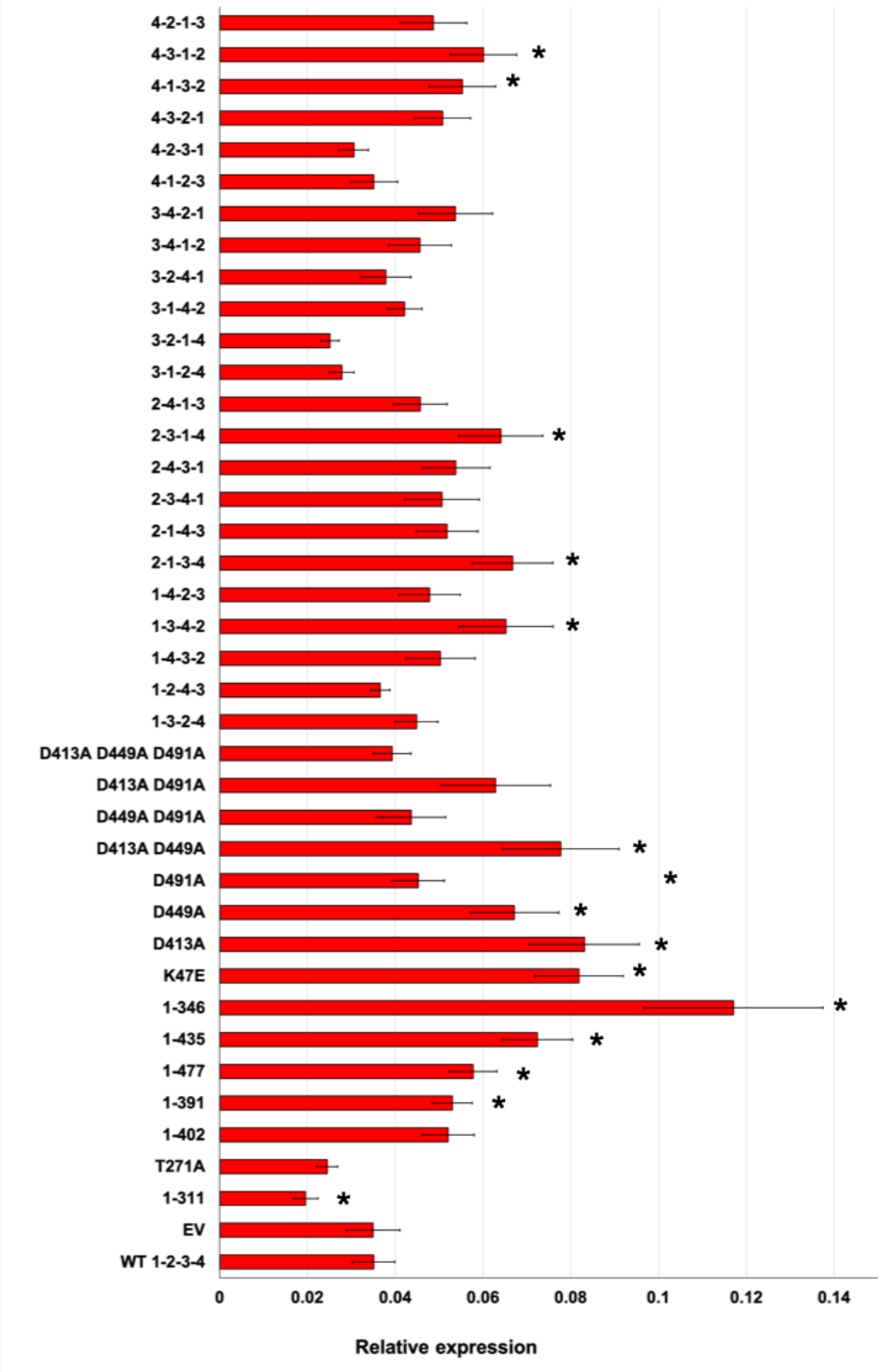

Figure 3. 9. Dual Luciferase reporter assay reveals large variability of CCaMK swaps to induce spontaneous *ENOD11* expression.

The interchanging of EF-hand loops within CCaMK structure resulted in CCaMK swaps with different GOF activities based on their ability to induce *ENOD11* expression in the absence of rhizobia. Asterisk denote statistically significant increase or decrease of

spontaneous *ENOD11* expression levels by the CCaMK mutants compared to CCaMK WT *ENOD11* expression induction levels in a pairwaise two-tailed test ($p<0.05$). Bars represent average expression of three biological replicates (each with three technical replicates) with each biological replicate comprising roots from 3-6 plants. Error bars represent S.E.

In order to create the CCaMK swaps, the EF-hand motif region that provides the seven oxygen ligands for coordination of the calcium ion was chosen (see chapter for EF-hand motif structure). This region comprises from residue 1 until residue 9 of the EF-loop and the three first residues of the EF-hand exiting helix, making a total of 12 residues. As a consequence, this region is considered the EF-hand loop despite not being structurally accurate (Strynadka and James, 1989). The CCaMK swaps were designed by placing each CCaMK EF-hand loop in between each pair of EF-hand helices and making every possible combination of EF-loops based on their position within CCaMK structure (Figure 3.8) and created by DNA synthesis.

An additional empty vector (EV) construct that lacked *CCaMK* was designed to use as a negative control. This construct contained the GUS gene encoding β-glucuronidase under the control of *pCCaMK* instead of *CCaMK* and should give low or no levels of spontaneous *ENOD11* gene expression similar to CCaMK WT as the symbiotic stimulus is not present. This construct would also ensure that the phenotype observed is specifically due to the CCaMK mutant inserted and not to the transformation event (a list of the constructs used in this experiment can be found in Appendix 1).

Results from the Dual-Luciferase reporter assay revealed that variants 1-311 and T271A, which are widely accepted as GOF versions of *CCaMK* (Gleason et al., 2006; Tirichine et al., 2007), were not able to induce spontaneous *ENOD11* expression (Figure 3.9). Previous assessments of spontaneous nodulation by these two mutants were performed after 6-8 weeks of incubation in sterile conditions as opposed to the immediate harvest of the material done in this method after *Agrobacterium-mediated* transformation period, suggesting these mutants' GOF activity might require longer periods of time to develop. However, truncated versions 1-477 and 1-435 did significantly induce *ENOD11* expression consistent with previous observations of these mutants' ability to induce

spontaneous nodule formation (Miller et al., 2013) and *ENOD11* being an early symbiotic marker dependent on CCaMK (Chabaud et al., 2002; Charron et al., 2004; Journet, 2001; Kosuta et al., 2003; Gleason et al., 2006). Unexpectedly, the truncated variant 1-346 was also able to significantly induce *ENOD11* expression at high levels (Figure 3.9), not observed in earlier published work (Gleason et al., 2006; Tirichine et al., 2006; Shimoda et al., 2012; Miller et al., 2013). It was previously shown that CCaMK 1-356, which also lacks the CaMBD and VLD, retains reduced levels of Ca^{2+}/CaM dependent kinase activity (Takezawa et al., 1996), which supports this variant's GOF activity. *ENOD11* expression has been reported from as early as 3-6 hours post-inoculation which rhizobia in the root epidermis to every stage of pre-infection and infection events in epidermal, cortical and nodule tissues (Charron et al., 2004; Journet, 2001). The high sensitivity of the Dual-Luciferase assay could explain why this 1-346 GOF phenotype was not previously identified as possibly less-sensitive methods were previously employed. However, the induction of *ENOD11* expression does not provide any information about what stage the nodulation process is arrested in. Interestingly, significant induction of *ENOD11* spontaneous expression was observed by the truncated version 1-391 but not by 1-402 suggesting for the first time a potential role for EF-hand 1 during symbiosis.

Impairment of calcium binding through either EF-hand 2, 3 or 4 of CCaMK results in GOF activity that give rise to spontaneous nodulation but also allows partial complementation of *ccamk* (Miller et al., 2013; Shimoda et al., 2012). Consistent with this, *ENOD11* expression was significantly induced by D413A and D449A mutants but surprisingly not by D491A (Figure 3.9). Furthermore, double CCaMK EF-hand point mutants which are impaired for calcium binging through two EF-hand motifs displayed different *ENOD11* gene expression abilities. Mutants containing the D491A mutation where calcium binding at EF-hand 4 is abolished, showed no spontaneous gene induction as opposed to the double mutant D413A-D449A that did (Figure 3.9). This was also consistent with the lack of spontaneous *ENOD11* induction by the triple EF-hand point mutant D413A-D449A-D491A. Spontaneous nodule formation was previously observed in all single, double and triple EF-hand point mutants (Miller et al., 2013) but spontaneous *ENOD11* gene expression by these mutants was not observed in the present experiment (Figure 3.9). However, similar to 1-311 and T271A,

spontaneous nodulation induced by these mutants was previously assessed after longer periods of time than for spontaneous gene expression in this assay. Therefore, longer periods of incubation could potentially be needed in order to detect the GOF activity for these mutants.

It was also very surprising that the kinase-dead K47E mutant was also able to induce high levels of spontaneous *ENOD11* expression (Figure 3.9). Mutation of the highly conserved lysine at the ATP binding site was thought to be sufficient to remove the kinase activity from CCaMK. However, these results suggest that further mutations might be needed to obtain a fully kinase-dead CCaMK mutant.

Swainsbury et al. (2012) demonstrated that EF-hand 2 and 3 have similar calcium binding capabilities with an affinity for calcium ions of 200 nM, appropriate for the perception of calcium spiking (625 – 850 nM) (Ehrhardt et al., 1996b). Since the ligands for calcium ion coordination are only provided by the EF-hand loop and EF-hand 2 and 3 having similar affinities for calcium, the obvious expectation was that exchanging the loops from these two EF-hands would result in no difference in CCaMK symbiotic capabilities. Indeed, the mutant 1-3-2-4 showed no higher ability to induce spontaneous *ENOD11* expression than WT. However, when this mutant is further modified so that EF-hand 4 position is also altered, variant 1-3-4-2, GOF activity was observed and *ENOD11* spontaneous gene expression raised to significant levels compared to WT. If EF-hands 2 and 3 were completely interchangeable due to their similar calcium ion affinities, variant 1-2-4-3 should have also behaved as a GOF, which was not observed. This was further demonstrated by variants 2-1-3-4 and 2-3-1-4 GOF activities that were not observed in their opponent variants 3-1-2-4 and 3-2-1-4, respectively. The importance of EF-hand 4 in the establishment of both symbioses (Shimoda et al., 2012) but also specifically in maintaining CCaMK inactive through calcium binding at basal levels required for Thr271 autophosphorylation (Swainsbury et al., 2012; Miller et al., 2013) was demonstrated, further supporting the absence of GOF activity in calcium binding impaired EF-hand 4 mutants observed in this experiment. Consequently, modification of EF-hand motif 4 through interchanging EF-loops was expected to have a major impact on CCaMK activity. Only were mutants 1-3-4-2, 4-1-3-2 and 4-3-1-2 able to induce spontaneous *ENOD11* expression while the remaining variants with EF-loop 4 interchanged position showed similar behaviour as WT.

Overall, the Dual-Luciferase assay does not exclude the possibility that many of these different helix-loop-helix combinations could still allow activation of the symbiotic signalling pathway in the presence of rhizobial and/or mycorrhizal signals. In fact, some of these variants that showed GOF activity might also induce formation of fully mature nodules and thus, allow symbiosis. Likewise, mutants with no apparent GOF activity could be able to allow nodulation at same, lower or higher levels than WT. This could also be the case during mycorrhization and in fact, it might also be possible that those CCaMK EF-hand swaps with no nodulation ability might allow mycorrhization.

2.5. Assessment of spontaneous *NIN* expression in *Nicotiana benthamiana* leaves

A further spontaneous gene induction test was performed in a heterologous system for mutants 1-311 and T271A which are well known for their GOF activities but were not able to induce spontaneous *ENOD11* expression in the Dual-Luciferase reporter assay. *Nicotiana benthamiana* leaves was the system of choice for its high efficiency and speed of transformation. In this case, *NIN* was chosen as the symbiotic transcriptional marker to test its induction by CCaMK mutants as the CCaMK-CYCLOPS complex was shown to activate *NIN* promoter through direct binding. In fact, a *pNIN:GUS* fusion was previously used to demonstrate the ability of T265D (*Lotus japonicus* equivalent of T271A in *Medicago truncatula*) in conjunction with CYCLOPS to transactivate *NIN* promoter in *Nicotiana benthamiana* leaf cells, so a similar approach was followed (Singh et al., 2014). Constructs were designed containing either CCaMK WT, 1-311, T271A or 1-435 along with *pNIN:GUS* and CYCLOPS for *Agrobacterium tumefaciens*-mediated transformation of *Nicotiana benthamiana* leaves. GUS staining results after 2 days of transformation, confirmed the GOF activity of the three mutants tested as previously reported (Miller et al., 2013) whilst WT did not show any spontaneous gene induction ability (Figure 3.10). However, any differences in the level of gene expression induction between the GOF mutants cannot be reliably identified based on the visual differences in the shade of blue staining. Although the 1-311 and T271A mutants showed the expected phenotype in *Nicotiana benthamiana* leaves in the GUS staining experiment but

not in the Dual-Luciferase assay, the latter represents a more sensitive and reliable method as it allows to obtain degrees of GOF activity rather than positive or negative results (Figure 3.9). Additionally, transient expression in a heterologous system such as *Nicotiana benthamiana* and in different tissues like the leaves might occur at a different pace and at different levels than in *Medicago truncatula* roots.

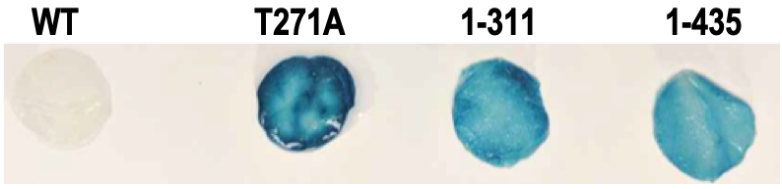

Figure 3. 10. CCaMK GOF mutants induce spontaneous expression of NIN in *Nicotiana benthamiana* leaves.

Nicotiana benthamiana leaves were infiltrated with *Agrobacterium tumefaciens* transformed with constructs containing either *CCaMK WT, T271A, 1-311* or *1-435*. Leaf discs (1 cm diameter) were GUS stained overnight and chlorophyll was removed by incubation in 70% ethanol for better visualisation of results. As expected, GOF CCaMK variants induced spontaneous gene expression which resulted in blue staining of the leaves, while CCaMK WT did not induce any gene expression and gave no blue staining.

Based on the Dual-Luciferase assay and *Nicotiana benthamiana* transient expression results, CCaMK mutants were further tested in planta in the presence of *Sinorrhizobium meliloti*. This would help to fully understand their symbiotic capabilities during the native conditions.

2.6. Assessing CCaMK swap ability to allow nodulation

In order to identify the CCaMK mutants' ability to decode calcium spiking and allow nodulation, constructs were re-designed for testing in *Medicago truncatula* in the presence of *Sinorrhizobium meliloti*. These constructs were designed similarly to the constructs employed previously for transient expression in *Nicotiana benthamiana*. However, CYCLOPS was not necessary in these constructs as the native *Medicago truncatula* CYCLOPS was already present in the plant and therefore, *CYCLOPS* was replaced in these constructs by *dsRed*

for selection of positively transformed plants, as employed previously in the Dual-Luciferase assay. Since *NIN* was discovered to be involved in the regulation of AM symbiosis as well as in nodulation (Guillotin et al., 2016), these constructs also contained the *pNIN:GUS* fusion suitable for future testing of symbiotic gene induction during both nodulation and mycorrhization if desired (Figure 3.11). As a positive control for nodulation, *Medicago truncatula* A17 wild-type plants were transformed with the same EV construct used for the Dual-Luciferase assay (Chapter three, Section 2.3).

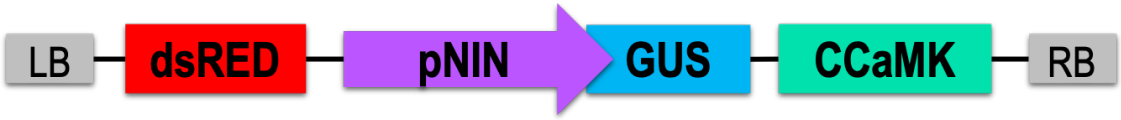

Figure 3. 11. Schematic representation of insert composition of genetic constructs used for the assessment of nodulation in hairy-root transformed *Medicago truncatula* roots.

All constructs contained: *dsRED* under the control of the constitutive *pAtUBI10* for positively transformed plant selection; *GUS* reporter gene under the control of *NIN* promoter used as a rhizobial-symbiosis transcriptional marker; and *CCaMK* under the control of *CCaMK* native promoter (different variants tested). In order to ensure its integration within the plant genome, *CCaMK* was placed at the right border (RB) as T-DNA insertion starts at this border.

Results showed that T271A fully complemented the *ccamk* mutant phenotype with similar levels of fully mature nodules as WT whilst variant 1-311 showed no ability to induce nodulation (Figure 3.14 and Appendix 2), as previously observed (Gleason et al., 2006; Tirichine et al., 2006; Miller et al., 2013; Shimoda et al., 2012). Strikingly, the kinase-dead K47E mutant was also able to induce similar levels of nodule formation (both pink and white) although in a reduced number of plants compared to WT. As previously shown, single EF-hand point mutants were able to partially complement *ccamk*, as fully matured nodules were observed but in a significantly reduced number compared to WT. However, double EF-hand point mutants D413A-D449A and D449A-D491A fully complemented *ccamk* with no apparent difference to WT while D413A-D491A was only able to allow formation of mature nodules to a significantly reduced number compared to WT

(Figures 3.12, 3.14 and Appendix 2). This conflicts with previous observations of the double EF-hand point mutants being unable to induce mature nodule formation but able to induce spontaneous nodulation (Miller et al., 2013). Shimoda et al. (2012) showed that the *Lotus japonicus* CCaMK variant equivalent to D413A-D449A has the ability to fully complement *ccamk*, matching the observed behaviour of this mutant in the current experiment. It is noticeable that although some of these variants are able to induce the formation of a similar number of nodules as WT, their nodulation ability is only observed in a reduced number of plants (Table 3.2), highlighting CCaMK's need of calcium sensing through its three EF-hand motifs to efficiently decode the symbiotic calcium signal. This is further demonstrated by the inability of D413A-D449A-D491A mutant to allow nodulation in the present experiment.

The truncated variant 1-391, which contains EF-hand 1's incoming helix and loop but lacks the exiting helix allowed formation of significantly higher number of nodules than WT. These nodules were unable to accommodate rhizobia as indicated by their white colour (not shown). On the contrary, the 1-402 mutant that did contain the entire EF-hand 1 (incoming helix-loop-exciting helix) did not induce any nodule formation. These results suggest that despite the lack of calcium binding to EF-hand 1, this EF-hand motif does indeed have a role in the regulation of CCaMK's activity.

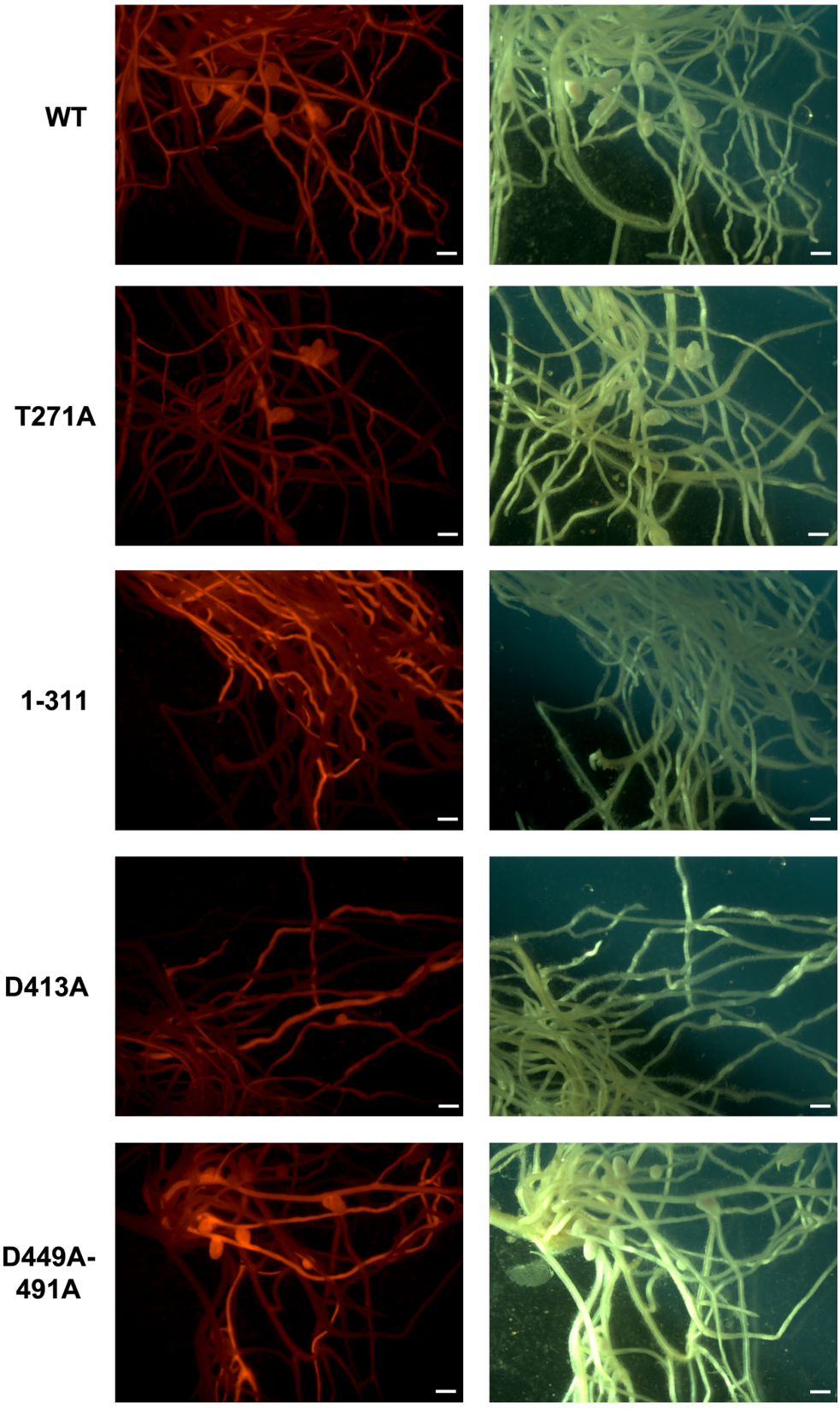

Figure 3. 12. Representative images of nodules obtained from CCaMK variants.

As previously reported, CCaMK WT, T271A and single CCaMK EF-hand point mutant D413A give rise to mature nodules in the presence of rhizobia while the 1-311 does not.

In contrast to previous reports, the double CCaMK EF-hand point mutant D449A-D491A is also able to complement *ccamk* and give rise to fully mature nodules. Roots were visualised using dsRED fluorescence (left panels) for confirmation of plant transformation and with the bright field (right panels). The white or pink colour of nodules cannot easily be distinguished in these images. Scale bar = 1 mm.

Truncated variants lacking part or the entire VLD, 1-477 and 1-346 did not allow nodulation as previously shown (Gleason et al., 2006). However, 1-435 was able to induce the formation of a reduced number of white nodules compared to WT but did not allow rhizobial infection. These nodules might be spontaneous despite the presence of rhizobia in the assay and this result is consistent with previous publications (Miller et al., 2013).

Mutant 1-3-2-4, where EF-hand loops 2 and 3 were interchanged, did not allow formation of fully mature nodules (pink) nor formation of spontaneous nodules (white). This confirmed that despite having similar calcium binding affinities, EF-hand 2 and 3 are not interchangeable. Interestingly, 1-2-4-3 and 1-3-4-2, which had their EF-loops 1 and 4 at the same positions but swapped EF-loops 2 and 3, were able to partially complement *ccamk*. These variants allowed formation of nodules capable of accommodating rhizobia (Figure 3.13), identified by their visually detectable pink colour. Moreover, the levels of complementation in terms of the number of fully mature nodules formed by these mutants were comparable to those produced by the single EF-hand point mutants and D413A-D491A (Figure 3.14 and Appendix 2). Although the calcium binding capabilities of CCaMK swaps' EF-hand motifs have not been assessed, their phenotypic resemblance might be an indication of calcium binding impairment in one or two EF-hand motifs of 1-2-4-3 and 1-3-4-2 mutants that still enabled partial complementation of *ccamk*.

It was also interesting to observe that both mutants 1-4-3-2 and 1-4-2-3 which are only different in their EF-loop 2 and 3 positions, produced the same phenotype. These mutants induced the formation of nodules that did not accommodate rhizobia, as indicated by their white colour (Figure 3.13). Since nodules were counted at the same time for all CCaMK variants and the incubation time was sufficient for WT and T271A to produce fully mature nodules, it is

possible to consider these white nodules as spontaneous. However, it cannot be ruled out that the infection process might be delayed in these mutants rather than completely abolished. This might also be the case for mutants 2-3-1-4, 3-4-1-2 and 4-2-3-1 that also gave rise to a reduced number of white nodules.

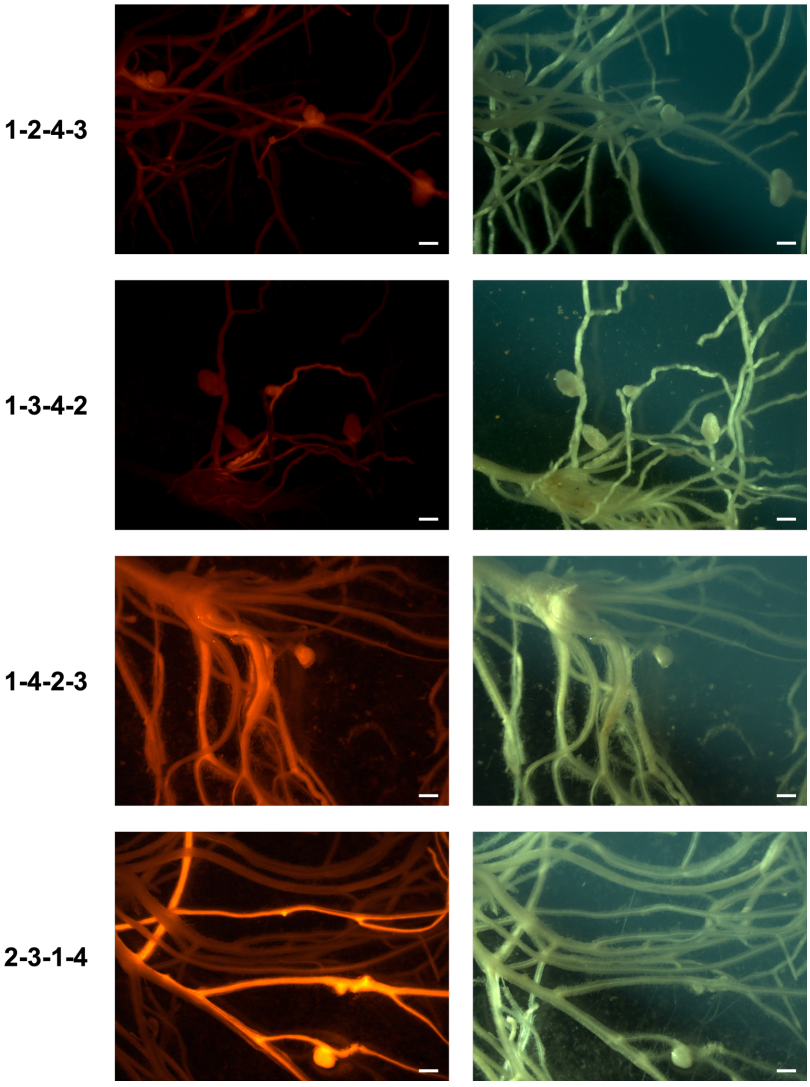

Figure 3. 13. Representative images of nodules obtained from CCaMK swaps.

Roots were visualised using dsRED fluorescence (left panels) for confirmation of plant transformation and with the bright field (right panels). The white or pink colour of nodules cannot easily be distinguished in these images. Scale bar = 1 mm.

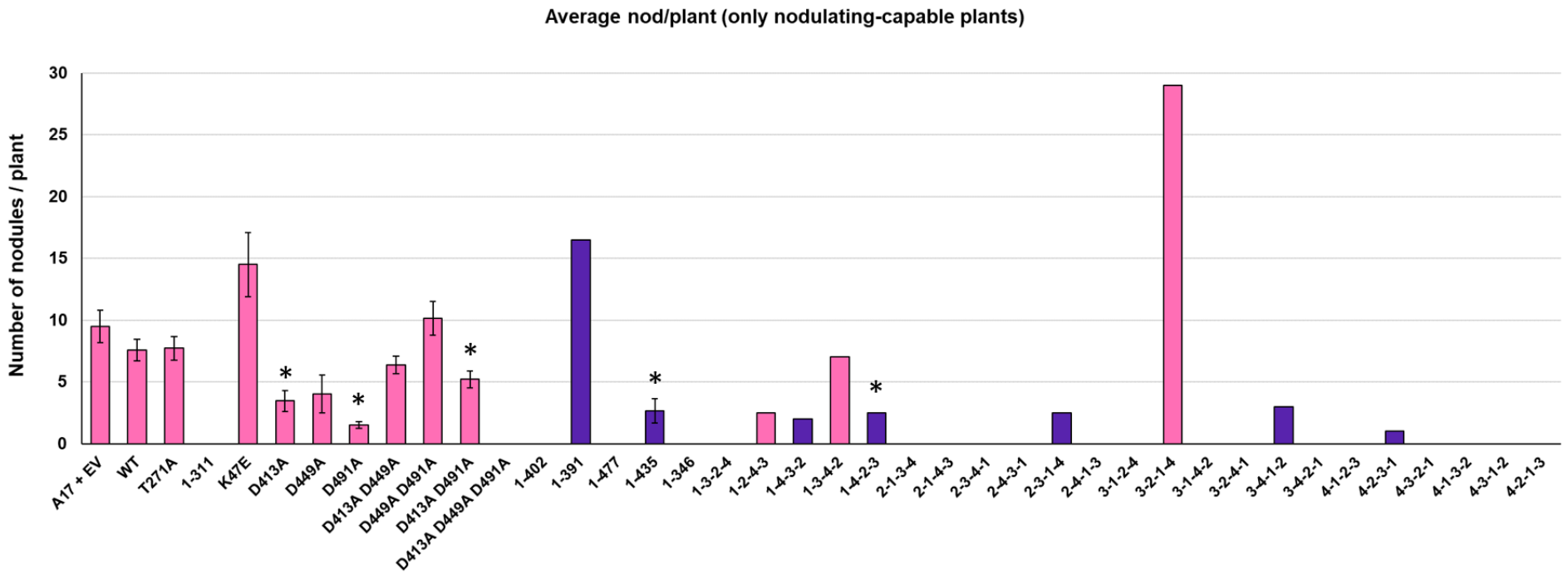

Figure 3. 14. CCaMK swaps showed different nodulation capabilities.

Nodules were obtained from a low number of CCaMK swaps. Bars represent average number of nodules of plants assessed in at least three technical replicates. While each replicate was comprised of at least 6-10 plants, each bar of the graph only includes those plants which gave rise to either spontaneous and / or mature nodules to facilitate the visualisation of the data without impacting on the results. The nodulation capability of certain CCaMK variants was very rare and was only observed in one or two plants of the total number of plants tested across all technical replicates and therefore, a statistical analysis was not possible to perform on these variants. However, this data still revealed the nodulation capability of the CCaMK variants and indicates that a higher number of plants need to be tested in order to achieve statistical significance. Pink bars correspond to CCaMK variants which were able to produce mature nodules and purple bars correspond to CCaMK variants which produced white nodules, potentially

spontaneous. A bar chart of the data comprising all plants tested can be found in Appendix 2 and the full number of plants tested and plants producing nodules can be seen in Table 3.2. Asterisk denote statistically significant increase or decrease of nodule number induced by the CCaMK mutants when at least three plants gave nodules compared to CCaMK WT in a pairwaise two-tailed student t-test ($p<0.05$). Error bars represent S.E. and were only added to those bars containing number of nodules of at least three plants.

Lastly, the mutant 3-2-1-4 fully complemented *ccamk* as formation of a high number of mature nodules was observed. However, this was a rare event that only occurred in 1 plant out of the 25 tested. This low frequency was also obtained for the other EF-hand swaps, where a very low number of plants displayed their ability to partially or fully allow nodulation and a high number of plants were required to be tested. This is not surprising as for instance, the double EF-hand point mutant's ability to induce fully mature nodule formation observed in these experiments was not shown in previous publications. These experiments revealed a lot of information about the importance of the EF-hand motifs of CCaMK and allowed the identification of CCaMK EF-hand mutants that enabled complementation of the *ccamk* mutant. A higher number of plants should be tested for these mutants to fully confirm their phenotypes, particularly for those EF-hand swaps that did not show any nodulation capabilities.

3. Discussion

Detailed study of the effect of native EF-loop interchanging within CCaMK structure has shown for the first time that the primary sequence of EF-hand motif is one of the main factors influencing its calcium signal response. Since the EF-loop sequence follows a conserved pattern (Strynadka and James, 1989), their interchange should not induce any major changes in the EF-hand motif tertiary structure. Moreover, if tertiary structure had a higher influence than the primary sequence on the calcium binding ability, interchanging the native EF-loops should have no effect on the ability of CCaMK to decode calcium spiking and allow symbiosis. However, this is not the case as the importance of the primary sequence of the EF-hand motif was highlighted by 1-3-2-4 in which EF-hand motifs 2 and 3 of similar calcium binding abilities (similar equilibrium dissociation constant, *Kd*) (Swainsbury et al., 2012) were swapped and yet this mutant was not able to either induce spontaneous *ENOD11* expression nor complement *ccamk*. This phenotype matches with CCaMK D413A-D449A-D491A triple EF-hand point mutant phenotype, in which calcium binding is impaired at EF-hand motifs 2, 3 and 4. However, the phenotypic resemblance of mutants D413A-D449A-D91A and 1-3-2-4 might not mean that the 1-3-2-4 variant has its calcium binding ability completely abolished but could suggest its similar structural

arrangement to the triple EF-hand point mutant. Even though theoretically the EF-hand motif tertiary structure was minimally altered by interchanging EF-loops 2 and 3, their primary sequences are different. It is known that residues at the EF-loops establish interactions with residues at the EF-helices but also with the EF-loop of the other member of the EF-hand pair (Strynadka and James, 1989). As a consequence, modification of the EF-hand motif primary sequence could be causing major structural changes in the EF-hand pair that influence the ability of CCaMK to respond to the symbiotic calcium signal. Additionally, these EF-hand pair structural alterations might also have an effect in other regions of the protein and possibly block other stages of CCaMK's mechanism of activation. This shows the need of a crystal structure that could help discriminate the effects of native EF-loop interchanging on CCaMK structure and mechanism of activation. It was previously shown that CCaMK triple EF-hand point mutant was not able to complement the *ccamk* phenotype as no infection threads or nodule-like structures (spontaneous nodules) were formed (Shimoda et al., 2012). Similarly, this could also be the case in mutant 1-3-2-4, consistent with the results of the Dual-Luciferase and nodulation tests.

Two out of the 23 CCaMK swaps were able to partially complement *ccamk*. These were mutants 1-2-4-3 and 1-3-4-2 that gave rise to fully mature nodules in a reduced number compared to WT. Strikingly, their EF-loops 1 and 4 are placed at the same positions in both mutants but EF-loops 2 and 3 are swapped. It is also interesting to highlight that 1-2-4-3 maintains one EF-hand pair intact (1-2) while the other pair has EF-loops 3 and 4 placed in opposite order (4-3) than WT (3-4). However, mutant 1-3-4-2 contains interchanged loops in both EF-hand pairs. Consistently, these mutants did not behave in an identical manner as, unlike 1-2-4-3, the mutant 1-3-4-2 additionally showed GOF activity due to its ability to induce spontaneous *ENOD11* expression in the Dual-Luciferase assay (Figure). The ability to both induce spontaneous gene expression and partially complement *ccamk* resembles the phenotypes observed in the single EF-hand point mutants D413A and D449A which lack calcium binding at EF-hands 2 and 3. This single EF-hand point mutants were shown to induce formation of infection threads and fully mature (infected) nodules (Shimoda et al., 2012), but also spontaneous nodules in the absence of rhizobia (Miller et al., 2013). Since a correlation between spontaneous *ENOD11* expression and spontaneous

nodulation has been considered, 1-3-4-2 might also be able to induce formation of infection threads and spontaneous nodules.

On the contrary, 1-2-4-3 allowed partial complementation of *ccamk* as fully mature nodules were formed (Figure 3.14 and Appendix 2), but no spontaneous *ENOD11* expression was observed (Figure 3.9). Despite the link between nodulation and *ENOD11* expression, the time when gene expression was assessed might not be appropriate for this mutant and its lack of *ENOD11* expression induction in the absence of rhizobia does not discard the possibility of spontaneous nodulation ability. However, this could also mean that the 1-2-4-3 mutant does not have GOF activity and that it needs to perceive the calcium signal in order to activate. In fact, this mutant's ability to induce the formation of fully mature nodules shows its ability to decode the calcium spiking. The double EF-hand point mutants D413A-D491A and D449A-D491A, both have calcium binding impaired at EF-hand 4 and like 1-2-4-3, showed no ability to induce *ENOD11* expression in the absence of rhizobia but did allow full complementation of *ccamk* phenotype. This suggests that calcium binding through either EF-hand 2 or 3 could be sufficient to regulate CCaMK activation and allow decoding of calcium spiking. Nevertheless, spontaneous nodulation was previously observed in these double EF-hand point mutants (Miller et al., 2013) which demonstrates their GOF ability despite not being able to induce spontaneous *ENOD11* expression ability in the Dual-Luciferase assays. Interchange of EF-hand loops 3 and 4 in mutant 1-2-4-3 might be causing calcium impairment to EF-hands 3 and 4 or a structural arrangement similar to either D413A-D491A or D449A-D491A, explaining their phenotype resemblance. In order to clarify whether this mutant constitutes a deregulated version of CCaMK, further assessment of its spontaneous nodulation ability would be necessary.

Full complementation of *ccamk* was only achieved by one of the CCaMK swaps. This was 3-2-1-4, which allowed formation of fully mature nodules at similar levels than WT but was unable to induce spontaneous *ENOD11* expression, suggesting this mutant's need of calcium spiking in order to activate the CSSP.

Despite the presence of rhizobia in the soil in the nodulation test, white nodules produced by some of the CCaMK swaps could be considered spontaneous. The fact that WT CCaMK along with other mutants such as T271A and EF-hand point

mutants, were able to induce the formation of fully mature nodules after three weeks indicates that this time period is sufficient for nodulation with rhizobia. Consequently, it was expected that if the CCaMK swaps were able to allow nodulation, fully mature nodules would be formed during this time. Mutant 2-3-1-4 gave rise to a reduced number of white nodules as well as induced spontaneous *ENOD11* expression. Although a delay in rhizobial infection could not be discarded due to the presence of rhizobia in the soil, 2-3-1-4 can be confirmed as a GOF mutant of CCaMK. In addition, 1-4-3-2, 1-4-2-3, 3-4-1-2 and 4-2-3-1 also induced white nodule formation but were unable to induce spontaneous *ENOD11* expression. Considering that the time of incubation with rhizobia was sufficient to allow nodulation and that these white nodules are spontaneous, the lack of *ENOD11* expression in the Dual-Luciferase assays suggests potential varying degrees of GOF activity for the CCaMK swaps. This can be appreciated in both CCaMK mutant controls and swaps. Since these mutants might induce *ENOD11* expression at different times depending on their amount of GOF activity, the timing when the gene expression was measured might not be suitable for all the CCaMK swaps. Alternatively, the fact that certain CCaMK swaps induced *ENOD11* expression but did not form nodules might indicate an early arrest of the nodulation process. This is consistent with the fact that *ENOD11* expression is induced very early during Nod factor perception and correlates with the different stages of pre-infection and infection during nodulation (Journet, 2001). Therefore, spontaneous *ENOD11* expression measurement provides information about whether the CCaMK swaps retain any ability to induce the CSSP but not to what extent.

It was previously shown that CCaMK is required for both IT formation and nodule organogenesis (Hayashi et al., 2010). However, there is a different requirement of Ca^{2+}/CaM by CCaMK to allow these processes. Ca^{2+}/CaM were not required for CCaMK activation in the cortex as the kinase-only version of CCaMK, 1-311, was sufficient to allow nodule organogenesis but did not support formation of IT or rhizobial colonisation (Gleason et al., 2006). In contrast, formation of IT requires CCaMK to be activated by the CSSP upstream genes, demonstrating the need of CaM and Ca^{2+} signal perception in the epidermis (Hayashi et al., 2014). Consistent with this, the CCaMK swaps could be classified into three categories based on their ability to allow full infection, nodule organogenesis or

not allowing symbiosis. Those CCaMK swaps that spontaneously induced *ENOD11* expression and/or formed white nodules might be have impaired calcium binding capabilities or no ability to decode the calcium spiking and similarly to 1-311, these might only activate the CSSP in the cortex. CCaMK swaps that allowed partial or full complementation of the *ccamk* phenotype could potentially have retained certain levels of calcium spiking decoding which enabled formation of epidermal ITs and rhizobial colonisation in order to produce fully mature nodules (pink nodules). Lastly, CCaMK swaps that did not induce spontaneous gene expression or nodule organogenesis could have possibly lost their kinase activity, rendering them unable to activate the CSSP.

The Dual-Luciferase reporter assay and nodulation test allowed the identification of new interesting CCaMK mutants with symbiotic capabilities. It is worth noting that more than 50% of the CCaMK swaps were unable to show either GOF activity or nodulation capability. However, the lack of activity of these CCaMK swaps during nodulation does not indicate a lack of activity at all. Conversely, these mutants might have lost their specificity to respond to the symbiotic calcium spiking but gained the ability to respond to a different calcium signal. The structure of calcium oscillations induced by both rhizobial and AM species were found to be very similar (Sieberer et al., 2012; Sun et al., 2015b). Sieberer et al. (2012) also showed that both symbionts, rhizobia and AM, induce rapid and periodic calcium oscillations in those cells that are being infected while poorly periodic calcium oscillations are found in neighbouring uninfected cells. Interchanging the native EF-loops of CCaMK might have resulted in some CCaMK swaps that are not able to discriminate these two types of calcium oscillation patterns or might only be able to perceive one or the other, altering their ability to allow symbiosis. Additionally, many different patterns of calcium oscillations are induced upon biotic and abiotic stimuli in plants (Kudla et al., 2010). Calcium binding proteins are responsible for the perception and specific decoding of those calcium oscillations through their EF-hand motifs (DeFalco et al., 2010). The new helix-loop-helix combinations might provide the CCaMK swaps with the ability to decode different calcium signals in response to different external stimuli.

The present study has shown the importance of the EF-hand motif primary sequence for the specificity to the calcium signal response. However, the

implications of altering the EF-hand motif structure on the protein's activity are not yet known. It was previously reported that phosphorylation at residue Thr271 is required for negative regulation of CCaMK and is calcium dependent. This is consistent with T271A mutant's ability to induce spontaneous nodulation due to its lack of autophosphorylation (Takezawa et al., 1996; Gleason et al., 2006; Tirichine et al., 2006; Miller et al., 2013). Since GOF activity is associated to the lack of Thr271 autophosphorylation which is dependent on calcium signal perception, information about the autophosphorylation ability of the CCaMK swaps would also help to identify whether their phenotype is due to impaired calcium binding.

Table 3. 1. Experimental conditions tested for *Medicago truncatula* seedling transformation.

Component	Conditions		
Silwett L-77	0.001%	0.0025%	0.005%
OD600 *A. tumefaciens*	0.25	0.5	0.75
Co-cultivation period (h)	40	48	60
Seedling age (days)	2	3	4
A. tumefaciens strain	GV3101	AGL1	

The table shows the different concentrations of the surfactant Silwett L-77, optical densities at 600 nm of two different strains of *Agrobacterium tumefaciens*, the co-cultivation periods of *Medicago truncatula* seedlings with *Agrobacterium* and the age of the seeds in days. Different but not all the combinations of these conditions were tested as described in the main text.

Table 3. 2. CCaMK swaps were tested for their nodulation capabilities in a high number of plants.

CCaMK mutant	Nodulating/tested plants
A17 + EV	24 / 27
WT 1-2-3-4	30 / 44
T271A	31 / 48
1-311	0 / 43
K47E	4 / 27
D413A	16 / 43
D449A	13 / 54
D491A	3 / 53
D413A-D449A	21 / 42
D449A-D491A	9 / 41
D413A-D491A	19 / 46
D413A-D449A-D491A	0 / 33
1-402	0 / 35
1-391	2 / 37
1-477	0 / 32
1-435	3 / 24
1-346	0 / 34
1-3-2-4	0 / 28
1-2-4-3	2 / 43
1-4-3-2	1 / 20
1-3-4-2	3 / 35
1-4-2-3	2 / 28
2-1-3-4	0 / 32
2-1-4-3	0 / 12
2-3-4-1	0 / 15
2-4-3-1	0 / 14
2-3-1-4	2 / 40
2-4-1-3	0 / 24
3-1-2-4	0 / 14
3-2-1-4	1 / 25
3-1-4-2	0 / 35
3-2-4-1	0 / 41
3-4-1-2	1 / 38
3-4-2-1	0 / 31
4-1-2-3	0 / 37
4-2-3-1	1 / 34
4-3-2-1	0 / 23
4-1-3-2	0 / 41
4-3-1-2	0 / 37
4-2-1-3	0 / 37

Chapter Four - Kinase assay trials to determine the T271-autophosphorylation capability of the CCaMK swaps

1. Introduction

CCaMK has the exceptional ability to discriminate between the basal [Ca^{2+}] and those during the symbiotic Ca^{2+} spiking (Chapter One, Section 1.5). This is due to the structure of CCaMK which contains a CaMBD for the indirect sensing of Ca^{2+} and four EF-hand motifs, three of which can directly bind Ca^{2+} (Swainsbury et al., 2012; Miller et al., 2013; Patil et al., 1995). The CCaMK EF-hand motifs are arranged in pairs with one pair composed of EF-hand 1 and 2, while EF-hands 3 and 4 form the other pair (Shimoda et al., 2012) and with no cooperativity between the members of each pair (Swainsbury et al., 2012) (Chapter One Section 5.1). CCaMK EF-hand motifs possess different calcium binding capabilities: EF-hand 1 is a non-calcium binding EF hand motif, EF-hands 2 and 3 are low affinity calcium binding sites and EF-hand 4 has high-affinity for calcium. Based on this, CCaMK was predicted to have EF-hand 4 bound to Ca^{2+} at basal [Ca^{2+}] due to its high affinity for Ca^{2+} (Swainsbury et al., 2012). The perception of Ca^{2+} during basal [Ca^{2+}] results in Thr-271 autophosphorylation which induces the formation of a hydrogen network between the kinase and CaMB domains that keeps CCaMK inactive but primed for activation (Miller et al., 2013). Upon perception of the symbiotic stimulus and generation of the nuclear calcium spiking, the three CCaMK Ca^{2+} binding EF hand motifs bind Ca^{2+} inducing a conformational change that allows calmodulin binding to CCaMK. This interrupts the hydrogen network, releasing the kinase domain from autoinhibition. Finally, CCaMK phosphorylates CYCLOPS which activates the specific symbiotic signalling pathway (Miller et al., 2013) (See Chapter One, Section 5.3 for full CCaMK mechanism of activation).

It has been demonstrated that the primary sequence of the EF-hand motif encodes specific information that allows CCaMK to respond to the symbiotic Ca^{2+} spiking (Chapter Three). Consistently, interchanging the native EF-loops of CCaMK which was predicted to not cause any changes in tertiary structure, resulted in different nodulation phenotypes: some CCaMK swaps allowed formation of fully mature nodules, others CCaMK swaps induced formation of white and/or pink nodules and induced spontaneous gene expression, and the

remaining CCaMK swaps were completely unable to induce nodule organogenesis and infection (Chapter Three). In addition, this result proved that despite having apparently similar structural arrangements, each individual EF-hand motif has a specific role in the regulation of CCaMK activity during symbiosis determined by their primary sequence.

In order to keep CCaMK inactive, the autophosphorylation of Thr271 is required which is dependent on Ca^{2+} (Takezawa et al., 1996; Sathyanarayanan et al., 2000, 2001; Gleason et al., 2006; Tirichine et al., 2006). The binding of Ca^{2+} through the EF-hands, therefore, is not only required for CCaMK activation during the symbiotic Ca^{2+} spiking but also for the negative regulation of CCaMK through autophosphorylation. This is supported by the fact that the truncated versions of CCaMK lacking part or the entire VLD and thus, with impaired or abolished Ca^{2+} binding ability, gave rise to spontaneous nodulation. Therefore, these CCaMK mutants have the ability to activate the downstream signalling in the absence of the symbiotic stimuli (Miller et al., 2013). Interestingly, these truncated mutants with spontaneous nodulation ability are also defective in Thr271 autophosphorylation (Miller et al., 2013). Consistently, the Thr to Ala mutation at position 271 which abolishes autophosphorylation at this position results in the CCaMK T271A mutant which has spontaneous nodulation ability in addition to fully complements the *ccamk* phenotype.

Since spontaneous nodulation appears to be linked to the absence of Thr271 autophosphorylation, it could be hypothesised that those CCaMK swaps that gave rise to spontaneous nodule formation also lack T271 autophosphorylation (Chapter Three). Moreover, autophosphorylation at 271 has been proved to be dependent on Ca^{2+} binding and therefore, the lack of Thr271 autophosphorylation could also be an indication of an impaired or abolished Ca^{2+} binding ability to the EF-hand motifs of the CCaMK swaps. Therefore, assessing the Thr271 autophosphorylation levels of those CCaMK swaps would give further insight about the role of the EF-hand motifs of CCaMK during symbiosis.

This chapter describes the experimental procedures followed for the purification of CCaMK and the kinase assay trials performed for attempting to determine the autophosphorylation levels of the CCaMK swaps. Additionally, the purification of

CCaMK would also allow assessment of the CCaMK swaps to interact with CaM and to interact with and phosphorylate CYCLOPS.

2. Results

2.1. Expression and purification of MBP-CCaMK using a GGC expression vector from *E. coli* BL21 DE3 cells

Full-length *Medicago truncatula* CCaMK had been previously purified using an expression and purification method in *E. coli* BL21 DE3 cells developed by Akira Miyahara after which successful phosphorylation studies of CCaMK were undertaken (Miller et al., 2013; Tirichine et al., 2006). Therefore, this experimental procedure was chosen for the purification of full-length CCaMK (Chapter Two, Section 9.1) and was designated as Method 1 (Table 4.1).

Table 4. 1. Differences in the methods used for purification of CCaMK.

	Method 1	**Method 2**	**Method 3**	**Method 4**
Gene expression induction	IPTG, 28°C, 2 hours	IPTG, 18°C, overnight	IPTG, EGTA, 18°C, overnight	IPTG, 28°C, 2 hours
Protease inhibitor	✗	✓	✓	✓
EGTA in lysis and washing buffers	✗	✓	✓	✓
Lysozyme treatment	✗	✓	✓	✓
Benzonase nuclease	✗	✓	✓	✓

This method made use of a maltose binding protein (MBP) fusion vector pMaLc2x (New England Biolabs) for expression of full-length CCaMK in *E. coli* BL21 DE3 cells. MBP fusions have been proven to be a very successful method for increasing the solubility of proteins in *E. coli* and as a result, high yields of purified

protein are obtained (Kapust and Waugh, 1999). However, the ligation of the *CCaMK* cDNA into the pMaLc2x vector required a traditional cloning method based on the use of restriction digestion enzymes which constitute a low efficient method for construct building due to inefficient ligation steps and the requirement of appropriate restriction sites selection. The results presented in Chapter Three allowed the selection of some CCaMK swaps for further study based on their interesting phenotypes. However, these CCaMK swaps still constituted a considerably large number of protein variants to test for their Ca^{2+}-induced Thr271 autophosphorylation abilities. Therefore, this raised the need of a faster and more efficient method of building constructs for protein purification.

GGC has been proved to be a very fast and efficient method of cloning based on the use of type IIS restriction enzymes that allow a restriction digestion and ligation in a single reaction through the presence of unique fusion sites (Weber et al., 2011) (Chapter Two, Section 3.2). A GGC-compatible MBP-fusion vector was available in the lab that was designed by combining parts of the pMalc2x and the level 2 GGC pL2V vectors. However, this vector had not been tested yet for protein expression and purification in *E. coli*. Due to the need of a faster construct building method, this new “hybrid” GGC-compatible MBP-fusion vector, named pL2V-MBP-LacZ (Figure 4.3), was desired to be tested for expression and purification of CCaMK.

The pL2V-MBP-LacZ vector was built by performing a GGC reaction in which the red colour selectable marker CRed (encoding the canthaxanthin biosynthesis operon) (Misawa et al., 1995, 1990) located between the left and right borders of the GGC pL2V (Figure 4.1) was replaced with the sequences of the *Lac* repressor and *MBP*.

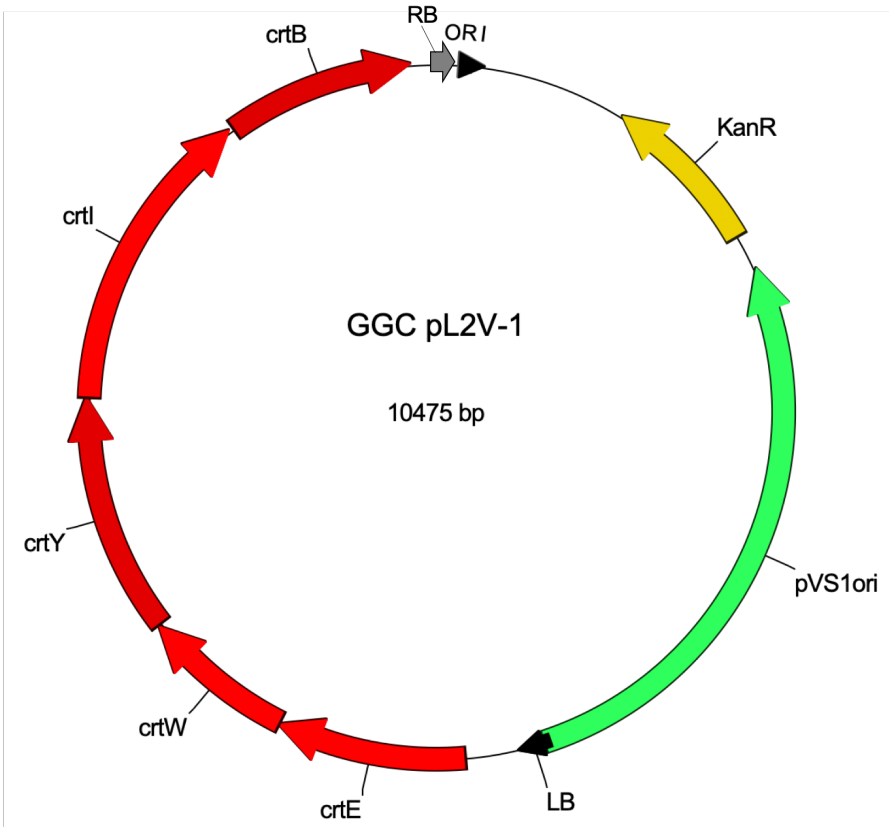

Figure 4. 1. Plasmid map of the Golden Gate cloning (GGC) level 2 vector from Weber et al., (2011).

The 5 elements of the red colour selectable marker CRed (encoding the canthaxanthin biosynthesis operon located between the left and right borders of the GGC pL2V) are indicated in different shades of red, the origin of replication for *E. coli* is indicated by a black triangle (ORI), the origin of replication for *Agrobacterium* is shaded in green (pVS1ori) and the kanamycin resistance gene (KanR) is shaded in yellow. The left border (LB) is indicated by a black arrow and the right border (RB) by a grey arrow.

However, the sequence of the GGC pL2V backbone containing the KanR gene, one origin of replication for *E. coli* and one origin of replication for *Agrobacterium* were maintained as previously designed (Weber et al., 2011). The presence of the *Agrobacterium* origin of replication has been demonstrated to not cause any alterations in *E. coli* since the GGC plasmids (containing both the *E. coli* and *Agrobacterium* origins of replications) are successfully used for plasmid propagation in *E. coli*. Likewise, these GGC plasmids are also used for *Agrobacterium*-mediated plant transformation (Chapter Three) and deleterious

effects have never been observed because of the presence of the *E. coli* origin of replication (Weber et al., 2011). The *Lac* repressor (*LacI*) is part of the *lac* operon in bacteria, composed of three genes that encode proteins involved in the transport and metabolism of lactose. The LacI is responsible for the repression of transcription of the operon and this repression can be overridden by the presence of lactose or its structural mimic IPTG. Therefore, either lactose or IPTG presence allows the initiation of the *lac* operon transcription. IPTG inducible promoters which are regulated by the LacI allow the tight regulation of protein expression as transcription can be activated when desired and not at earlier stages when impairment of cell growth might occur (Jonasson et al., 2002). Therefore, these promoters have been widely used for efficient recombinant protein purification. These promoters include the *lac* promoter (Gronenborn, 1976) which was chosen in this case for driving the expression of the *LacI* in pMaLc2X and the untested pL2V-MBP-LacZ vectors (Figures 4.2 and 4.3, respectively).

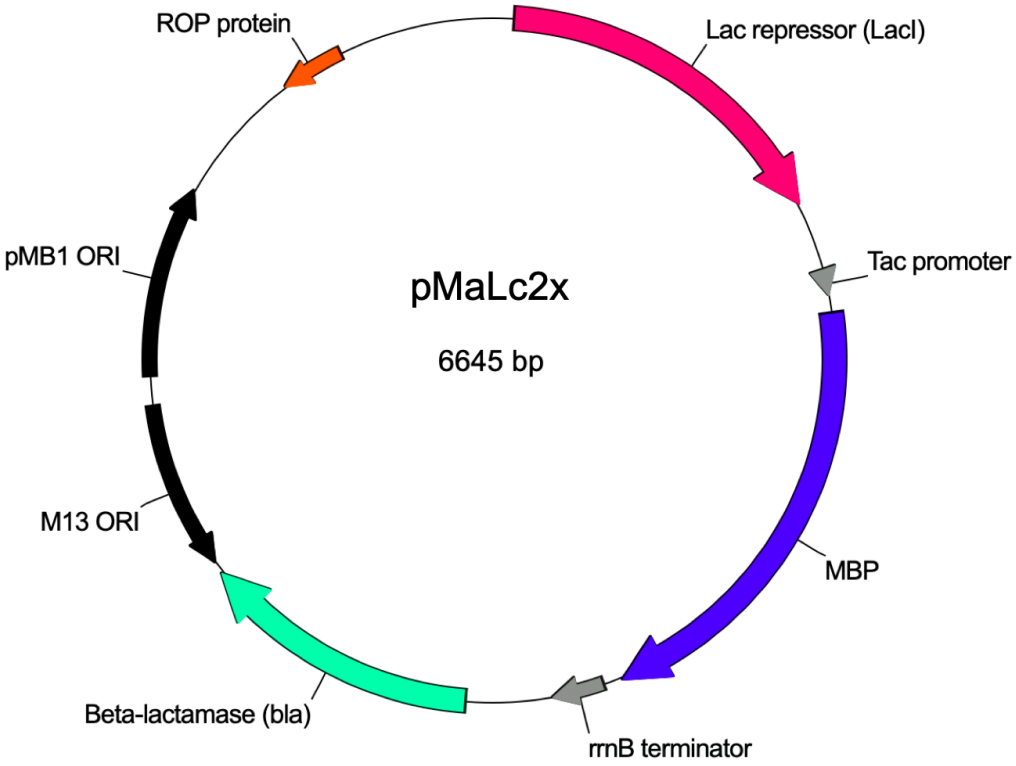

Figure 4. 2. Plasmid map of the pMaLc2x vector.

The Lac repressor (LacI) is shaded in pink, the Tac promoter is indicated by a grey triangle, the maltose-binding protein (MBP) is shaded in blue, the rrnB terminator is

indicated by a grey arrow, the Beta-lactamase (bla) is shaded in turquoise, the M13 origin of replication (M13 ORI) and pMB1 ORI are shaded in black, and the Rop protein is shaded in orange.

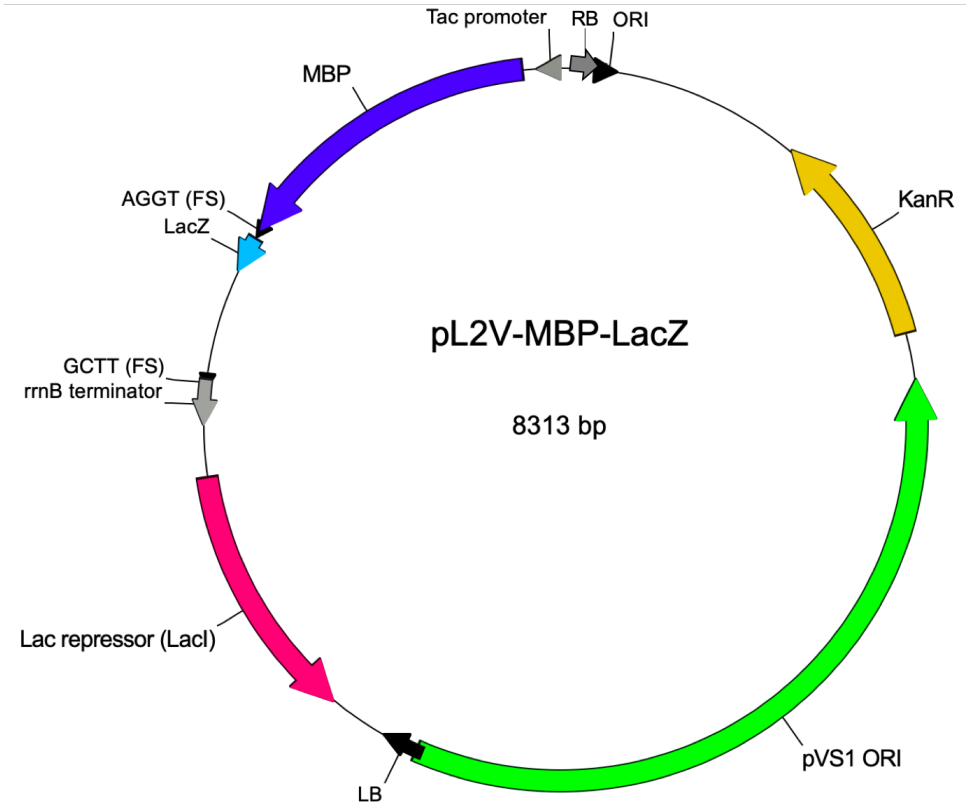

Figure 4. 3. Plasmid map of the new pL2V-MBP-LacZ expression plasmid.

The Lac repressor (LacI) is shaded in pink, the Tac promoter is indicated by a grey triangle, the maltose-binding protein (MBP) is shaded in blue, the GGC fusion sites for insertion of *CCaMK* gene are indicated as AGGT (FS) and GCTT (FS) by black triangles, the *LacZ* gene is indicated by a light blue arrow, the rrnB terminator is indicated by a grey arrow, the *Beta-lactamase* (bla) is shaded in turquoise, the origin of replication for *E. coli* is indicated by a black triangle (ORI), the origin of replication for *Agrobacterium* is shaded in green (pVS1ori) and the kanamycin resistance gene (KanR) is shaded in yellow. The left border (LB) is indicated by a black arrow.

Additionally, the *lac-trp* hybrid promoter *tac*, also inducible by IPTG, has been shown to be a strong promoter for recombinant protein expression (Amann et al., 1988; de Boer et al., 1983) and was placed to drive the expression of MBP in the pMaLc2X and the untested pL2V-MBP-LacZ vectors (Figures 4.2 and 4.3). In

addition, a *LacZ* fragment was inserted downstream of MBP for white/blue selection of clones similar to the GGC-compatible vectors (Weber et al., 2011). At both sides of *LacZ*, two BpiI type IIS restriction sites (Chapter Two, Section 3.1) were placed in reversed orientation for the replacement of *LacZ* with the gene of interest during the GGC reaction (Figure 4.3). A summary of the main elements of each plasmid can be found in Table 4.3.

Table 4. 2. Main components of the plasmids used for expression and purification of CCaMK.

Plasmid component	GGC pL2V-1	pMaLc2x	pL2V-MBP-LacZ
Insert	*cRed*	*LacI* + *MBP*	*LacI* + *MBP*
Origin of replication	pMB1 derivative (*E. coli* 500-700 copies/cell) + pVS1 (*Agrobacterium*)	pMB1 (*E. coli* 15-20 copies/cell)	pMB1 derivative (*E. coli* 500-700 copies/cell)
Antibiotic resistance	Kanamycin	Ampicillin	Kanamycin
Restriction site	BpiI	Polylinker (multiple restriction sites)	BpiI
Cloning method	GGC	Traditional	GGC

After the insertion of *CCaMK* in place of the *LacZ* in the untested pL2V-MBP-LacZ vector, purification of *MBP-CCaMK WT* from *E. coli* BL21 DE3 (named *E. coli* DE3 from this point onwards) was performed strictly following the protocol in Method 1 (Table 4.1; Chapter Two, Section 9.1). However, since the detection of Ca^{2+}-dependent T271 autophosphorylation was desired in the purified protein, it was necessary to obtain a dephosphorylated CCaMK after purification. The *E. coli* BL21(DE3)-V2R-pACYC LamP (Wernimont et al., 2010) host strain co-expressing the λ protein phosphatase from the bacteriophage lambda (λ) (named *E. coli* DE3 + P from this point onwards) was kindly provided by Kyle W. Bender which was proven effective for obtaining purified dephosphorylated CPK28 (Bender et al., 2017). Therefore, MBP-CCaMK WT was also purified from the *E.*

coli DE3 + P strain for its comparison with the purified protein from the *E. coli* DE3 (lacking the phosphatase) strain during the assessment of Ca^{2+}-induced autophosphorylation of CCaMK. In order to identify whether these two versions of the purified MBP-CCaMK WT were stable and functional proteins, kinase assays were performed for the detection of the autophosphorylation levels of CCaMK in the presence and absence of Ca^{2+}. More specifically, each version of MBP-CCaMK WT was tested under five conditions (Figure 4.4): in the presence of Mg^{2+} with added the Ca^{2+}-chelator EGTA (this condition was considered equivalent to basal [Ca^{2+}] or the absence of Ca^{2+} spiking); in the presence of Mg^{2+} and either 0.2, 0.4 or 0.6 mM of Ca^{2+}; and lastly, the purified proteins were incubated with water-only (condition named as "none") which allowed the identification of the phosphorylation levels of each protein straight after purification (Chapter Two, Section 9.1 and 9.4).

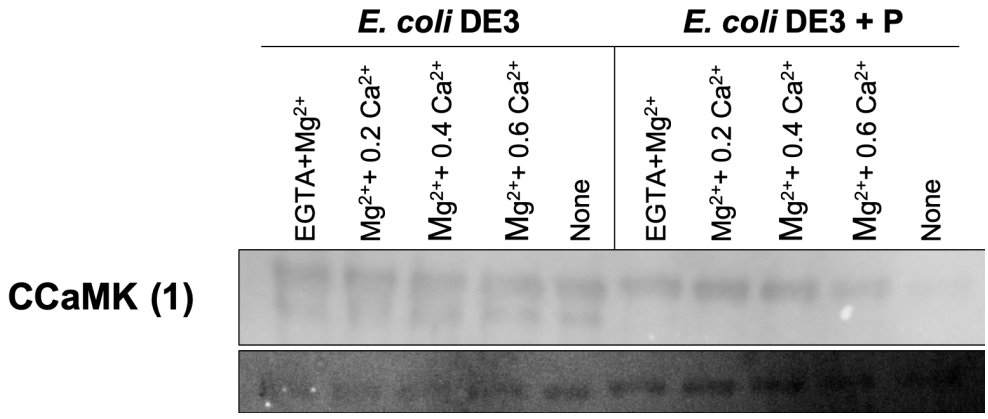

Figure 4. 4. Detection of CCaMK WT Ca^{2+}-dependent autophosphorylation by western blotting using the pIMAGO technology.

MBP-CCaMK WT was purified from both *E. coli* BL21 DE3 (*E. coli* DE3) and *E. coli* BL21(DE3)-V2R-pACYC LamP host strain (*E. coli* DE3 + P) co-expressing the λ protein phosphatase from the bacteriophage lambda (λ). The two *MBP-CCaMK WT* proteins were tested in the presence of 10 mM Mg^{2+} with added 5 mM Ca^{2+}-chelator EGTA (this condition was considered equivalent to basal cellular [Ca^{2+}] or the absence of Ca^{2+} spiking); in the presence of 10 mM Mg^{2+} and either 0.2, 0.4 or 0.6 mM of Ca^{2+} (Mg^{2+}+ 0.2 Ca^{2+}; Mg^{2+}+ 0.4 Ca^{2+}; Mg^{2+}+ 0.6 Ca^{2+}, respectively); and lastly, the purified proteins were incubated with water-only (condition labelled as "none") to detect phosphorylation levels of each protein after purification.

2.2. Detection of Ca^{2+}-dependent autophosphorylation of CCaMK WT via the pIMAGO technology

In order to detect the Ca^{2+}-dependent autophosphorylation levels of MBP-CCaMK WT purified from *E. coli* BL21 DE3 either co-expressing or lacking the λ phosphatase, the non-antibody strategy pIMAGO (Iliuk and Tao, 2015) was used for autophosphorylation detection during western blotting. The pIMAGO technology allows the specific detection of any phosphate groups regardless whether the phosphorylation occurs at Ser, Thr or Tyr residues and has been successfully used for previous Ca^{2+}-induced phosphorylation studies of other Ca^{2+} binding proteins (Bender et al., 2017). Since assessment of the Ca^{2+}-induced autophosphorylation at Thr271 of CCaMK WT was desired, the pIMAGO technology could appear unsuitable for this purpose due to the lack of specificity in the detection of any phosphate groups (detection on either Ser, Thr or Tyr). However, it was possible that this technology could be appropriate as the residue Thr271 of CCaMK has previously been shown to be the main autophosphorylation site of CCaMK (Miller et al., 2013).

The pIMAGO detection of the autophosphorylation levels of CCaMK WT purified from either *E. coli* DE3 + P (co-expressing the λ phosphatase) or *E. coli* DE3 (lacking the λ phosphatase) host strains revealed differences between the two purified proteins. As it can be observed in Figure 4.4, when purification was performed from *E. coli* DE3, an additional band below the CCaMK expected size (~110 kDa: MBP 42.5 kDa + CCaMK 58 kDa) band was obtained. In addition, no differences in phosphorylation levels under the five different conditions mentioned above could be observed, indicating that this protein was possibly not stable or in the right structural state to respond to Ca^{2+}. However, when CCaMK WT was purified from *E. coli* DE3 + P, a unique band of the expected size and a gradual increase in the autophosphorylation levels over increasing [Ca^{2+}] was observed, with low levels of autophosphorylation in the “none” condition (Figure 4.4). These results confirmed that co-expressing the phosphatase in *E. coli* DE3 cells allowed the purification of a more stable and active version of CCaMK WT and it was therefore decided that the *E. coli* DE3 + P host strain would be used for all following protein purification experiments. In addition, the pIMAGO technology seemed to be sensitive enough to detect the changes in CCaMK

autophosphorylation in the presence and absence of Ca^{2+} and was also decided to be used for future experiments.

After the protein purification and Ca^{2+}-dependent autophosphorylation detection methods were confirmed to be suitable for CCaMK autophosphorylation studies, a further test was decided to be performed including the CCaMK T271A mutant which is impaired for Ca^{2+}-dependent autophosphorylation (Miller et al., 2013). The CCaMK T271A mutant would constitute the negative control of future autophosphorylation studies of the CCaMK swaps and this would also be a further confirmation of the suitability of these methods for these studies. Since the CCaMK T271A was going to be purified, the CCaMK WT was purified again alongside it. This version of the purified CCaMK WT was named as CCaMK (2) (Table 4.2) and was compared to the previously purified and tested CCaMK WT (Figure 4.4) named as CCaMK (1) (Table 4.2) to confirm the reproducibility of the purification method employed.

Table 4. 3. Different batches of purified CCaMK following the methods summarised in Table 4.1.

CCaMK batch	Expression vector	Purification method
CCaMK (1)	pL2V-MBP-LacZ	Method 1
CCaMK (2)	pL2V-MBP-LacZ	Method 1
CCaMK (3)	pL2V-MBP-LacZ	Method 2
CCaMK (4)	pL2V-MBP-LacZ	Method 3
pMaLc2x-CCaMK (5)	pMaLc2x	Method 4
pMaLc2x-CCaMK (6)	pMaLc2x	Method 3

Therefore, after purification of both CCaMK (2) and T271A, their Ca^{2+}-dependent autophosphorylation levels were tested in the presence and absence of Ca^{2+} by western blotting using the pIMAGO technology, and CCaMK (1) (Figure 4.4) was included as a control. In this case and based on the results shown in Figure 4.4, the kinase assays were performed under four conditions which included the absence of Ca^{2+}, presence of 0.2 mM of Ca^{2+}, in the presence of both 0.2 mM Ca^{2+} and CaM, and water-only ("none") (Figure 4.5).

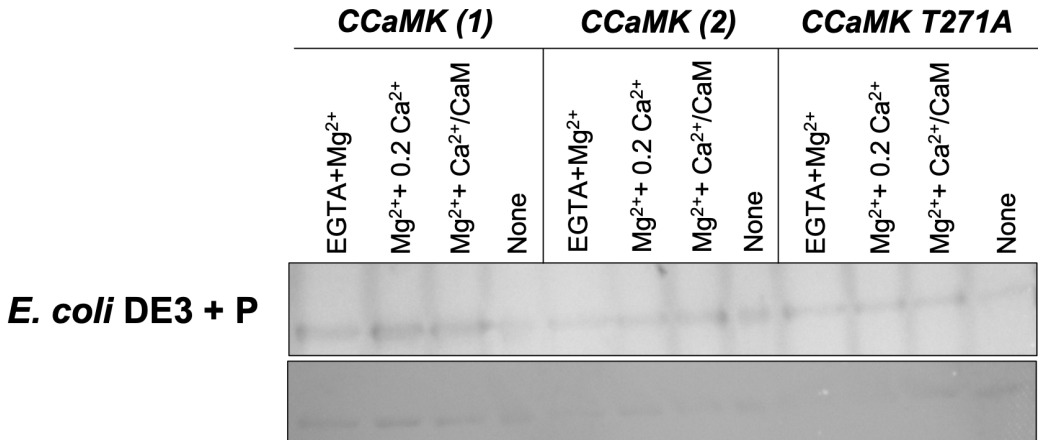

Figure 4. 5. Detection of CCaMK WT and T271A Ca^{2+}-dependent autophosphorylation by western blotting using the pIMAGO technology.

Two different batches of purified CCaMK WT (CCaMK (1) and CCaMK (2)) were included in addition to CCaMK T271A and kinase assays were performed under four conditions which included: in the presence of 10 mM Mg^{2+} with added Ca^{2+}-chelator 5 mM EGTA (EGTA+ Mg^{2+}), in the presence of 10 mM Mg^{2+} and 0.2 mM of Ca^{2+} (Mg^{2+}+ 0.2 Ca^{2+}) and lastly, the purified proteins were incubated with water-only (condition labelled as "none") to detect phosphorylation levels of each protein after purification.

Surprisingly, despite strictly following the experimental procedures explained above, the obtained results were different. Although a unique band of the expected size (~110 kDa) was still obtained for the three proteins tested under the four conditions, both the CCaMK (2) and T271A seemed to not respond to Ca^{2+} as changes in their Ca^{2+}-dependent autophosphorylation levels were not observed. In contrast, the phosphorylation levels of these proteins after purification were already high which is noticeable because of the strong intensity of the band obtained for the "none" condition. Therefore, since CCaMK (2) was

unable to show any Ca^{2+}-induced autophosphorylation and both CCaMK (2) and CCaMK T271A were purified side-by-side under the exact same conditions, it is possible that these two proteins may have been obtained in an inactive or misfolded state after purification. In contrast, CCaMK (1) showed lower levels of phosphorylation straight after purification ("none" condition) and was still able to respond to Ca^{2+} with visible increases in autophosphorylation in the Ca^{2+} and Ca^{2+}/CaM conditions compared to in the non-Ca^{2+} conditions (Figure 4.5). According to the CCaMK model of activation, binding of CaM to CCaMK (upon binding of Ca^{2+} through the CCaMK EF-hand motifs) inhibits the autophosphorylation of CCaMK at Thr271 in the presence of Ca^{2+} (Miller et al., 2013). This inhibition of Thr271 autophosphorylation by CaM has previously been observed using a state-specific antibody via western blotting (Miller et al., 2013). Consistently, it was expected that the addition of CaM would inhibit Ca^{2+}-dependent autophosphorylation as previously reported (Miller et al., 2013), but this was not observed (Figure 4.5). As a consequence, these results indicate that the purified CCaMK proteins were possibly not being obtained at their optimum structural state to allow their Ca^{2+}-induced activation according to what was previously observed.

These results suggested that the protein purification method employed may not be as reproducible and robust as originally thought, and that inactive or structure-defective proteins were being obtained. Since a high number of CCaMK swaps were potentially going to be purified, the protein purification protocol was required to produce reliable results. Furthermore, high levels of CCaMK phosphorylation after purification could be observed in the "none" condition despite the co-expression of the λ phosphatase (Figure 4.5). Therefore, changes to the protein purification protocol were first made with the aim of obtaining purified CCaMK in the right structural conformation with Ca^{2+}-dependent autophosphorylation ability.

2.3. Improvement of the CCaMK purification protocol and antibody detection of Ca^{2+}-dependent autophosphorylation of CCaMK

In Method 1 (Table 4.1), the induction of gene expression was performed at 28°C for 2 hours. However, the application of low temperatures over long periods of incubation during gene expression induction has been proved to result in correct

folding of recombinant proteins because the protein production slows down which reduces the probability of protein aggregation (Vera et al., 2007; Schein, 1989). Therefore, the gene induction was tested overnight in the presence of IPTG at 18°C rather than at 28°C for 2 hours.

A higher protein purification yield was also desired as it would increase the probability of producing higher amounts of high-quality protein. Therefore, the possible deleterious effect of proteolytic enzymes after cell lysis was intended to be solved by adding a commercially available protease inhibitor cocktail (Chapter Two, Section 9.2). In addition, the presence of metal chelators such as ethylenediaminetetraacetic acid (EDTA) and ethylene glycol-bis(β-aminoethyl ether)-N,N,N′,N′-tetraacetic acid (EGTA) is known to inactivate metalloproteases and therefore stop these enzymes from cleaving the purified proteins (Barletta et al., 1996). Therefore, in order to increase the amount of metal chelator, EGTA was added in addition to EDTA to the lysis and washing buffers used during CCaMK purification (Table 2.12). In addition, the presence of EGTA would also remove any free-Ca^{2+} which theoretically should not allow any Ca^{2+}-induced autophosphorylation of CCaMK and thus, reduce the autophosphorylation levels of the purified protein. Furthermore, EGTA was also added during the induction of gene expression in the presence of IPTG as this was previously reported to be successful in the purification of dephosphorylated proteins (Bender et al., 2017). Since the effect of adding EGTA during induction with IPTG was not previously established within the protocol for CCaMK purification, two versions of the protein purification protocol were performed which differed in the absence or presence of EGTA during gene expression induction with IPTG (Methods 2 and 3, respectively; Table 4.1). Therefore, CCaMK WT was purified twice following Methods 2 and 3 (Table 4.1), and the purified proteins were named as CCaMK (3) and CCaMK (4) (Table 4.2) respectively (Figure 4.6).

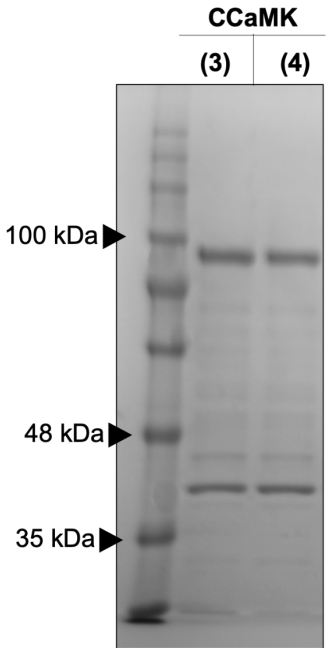

Figure 4. 6. CCaMK WT (3) and (4) were purified following Methods 2 and 3 in Table 4.1, respectively and run in an SDS-PAGE gel for size identification.

Both methods yielded approximately 400-800 ng/μL of MBP-CCaMK protein. A strong band of approximately 40 kDa always appeared below the band from MBP-CCaMK (~110 kDa), very likely corresponding to cleaved MBP due to its size (~42.5 kDa).

Moreover, a 20-minute incubation step with lysozyme was added in both Methods 2 and 3 (Table 4.1) in order to enzymatically digest the cell walls prior to mechanical cell breakage with the French press cell disrupter (Smékal, 1973). This would ensure maximum cell lysis and protein extraction. Additionally, it was recommended by the lysozyme manufacturer (Thermo Fisher Scientific) to use both lysozyme and a nuclease such as DNaseI for the effective lysis of *E. coli* cells. The use of a nuclease would remove the nucleic acids from the sample, reducing the viscosity of the cell lysate and increasing the protein extraction yield. Therefore, the Benzonase Nuclease (Sigma-Aldrich), which is able to degrade all forms of DNA and RNA, was also added in both Methods 2 and 3 after the incubation with lysozyme in order to improve the efficiency of the French press cell lysis (Structural Genomics Consortium et al., 2008).

The modifications made to the protein purification method did not produce higher concentrations of protein than the previous purification method, with both strategies yielding approximately 400-800 ng/μL MBP-CCaMK protein. However, the concentration of protein does not constitute an indication of high-quality protein and kinase assays were necessary to conclude whether the purified protein was an active protein. It was noticeable that a strong band of approximately 40 kDa always appeared below the band from MBP-CCaMK (~110 kDa), very likely corresponding to cleaved MBP due to its size (~42.5 kDa) (Figure 4.6). CCaMK (3) and (4), induced either in the absence or presence of EGTA respectively during induction with IPTG, were tested for Ca^{2+}-dependent autophosphorylation. In contrast to earlier experiments, in this case the pIMAGO technology was not used for detection of autophosphorylation in western blotting. In the previous test to detect Ca^{2+}-dependent autophosphorylation of CCaMK, high levels of phosphorylation were detected even when the protein was only incubated with water ("none') (Figure 4.5). The pIMAGO technology is able to detect any phosphate groups regardless whether on Ser, Thr and/or Tyr residues. However, Ca^{2+}-induced autophosphorylation specifically on Thr was desired to be tested and therefore, a commercially available antibody specific for the detection of phosphorylated-Thr was chosen instead of pIMAGO (Chapter Two, Section 9.5).

A kinase assay was performed to detect Ca^{2+}-dependent autophosphorylation on the CCaMK (3) and (4) proteins (purified using Methods 2 and 3, respectively; Table 4.1) and CCaMK (1) (Table 4.2) was included as a control. Using a commercially available antiphosphothreonine antibody (α-PThr) from Sigma, no difference in the autophosphorylation levels of CCaMK was observed either in the presence or absence of Ca^{2+}. Moreover, detectable levels of Thr-phosphorylation could be observed in the "none" condition despite the addition of EGTA (Ca^{2+} chelator) and the co-expression of the λ phosphatase (Figure 4.7).

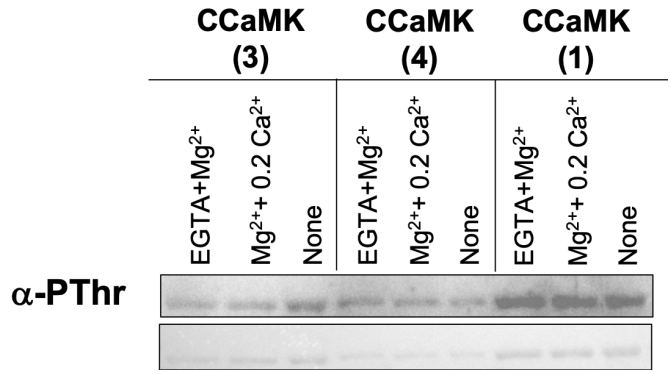

Figure 4. 7. Detection of CCaMK WT Ca^{2+}-dependent autophosphorylation using a commercially available antiphosphothreonine antibody (α-PThr).

CCaMK (3) and (4) proteins (purified using Methods 2 and 3, respectively; Table 4.1) and CCaMK (1) (Table 4.2) included as a control, were tested for Ca^{2+}-dependent autophosphorylation. Kinase assays were performed under three conditions which included the absence of Ca^{2+} (EGTA+Mg^{2+}), 10 mM Mg^{2+} in the presence of 0.2 mM of Ca^{2+} (Mg^{2+}+ 0.2 Ca^{2+}) and water-only ("none"). Detectable levels of Thr-phosphorylation could be observed in the "none" condition despite the addition of EGTA (Ca^{2+} chelator) and the co-expression of the λ phosphatase during protein purification. No differences in the autophosphorylation levels of CCaMK were observed either in the presence or absence of Ca^{2+}.

This suggests that CCaMK (3) and (4) for unknown reasons, were still non-active proteins after purification as they were not able to respond to Ca^{2+} concentrations equivalent to those during symbiotic Ca^{2+} spiking and employed in previous autophosphorylation studies (Shimoda et al., 2012; Miller et al., 2013). Moreover, co-expression of the λ phosphatase seemed to be insufficient to stop the phosphorylation of CCaMK by endogenous *E. coli* protein kinases as previously reported for other recombinant proteins (Yang and Liu, 2004).

Despite the lack of response of the newly purified CCaMK WT proteins to 0.2 mM of Ca^{2+}, it was considered whether the proteins would respond to higher [Ca^{2+}]. In fact, there was the possibility that the purification protocol was producing structurally altered proteins that may respond to Ca^{2+} differently from CCaMK WT. Therefore, both CCaMK (3) and (4) were subjected to another Ca^{2+}-dependent autophosphorylation test that included a significantly higher [Ca^{2+}] corresponding to 10 mM (Figure 4.8). None of the two CCaMK proteins showed

any changes in Ca^{2+}-dependent autophosphorylation. Consequently, this confirmed that neither CCaMK (3) or (4) were able to autophosphorylate on Thr in a Ca^{2+}-dependent manner (Figure 4.8).

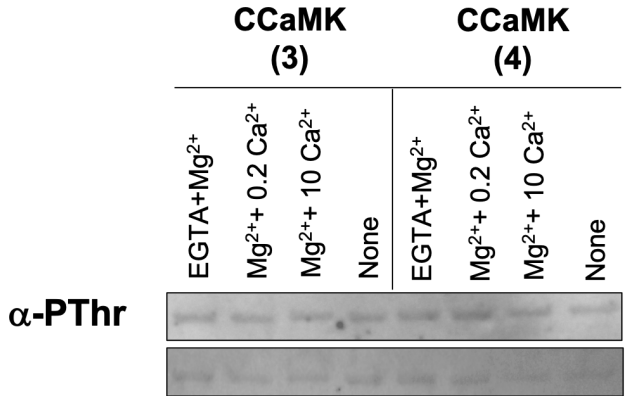

Figure 4. 8. Detection of CCaMK WT Ca^{2+}-dependent autophosphorylation using a commercially available antiphosphothreonine antibody (α-PThr).

CCaMK (3) and (4) proteins (purified using Methods 2 and 3, respectively; Table 4.1) were tested for Ca^{2+}-dependent autophosphorylation in the presence of higher [Ca^{2+}]. Kinase assays were performed under four conditions which included the absence of Ca^{2+} (5 mM EGTA and 10 mM of Mg^{2+}; EGTA+Mg^{2+}), presence of 0.2 mM of Ca^{2+} (Mg^{2+}+ 0.2 Ca^{2+}), presence of 10 mM of Ca^{2+} (Mg^{2+}+ 10Ca^{2+}) and water-only ("none"). Detectable levels of Thr-phosphorylation could be observed in the "none" condition despite the addition of EGTA (Ca^{2+} chelator) and the co-expression of the λ phosphatase during protein purification. No differences in the autophosphorylation levels of CCaMK were observed either in the presence or absence of Ca^{2+}.

After several rounds of purification, kinase assays and western blotting, similar results were obtained. The MBP-CCaMK fusion protein was previously reported to be successfully purified providing a good quality protein with kinase activity and able to be autophosphorylated on Thr in a Ca^{2+}-dependent manner (Miller et al., 2013). Despite this experimental protocol being strictly followed, good quality protein could not be obtained even when potential improvements were attempted. However, it is important to realise that the MBP fusion vector used in these experiments was different from the one previously used and in fact, had not been tested previously for protein expression and purification. Therefore, in order to identify whether the expression vector used for CCaMK expression in *E. coli* DE3

+ P cells was responsible for the bad quality CCaMK protein obtained after purification, it was decided to express and purify CCaMK WT protein from the pMaLc2x-MBP fusion vector used previously by Akira Miyahara (Tirichine et al., 2006; Miller et al., 2013).

2.4. Purification of CCaMK using the pMaLc2x MBP fusion vector and antibody detection of Ca^{2+}-dependent autophosphorylation

The pMaLc2x-MBP-CCaMK was purified following Method 2 (Chapter Two, Section 9.2) which contained a series of additions/modifications of the original purification protocol (Method 1, Tirichine et al., 2006). While most of the additions such as the treatments with Lysozyme and Benzonase nuclease were considered minor changes that could clearly improve the protein purification process, the difference between the gene expression induction for 2 hours at 28 °C and overnight at 18 °C was still unclear. This is due to the fact that none of the purified CCaMK proteins obtained by the different methods employed (Table 4.1) showed any activity (lack of Ca^{2+}-induced Thr-autophosphorylation). Therefore, both the gene expression induction for 2 hours at 28 °C and overnight at 18 °C were compared and two batches of the pMaLc2x-MBP-CCaMK WT were produced. The MBP-CCaMK protein that was induced at 28 °C for 2 hours was named as pMaLc2x-CCaMK (5) and the protein induced overnight at 18 °C was named as pMaLc2x-CCaMK (6) (Table 4.2).

It was very surprising to observe that the same experimental procedure followed for the purification of pL2V-MBP-CCaMK (previously untested GGC-compatible MBP fusion vector) produced a very high yield of protein when used for the purification of CCaMK from the pMaLc2x fusion vector (Figure 4.9). A concentration between 1.5 and 2.5 μg/μL was obtained for the two purified CCaMK proteins under the different induction conditions (Figure 4.9), as opposed to the previously protein concentrations obtained of 400-800 ng/μL (Figure 4.5). While a band of ~42 kDa corresponding to the size of MBP was still obtained below MBP-CCaMK after the pMaLc2x-MBP-CCaMK purification, the ratio of MBP-CCaMK to cleaved MBP was very high indicating that the majority of the purified product corresponded to MBP-CCaMK (Figure 4.9).

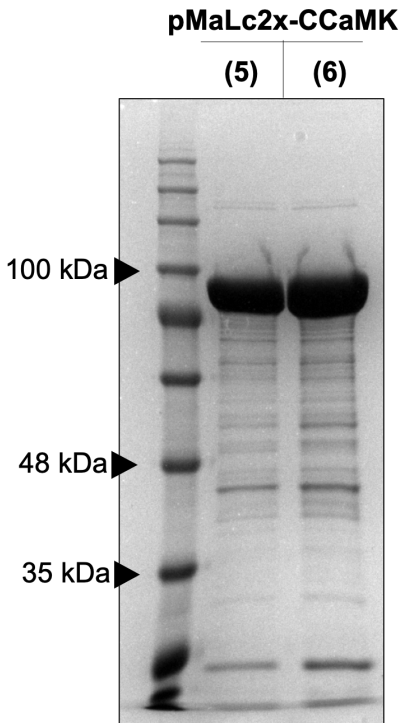

Figure 4. 9. pMaLc2x-CCaMK WT was purified twice following Methods 3 and 4 in Table 4.1 and run on an SDS-PAGE gel for size identification.

A concentration between 1.5 and 2.5 μg/μL MBP-CCaMK protein was obtained. A strong band of approximately 110 kDa was obtained corresponding to MBP-CCaMK. A band 40 kDa was still obtained very likely corresponding to cleaved MBP due to its size (~42.5 kDa), but the ratio MBP-CCaMK:MBP is much higher than when CCaMK was purified using the pL2V-GGC vector.

This suggested that the modifications made to Method 1 were indeed beneficial and that good protein yields could be obtained. Moreover, a higher protein concentration was obtained for the pMaLc2x-CCaMK (6) than for pMaLc2x-CCaMK (5), as can be observed in Figure 4.9. However, a high protein concentration was not considered indicative of good protein quality and these two MBP-CCaMK proteins purified from the pMaLc2x vector were therefore tested for their ability to autophosphorylate on Thr in a Ca^{2+}-dependent manner.

Kinase assays were performed for both the pMaLc2x-CCaMK (5) and (6) along with the CCaMK (1) (GGC backbone) for comparison and this was followed by detection of Thr-autophosphorylation using the α-PThr antibody from Sigma as previously (Figure 4.10).

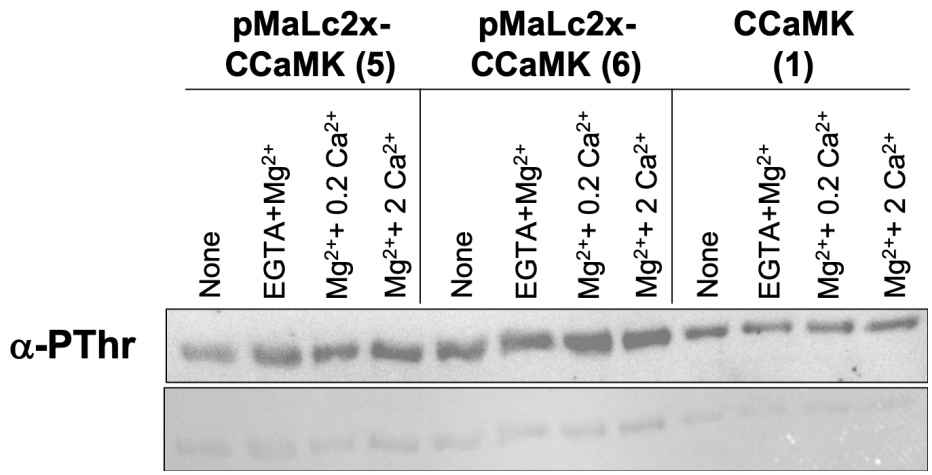

Figure 4. 10. Detection of Ca^{2+}-dependent autophosphorylation of MBP-CCaMK WT expressed and purified from the pMaLc2x vector using the commercially available antiphosphothreonine antibody (α-PThr).

Kinase assays were performed for both the pMaLc2x-CCaMK (5) and (6) (Table 4.2) along with the CCaMK (1) (GGC backbone) for comparison under four conditions, as indicated: absence of Ca^{2+} consisting of 5 mM EGTA and 10 mM Mg^{2+} (EGTA+Mg^{2+}), presence of 10 mM Mg^{2+} and 0.2 mM of Ca^{2+} (Mg^{2+}+ 0.2 Ca^{2+}), presence of 10 mM Mg^{2+} and 2 mM of Ca^{2+} (Mg^{2+}+ 2 Ca^{2+}) and water-only ("none").

Surprisingly, the pMalc2x-CCaMK (6) (expression overnight at 18 °C) was able to respond to 0.2 mM of Ca^{2+} with increasing levels of Thr autophosphorylation compared to in the absence of Ca^{2+} (Figure 4.10) as previously reported (Miller et al., 2013). Additionally, the increased amount of Ca^{2+} from 0.2 to 2 mM caused a reduction in Thr-phosphorylation also consistent with previous published results (Miller et al., 2013). In contrast, neither the pMaLc2x-CCaMK (5) (expression at 28 °C) nor the CCaMK (1) were able to respond to Ca^{2+} according to what was previously reported (Figure 4.10). Consequently, this suggested that the GGC-compatible MBP fusion vector available in the lab was actually not allowing the purification of a good quality CCaMK protein. In addition, these results also demonstrated that the new version of the purification protocol including the gene induction step at lower temperatures for a longer period of time had a positive effect and allowed the production of a well-folded fully active purified protein.

3. Discussion

3.1. Assessing the Ca^{2+}-dependent autophosphorylation levels of CCaMK

The work presented in this chapter has established the experimental procedures required for assessment of the Ca^{2+}-dependent Thr-autophosphorylation capabilities of CCaMK, and therefore, of the CCaMK swaps. The new hybrid MBP fusion vector, pL2V-MBP-LacZ, composed of the vector backbone from the GGC pL2V and the LacI and MBP elements from the pMaLc2x (Figure 4.3; Table 4.3) was demonstrated not to be suitable for CCaMK purification. The assessment of Ca^{2+}-dependent autophosphorylation showed that the CCaMK protein purified using the pL2V-MBP-LacZ vector was not an active protein as changes in autophosphorylation were not observed in the presence of any [Ca^{2+}] regardless the method of detection employed during western blotting, either the pIMAGO or the α-PThr antibody (Figures 4.4, 4.5, 4.7 and 4.8). This was further confirmed by the fact that when CCaMK was purified using the pMaLc2x MBP fusion vector, detection of Ca^{2+}-dependent autophosphorylation was possible using the α-PThr antibody (Figure 4.10).

The pL2V-MBP-LacZ (Figure 4.3) was carefully built to contain the components that were thought necessary for high expression of CCaMK from the pMaLc2x vector (Figure 4.2) but also, containing the necessary elements of the GGC pL2V vector (Figure 4.1) that would enable to clone into via GGC (Figure 4.3; Table 4.3). It is important to point out that the new pL2V-MBP-LacZ vector contained two origins of replication, one for *E. coli* of a different sequence from that in the pMaLc2x vector and one for *Agrobacterium*. It is important to realise that the pMaLc2x backbone also contained the sequence of the *Rop* gene, also known as *Rom* (RNA one modulator) which has an important function during plasmid replication and in conjunction with the pMB1 origin of replication (~15-20 copies/cell) is responsible for maintaining the low copy number of the plasmid (Atlung et al., 1999). High-copy plasmids can be thought as ideal for obtaining a high protein yield, but this is not always the case. In fact, a high copy number may cause an excessive metabolic burden that decreases cell growth and stability of the plasmid but could also lead to protein aggregation and defects in

post-translational modifications that reduce the protein yield (Rosano and Ceccarelli, 2014; Birnbaum and Bailey, 1991). Consistently, the pL2V-MBP-LacZ contained the backbone of the GGC pL2V which is derived from the pUC vectors, considered high-copy number plasmids due to their origin of replication corresponding to a pMB1 derivative that allows the production of 500-700 plasmid copies per cell (Minton, 1984; Weber et al., 2011; Lin-Chao et al., 1992). As a result, the difference in copy number between the pMaLc2x (~15-20 copies/cell) and the pL2V (500-700 copies/cell) vector backbones might be responsible for the inability to obtain a good quality CCaMK protein when using the pL2V-MBP-LacZ for expression. Since Ca^{2+}-dependent autophosphorylation of the CCaMK swaps is still desired to be addressed, a GGC-compatible MBP fusion vector would still be necessary for facilitating the construct building for purification of the CCaMK swaps. This construct could be built by simply substituting the polylinker region (containing multiple restriction sites for traditional cloning located downstream of the *MBP* in the pMaLc2x vector) for the sequence of *LacZ* flanked by two BpiI sites placed in reverse orientation from each other, which would allow the insertion of the sequence of CCaMK by a GGC reaction. As a result, the new vector would be exactly the same as the pMaLc2x MBP fusion vector but compatible for GGC.

The use of the pIMAGO technology (Iliuk and Tao, 2015) was also confirmed for the detection of the Ca^{2+}-dependent phosphorylation of CCaMK (Figure 4.1 and 4.2). However, the ability of the pIMAGO reagent to detect phosphate groups on either Ser, Thr or Tyr residues did not allow detection of significant increases in autophosphorylation between the presence and absence of Ca^{2+}. However, it is also worth mentioning that the pIMAGO technology was not used for detection of the Ca^{2+}-dependent autophosphorylation of the MBP-CCaMK expressed from the pMalc2x vector (pMalc2x-CCaMK (6) in Table 4.2). The ability of pMaLc2x-CCaMK (6) to autophosphorylate on Thr271 in a Ca^{2+}-dependent manner was observed via detection with the α-PThr antibody (Figure 4.10) and pIMAGO might be sensitive enough to detect it as well. The lack of specificity of the pIMAGO reagent in the detection of phosphate groups was the reason why the α-PThr antibody was thought to be a better choice for Ca^{2+}-dependent

autophosphorylation detection in CCaMK since detection of Thr271 autophosphorylation was actually the aim of these experiments. Despite the specificity of the antibody for phosphorylated threonines and its ability to detect the Ca^{2+}-dependent autophosphorylation of CCaMK purified using the pMaLc2x vector (Figure 4.10), this method was not guaranteed to only show the autophophorylation at Thr271 of CCaMK, which was previously demonstrated to be the main autophosphorylation site of CCaMK (Miller et al., 2013). The existence of other phosphorylatable Thr residues in CCaMK cannot be ruled out and therefore, a state specific antibody that would detect specifically the phosphorylated Thr271 residue would be ideal for future assessments of Thr271 autophosphorylation of the CCaMK swaps, as used in published studies (Miller et al., 2013). Alternatively, radioactive phosphate γ-^{32}p could also be employed for autophosphorylation detection as its use in *in vitro* kinase assays has also been shown to be successful for the assessment of the kinase activity of CCaMK (Shimoda et al., 2012). The antibody detection of autophosphorylation does not only show the autophosphorylation that occurred during the kinase assays but also any phosphorylation that occurred during expression in *E. coli* and purification of the protein, possibly making it more difficult to visibly identify differences in phosphorylation. This could be observed when both pIMAGO and the α-PThr antibody were used for detection of autophosphorylation of CCaMK as high levels of phosphorylation could be detected in the purified protein incubated with water only. This resulted in very subtle differences in autophosphorylation visually detected between the presence and absence of Ca^{2+} (Figure 4.10). Therefore, radiation could constitute a more sensitive, non-saturating method for visually detecting differences in Ca^{2+}-dependent autophosphorylation of CCaMK if a state specific antibody was not available.

The encountered challenges mentioned above and the lack of time for further experiments once the troubleshooting was done resulted in the inability to test the Ca^{2+}-dependent Thr271-autophosphorylation ability of the CCaMK swaps. Despite this, the results presented in Chapter Three and the published literature regarding the autophosphorylation and Ca^{2+} binding capabilities of many identified CCaMK mutants still allow to make predictions about some of the

CCaMK swaps' ability to bind Ca^{2+} through their EF-hands and their autophosphorylation capabilities.

3.2. Potential impact of interchanging EF-loops on Ca^{2+}-dependent Thr271-autophosphorylation of CCaMK

The interchange of the EF-hand loop primary sequences of CCaMK was performed considering that the tertiary structure of the EF-hand motifs and overall of CCaMK would not be disturbed (Chapter Three). Since the EF-hand motifs 2 and 3 of CCaMK were previously demonstrated to have similar calcium binding affinities (Swainsbury et al., 2012), their interchange was predicted to not have any effect on the ability of CCaMK to activate the signalling response to the symbiotic Ca^{2+} spiking. However, this was not the case as neither nodulation nor spontaneous gene expression was induced by CCaMK 1-3-2-4 (Chapter Three, Figure 3.5 and Figure 3.7). In addition to CCaMK 1-3-2-4, over 50% of the CCaMK swaps also behaved in a similar manner as neither formation of fully mature nodules nor spontaneous gene expression were observed for these mutants (Chapter Three, Figure 3.6 and Figure 3.7).

As discussed in Chapter Three, the lack of nodulation complementation or spontaneous gene expression could be due to the modification of the Ca^{2+} binding properties or Ca^{2+} binding impairment to the EF-hand motifs of the CCaMK swaps and this could impact on their Ca^{2+}-dependent Thr271-autophosphorylation capabilities. For instance, this is the case for the triple EF-hand point CCaMK mutant which has Ca^{2+} binding impaired through EF-hands 2, 3 and 4 (Swainsbury et al., 2012) and was not able to autophosphorylate on Thr271 in the presence of Ca^{2+} (Miller et al., 2013). Consistently, the Thr271 autophosphorylation is dependent on Ca^{2+} binding through the EF-hands (Sathyanarayanan et al., 2001; Miller et al., 2013). Therefore, the inability of the CCaMK 1-3-2-4, along with the other CCaMK swaps, to allow nodulation complementation could imply that these CCaMK swaps might also be impaired in Ca^{2+} binding through their EF-hand motifs and that would not be able to autophosphorylate on Thr271 either. In addition, the CCaMK single and double

EF-hand point mutants with impaired Ca^{2+} binding through either one and/or two EF-hand motifs were also found to be defective in Thr271 autophosphorylation although partial complementation and spontaneous gene expression was induced by these mutants (Miller et al., 2013; Chapter Three of this work). Both the CCaMK 1-3-4-2 and 2-3-1-4 were able to induce nodule organogenesis and spontaneous gene expression (Chapter Three, Figure 3.5 and Figure 3.7) which resembles the phenotype of the single and double EF-hand point mutants of CCaMK. It therefore follows that the CCaMK swaps 1-3-4-2 and 2-3-1-4 might also be unable to perform Thr271 autophosphorylation in the presence of Ca^{2+} due to impairment of Ca^{2+} binding to one and/or two of their EF-hand motifs. Lastly, CCaMK 3-2-1-4 was the only CCaMK swap that enabled full complementation of the *ccamk* mutant as fully mature nodules were observed although at lower frequency than CCaMK WT (Chapter Three, Figure 3.6 and Figure 3.7). However, the CCaMK 3-2-1-4 was unable to induce spontaneous gene induction. As a result, the full complementation but lack of spontaneous gene expression ability of the CCaMK 3-2-1-4 could be resembling CCaMK WT phenotype. Along with the lack of spontaneous gene expression, this indicates that CCaMK 3-2-1-4 might have actually preserved some Thr271 autophosphorylation ability in the presence of Ca^{2+}. Therefore, the CCaMK 3-2-1-4 might be able to bind Ca^{2+} through the three EF-hand motifs, allowing its negative regulation via Thr271-autophosphorylation and indicating that this CCaMK swap might require the Ca^{2+} spiking in order to be activated. Nevertheless, the modification of the EF-hand motif sequences could result in alterations to the overall protein structure. This supports the fact that the CCaMK 3-2-1-4 allowed full complementation of the *ccamk* mutant and indicates that the new helix-loop-helix combinations present in this CCaMK swap might result in a protein of a structural arrangement similar enough to CCaMK WT that allows it to respond to Ca^{2+} spiking. Conversely, the ability of CCaMK 3-2-1-4 to fully complement *ccamk* was only observed in a low number of plants (Chapter Three) and it could be hypothesised that the structural arrangement adopted by this CCaMK swap might not be identical to CCaMK WT, thus explaining its low frequency of nodulation complementation.

3.3. The EF-hand motifs may also have a structural role within CCaMK structure

It was revealed in Chapter Three that the truncated versions 1-477, 1-435 and 1-346 of CCaMK lacking either EF-hand 4, EF-hand 3 and 4 or the entire VLD respectively, were able to induce spontaneous gene expression (Figure 3.5). Consistently, these variants were not able to complement the *ccamk* mutant phenotype although 1-435 gave rise to a reduced number of white nodules, very likely to be spontaneous as previously reported (Miller et al., 2013). Based on these results from the truncated CCaMK mutants, it could be predicted that a truncated version lacking EF hands 2, 3 and 4 would also give rise to spontaneous gene expression and spontaneous nodulation but would not be able to allow complementation of *ccamk*. Indeed, the truncated CCaMK 1-402 which lacked EF-hands 2, 3 and 4 but preserved the non Ca^{2+} binding EF-hand 1 did not allow *ccamk* complementation or spontaneous gene expression (Figure 3.5 and Figure 3.6). Based on the prediction that a putative biotin binding site could be located between residues 389 and 399 in lily CCaMK (393-402 in MtCCaMK) (Patil et al., 1995), the truncated variant CCaMK 1-391 was additionally created lacking this entire putative biotin binding site to test whether this region could play any role in CCaMK regulation. Like 1-402, the CCaMK 1-391 lacked also EF hands 2, 3 and 4 but also part of the EF-hand 1, specifically the exiting helix. Since EF-hand 1 is a non Ca^{2+} binding EF-hand motif, theoretically the removal of its exiting helix should not have any different impact than the removal of the entire VLD from CCaMK as in 1-346, but this was not the case. In contrast to 1-402, the 1-391 variant was able to induce spontaneous gene expression but also to fully complement the *ccamk* phenotype (Chapter Three, Figure 3.5 and Figure 3.6) indicating a potential role for this region containing the predicted putative biotin binding site. Therefore, this result indicates that the exiting helix of EF-hand 1 has a potential structural role in regulating the mechanism of activation of CCaMK.

It is known that EF-hand 1 of CCaMK is unable to bind Ca^{2+} because it lacks two key residues for the coordination of Ca^{2+} (Swainsbury et al., 2012) but whether EF-hand 1 plays a role in CCaMK regulation remains as yet unclear. However, it has been shown that the binding of Ca^{2+} is not the only function of the EF-hand motifs but that they can also contribute structurally to the protein's regulation. It

is important to note that the non-Ca^{2+} binding EF-hand 1 of CCaMK is located immediately upstream of the CaMBD within the CCaMK structure and thus, it could be hypothesised that the role of this EF-hand could be to assist the binding of CaM to CCaMK. Moreover, the binding of Ca^{2+} to the EF-hand motifs of CCaMK during the perception of the Ca^{2+} spiking results in a conformational change that allows the binding of CaM and thus, in activation of CCaMK (Miller et al., 2013). This conformational change due to the binding of Ca^{2+} to EF-hands 2, 3 and 4 could be responsible for the exposure of EF-hand 1 to allow CaM binding that might be structurally buried during basal [Ca^{2+}]. The structural role of the EF-hand motifs has previously been reported in the mammalian ryanodine receptors (RYR). The structure of the RYR includes a CaMBD and a CaM-like domain composed of four EF-hand motifs arranged in pairs, designated as EF-hands 1, 2, 3 and 4 from the N-terminal to the C-terminal end (Xu et al., 2017). It was previously shown that the RYR1 and RYR2 have CaMBDs that only differ in four amino acid residues. However, CaM activates RYR1 but inhibits RYR2. Interestingly, the four different residues at the CaMBD of RYR1 and RYR2 were found to not be responsible for CaM-isoform specific regulation of the RYR (Yamaguchi et al., 2003). Consistently, it was demonstrated that the CaMBD and EF-hand 2 of RYR1 interact (Xiong et al., 2006; Gangopadhyay and Ikemoto, 2008). Moreover, CaM-isoform specific regulation of RYR1 and RYR2 requires the interaction between both EF-hands 1 and 2 with the CaMBDs of the RYRs (Xu et al., 2017). Similarly, the EF-hand 1 of CCaMK might have a structural role in the regulation of CCaMK activity, and perhaps might also be required for CaM binding to CCaMK. If this is the case, the phenotype of those CCaMK swaps in which the EF-loop 1 was replaced with another EF-hand loop of CCaMK might be due to altered or impaired CaM binding. In fact, these CCaMK swaps might be able to bind a different isoform of CaM that does not allow their activation in response to Ca^{2+} spiking resulting in the lack of *ccamk* complementation. Alternatively, the replacement of EF-loop 1 with another EF-loop might cause the opposite effect and a premature binding of CaM could result in the activation of the CSSP in the absence of the symbiont.

3.4. Potential effects of interchanging EF-loops in the CCaMK interaction with CYCLOPS

It has previously been shown that the region between the CaMBD and the EF-hand 2 of CCaMK is required for the interaction between LjCCaMK and CYCLOPS in yeast (Yano et al., 2008). These results along with the results obtained from 1-391 and 1-402 mutants presented above suggest that EF-hand 1 might also have a role in facilitating the interaction between CCaMK and its interacting partner CYCLOPS. Moreover, this could also suggest a potential role for biotin in the regulation of the CYCLOPS-CCaMK interaction since the lack of the biotin binding site in 1-391 allowed *ccamk* complementation and spontaneous gene expression while its presence in 1-402 abolished both phenotypes (Chapter Three, Figure 3.5 and 3.6). Moreover, the new helix-loop-helix combinations within the CCaMK swaps might also have an impact on the interaction between CCaMK and CYCLOPS. This is due to the fact that the amino acid sequences of those new helix-loop-helix combinations are different from CCaMK WT and although the overall tertiary structure might not have been modified, small structural changes might have occurred. As a consequence, these changes might result in a structural conformation that does not allow interaction with and/or phosphorylation of CYCLOPS. Therefore, it would be interesting to test the ability of the CCaMK swaps to interact with CYCLOPS, which would also provide further information about potential structural changes that might occur when interchanging EF-loops. The interaction between CCaMK and CYCLOPS have previously been assessed by both yeast-two-hybrid (Y2H) and in vitro kinase assays and thus similar experiments could be performed for the CCaMK swaps (Yano et al., 2008; Shimoda et al., 2012).

In order to confirm the hypotheses presented above, further studies of Ca^{2+}-dependent Thr271 autophosphorylation, Ca^{2+} binding and interaction with either CaM and/or CYCLOPS need to be performed and would help to characterise the phenotypes observed for the CCaMK swaps. These tests can now be performed on the CCaMK swaps since the experimental protocols for purification of CCaMK and in vitro kinase assays have now been established as presented in this chapter.

Chapter Five - Investigating the role of CCaMK during salt stress

1. Introduction

Plants are subjected to many environmental stress factors such as drought, salinity, high and low temperatures and microbial pathogen attacks, that put their growth and survival abilities at risk, causing major losses in agricultural yields (Singh et al., 2011; Arshad et al., 2017; Farooq et al., 2017; Sehgal et al., 2018). These biotic and abiotic stresses induce the activation of different signalling pathways that result in specific plant responses which are essential for plant adaptation (Suzuki et al., 2014). Ca^{2+} has been shown to be a key element in the activation of these specific signalling pathways as changes in cytosolic Ca^{2+} concentrations ($[Ca^{2+}]_{cyt}$) have been observed in response to environmental stimuli. Ca^{2+} signatures of a defined pattern (amplitude, frequency, duration and spatial distribution) are generated in response to these stimuli and as result of the activation of different pumps, channels and transporters, which are then decoded by specific Ca^{2+} sensors (McAinsh and Pittman, 2009; Kudla et al., 2010; Dodd et al., 2010).

High salinity resulting from the accumulation of high amounts of NaCl causes both osmotic and ionic stress to the plant. The osmotic effects of salt stress appear at early stages causing a reduction of the root growth and leaf expansion rates while the ionic effects caused by the presence of toxic amounts of Na^+ and Cl^- appear later leading to cellular damage and death (Munns, 2002). Despite the ionic effects of salt stress being observed later, the influx of Na^+ occurs early (Zörb et al., 2009) and has been suggested to act as a signal for the potential salinity adaptation of the plant when NaCl is still not present at toxic levels (Ismail et al., 2014). However, although some of the Na^+ influx transporters have been identified in *Arabidopsis,* the molecular mechanisms by which the plant perceives the increase in cytosolic Na^+ levels were not fully clear (Amtmann et al., 2006; Guo et al., 2008; Jin et al., 2015). A recent study by Jiang et al. (2019) in *Arabidopsis thaliana* uncovered a salt-sensitivity mechanism in which Na^+ ions bind to glycosyl inositol phosphorylceramide (GIPC) sphingolipids in the plasma membrane to gate Ca^{2+} influx channels and the glucuronosyltransferase

monocation-induced $[Ca^{2+}]_{cyt}$ increases 1 (MOCA1) is required for salt-induced depolarization of the cell-surface potential, Ca^{2+} spikes and waves, Na^+/H^+ antiporter activation and regulation of growth.

Salt stress has been shown to induce rapid and transient increases in $[Ca^{2+}]_{cyt}$ that last approximately 200 s in roots of *Arabidopsis thaliana* (Tracy et al., 2008; Jiang et al., 2013). However, Na^+ also showed the ability to induce the propagation of a wave-like $[Ca^{2+}]$ increase from the point of perception at the root tip towards the shoot. This Ca^{2+} wave moves at a steady ~396 μm/s through the cortical and endodermal cell layers but was not observed in the epidermal root cells (Choi et al., 2014). Additionally, a Ca^{2+} wave was also observed that moved through the cortex and endodermis from the tip of NaCl stimulated lateral roots towards the main root and shoot, ultimately reaching the aerial part of the plant (Choi et al., 2014). This effect was Na^+ specific as when sorbitol (the osmotic control for NaCl) was applied, the changes in Ca^{2+} were not observed (Choi et al., 2014). This long-distance transmission of Ca^{2+} waves highlights the importance of Ca^{2+} during the salt stress response.

Different environmental stresses have been shown to induce intracellular Ca^{2+} signatures that encode information and lead to the activation of specific signal transduction pathways (McAinsh and Pittman, 2009). This is supported by the observation that application of the two different abiotic stimuli (NaCl and H_2O_2) caused similar increases in $[Ca^{2+}]_{cyt}$ when applied individually, but a significantly higher $[Ca^{2+}]_{cyt}$ increase occurred (additive effect) when both stimuli were applied simultaneously in *Arabidopsis thaliana* (Jiang et al., 2013). A similar additive effect on the increase of $[Ca^{2+}]_{cyt}$ was observed in *Arabidopsis* when pathogen-associated molecular patterns PAMPs (biotic) and NaCl (abiotic) were applied simultaneously indicating the potential activation of different Ca^{2+} channels by these stresses (Cao et al., 2017).

Most of the information about salt stress-induced Ca^{2+} signalling has been obtained from the experimental work performed on the model plant *Arabidopsis thaliana* and this information is considered applicable to other plant species. However, whether the Ca^{2+} signature induced by NaCl in *Medicago truncatula* is

similar to the one in *Arabidopsis* has not been confirmed yet. *Medicago truncatula* is a model legume wildly used for the study of plant-microbe interactions, particularly for the study of the symbiotic interaction with AMF and rhizobia (Rose, 2008). At the centre of the symbiotic signalling pathway, nuclear Ca^{2+} spiking induces the activation of CCaMK which constitutes the Ca^{2+} spiking decoder and is essential for the activation of downstream signalling processes. Interestingly, CCaMK has also been reported to have an additional role during abiotic stresses in legumes such as pea and non-legumes such as wheat, rice and maize (Chapter One, Section 3.7).

Abiotic stresses such as cold, drought and high salinity have also been shown to increase the cellular levels of the phytohormone abscisic acid (ABA) (Cutler et al., 2010; Raghavendra et al., 2010; Yoshida et al., 2014). ABA is responsible for the regulation of developmental processes such as root growth and plant stress responses. Strikingly, the same stress signals that induce the increase of cellular ABA levels also raise the levels of intracellular Ca^{2+} in the form of Ca^{2+} signatures. In fact, both increases in cellular ABA and Ca^{2+} have been proposed to potentially be interconnected as a part of tightly regulated signalling networks (Edel and Kudla, 2016). High salinity caused by the presence of high concentrations of NaCl was found to increase the expression levels of *CCaMK* in roots of pea (Pandey et al., 2002). In contrast, wheat *CCaMK* expression levels were downregulated in roots in the presence of NaCl or ABA (Yang et al., 2011). However, the expression levels of both *CCaMK* from maize and rice were upregulated in the presence of increased ABA in response to abiotic stresses (Shi et al., 2012; Ma et al., 2012) (Chapter One, Section 3.7).

Therefore, this raises the question of whether CCaMK is able to respond to the abiotic stress-induced Ca^{2+} signal(s) in addition to its role during plant-microbe symbiosis as the Ca^{2+} spiking decoder. If this were the case, CCaMK would have the ability to discriminate not only between the two symbiotic Ca^{2+} signals (from AMF and rhizobia) but also between the abiotic and biotic stress Ca^{2+} signals. However, the activation of either the CSSP or the abiotic stress signalling response would also depend on the interaction of CCaMK with the corresponding interacting partner. CYCLOPS has been demonstrated to be the specific

interacting partner of CCaMK during plant-microbe symbiosis (Yano et al., 2008). Therefore, would also CYCLOPS be involved in the response of CCaMK to the salt stress-induced Ca^{2+} signal? If so, are there other components of the CSSP involved during salt stress?

In order to address these questions, *M. truncatula ccamk* mutant seedlings were subjected to different concentrations of NaCl and their root growth capabilities were compared to that of the WT plant. In addition, the root growth of *ipd3-1 (cyclops), dmi1-1, dmi2-1, nin-1, nsp1-2 and nsp2-2* mutants were also assessed. Furthermore, expression levels of *CCaMK* were also measured in the presence and absence of NaCl along with the expression levels of salt marker genes in WT *Medicago truncatula* seedlings.

2. Results

2.1. In vitro assessment of the root growth capability of *Medicago truncatula* symbiotic gene mutants during salt stress

The decrease in plant root growth is an important effect observed under salt stress conditions and has been shown to occur in *Medicago truncatula* (de Lorenzo et al., 2007). Additionally, the *Medicago truncatula* genotype Jemalong A17 (A17) was found to have a high salinity tolerance as concentrations over 120 mM NaCl were required to reduce root growth *in vitro* (de Lorenzo et al., 2007). Therefore, the root growth capabilities of the *Medicago truncatula* A17 WT (named as WT from this point) and the *dmi3-1* (*ccamk*) mutant seedlings were assessed in the presence of different concentrations of NaCl ([NaCl]) in order to identify whether CCaMK is involved in the salt stress response. *In vitro* tissue culture was chosen as the first screening method as has been demonstrated to be a reliable and fast system for initial studies of the salt stress response in seedlings (Ahmed et al., 2014; de Lorenzo et al., 2007; Zahaf et al., 2012). Based on the information provided in the *Medicago truncatula* Handbook developed by the Noble Research Institute (https://www.noble.org/medicago-handbook/), four concentrations of NaCl, (0, 100, 150 and 200 mM) were chosen for the treatment of the *Medicago truncatula A17* seedlings *in vitro* (See Chapter Two Methods, Section for experimental procedure). In the *Medicago truncatula Handbook* is indicated that after the overnight germination, seedlings were grown for three

days before being moved to the NaCl-containing medium plates. However, seedlings were found to be very sensitive to contamination when moved between plates despite their careful handling under sterile conditions. Therefore, after the overnight germination (one day-old), the seedlings were directly placed on sterile BNM-agar plates (Chapter Two, Table 2.6) containing the desired [NaCl] to be tested, with their root tip placed over a straight line drawn on the plates. This would ensure that only root growth was measured and enable the comparison between the mutant and WT (Figure 5.1).

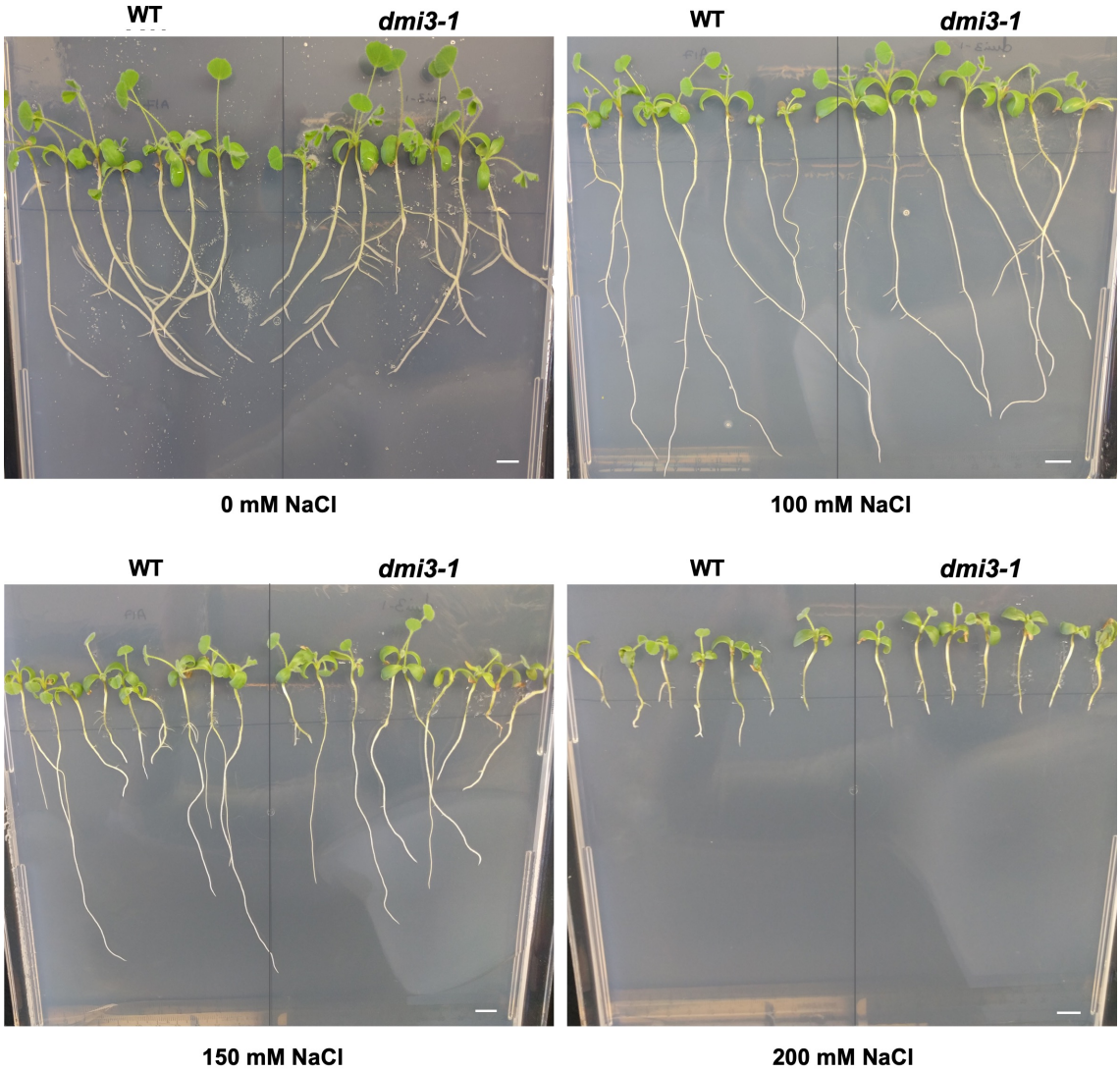

Figure 5. 1. Root growth assessment in *Medicago truncatula* WT and *dmi3-1* after in vitro treatments with different concentrations of NaCl.

Germinated seedlings of *Medicago truncatula* WT and *dmi3-1* were placed on BNM-agar plates with different [NaCl] (as indicated), ensuring that their root tip was in contact with the agar. A straight horizontal line was drawn on the plates to mark the start point of growth and the root tips of the seedlings were placed on top. Plates were placed vertically

in a controlled growth condition cabinet (23°C, 16 h photoperiod) for 8 days, after which the photos were taken. Scale bar = 1 cm.

Additionally, each plate was prepared containing an agar-medium composed of a fixed amount of Buffered Nodulation Medium (BNM) but different concentrations of NaCl and then topped up with deionised water in order to achieve the same final volume of medium in each plate. This would remove the possibility of obtaining different phenotypes based on the differing amounts of nutrients among plates rather than based on the [NaCl]. After 8 days of seedling growth at the different [NaCl], the root length of each seedling was measured from the straight line.

The measurement of root growth obtained from an average of 15 plants for each [NaCl] and each genotype, tested over two experimental repetitions, showed that there was not statistically significant difference in root growth between A17 WT (WT) and the *dmi3-1* mutant at the different [NaCl] (Figures 5.1 and 5.2).

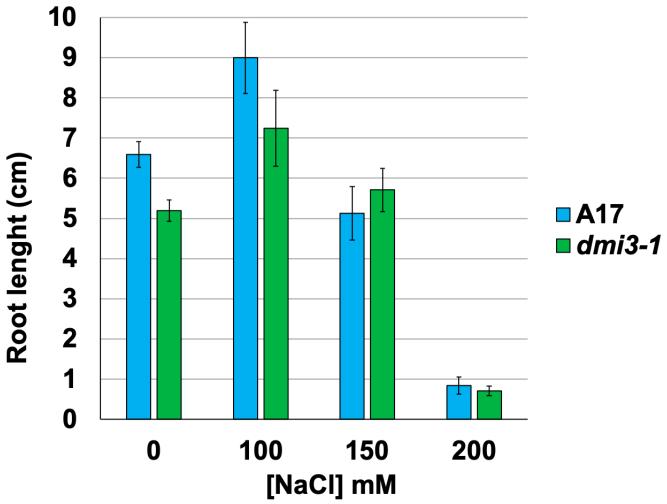

Figure 5. 2. Differences in root growth were observed between *Medicago truncatula* WT and *dmi3-1*.

The *dmi3-1* mutant showed a significant reduction in root growth compared to WT in the absence of NaCl. In the presence of either 100, 150 or 200 mM of NaCl, differences were not significant between the WT and *dmi3-1* mutant. The assessment of root growth was performed after 8 days of incubation in a controlled growth condition cabinet (23°C, 16 h photoperiod). The asterisk denotes statistically significant difference in root length

relative to WT under each [NaCl] in pairwise two-tailed t-tests ($p<0.05$). Numbers indicate the root length in cm measured from the start point of growth determined by a straight line drawn on the plates. Bars represent average of at least two biological replicates. Error bars represent S.E.

However, the *dmi3-1* mutant showed a significant decrease in root growth in the 0 mM NaCl plates compared to WT. Moreover, it was interesting to see that both genotypes showed a similar trend of root growth: in the presence of a relatively low [NaCl] (100 mM), both genotypes showed an increase in root growth compared to in the absence of NaCl but this increase was only statistically significant in WT; when in the presence of a higher [NaCl] of 150 mM, both genotypes showed similar levels of root growth to that observed in the absence of NaCl; lastly, 200 mM of NaCl reduced the root growth to statistically significant lower levels than in the absence of NaCl in both genotypes (Figure 5.2).

The fact that both genotypes showed a similar trend at the different [NaCl] (Figure 5.2) raised the question of whether other symbiotic gene mutants would also follow this pattern. Since there was a large difference in root growth between the 150 mM and 200 mM conditions, it was also questioned whether the treatment with an intermediate concentration of 175 mM would allow to see a more acute difference in root growth between genotypes. Moreover, the highest [NaCl] that was applied which corresponded to 200 mM was found to not completely abolish root growth in either WT or *dmi3-1* and therefore, a higher [NaCl] was interesting to test (Figure 5.2). As a consequence, six different [NaCl] (Chapter Two, Table 2.6) were chosen for a new experiment performed under the same experimental procedure explained above. In this case, the genotypes chosen included the WT and *dmi3-1* in addition to *ipd3-1*, *dmi1-1*, *dmi2-1, nsp1-2, and nsp2-2* mutants, which are knockouts of members of the CSSP (See Chapter One, Section 4.5 for the role of each of these genes).

Figure 5.3 shows the difference in root growth between each genotype at 0, 100, 150, 175, 200 and 300 mM of NaCl.

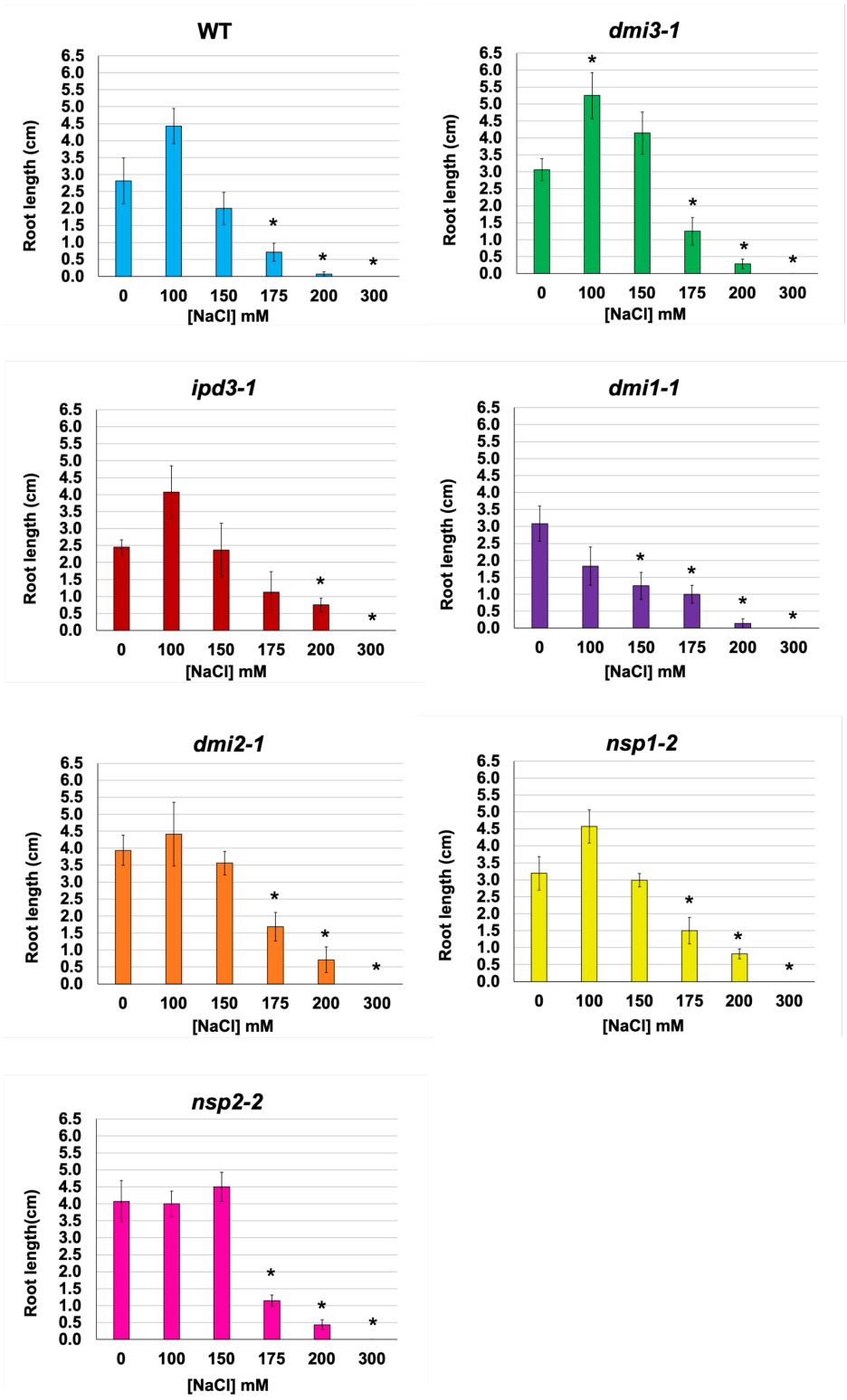

Figure 5. 3. Assessment of the root growth capabilities of *Medicago truncatula* WT and symbiosis defective mutants during salt stress.

The root growth of WT and *dmi3-1, ipd3-1, dmi2-1* and *nsp1-2* mutants under the different [NaCl] tested followed a similar trend. This trend corresponds to a slight increase in root growth at 100 mM of NaCl followed by a root growth decrease at increasing [NaCl] of 150, 175 and 200 mM. At 300 mM of NaCl, root growth was

completely abolished for all the genotypes tested. The *dmi1-1* and *nsp2-2* mutants showed a different pattern of root growth from WT with a decrease in root growth at higher [NaCl] than 100 mM in the case of *dmi1-1*. The *nsp2-2* showed tolerance to salt until 150 mM of NaCl and root growth decreased at 175 and 200 mM of NaCl. The assessment of root growth was performed after 8 days of incubation in a controlled growth condition cabinet (23°C, 16 h photoperiod). The asterisk denotes statistically significant difference in root length of each genotype at each [NaCl] relative to 0 mM of NaCl in pairwise two-tailed t-tests ($p<0.05$). Numbers indicate the root length in cm measured from the start point of growth determined by a straight line drawn on the plates. Bars represent average of at least two biological replicates. Error bars represent S.E.

This experiment was performed for two experimental repetitions with an average total of 8 plants per condition as a first screen to identify whether these genes have a role during the salt stress response. Interestingly and consistent with the experiment performed above (Figure 5.2), WT and most of the mutants showed a similar NaCl response pattern. A treatment of 100 mM NaCl induced a slight increase in root growth compared to the absence of NaCl. In contrast, the application of higher concentrations of NaCl corresponding to 150, 175, 200 and 300 mM caused a reduction in root growth that was most acute- at the highest concentrations of NaCl, compared to plants grown in the absence of NaCl (Figure 5.3). This slight increase in root growth at moderate [NaCl] is consistent with previous studies which showed the initial adaptive responses of some crops to salinity (Rewald et al., 2013). However, *dmi1-1* and *nsp2-2* mutants showed an exceptional salt response pattern. The *dmi1-1* mutant showed a downward root growth trend directly from the lower [NaCl] (100 mM) while a considerably higher [NaCl] (175 mM) was required to see any reduction in root length growth in the *nsp2-2* mutant (Figure 5.3).

Although the root growth followed a similar trend, different responses to NaCl were obtained for each individual genotype (Figure 5.3). It was previously reported that the A17 is a highly tolerant *Medicago truncatula* ecotype to salt stress and a [NaCl] of at least 120 mM was required to show signs of a salt stress response *in vitro* (de Lorenzo et al., 2007). Consistently, under the current experimental conditions, the A17 WT required 175 mM of NaCl to show a

statistically significant reduction in root length growth compared with the absence of NaCl. Although this result was also observed in the *dmi3-1, dmi2-1, nsp1-2 and nsp2-2* mutants, 100 mM NaCl induced a statistically significant increase in root length growth in *dmi3-1* plants compared to the no-salt condition (0 mM NaCl) that also occurred but was not statistically significant in the WT, *ipd3-1*, *dmi2-1 and nsp1-2* mutants. In contrast, despite the *ipd3-1* mutant root growth halved from 0 mM to 175 mM of NaCl, a higher [NaCl] of 200 mM was required in this case to show a statistically significant decrease in root growth compared to in the absence of NaCl. Additionally, while most genotypes required at least 175 mM of NaCl to have a statistically significant decrease in root growth compared to in the absence of NaCl, the *dmi1-1* mutant showed a higher sensitivity to salt as a 150 mM of NaCl was enough to significantly reduce the root growth compared to at 0 mM.

The measurement of root length from the growth start point allowed the comparison among all the genotypes at each [NaCl]. A second analysis of the same data presented in Figure 5.3. was performed in order to compare the response of each mutant to each [NaCl] against the WT. Therefore, these same data presented in Figure 5.3 was re-analysed and re-plotted in order to facilitate the visual identification of the NaCl response differences among the genotypes studied (Figure 5.4). While there was no statistically significant difference in root growth among all genotypes tested in the absence of NaCl (0 mM), differences were observed at the different [NaCl] (Figure 5.4). At a 100 mM of NaCl, there was still no significant differences in root growth among all genotypes. However, at a [NaCl] of 150 mM the *dmi3-1, dmi2-1 and nsp2-2* mutants had statistically significant longer roots than WT. The [NaCl] of 175 mM seemed to reduce root growth to similar levels among all the genotypes as no statistically significant differences were observed. In contrast, at 200 mM NaCl, the root growth of *ipd3-1, nsp1-2* and *nsp2-2* mutants was significantly higher than that of A17 (Figure 5.4). Lastly, 300 mM of NaCl completely abolished root growth in all genotypes.

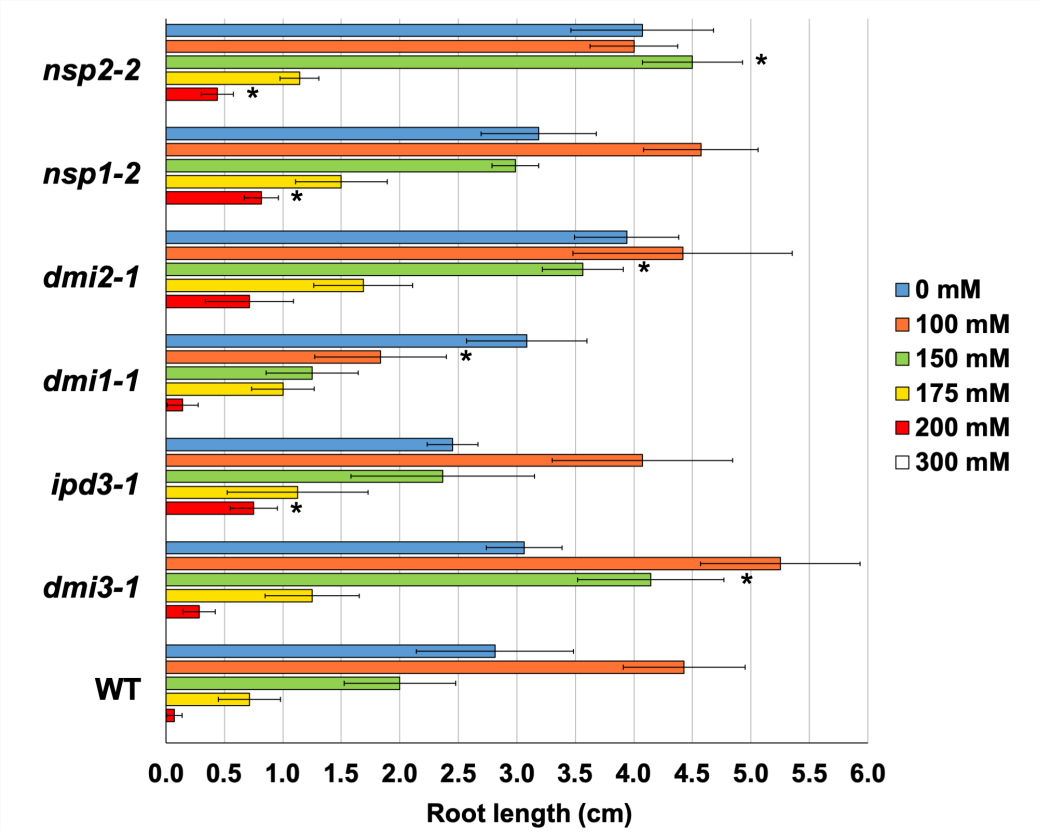

Figure 5. 4. Comparison of the root growth of *Medicago truncatula* WT and symbiotic defective mutants under different [NaCl].

The data presented in Figure 5.3. was re-analysed in order to compare the root growth during salt stress among the genotypes tested at different [NaCl]. This re-analysis is represented in the bar chart presented above in order to facilitate the visual identification of the root growth differences among these genotypes. In the absence of NaCl, all mutants showed the same root growth capability as WT. At 100 mM of NaCl, the root growth of the *dmi1-1* mutant was reduced compared to WT. At 150 mM, a decrease in root growth was obtained for the *dmi3-1, dmi2-1* and *nsp2-2* mutants compared to WT. All genotypes showed similar levels of root growth at 175 mM of NaCl. At 200 mM of NaCl, the *ipd3-1, nsp1-2* and *nsp2-2* mutants showed a reduced root growth compared to WT. The root growth of all genotypes was abolished in the presence of 300 mM of NaCl. The asterisk denotes statistically significant difference in root length of each genotype at each [NaCl] relative to WT in pairwise two-tailed t-tests ($p<0.05$). Numbers indicate the root length in cm measured from the start point of growth determined by a straight line drawn on the plates. Bars represent average of at least two biological replicates. Error bars represent S.E.

2.3. Assessment of the root growth capability of *Medicago truncatula* symbiotic gene mutants during salt stress under greenhouse conditions

The results presented above suggest that some members of the CSSP might be involved in the salt stress response. However, to confirm these results in a more "real-life scenario", a similar experiment was performed in soil instead of agar plates. The root growth was assessed in the same genotypes that were tested on plates in addition to the *nfp-1* and *nin-1* mutants as *NFP* and *NIN* are also important members of the CSSP (See Chapter One, Section 4.5 for relevant information about these genes). However, the test conditions were adjusted due to this experiment being performed under greenhouse conditions rather than on plates. Firstly, following the indications stated in the *Medicago truncatula* Handbook and due to the fact that the seedling roots would be placed in to the soil (rather than placed on top of an agar-medium), lower [NaCl] were chosen for the assessment of root growth in greenhouse conditions that corresponded to 0, 50 and 100 mM. Similar to the *in vitro* conditions used in the previous experiment presented above, overnight germinated seedlings of each genotype were placed directly into the soil, but plants were grown for 5 days before treatment with NaCl. After 2 weeks of watering the plants with the chosen [NaCl], the root lengths were measured approximately from the junction between shoot and root. Three out of the four technical repetitions of this experiment were performed by Velindah Chibomba, a co-supervised MSc student, and each of the technical repetitions included 10 plants per genotype per [NaCl].

Overall, the measurement of root lengths from plants treated with NaCl in soil showed that every genotype tested shared a similar trend of root length change in response to the NaCl treatments (Figure 5.5A). The [NaCl] of 50 mM had no significant impact on root length in any of the genotypes compared to the absence of NaCl. In contrast, the 100 mM NaCl caused a reduction in the root lengths to statistically significant levels in all the genotypes, with the exception of the *dmi2-1* mutant. Strikingly, the *dmi2-1* mutant showed a higher resistance to NaCl as no changes in root length were observed at any of the NaCl treatments (Figure 5.5A).

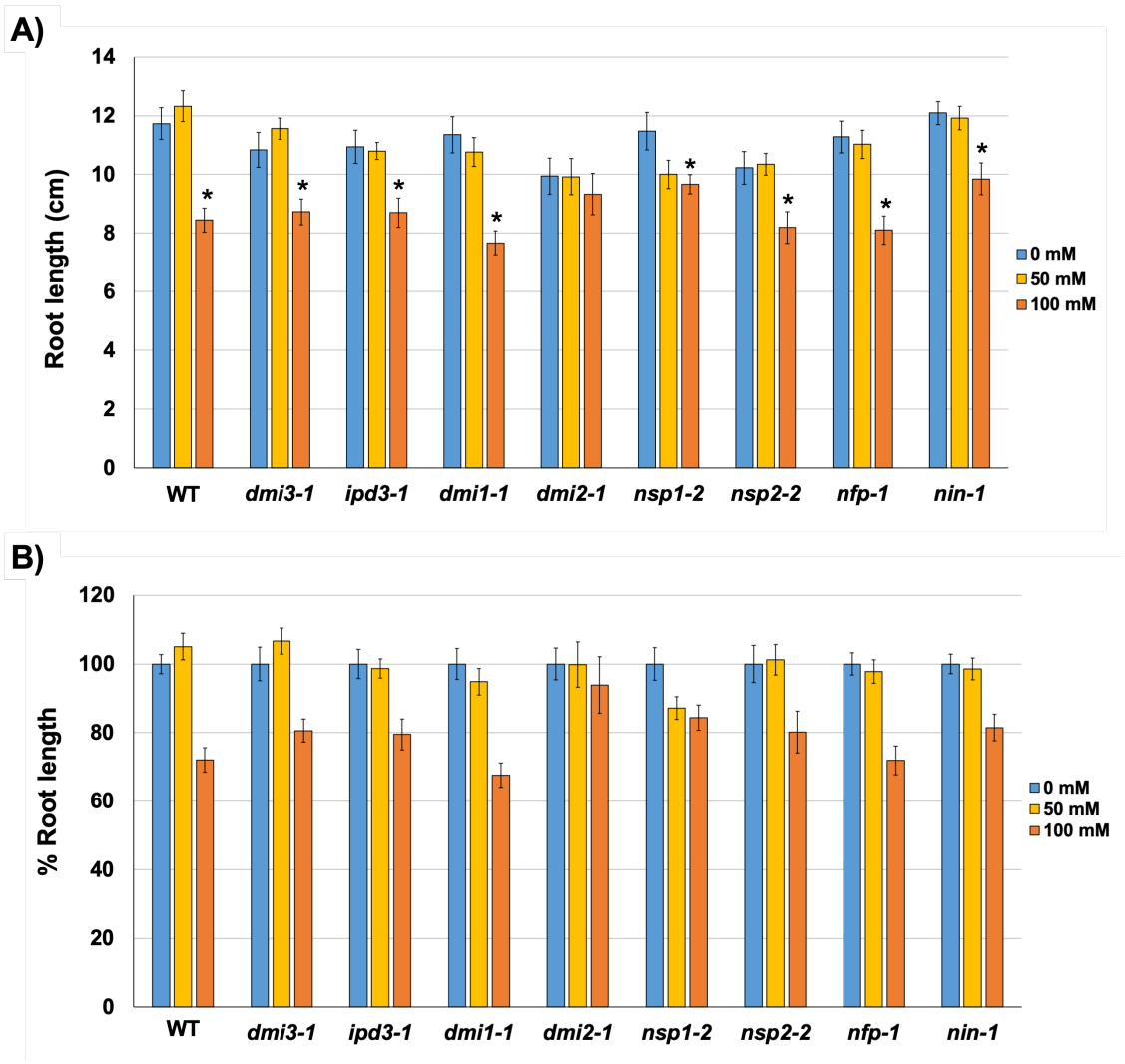

Figure 5. 5. Assessment of root length in *Medicago truncatula* WT and symbiosis defective mutants during salt stress under greenhouse conditions.

Measurement of root length in *Medicago truncatula* WT and the *dmi3-1, ipd3-1, ipd3-1, dmi1-1, nsp1-2, nsp2-2, nfp-1* and *nin-1* mutants grown in soil for 5 days and then watered with BNM medium with containing or lacking NaCl for 2 weeks. (A) All genotypes tested show a similar pattern of root length under the different [NaCl] tested. In the absence of NaCl and in the presence of 50 mM of NaCl, similar values of root length were obtained for all the mutants compared to WT. In the presence of 100 mM of NaCl, all mutants except *dmi2-1* showed reduced root lengths compared to WT. Numbers indicate the root length in cm measured approximately from the root-shoot junction. (B) In order to assess root growth of the different genotypes under salt-stress, the data presented in panel A was re-analysed and expressed a percentage (%) of root length in the non-salinized plants. The root growth trend for all the genotypes under the three

different NaCl conditions was consistent with the trend obtained from root length expressed in cm in panel A. However, changes in root growth among all the genotypes were not significantly different. The asterisk denotes statistically significant difference in root length (A) and root growth percentage (B) of each genotype at each [NaCl] relative to WT in pairwise two-tailed t-tests ($p<0.05$). Bars represent average of at least three biological replicates. Error bars represent S.E.

In order to identify differences in root growth during salt stress between the A17 and the symbiotic mutant genotypes tested under greenhouse conditions, normalisation of the data was required due to the inability to stablish an accurate start point of the root growth under this experimental procedure. Therefore, the root length data obtained at the different [NaCl] were represented as a percentage of the root length in the no-salt condition (Bottom panel Figure 5.5). This allowed the identification of how much root growth occurred in each genotype at each [NaCl], considering that root growth was 100% in the absence of NaCl and then the comparison to the root growth occurred in A17 plants at the same [NaCl]. The normalised data showed that there were no statistically significant differences among all genotypes at each [NaCl] (Figure 5.5B). However, it is noticeable that the decrease in root length in the presence of the highest salt concentration (100 mM NaCl) only induced an approximately 20-30% decrease in the root length (Figure 5.5B) which corresponds to a difference of 2-4 cm (Figure 5.5A) from the non-salinity condition. Therefore, there might be the possibility that a higher [NaCl] would be required to produce a more severe phenotype. This then would allow to observe more clearly the NaCl response differences among the genotypes under greenhouse conditions.

2.4. Identification of salt stress transcriptional markers in *Medicago truncatula* roots

The results obtained from the root growth assessment in the presence of different [NaCl] suggests that some members of the CSSP might be involved in the salt stress response in roots of *Medicago truncatula*. In order to further confirm these results, an analysis of the gene expression levels of the symbiotic genes *DMI3, IPD3, DMI1, DMI2, NSP1, NSP2, NFP* and *NIN* during salt stress was carried out from roots subjected to different NaCl treatments by qRT-PCR. However, it was

first necessary to identify specific transcriptional markers of salt stress to confirm that the NaCl treatments were actually causing stress in the plants. Some of these genes were identified from published literature associated with the model plant *Arabidopsis thaliana*. The *Medicago truncatula* orthologous genes to the *Arabidopsis thaliana* salt markers were identified by performing nucleotide Basic Local Alignment Search Tool (BLAST) searches and selecting the top-hit sequences obtained. Then, the potential *Medicago truncatula* salt markers were selected based on those top-hit sequences which showed gene expression induction during treatments with NaCl in the published microarray datasets available on the *Medicago truncatula* Gene Expression Atlas (MtGEA) (Benedito et al., 2008). This was the case of the genes *MtbZIP46* and *MtABI5-7* which were identified through BLAST alignments using the sequence of *A. thaliana ABA responsive element-binding factor 4* (*AtABF4*) (Choi et al., 2000; Uno et al., 2000). The *MtLEA14* was also found to be upregulated during NaCl treatments in the MtGEA and was identified following a similar procedure than above using the *AtLEA14* gene sequence as a template (Miura and Furumoto, 2013). The genes *MtbZIP44* and *MtbZIP11* were obtained through a BLAST search using the soybean *bZIP110* (*GmbZIP110*) sequence which showed to have important roles during the salt stress response (Xu et al., 2016). These genes were further confirmed to be upregulated during treatments with NaCl by searches in the MtGEA and selected as potential salt transcriptional markers in *Medicago truncatula*. In addition, some of the candidate transcriptional markers chosen for this experiment were also selected from published literature associated with *Medicago truncatula* genes involved in salt stress. This is the case of *MtCBF4, MtCAT* and *MtCorA1* which were found to be upregulated during salt stress conditions (Li et al., 2011; Mhadhbi et al., 2011; de Lorenzo et al., 2007).

In order to confirm that the genes selected were indeed transcriptional markers of salt stress in *Medicago truncatula*, their expression levels under different [NaCl] were first tested by RT-PCR, using the housekeeping gene *Elongation Factor 1*α (*EF1*α) as a control. This was initially tested using plant material obtained from *in vitro* treatments with 0, 50, 100 and 150 mM of NaCl during 6h and 24h in roots of *Medicago truncatula*, following the same experimental procedure as explained in Section 2.1 of this chapter (Figure 5.6).

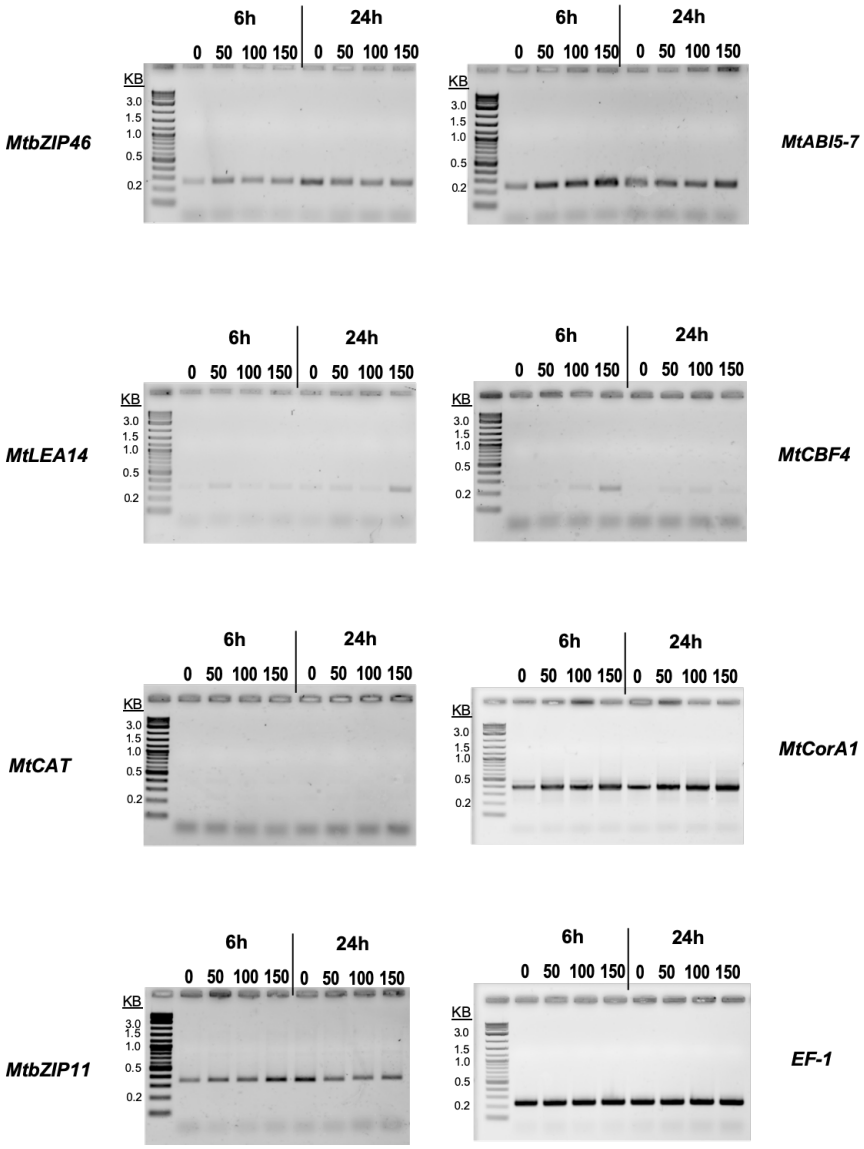

Figure 5. 6. Expression of potential salt marker genes in *Medicago truncatula* roots treated with different [NaCl] for 6 h and 24 h in vitro was assessed by RT-PCR.

Changes in the expression levels of *MtbZIP46, MtABI5-7, MtLEA14, MtCB4, MtCorA1* and *MtbZIP11* were observed in the presence of different [NaCl] which corresponded to 0 mM (0 in the figure), 50 mM (50), 100 mM (100) and 150 mM (150), at both 6h and 24 h. The *MtCAT* was not expressed under these experimental conditions. The expression levels of the housekeeping gene *EF1*α were used as a reference. The gene amplification expected sizes were the following: 244 bp *MtbZIP46*, 242 bp *MtABI5-7*, 297 bp *MtLEA14*, 227 bp *MtCBF4*, 225 bp *MtCAT*, 467 *MtCorA1*, 340 bp *MtbZIP11* and 222 bp *EF1*α. The 1 kb Plus DNA ladder (NEB) was used for fragment size identification.

At 6h, the expression levels of *MtABI5-7*, *MtCBF4*, *MtCorA1* and *MtbZIP11* gradually increased as the [NaCl] also increased while no changes in expression were observed for *MtbZIP46* and *MtLEA14*. After 24h, the *MtABI5-7*, *MtCBF4* and *MtCorA1* along with *MtLEA14* expression levels also increased over increasing [NaCl] while the *MtbZIP11* and *MtbZIP46* expression decreased as the [NaCl] increased, in contrast with the results obtained after 6h. The aim of this experiment was not only to identify transcriptional markers of salt stress but also to determine whether the expression levels of members of the CSSP change under salt stress. Therefore, the same plant material was used to check the expression levels of *DMI3, IPD3, DMI1, DMI2, NSP1, NSP2,* and *NFP* (Figure 5.7). After 6h of treatment with the different [NaCl], the *DMI3, IPD3, DMI2, NSP2,* and *NFP* genes showed fluctuations in their expression levels, while no gene expression was observed for *DMI1 and NSP1*. However, after 24h of NaCl treatment, the expression levels of *DMI3* and *IPD3* at 150 mM of NaCl were clearly higher than those in the no-salt condition. Consistent with the results observed after 6h of treatment with NaCl, the *NSP2* expression levels also showed fluctuations at the different [NaCl] while in the case of *NFP*, expression levels decreased gradually with increasing [NaCl]. Additionally, while *DMI1* and *NSP1* were not expressed under any condition, *DMI2* gene expression level showed a slight increase at 150 mM compared with the absence of NaCl. These results further suggest that the members of the CSSP *DMI3, IPD3, DMI1, DMI2, NSP1, NSP2 and NFP* might be involved in the salt stress response.

The plant material generated for the measurement of root growth under salt treatments by Velindah Chibomba (Section 2.2 of this chapter) was stored at -80°C for future gene expression analysis by qRT-PCR. Therefore, an additional RT-PCR test was performed from this material for the selection of the transcriptional markers of salt stress (Table 5.1) to use in the future qRT-PCR experiment. In this case, the expression of the potential salt stress transcriptional markers was assessed in both roots and shoots after 2 weeks of treatment with 0, 50 and a 100 mM of NaCl (Figure 5.8) (See section 2.2 of this chapter for experimental procedure followed for generation of plant material). The expression of *MtbZIP46, MtABI5-7, MtLEA14* and *MtbZIP11* increased noticeable from 0 to 100 mM of NaCl in roots of *Medicago truncatula*. However, the *MtCBF4, MtCAT*

and *MtCorA1* gene expression levels did not change from the absence to the presence of NaCl in roots. In shoots, the expression of *MtABI5-7, MtbZIP46* and *MtbZIP11* also increased from 0 to 100 mM of NaCl, but the expression levels of *MtCBF4* and *MtCorA1* did not change over increasing [NaCl]. In contrast to their expression in roots, *MtLEA14* and *MtCAT* were not expressed in shoots under these experimental conditions.

Since the assessment of the gene expression levels of members of the CSSP during salt stress was desired and plant-microbe symbiosis occur in roots, the transcriptional markers that were found upregulated in roots during salt stress by RT-PCR were chosen for further analysis by reverse transcription quantitative PCR (RT-qPCR). The use of RT-qPCR allows the quantification of gene expression levels of each gene tested and for statistical analysis of the results. In addition, RT-qPCR constitutes a more sensitive method of detection allowing more subtle differences in gene expression levels to be identified (VanGuilder et al., 2008). Therefore, based on the RT-PCR results from treatments with NaCl after 6h and 24h *in vitro* and after 2 weeks under greenhouse conditions, the *MtbZIP46, MtABI5-7* and *MtbZIP11* were chosen for further experiments as salt stress transcriptional markers in *Medicago truncatula*.

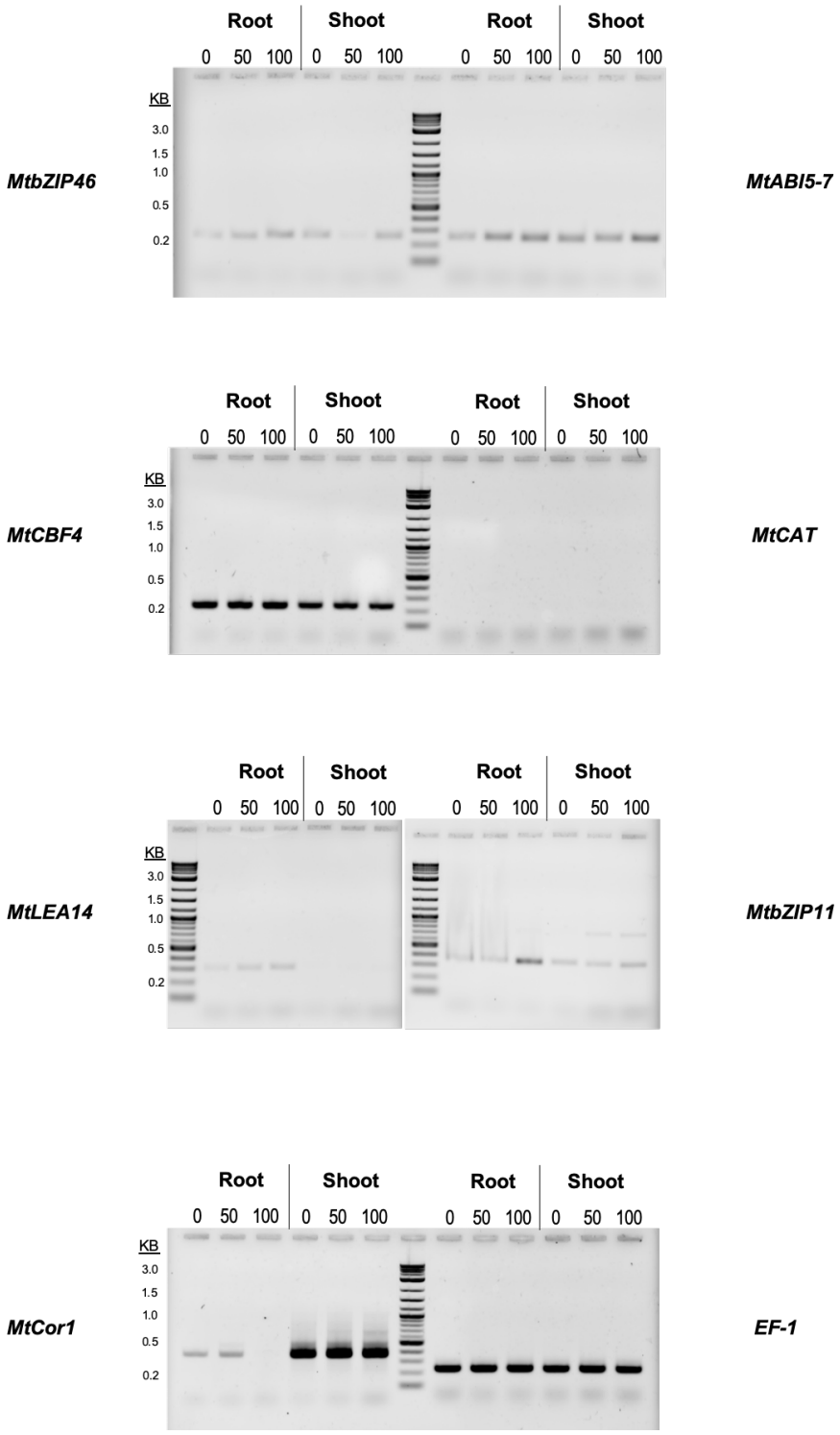

Figure 5. 7. Expression of potential salt marker genes in *Medicago truncatula* roots and shoots treated with different [NaCl] under greenhouse conditions was assessed by RT-PCR.

Plants were treated with different [NaCl] which corresponded to 0 mM (0 in the figure), 50 mM (50) and 100 mM (100), for 2 weeks in soil in controlled environment growth rooms (20°C light and 21°C darkness, 16 h photoperiod). All genes tested corresponding to *MtbZIP46, MtABI5-7, MtLEA14, MtCBF4, MtCAT, MtCorA1* and *MtZIP11* showed

differences in their expression levels over the conditions tested as opposed to the housekeeping gene EF-1 whose expression levels kept unchanged. *MtbZIP46, MtABI5-7* and *MtbZIP11* were chosen for future experiments as transcriptional markers of salt stress in *Medicago truncatula*. The gene amplification expected sizes were the following: ~244 bp *MtbZIP46*, 242 bp *MtABI5-7*, 297 bp *MtLEA14*, 227 bp *MtCBF4*, 225 bp *MtCAT*, 467 *MtCorA1*, 340 bp *MtbZIP11* and 222 bp *EF1*α. The 1 kb Plus DNA ladder (NEB) was used for fragment size identification.

2.5. Assessment of gene expression levels of members of the CSSP during salt stress in *Medicago truncatula* roots

Since the plant root material generated by Velindah Chibomba constituted three independent technical repetitions with 10 plants per genotype per condition (Section 2.2 of this chapter), this material was chosen for the gene expression analysis of the CSSP genes during salt stress by RT-qPCR (Figure 5.9). Consistent with the RT-PCR results, *MtbZIP46, MtABI5-7* and *MtbZIP11* showed increasing levels of gene expression as the [NaCl] increased from 0 to 100 mM. However, the increased gene expression levels in the presence of 50 and 100 mM of NaCl were only statistically significant for *MtbZIP46* when compared to in the 0 mM condition. The fact that the levels of gene expression for these genes were increasing with the [NaCl] indicated that the NaCl treatments were indeed causing a salt stress and that expression levels of the CSSP genes could be checked in this material. However, it is important to consider that the methodology followed in this case to generate the plant material (moderate [NaCl] for long period of incubation in soil) may not be the most appropriate in order to obtain differences in gene expression to statistically significant levels. For instance, published studies of gene expression during salt stress in *Medicago truncatula* were based on plant material obtained following more “aggressive” procedures by incubating the plants for short periods of time (24 and 48 h) with higher [NaCl] over 150 mM *in vitro* (Mhadhbi et al., 2013, 2011). Despite these considerations, the material generated by Velindah Chibomba showed a root length phenotype during the NaCl treatments (Figure 5.5) and the results presented in Figure 5.9 show the increase in expression levels of the chosen salt marker genes over increasing [NaCl] consistent with the RT-PCR results (Figure 5.8).

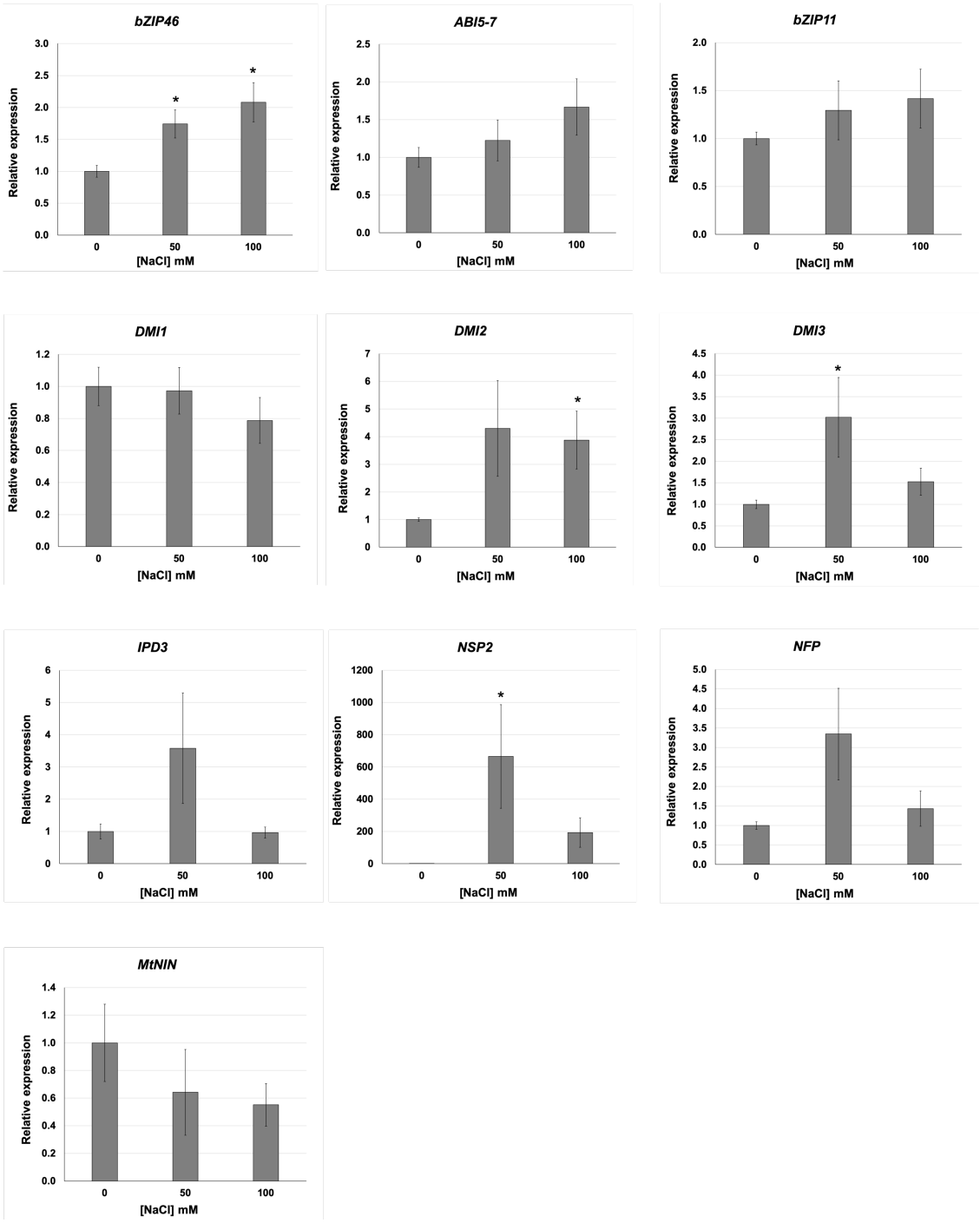

Figure 5. 8. The expression of members of the CSSP is induced in the presence of NaCl.

Expression of *DMI2*, *DMI3* and *NSP2* is induced in the presence of NaCl compared to in the absence of NaCl. The expression of the salt marker *bZIP46* increased over increasing [NaCl]. Asterisk denote statistically significant expression induction of each gene at 50 or 100 mM of NaCl relative to 0 mM of NaCl in a pairwise two-tailed t-test

($p<0.05$). Bars represent average expression of three biological replicates (each with three PCR technical replicates), as determined by RT-qPCR. Error bars represent S.E.

CCaMK (*DMI3*) expression was induced in the presence of 50 mM of NaCl to statistically significantly levels compared with the no-salt condition, but then the expression decreased in the presence of 100 mM of NaCl. The upregulation of *CCaMK* in the presence of NaCl (50 mM in this experiment) is consistent with the upregulation of the pea, maize and rice *CCaMK* during abiotic stresses (Ma et al., 2012; Shi et al., 2012; Pandey et al., 2002). Nevertheless, the fact that a higher [NaCl] corresponding to 100 mM induces a decrease in *CCaMK* expression levels had not previously been observed. As explained above, the plant material used for these RT-qPCR experiments was generated by treatment with moderate [NaCl] as opposed to the shorter incubations with higher [NaCl] performed in previous publications. In this case, the 100 mM of NaCl might be inducing a more severe stress that activates the plant abiotic stress mechanisms and thus, inhibits root growth which might correspond to reduced levels of *CCaMK* expression. Conversely, the 50 mM might indeed induce a moderate salt-stress that activates the plant adaptation mechanisms that stimulates root growth and corresponds to increased levels of *CCaMK* expression.

It was interesting to observe that the gene expression levels of CCaMK's interacting partner *IPD3* (*CYCLOPS*) showed a similar pattern to *CCaMK* (*DMI3*) with higher levels of expression at the 50 mM of NaCl condition, although these levels were not statistically significant compared to in the absence of NaCl. There are previous reports demonstrating the existence of other interacting partners of CCaMK during abiotic stresses such as the maize NAC84 transcription factor (Zhu et al., 2016b) and the pea p40 protein (Pandey et al., 2002) (Chapter One, Section 3.7). Consistently, *Medicago truncatula* CCaMK might have other interactor partners different from CYCLOPS and this further supports the potential specificity in the response of CCaMK to the abiotic stress calcium signal by interacting and activating different signalling components from the CSSP.

DMI2, the symbiotic co-receptor that interacts with the LysM receptor complex composed of LYK3-NFP during the recognition of the Nod and Myc factors (Endre et al., 2002; Gherbi et al., 2008; Stracke et al., 2002), showed increased levels of gene expression at a 100 mM of NaCl that were statistically significant compared to at 0 mM. This was particularly interesting because *DMI2* was expected to solely participate in the perception of the Nod and Myc factors due to its interaction with LYK3 and NFP that specifically recognise these symbiotic diffusible factors. In contrast with *DMI2*, the gene expression levels of *NFP* were not significantly increased at any [NaCl] in a t-test despite following a similar gene expression pattern to that of *DMI3* and *IPD3* with increased levels at 50 mM that then decreased at a 100 mM of NaCl.

DMI1 was characterised as a voltage-gated ion channel responsible for the extrusion of K^+ from the nucleoplasm during the symbiotic Ca^{2+} spiking (Charpentier et al., 2013). Therefore, the fact that the levels of *DMI1* gene expression did not change over the three conditions tested suggest that abiotic and biotic stimuli activate different channels and result in the generation of specific calcium signatures (Cao et al., 2017). Similarly, the transcription factor *NIN* did not show any changes in gene expression either over the three [NaCl] (Figure 5.9). This is consistent with the essential role of NIN for the activation of specific signalling components downstream of the Ca^{2+} spiking during nodulation (Schauser et al., 1999; Borisov et al., 2003; Marsh et al., 2007; Jin et al., 2016; Vernié et al., 2015) and mycorrhization (Guillotin et al., 2016).

The GRAS transcription factor NSP2, in complex with NSP1, was shown to interact with DELLA proteins (Chapter One, Section 4.5) which act as a bridge to the CCaMK-CYCLOPS complex. As a result, the NSP1-NSP2 heterocomplex is then able to activate nodulation (Catoira, 2000; Andriankaja et al., 2007; Kalo, 2005; Smit, 2005) and mycorrhization (Akiyama et al., 2005) specific genes for the establishment of the symbiotic interaction. In the presence of 50 mM of NaCl, the gene expression levels of *NSP2* increased very highly to statistically significant levels. These expression levels decreased in the presence of 100 mM of NaCl although still were statistically significant compared to in the absence of salt (Figure 5.9). This result is consistent with the fact that the GRAS transcription

factors have also been shown to participate during abiotic stress responses in other plant species (Ma et al., 2010; Li et al., 2018; Xu et al., 2015).

3. Discussion

CCaMK plays an essential role during plant-microbe symbiosis. In legumes, the perception of Nod and Myc factors at the plant root results in nuclear Ca^{2+} spiking which is decoded by CCaMK. CCaMK is placed immediately downstream of the Ca^{2+} spiking and may be able to discriminate between the Ca^{2+} spiking originated by AMF and rhizobia, activating the specific signalling response. The application of a saline solution to the roots of *Medicago truncatula* has been found to generate an intracellular Ca^{2+} signal of a monophasic pattern (Dr Ben Miller, personal communication, unpublished data). Surprisingly, this study has revealed that CCaMK is also involved in the salt stress response in *Medicago truncatula* and suggests that CCaMK could be responsible for the decoding of the salt-induced Ca^{2+} signal. The *dmi3-1* mutant showed an increased tolerance to salt as the root growth was significantly higher than in A17 at a 150 mM of NaCl *in vitro* (Figure 5.4). Moreover, despite not being statistically significant, the overall root growth of the *dmi3-1* in the presence of different [NaCl] was found to be higher than A17 (Figure 5.4). However, the assessment of root growth performed under greenhouse conditions provided a contrasting result to those obtained from the *in vitro* procedure as no differences in root growth were observed between the two genotypes under the different [NaCl] (Figure 5.5). It was previously shown that the *in vitro* screenings provide valid and useful results for the study of plant phenotypes during salt stress (de Lorenzo et al., 2007; Khan et al., 2016). However, contrasting results were also previously obtained between the *in vitro* and greenhouse experiments, for instance for the study of the salt stress response in different wheat lines (Khan et al., 2016). It is important to note that in the greenhouse experiment, the highest [NaCl] used corresponding to 100 mM only induced a moderate change in root growth (Figure 5.5) as opposed to the sharp reduction in root growth obtained when in the presence of higher [NaCl] during the *in vitro* experiment (Figure 5.3 and 5.4). Lower [NaCl] were employed in the greenhouse experiment because plants were going to be subjected to the treatment for a longer period of time, 2 weeks in soil as opposed to 8 days on plates and also following indications from previous salt stress response studies

in *Medicago truncatula* (MtGEA; de Lorenzo et al., 2007). However, the absence of larger changes in root growth in the presence of 100 mM of NaCl could be due to the need of longer incubation times and possibly, increasing the incubation time to 3-4 weeks could in fact provide more similar results to the *in vitro* experiment. Therefore, the root growth data obtained under the greenhouse conditions would not be used for development of the final conclusions and higher [NaCl] such as 120 and 150 mM or longer incubation times would be recommended for future assessments of root growth during salt stress in *Medicago truncatula*. Consequently, it can be concluded that the [NaCl] and the incubation times are important factors that need to be re-adjusted for obtaining more clear results when assessing the effects of salt stress under greenhouse conditions in *Medicago truncatula*.

In agreement with the differences observed in root growth between the A17 and *dmi3-1* genotypes (Figure 5.4), the *DMI3* gene was found to be significantly upregulated in the presence of 50 mM of NaCl compared with the no-salt condition. The increased salt tolerance of the *dmi3-1* mutant which showed a higher root growth than the A17 and the induction of *DMI3* expression in the presence of moderate [NaCl] confirmed the involvement of CCaMK during the salt stress response and supports the hypothesis of CCaMK being the decoder of the salt-induced Ca^{2+} signal that activates the specific signalling pathway responsible for conferring plant salt sensitivity. These results are also in agreement with previous studies which showed that CCaMK is involved in abiotic stress responses in pea, wheat, maize and rice (Pandey et al., 2002; Shi et al., 2012; Ma et al., 2012; Yang et al., 2011).

Since CYCLOPS/IPD3 is the main phosphorylation substrate of CCaMK/DMI3, it was expected that IPD3 may also be involved during the salt stress response in *Medicago truncatula*. The assessment of root growth in the *ipd3-1* mutant showed no statistical difference in root growth compared to A17 at any given [NaCl], except in the presence of a very high [NaCl] (200 mM) at which an increased root growth was observed for the *ipd3-1* mutant. This result suggested that IPD3 might be involved in the response to very high salinity, in contrast with the DMI3 response to moderate [NaCl] (Figure 5.4). In addition, the *IPD3* gene expression

pattern under salt stress was similar than that of *DMI3* with increased levels of gene expression at 50 mM of NaCl that then decreased in the presence of 100 mM. However, unlike *DMI3*, the increased *IPD3* expression levels at 50 mM of NaCl were not statistically significant indicating that IPD3 might not be involved in the salt stress response or might require higher [NaCl] to be upregulated (Figure 5.9). It was previously shown that in contrast to *dmi3-1*, the *ipd3-1* mutant of *M. truncatula* is not completely symbiosis defective as shortened infection threads and nodule primordia are generated in this mutant. It was recently identified the transcription factor IPD3L, as a functional partner of IPD3 due to the inability of the *ipd3l ipd3* double mutant to form infection threads or nodules (Jin et al., 2018). It was also found that there is functional redundancy between IPD3 and IPD3L, although *IPD3L* is expressed at lower levels than *IPD3 (Jin et al., 2018)*. As a consequence, it is possible that this functional redundancy was responsible for the lack of significant root growth changes obtained during salt stress (Figure 5.4). Therefore, it would be interesting to test the root growth capability of the *ipd3l idp3* double mutant. In addition, it could also be possible that in contrast to during symbiosis, *IPD3L* is the functional partner that expresses more highly than *IPD3* during salt stress and thus, assessing whether the expression levels of *IPD3L* change in the presence of NaCl would be an interesting future experiment. This could help to elucidate whether IPD3 and/or IPD3L are interactors of CCaMK during salt stress in *Medicago truncatula*. Consistently, other interactors of CCaMK in *Medicago truncatula* such as CIP73 or the *Medicago truncatula* orthologs of ZmNAC84, OsMPK1 and OsPP45 which were identified during abiotic stress would also be worth to test for interaction with CCaMK during the salt stress response in *Medicago truncatula*.

DMI2 encodes a leucine-rich repeat (LRR) receptor-like kinase (RLK) that participates in the transduction of the Nod and Myc factor signals as a part of the perception receptor complex composed of LYK3 and NFP (Endre et al., 2002; Stracke et al., 2002; Antolín-Llovera et al., 2014). After perception of the diffusible factors, DMI2 was found to have interacting partners that positively regulate nodulation such as the HMGR (Chapter One, Section 5.3) (Kevei et al., 2007; Venkateshwaran et al., 2015) and a plant MAPKK (Chen et al., 2012). In contrast, it was also identified another interacting partner and phosphorylation substrate of

both LYK3 and DMI2, the U-box E3 Ubiquitin ligase 1 (PUB1) which negatively modulates the early infection and establishment of the symbiotic interaction with AMF and rhizobia (Vernié et al., 2016; Mbengue et al., 2010). The *dmi2-1* mutant showed increased root growth ability at 150 mM of NaCl compared to A17 (Figure 5.4) consistent with the increased expression of *DMI2* in the presence of both 50 mM and 100 mM but that was only statistically significant at 100 mM of NaCl (Figure 5.9). This suggests the potential involvement of DMI2 in the perception/transduction of Na^+ which might confer salt sensitivity to the plant. However, although the root growth capability of the *nfp-1* mutant was not assessed, the NFP expression levels were found to not show any statistically significant changes in the presence of any [NaCl] indicating the lack of involvement during salt stress during under these experimental conditions. This supports the fact that NFP was shown to be responsible for the specific perception of Nod and Myc factors (Amor et al., 2003; Czaja et al., 2012; Maillet et al., 2011).

Since it was demonstrated to be part of the receptor complex responsible for the perception of Nod and Myc factors, DMI2 was not expected to have a role during salt stress. However, this is not very unusual as some members of the large family of LRR-RLKs have previously been reported to have roles during abiotic stress responses (Ye et al., 2017). For instance, a rice LRR-RLK encoding gene denoted as *OsSIK1* was upregulated during treatments with salt, drought and H_2O_2 (Ouyang et al., 2010). Another example is the *Salt-induced Receptor-Like Kinase Srlk*, a LRR-RLK whose expression levels were found to rapidly increase in the presence of 150 mM of NaCl in *Medicago truncatula* A17 roots (de Lorenzo et al., 2009). The fact that DMI2 acts in complex with other receptors (LYK3 and NFP) for the perception of the symbiotic diffusible signals raises the question of whether this would be the case during salt stress and therefore what the identity of these receptors/molecules might be. A possible option could be the GIPCs, recently identified in *Arabidopsis thaliana* to be responsible for binding Na+ in order to gate Ca^{2+} influx channels but this remains to be explored (Jiang et al. 2019). Conversely, there is more information available on the substrates/interactors of LRR-RLKs, particularly of DMI2. As mentioned earlier, PUB1 was found to be a phosphorylation substrate of DMI2 and interestingly, 25

members of the PUB gene family were found to be upregulated during salt stress in *Medicago truncatula* (Song et al., 2017). Therefore, DMI2 might be able to act as a co-receptor in different receptor complexes responsible for the perception of symbiotic diffusible factors and Na^+. This in turn would allow DMI2 to either interact with a positive or negative regulator of symbiotic signalling and enabling the activation of the specific response to either the symbiont or abiotic stress, respectively.

The symbiotic Ca^{2+} spiking was proposed to be generated by the concerted action of the CGNC15a, b and c channels that mediate the nuclear Ca^{2+} influx. CNGC15a, b and c also interact with the DMI1 voltage-gated channel, which mediates the efflux of the potassium counter-ions from the nucleus. Lastly the MCA8 Ca^{2+} ATPase that pumps the Ca^{2+} back into the ER (Capoen et al., 2011; Charpentier et al., 2016, 2013). CNGC15, DMI1 and MCA8 were found to be localised at both the outer and inner nuclear membrane (Capoen et al., 2011; Charpentier et al., 2013). Therefore, in order to activate the process of generating the symbiotic Ca^{2+} spiking, a second messenger is necessary for transporting the signal obtained from the plasma membrane where the perception of diffusible factors occur to the nucleus where the Ca^{2+} spiking machinery is localised. The identity of this second messenger remains to be confirmed but it has been suggested that mevalonate, the direct product of the HMGR1 which interacts with the co-receptor DMI2, could potentially be responsible for driving the signal to the nucleus (Venkateshwaran et al., 2015). Since, DMI2 was confirmed to participate in the salt stress response (Figure 5.4 and 5.9), it is possible that any of these members of the Ca^{2+} spiking generation machinery could be involved too. The *in vitro* assessment of root growth capability in the presence of different [NaCl] showed that the *dmi1-1* mutant was not different from A17 under all [NaCl], except in the presence of 100 mM at which root growth decreased significantly. This suggested that DMI1 could be involved in providing salt tolerance to *Medicago truncatula* under moderate salt stress. However, no significant differences in *DMI1* expression were observed in the absence or presence of any [NaCl] when measured from material treated for long time periods of incubation with NaCl (Figure 5.9). Since DMI1 is involved in the generation of Ca^{2+} spiking and Ca^{2+} signals tend to occur shortly after stimuli perception, the assessment of

DMI1 expression could be assessed after 6h or 24 h of NaCl treatment. This could help further clarify whether DMI1 has a role during the salt stress response in *Medicago truncatula*. Although the *CNGC15* and *MCA8* were not included as candidate genes involved in salt stress in the experiments presented in this chapter, it could be expected that these components of the Ca^{2+} spiking generation machinery were not involved during salt stress either. This is due to the fact that even in the case of having apparently similar patterns, the Ca^{2+} signatures generated upon perception of particular stimuli encode specific information possibly through the activation of different channels (Cao et al., 2017). Therefore, the Ca^{2+} signal originated in response to salt stress would probably be generated by the action of different channels from those involved in the symbiotic Ca^{2+} spiking generation. However, confirmation of whether CNGC15 and MCA8 are involved during salt stress would be recommended in order to validate this hypothesis. In order to do this, assessment of root growth of the *cngc15* and *mca8* mutants of *Medicago truncatula* could be performed under the same experimental conditions presented in this chapter as well as the assessment of gene expression levels of *CNGC15a, b* and *c* and *MCA8*.

Genes encoding GRAS-type transcription factors have been found to be extensively involved during biotic and abiotic stress responses. For instance, the *Arabidopsis thaliana* SCL7 is a GRAS type protein which was found to provide salt as well as drought tolerance (Ma et al., 2010). A rice GRAS gene, *GRAS23* was upregulated during NaCl, jasmonic acid and drought treatments and showed the potential ability to regulate the expression of several anti-oxidation related genes during these stresses (Xu et al., 2015). Consistently, the results presented in this chapter showed that the NSP1 and NSP2, GRAS transcription factors essential for nodulation and mycorrhization (Smit, 2005; Kalo, 2005), are potentially involved in the salt stress response of *Medicago truncatula*. This was observed during the assessment of root growth capabilities of *nsp1-2* and *nsp2-2* mutants which both showed enhanced root growth during the treatment with high [NaCl], 200 mM (Figure 5.4). In addition, the *nsp2-2* mutant also showed a statistically significant increase in root growth in the presence of 150 mM of NaCl compared with A17, similar to the results obtained for the *dmi2-1* and *dmi3-1* mutants (Figure 5.4). Consistently, the expression levels of *NSP2* increased

sharply in the presence of both 50 and 100 mM of NaCl further confirming the involvement of NSP2 during salt stress (Figure 5.9). Although the analysis of *NSP1* gene expression was not possible to perform by qRT-PCR, the RT-PCR studies at 6h and 24h of treatments with NaCl showed no levels of gene expression at any of the conditions, as opposed to NSP2 which did. Therefore, this and the root growth assessment results suggested that NSP1 might not be involved during salt stress but its interacting partner NSP2 is (Figure 5.7).

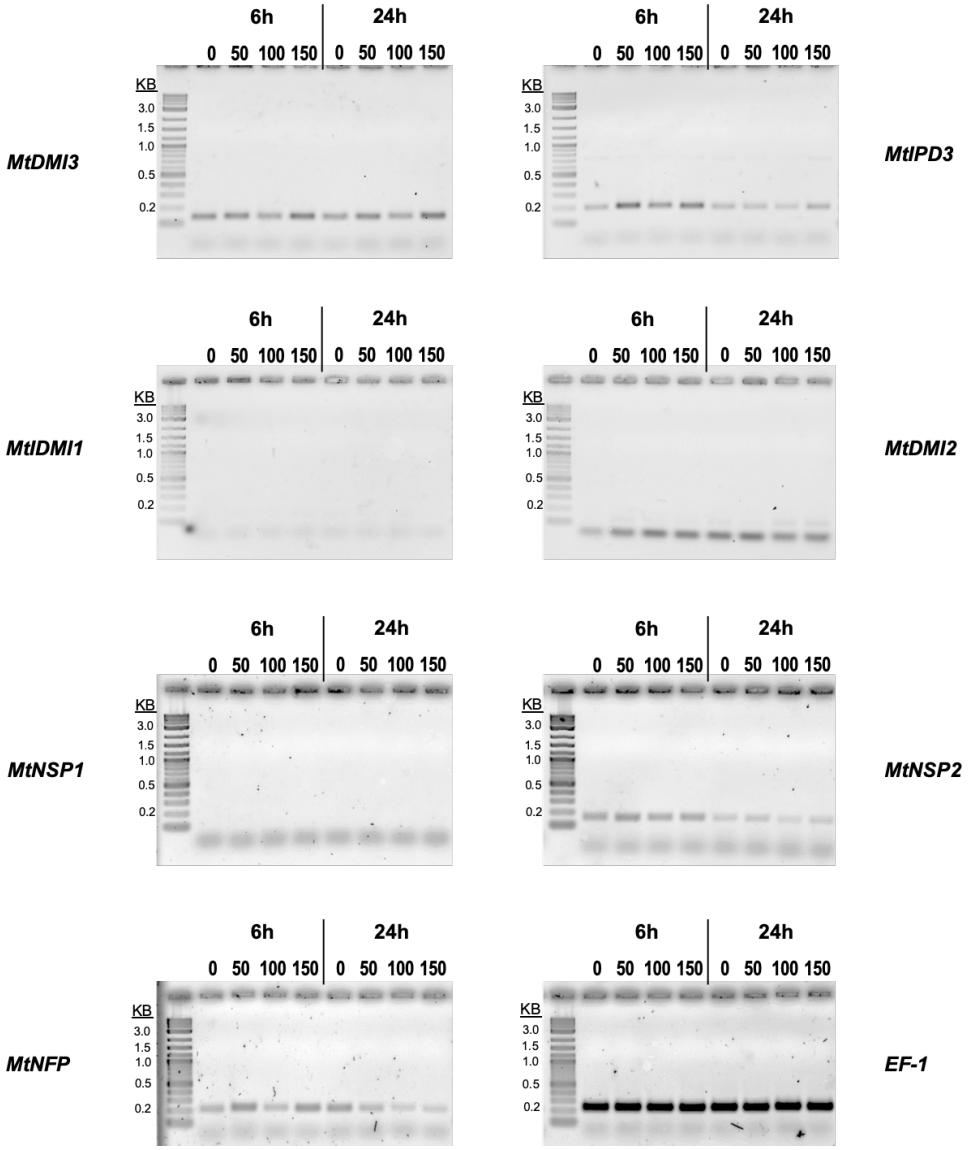

Figure 5. 9. Assessment of the expression of gene members of the CSSP in *Medicago truncatula* roots treated with different [NaCl] for 6 h and 24 h in vitro by RT-PCR.

The expression levels of *MtDMI3, MtIPD3, MtDMI2, MtNSP2 and MtNFP* fluctuated over the different [NaCl] which corresponded to 0 mM (0 in the figure), 50 mM (50), 100 mM

(100) and 150 mM (150), at both 6h and 24 h. *MtDMI1 and MtNSP1* expression was not detected under these experimental conditions. The expression levels of the housekeeping gene *EF1*α were used as a reference. The gene amplification expected sizes were the following: 130 bp *MtDMI3*, 193 bp *MtIPD3*, 123 bp *MtDMI1*, 121 bp *MtDMI2*, 135 bp *MtNSP1*, 153 *MtNSP2*, 194 bp *MtNFP* and 222 bp *EF1*α. The 1 kb Plus DNA ladder (NEB) was used for fragment size identification.

NSP2 was shown not to have any DNA binding activity and interacts with NSP1 which has the ability to bind to DNA (Hirsch et al., 2009). This interaction results in the formation of the NSP1-NSP2 heterocomplex and is actually required for NSP1 binding to the promoter of important downstream signalling components for the activation of nodulation and mycorrhization processes (Hirsch et al., 2009; Cerri et al., 2012; Smit, 2005; Kalo, 2005; Liu et al., 2011). However, NSP2 is also able to bind RAM1, another GRAS transcription factor essential during mycorrhization (Gobbato et al., 2012). This suggests that depending on the stimulus perceived, NSP2 function consists of the binding of transcription factors with DNA-binding capability for the transcriptional activation of specific signalling components. In fact, the NSP1-NSP2 heterocomplex was demonstrated that through the interaction with NSP2, DELLA proteins which also belong to the GRAS family, act as a bridge between the NSP1-NSP2 and CCaMK-CYCLOPS heterocomplexes. The experimental results of this chapter showed that CCaMK, but not its interactor/phosphorylation substrate CYCLOPS, is also involved during salt stress in *Medicago truncatula*. However, the link between CCaMK and NSP2 during salt stress appears as an interesting question from these results. Therefore, finding the identity of the CCaMK interactor during salt stress and the assessment of the involvement of DELLA proteins during salt stress could shed light on the connection between CCaMK and NSP2 during the salt stress response in *Medicago truncatula*.

Lastly, it is important to highlight that the gene expression levels were measured after long incubation with moderate [NaCl]. The assessment of gene expression after shorter periods of incubation such as 6 h and 24 h could be more suitable for representing early signalling responses since the generation of the Ca^{2+} spiking and the activation of the CSSP occur shortly after perception of the Nod

and Myc factors (Chapter One, Section 4). Therefore, assessing the expression of *DMI3, IPD3, DMI1, DMI2, NSP1, NSP2, DELLA, NFP, CNGC15* and *MCA8* could help to confirm the involvement of these genes during the salt stress response in *Medicago truncatula*.

From a common ancestor, the green algae chlorophytes diverged followed by the charophytes, the closest green algae relatives to land plants (Wodniok et al., 2011). Plant colonisation of the land dates ~450 Mya (million years ago) (Lenton et al., 2016) when AM presence in the environment also dated (Taylor et al., 1995; Redecker et al., 2000). It has been suggested that colonisation of the land, which was probably a very challenging process due to nutrient limitation, drought and salt stress among other issues, was probably facilitated by the development of AM-plant interactions (Selosse et al., 2015). This mutualistic interaction allowed the plants to obtain nutrients more efficiently while the fungus obtained a continuous source of energy for survival. However, the single origin of the symbiotic interaction with nitrogen-fixing symbiosis bacteria (rhizobia) is dated ~100 Mya and was proposed to have occurred through the recruitment of signalling components involved in the plant symbiotic interaction with AMF (Parniske, 2000; Werner et al., 2014). This shared evolutionary origin is consistent with the fact that a CSSP has been described from many studies on the model legumes *Lotus japonicus* and *Medicago truncatula*, among other plant species (Oldroyd, 2013).

The origin of some members of the CSSP such as DMI1 and CCaMK, was found to pre-date the plant colonisation of the land and the appearance of AMF as these two genes were already present in both chlorophytes and charophytes (Delaux et al., 2015). Based on the fact that there are not reported AM-charophytes associations, this suggest that both DMI1 and CCaMK might have additional roles than symbiotic. This further supports the results presented in this chapter regarding CCaMK role during salt stress. Although DMI1 was not found to participate in the salt stress response, that does not rule out DMI1 involvement in other abiotic or biotic stresses. Moreover, orthologs of *DMI1* as well as *NSP2* were found to be present in *Arabidopsis thaliana* which is a member of the plant family Brassicaceae and that cannot establish symbiotic interactions with AMF.

The fact that *DMI1* and *NSP2* were present in a plant species unable to interact with AMF suggests the non-symbiotic roles of these genes (Delaux et al., 2013). Consistently, NSP2 appearance also pre-dates AMF as was found present in the charophytes. This agrees with the increased *NSP2* expression and the significantly increased root growth capability of the *nsp2-2* mutant obtained during the treatments with NaCl explained in this chapter.

In contrast to *NSP2*, *IPD3* is not present in members of the Brassicaceae but was present in the charophytes (Delaux et al., 2015, 2013). Regarding the involvement of IPD3 during salt stress, the data presented in this chapter does not provide a firm conclusion as although the *ipd3-1* mutant showed an enhanced salt tolerance at high [NaCl] during the 200 mM of NaCl treatment, the gene expression analysis showed not significant changes in the presence of NaCl compared to in the absence. However, the role of IPD3 during others biotic or abiotic stresses cannot be ruled out either and is supported by the AMF pre-dated appearance of *IPD3* in evolution (Delaux et al., 2013). Since the levels of phytohormone abscisic acid (ABA) increase during plant abiotic stresses (Vishwakarma et al., 2017), treatments of the roots of the *ipd3-1* mutant with ABA could be performed to assess whether there are any phenotype changes. In addition, the expression levels of *IPD3* could also be assessed from plant root material treated with ABA. These experiments would provide further information on whether IPD3 plays a role during abiotic stress other than salt stress.

DMI2 constitutes an interesting case as orthologs were not found in the charophytes and its appearance seems to have occurred with the plant colonisation of the land (Delaux et al., 2015, 2013). This suggests that *DMI2* might have originated specifically for its role during the AMF and rhizobial symbioses. However, this cannot be the case as the results presented in this chapter confirmed that DMI2 is involved in the salt stress response in *Medicago truncatula.* Consequently, these results suggest that *DMI2* might have evolved earlier or at the same time than *DMI1* and *NSP2* which would support the role of DMI2 in both symbiosis and salt stress.

In order to clarify the results presented in this chapter, further experiments could be performed. For instance, the RNA-seq technology (Costa-Silva et al., 2017) could be used for the transcriptomic analysis of *Medicago truncatula* roots treated with NaCl, inoculated with rhizobia and AM, and during both salt stress and symbiosis. The comparison of the transcriptional profiles obtained for *Medicago truncatula* during these three conditions would help to identify genes that participate in both processes. Similar transcriptomics analyses have previously been performed in *Medicago truncatula* for either the identification of candidate genes involved in the response to abiotic stress such as drought (Zhang et al., 2014), salt stress (Li et al., 2011, 2009; Gruber et al., 2009) and during rhizobial and AM-symbioses (Boscari et al., 2013; Cabeza et al., 2014; Damiani et al., 2016; Garcia et al., 2017). However, specific transcriptomic studies to understand the overlap between these processes have not been performed in detail and would constitute an interesting future experiment to help reveal the common genetic elements among these signalling pathways.

In conclusion, this chapter shows that members of the CSSP have additional roles than during the plant symbiotic interactions with AMF and rhizobia. During the colonisation of the land, plants possibly recruited some of the signalling components involved during different abiotic and biotic responses for the development of mutualistic interactions with AMF and rhizobia to facilitate their survival. However, identification of salt stress specific signalling components is still required in order to dissect the symbiotic and salt stress signalling pathways and the results presented in this chapter started to address this. The establishment of symbiosis is a process that the plant is very likely to undertake during high salinity conditions and understanding both processes at the molecular level could help to improve the plant survival and increase crop yields.

Chapter Six - General discussion

1. The EF-hand motif primary sequence encodes information that confers specificity to CCaMK Ca^{2+}-spiking response

Perception of Nod and Myc factors at the plasma membrane of plant root hair cells results in the generation of the nuclear Ca^{2+} spiking. CCaMK lies immediately downstream of the Ca^{2+} spiking and is considered the central regulator of root endosymbiosis due to its ability to decode the Ca^{2+} spiking and activate the genetic components of the common symbiotic signalling pathway (CSSP) shared between the nodulation and mycorrhization symbioses (Singh and Parniske, 2012; Oldroyd, 2013). CCaMK is able to decode Ca^{2+}-spiking during nodulation and mycorrhization due to its exceptional ability to discriminate between basal [Ca^{2+}] and those during Ca^{2+} spiking. This ability is conferred by the CCaMK general structure, which consists of a kinase domain that allows transmission of information downstream through phosphorylation of target proteins, a CaMBD that allows indirect sensing of Ca^{2+} through the binding of Ca^{2+}-CaM, and a VLD composed of four EF-hand motifs, three of which are able to directly bind Ca^{2+} (Patil et al., 1995; Swainsbury et al., 2012).

The EF-hand motifs are essential for the regulation of CCaMK activity during symbiosis as truncated versions of CCaMK lacking one or two EF-hand motifs or the kinase-only version of CCaMK give rise to spontaneous nodulation in the absence of rhizobia (Chapter One, Section 5.2) (Gleason et al., 2006; Tirichine et al., 2006; Shimoda et al., 2012; Miller et al., 2013). Furthermore, the Asp to Ala mutation at the first position of the EF-hand loop (which impairs the binding of Ca^{2+} to either EF-hand 2, 3 and/or 4) results in CCaMK GOF activity as spontaneous nodulation in the absence of rhizobia is also induced by these mutants (Gleason et al., 2006; Tirichine et al., 2006; Shimoda et al., 2012; Miller et al., 2013). However, the fact that not all the single and double EF-hand point mutants of CCaMK possess the same nodulation and/or spontaneous nodulation abilities indicated that each individual EF-hand motif of CCaMK might have a specific role during the regulation of CCaMK activity. This was shown when the single EF-hand point CCaMK mutants with Ca^{2+} binding impaired in one of the EF-hand motifs allowed partial complementation of the *ccamk* nodulation phenotype in addition to induction of spontaneous nodulation in the absence of

rhizobia (Miller et al., 2013). In contrast, the double EF-hand point mutants with Ca^{2+} binding impairment to two EF-hand motifs of CCaMK were able to induce spontaneous nodulation with no ability to complement the *ccamk* phenotype (Miller et al., 2013). Similar to the double EF-hand point mutants, the triple EF-hand point mutant of CCaMK which lacks any Ca^{2+}-binding ability (Swainsbury et al., 2012) was able to induce spontaneous nodulation but did not allowed complementation of *ccamk*.

Nevertheless, contrasting results to those mentioned above were obtained from the work of this thesis for the double EF-hand point mutants of CCaMK. While D413A-D449A and D449A-D491A allowed full complementation of the *ccamk* phenotype, D413A-491A only complemented partially (Figure 3.9). This *ccamk* complementation ability of the double EF-hand point mutants of CCaMK had not been previously reported. Moreover, the fact that the double EF-hand point mutants differed in their complementation and/or spontaneous nodulation abilities clearly supports the potential individual roles of each of the EF-hand motifs of CCaMK. The potential individual role of each CCaMK EF-hand motif during regulation of CCaMK activity is supported by the fact that the EF-hand motifs of CCaMK possess different Ca^{2+} binding affinities (Swainsbury et al., 2012). Consistently, individual EF-hand motif roles have previously been reported in other Ca^{2+} binding proteins such as in the plant Slow Vacuole (SV) channel Two-pore Channel 1 (TPC1) (Schulze et al., 2011). TPC1 contains two canonical EF-hand motifs (Chapter One, Section 3.1) and activates upon increasing cytosolic [Ca^{2+}] (Schulz-Lessdorf and Hedrich, 1995). The impairment of Ca^{2+} binding through the Asp to Ala mutation at position 1 of the EF-loop of each TPC1 EF-hand motif revealed that EF-hand motif 1 of TPC1 does not bind Ca^{2+} during physiological [Ca^{2+}] (Schulze et al., 2011). Therefore, the Ca^{2+} binding through this EF-hand motif was found not to be necessary for activity of the channel. The TPC1 EF-hand 1 was found to act as a modulator of the Ca^{2+} binding to the TPC1 EF-hand motif 2 which possess high affinity for Ca^{2+}. Finally, the binding of Ca^{2+} through the TPC1 EF-hand motif 2 results in the opening of the channel (Schulze et al., 2011).

The factors conferring the Ca^{2+} binding properties to the EF-hand motif remains yet unclear. It is known that the EF-hand motif structure consists of two helices, the incoming and exiting helices, connected by a loop and that the latter provides the conserved seven ligands required for coordination of the Ca^{2+} ion (Chapter One, Section 3.1) (Strynadka and James, 1989). While the primary sequence of the EF-hand loop including both the Ca^{2+} chelating and non-chelating amino acid residues has been considered a major contributor to the Ca^{2+} binding affinity of the EF-hand motif, the EF-hand motif helices also contribute to this (Gifford et al., 2007). This was highlighted in previous studies using chimeras of the cardiac troponin C (TnC) and calmodulin (CaM) which are approximately 51% homologous in amino acid sequence (Wang et al., 1998). The structure of both TnC and CaM consists of two globular domains, the N- and C-terminal lobes, connected by a linker each composed of two EF-hand motifs of different Ca^{2+}-binding affinities (Herzberg and James, 1988; Babu et al., 1988). The substitution of the third and fourth EF-hand motifs of TnC into CaM resulted in no changes to the Ca^{2+} binding ability of the C-terminal region of CaM. However, substitution of the third EF-hand motif of TnC alone into CaM did result in a 10-fold increase in the Ca^{2+} binding affinity of CaM (George et al., 1993). This demonstrates the essential role of the EF-hand motif 3 in conferring high affinity for Ca^{2+} to the entire C-terminal EF-hand pair of TnC. However, when each component of TnC EF-hand 3 (incoming helix, loop, exiting helix) was individually substituted into CaM, differences were observed for each component (Wang et al., 1998). The substitution of each TnC EF-hand 3 component into CaM resulted in different increases in the Ca^{2+} binding affinity of the EF-hand with the exiting helix responsible for the most dramatic increase (Wang et al., 1998). As a result, this demonstrates that the EF-helices also contribute to the Ca^{2+} binding properties of EF-hand motifs.

In order to better understand how the EF-hand motif functions and identify whether their primary sequence and/or their tertiary structure is responsible for the individual role of each EF-hand motif, the native EF-loops of CCaMK were interchanged creating a total of 24 CCaMK variants including WT (Chapter Three). Each EF-loop of CCaMK was placed in between each CCaMK native pair of EF-helices. This allowed the mutagenesis of the CCaMK EF-hand motifs without the potential alteration of their tertiary structure since each EF-loop was

exchanged for another EF-loop without disrupting the canonical structure of the EF-hand motif (Chapter Three). The assessment of nodulation and spontaneous gene expression capabilities of the CCaMK swaps revealed that more than 50% of the CCaMK swaps were unable to allow nodulation or spontaneous gene expression (Figure 3.9, 3.14 and Appendix 2). This suggests that most of the CCaMK swaps contained new helix-loop-helix combinations that are unable to decode the symbiotic Ca^{2+} spiking. In contrast, a limited number of CCaMK swaps were able to fully or partially complement the *ccamk* phenotype and/or were able to induce spontaneous gene expression (Figure 3.9, 3.14 and Appendix 2) which suggests that their helix-loop-helix combinations are suitable for decoding of the Ca^{2+} spiking. The interchanging of the EF-loops of CCaMK was predicted to have a minimal impact on the tertiary structure of the new helix-loop-helix combinations since each native EF-loop of CCaMK was replaced with another native CCaMK EF-loop. Since it is likely that no significant changes occurred to the EF-hand tertiary structure, these results demonstrate that the primary sequence of the EF-hand motif encodes specific information for the regulation of CCaMK activity (Chapter Three) (Figure 6.1).

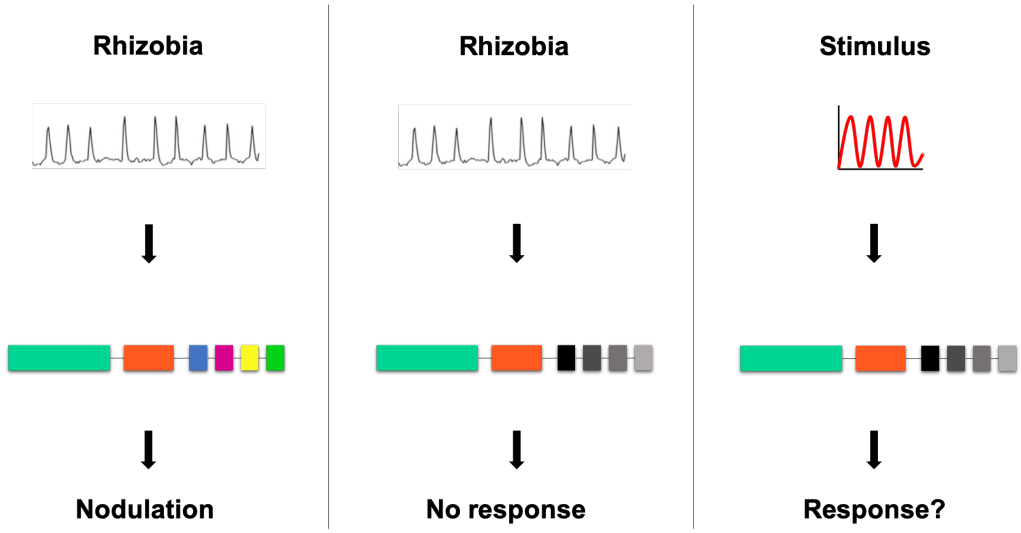

Figure 6. 1. The primary sequence of the EF-hand motif encodes specific information that allows the protein to respond to a particular Ca^{2+} signal.

Replacement of the EF-hand motif loops with others of different primary sequence might enable the CCaMK protein to respond to a different Ca^{2+} signal. CCaMK has the ability to respond to the Ca^{2+} spiking induced by rhizobia. However, if the EF-hand loops of CCaMK were replaced by other EF-hand loops of different primary sequence, CCaMK

would not be able to respond to the Ca^{2+} spiking. In contrast, CCaMK with these new EF-hand loop sequences could be able to respond to the Ca^{2+} signals induced by a different stimulus. The CCaMK kinase domain is shaded in turquoise, the calmodulin binding domain (CaMBD) is shaded in orange, the EF-hand loop 1 is shaded in blue, the EF-hand loop 2 is shaded in pink, the EF-hand loop 3 is shaded in yellow, the EF-hand loop 4 is shaded in green. The replacement of the native EF-hand loops of CCaMK has been represented by different grey shades on the EF-hand loops.

The replacement of an EF-hand loop within an EF-hand motif entails that new interactions between the residues from the loop and/or the helices are formed. Although the main tertiary structural arrangement of the CCaMK EF-hand motifs was not altered, these new residue interactions could potentially induce minor changes on the EF-hand motif structure conformation upon Ca^{2+} binding that ultimately could lead to changes in the EF-hand Ca^{2+} binding properties such as their Ca^{2+}-binding affinity. This raises the question of whether these new helix-loop-helix combinations did not allow the CCaMK swaps to respond to the Ca^{2+} spiking because of the lack of Ca^{2+} binding to their EF-hand motifs or alternatively, because of changes to their Ca^{2+} binding affinities to different values from those of CCaMK WT EF-hand motifs. The change in the EF-hand Ca^{2+} binding affinities could result in the loss of their ability to respond to the symbiotic Ca^{2+} spiking. However, the inability of a mutant to respond to Ca^{2+} spiking does not exclude the potential for the mutant protein to gain ability to respond to an additional Ca^{2+} signature or signatures other than the Ca^{2+} spiking (Figure 6.1).

Therefore, changes in the Ca^{2+} binding affinity of the EF-hand motifs could have an impact on the activity of CCaMK since the altered Ca^{2+} binding affinities of the EF-hand motifs might activate the CCaMK swaps during the response to a Ca^{2+} signal other than Ca^{2+} spiking. This impact on the protein activity caused by altered EF-hand Ca^{2+} binding affinities has been previously reported in other proteins such as the photoprotein aequorin from the luminous jellyfish *Aequorea victoria* (Shimomura et al., 1962). Aequorin possesses four EF-hand motifs (helix-loop-helix structure), three of which can bind Ca^{2+} (Head et al., 2000). However, the Ca^{2+}-triggered luminescence of aequorin does not occur via the binding of

Ca^{2+} through the three aequorin Ca^{2+}-binding EF-hand motifs. Instead, it was reported that EF-hand 1 of aequorin, and specifically the sequence of the EF-hand 1 loop was responsible for the Ca^{2+}-induced luminescence of aequorin (Inouye and Sahara-Miura, 2016) which further supports the potential individual roles of each EF-hand motif within the protein function. The identification of the EF-hand 1 loop of aequorin as being responsible for its Ca^{2+}-triggered luminescence by Inouye and Sahara-Miura (2016) was made by substitution of this loop for other EF-loops from other Ca^{2+} binding proteins. This constitutes a similar experimental approach to understanding the EF-hand motif structure-function relationship that was undertaken in the work of this thesis. Interestingly, the work by Inouye and Sahara-Miura (2016) also revealed that modification of the EF-hand 1 loop primary sequence of aequorin by replacement with another EF-loop of different amino acid residues resulted in changes in the Ca^{2+} binding affinity of that EF-hand motif. As a result, the new Ca^{2+} binding affinities of EF-hand motif 1 caused a change in the pattern of luminescence of Aequorin but did not completely abolish its luminescence activity (Inouye and Sahara-Miura, 2016). This demonstrates that indeed, modification of the EF-hand loop sequences does result in changes to their Ca^{2+}binding affinities that ultimately have an impact on the overall protein activity. However, changing the sequence of the EF-loops also has an impact on the EF-helices as interactions between residues from helices and loop occur within the EF-hand. Consequently, it cannot be ruled out that the changes in EF-hand Ca^{2+} binding affinities might be a consequence of the changes occurred on both helices and loop despite the modifications having been made only in the EF-loops (Reviewed in Chapter Three). Changes in the Ca^{2+} binding affinities of the EF-hands could also be the case for the CCaMK swaps as many of them were unable to allow nodulation or spontaneous nodulation (Figure 3.9), suggesting that potential changes to their Ca^{2+} binding affinities might have occurred which might not allow or modify the ability of the CCaMK swaps to respond to the Ca^{2+} spiking. Therefore, the assessment of the Ca^{2+} binding capabilities and affinities of the EF-hand motifs of the CCaMK swaps by techniques such as isothermal titration calorimetry (ITC) would contribute to shed further light on the EF-hand motif structure-function relationship. The experimental procedures for the measurement of the Ca^{2+} binding affinities of the CCaMK EF-hand motifs have previously been established

and similar procedures could be followed for the CCaMK swaps (Swainsbury et al., 2012). Alternatively, the prediction of Ca^{2+}-binding affinities based on primary sequence could also be possible. Mazumder et al. (2014) developed a method based on position-specific scoring metrics that allowed to predict the Ca^{2+}-binding affinities of EF-hand motifs from their amino acid sequences with an accuracy between 87 and 90%. Using this method, 58 EF-hand protein sequences with 153 binding loops were predicted within the whole *Entamoeba histolytica* proteome. In addition, this method allowed the identification of 36 Ca^{2+}-binding sites, 24 of low-affinity and 12 high-affinity for Ca^{2+} within the *E. histolytica* proteome. The predicted affinities were experimentally validated by isothermal titration calorimetry, demonstrating the suitability of this computational method for predicting Ca^{2+} binding affinity of the EF-hand motifs based on their primary sequence (Mazumder et al., 2014). Similarly, this tool could also be used to predict the changes in Ca^{2+}-binding affinity potentially occurred upon modification of the EF-hand motif primary sequence of Ca^{2+}-binding proteins like CCaMK.

Ca^{2+}-binding to the EF-hand motifs of CCaMK results in the exposure of a hydrophobic surface that allows the interaction with target proteins (Swainsbury et al., 2012). Indeed, the region within CCaMK structure responsible for the interaction with the target protein CYCLOPS was found to be located between the CaMBD and EF-hand 2 of CCaMK (Yano et al., 2008). The interchanging of EF-loops within the CCaMK structure might have also conferred CCaMK swaps different hydrophobic exposure abilities than that of the CCaMK WT. Previous studies using TnC and CaM chimeras (structures described above) revealed that exchanging EF-hand motifs between these two Ca^{2+} binding proteins did alter the hydrophobic exposure of these chimeras (Jensen et al., 2015). In the work by Jensen et al. (2015), each entire EF-hand motif of TnC was substituted into CaM constituting a total of four chimeras named as CaM(1TnC) which contained EF-hand motif 1 of TnC in place of the CaM EF-hand 1 motif within CaM, CaM(2TnC), CaM(3TnC) and CaM(4TnC). Overall, the Ca^{2+}-induced exposure of hydrophobic surfaces was reduced in all four chimeras but the target-binding affinity was only reduced in the CaM(1TnC) and CaM(2TnC) while no changes were observed in the target-binding ability of CaM(3TnC) and CaM(4TnC). Furthermore, the reduced target-binding affinity of the CaM(1TnC) and CaM(2TnC) chimeras was suggested to be caused by the N-terminal lobe of these chimeras adopting a

structural arrangement upon Ca^{2+} binding that is different than that of CaM N-terminal lobe (Jensen et al., 2015). These results highlight the importance of the structural role of the EF-hand motif within the protein structure and that Ca^{2+}-binding to the same EF-hand motif placed in two different protein scaffolds could lead to activation of different target proteins (Figure 6.2). This support the hypothesis that modification of the native CCaMK EF-hand motifs could be responsible for altered or impaired hydrophobic surface exposure in some of the CCaMK swaps. The differences in the hydrophobic surface exposure might occur due to the structural arrangements adopted by the CCaMK swap EF-hand motifs that could potentially be different from that of the native CCaMK EF-hand motifs. As a result, these structural changes could possibly lead to negative effects on the ability of CCaMK to interact with the target protein CYCLOPS upon Ca^{2+} spiking perception, which could be another reason why most of the CCaMK swaps were not able to fully complement the *ccamk* mutant (Figure 3.9).

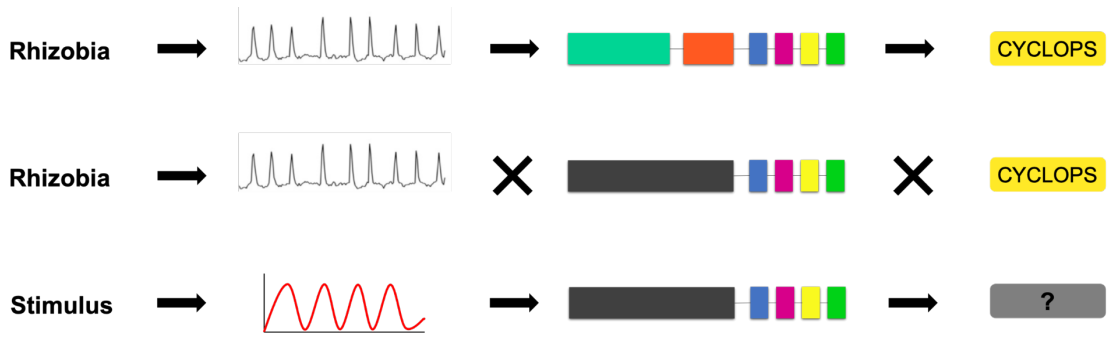

Figure 6. 2. EF-hand motifs of a particular primary sequence within different protein scaffolds might activate distinct target proteins, highlighting the importance of the structural role of the EF-hand motifs.

CCaMK EF-hand motifs allow the perception of the Ca^{2+} spiking induced by rhizobia and results in CCaMK activation which in turn, allows the activation of its target protein CYCLOPS. However, according to the mechanism of activation of CCaMK, placing the EF-hand motifs of CCaMK in a different protein scaffold would not allow the same response to the rhizobia-induced Ca^{2+} spiking. In contrast, this protein scaffold with added CCaMK EF-hand motifs may unable the respond to the Ca^{2+} signal induced by a different stimulus from rhizobia and as a result, in the activation of a different target protein other than CYCLOPS. The CCaMK kinase domain is shaded in turquoise, the calmodulin binding domain (CaMBD) is shaded in orange, the EF-hand loop 1 is shaded

in blue, the EF-hand loop 2 is shaded in pink, the EF-hand loop 3 is shaded in yellow, the EF-hand loop 4 is shaded in green. The different protein scaffold from CCaMK is represented in dark grey, CYCLOPS is shaded in yellow and a different target protein from CYCLOPS is represented by a question mark and shaded in lighter grey.

As demonstrated by several studies mentioned above, modification of the EF-hand motif primary sequence could lead to changes in Ca^{2+}-binding affinity, structural conformation and exposure of hydrophobic surfaces for interaction with target proteins. An important part of the mechanism of regulation of CCaMK activity is the autophosphorylation on Thr271 which depends on Ca^{2+} binding during basal [Ca^{2+}] and keeps CCaMK in the inactive state but primed for activation (Sathyanarayanan et al., 2000, 2001; Miller et al., 2013). Since the binding of Ca^{2+} (most likely to be through EF-hand 4 of CCaMK because of its high affinity) is required for Thr271 autophosphorylation, the interchanging of the native EF-loops of CCaMK might have also altered this process (Swainsbury et al., 2012; Miller et al., 2013). The binding of Ca^{2+} through the EF-hand motif causes a conformational change which also occurs in the CCaMK EF-hand motifs (Swainsbury et al., 2012). Similarly, the replacement of CCaMK EF-loop 4 with another EF-loop might be altering the Ca^{2+}-binding capability of EF-hand 4 of the CCaMK swaps. As a result, EF-hand 4 might adopt a different structural rearrangement that ultimately affect the ability of CCaMK to autophosphorylate on Thr271. Therefore, the assessment of Thr271 autophosphorylation capabilities of the CCaMK swaps would also provide further knowledge about the link between structure and function of the EF-hand motifs of CCaMK. The experimental procedures for purification and kinase assays of CCaMK have been developed in this thesis (Chapter Four) which would facilitate further studies of the CCaMK swaps. Lastly, the resolution of the crystal structure of CCaMK and the use of in-silico predictions have been previously performed for other Ca^{2+} binding proteins such as CaM (Piazza et al., 2017), and would allow the visual detection of structural changes that might be occurring when the EF-hand motif sequences of CCaMK are modified.

2. CCaMK might be involved during salt stress as a Ca^{2+} signal decoder

CCaMK was found to be upregulated during salt stress in *Medicago truncatula* (Figure 5.9). Consistently, the *dmi3-1* (*ccamk*) mutant showed a higher tolerance to salt stress as the root growth of *dmi3-1* significantly increased compared to WT in the presence of 150 mM of NaCl (Figure 5.4). These results suggest that in addition to be the Ca^{2+} spiking decoder, CCaMK could also be involved in the salt stress response as a decoder of the potential Ca^{2+} signal induced by salt in *Medicago truncatula*. In addition, a Ca^{2+} signal of a monophasic pattern (single increase in $[Ca^{2+}]_c$) was observed in *Medicago truncatula* upon treatment with NaCl (Miller, personal communication), demonstrating that salt indeed induces a Ca^{2+} signal in *Medicago truncatula*. However, how CCaMK would be able to discriminate between the symbiotic and salt-stress Ca^{2+} signals and activate the specific components of one signalling pathway or the other remain yet unknown.

It has previously been reported that the frequency of Ca^{2+} oscillations confers specificity to the activation of particular transcription factors in mammalian cells (Dolmetsch et al., 1998; Smedler and Uhlén, 2014). Similarly, the use of artificially imposed $[Ca^{2+}]_c$ oscillations revealed that in plants, different sets of genes are up- and down-regulated in response to Ca^{2+} signatures of different amplitudes and frequencies (Whalley and Knight, 2013). These studies demonstrated that Ca^{2+} signatures of different patterns (amplitude, duration and frequency) are able to activate the expression of different genes and therefore, different Ca^{2+} signal decoders would specifically be activated. For instance, the ability to decode different Ca^{2+} oscillation frequencies has previously been observed in other Ca^{2+} decoders such as the CaM-dependent protein kinase II (CaMKII) (De Koninck and Schulman, 1998). Upon the generation of the Ca^{2+} signal, CaMKII binds Ca^{2+}-bound CaM which induces the autophosphorylation of Thr286 of CaMKII. The Thr286 autophosphorylation increases the affinity of CaMKII for CaM which allows CaM-trapping and provides autonomy to CaMKII to remain active after CaM dissociation (Chapter One, Section 3.5). The ability of CaMKII to decode different $[Ca^{2+}]_c$ oscillation frequencies was observed through the use of artificially imposed $[Ca^{2+}]_c$ oscillations. This study revealed that the response of CaMKII was significantly greater when a higher frequency of Ca^{2+} pulses was applied rather than lower frequencies (De Koninck and Schulman, 1998). In addition, CaMKII showed an increased activity autonomy in response to $[Ca^{2+}]_c$

oscillations of higher frequency (De Koninck and Schulman, 1998). Therefore, the different degrees of responsiveness and autonomous activity obtained for CaMKII for the different Ca^{2+} signatures were suggested to be responsible for the specificity in the activation of CaMKII (De Koninck and Schulman, 1998). The structure of CCaMK has features that resemble the mammalian CaMKII and the CaMBD of CCaMK is 79% homologous to the α-subunit of CaMKII (Patil et al., 1995). Ca^{2+} spiking consists of the [Ca^{2+}] oscillation (Chapter One, Section 4.4) while the salt-stress Ca^{2+} signal in *M. truncatula* has been observed to correspond to a single increase and decrease of the [Ca^{2+}] (monophasic; Miller, personal communication). Therefore, like CaMKII, it is possible that CCaMK also has the ability to respond to different Ca^{2+} signatures (Ca^{2+} spiking and the salt-stress Ca^{2+} signal).

It is important to realise that although CaMKII has the ability to specifically respond to different Ca^{2+} signatures (De Koninck and Schulman, 1998), CaMKII relies on CaM for the perception of the Ca^{2+} signal before being able to decode it. The ability of CaM to perceive the Ca^{2+} signal is due to its structure which consists of two globular domains each of which contain two EF-hand motifs of different affinities for Ca^{2+} (Johnson et al., 1996). The various conformational states that CaM can adopt and the different Ca^{2+} binding properties of N- and C-terminal lobes allow CaM to specifically regulate a vast array of target proteins and the decoding of a wide range of Ca^{2+} signatures (Chin and Means, 2000; Samanta and Parekh, 2017; Villarroel et al., 2014). Unlike CaMKII, CCaMK has the additional ability to perceive the changes in [Ca^{2+}] through the three Ca^{2+}-binding EF-hand motifs also included in its structure (Chapter One, Section 5.1) and therefore, CCaMK does not entirely rely on CaM for perception of Ca^{2+}. Instead, CCaMK possess a second mode of regulation by Ca^{2+}/CaM which constitutes an important part of the mechanism of activation of CCaMK during symbiosis (Miller et al., 2013). As explained in the previous paragraph, the upregulation of *CCaMK* during salt stress in *Medicago truncatula* (Figure 5.9) and the increased salt tolerance of the *dmi3-1* (*ccamk*) mutant (Figure 5.4) suggest that CCaMK might have the ability to respond to both the symbiotic and salt-stress Ca^{2+} signatures. The fact that the activation of CCaMK occurs after a certain number of [Ca^{2+}] spikes and in response to a particular pattern of [Ca^{2+}]

oscillations (Ca^{2+} spiking) (Chapter One, Section 4.4) suggests that the EF-hand motifs of CCaMK bind Ca^{2+} under specific conditions. Moreover, the Ca^{2+} binding affinities of the CCaMK EF-hand motifs might be responsible for the ability of CCaMK to decode the Ca^{2+} spiking, as explained in previous paragraphs. Therefore, it seems unlikely that the EF-hand motifs of CCaMK would also bind Ca^{2+} during salt stress in a similar manner than during symbiosis. For instance, it is possible that their Ca^{2+} binding affinities do not allow all three-Ca^{2+} binding EF-hand motifs of CCaMK to bind Ca^{2+} in response to the salt-stress Ca^{2+} signal. In fact, it could be possible that CCaMK EF-hand motifs do not bind Ca^{2+} during the response to the salt-induced Ca^{2+}-signature but instead, CCaMK relies on CaM to specifically respond to this signal during salt-stress in a similar manner to CaMKII. It is important to highlight that different isoforms of CaM exist in plants which increase the number of target proteins that CaM is able to activate and Ca^{2+} signals that CaM can decode (Lee et al., 2000, 1999). Consequently, it could also be hypothesised that the CaM isoform that regulates CCaMK during symbiosis might be different than the isoform involved during salt stress, which would explain the involvement of CCaMK during both salt stress and symbiosis. For instance, the NAD kinase (NADK) of soybean is activated by the constitutively expressed CaM1 but inhibited by the stress-induced CaM4. However, it was found that both CaM1 and CaM4 have the ability to respond to the same Ca^{2+} signatures and that the differential regulation of their target protein is achieved through the different conformational states that CaM isoforms adopt once bound to the target (Walton et al., 2017). This could also be the case for CCaMK which might be differentially regulated by CaMs during salt stress and symbiosis (Figure 6.3).

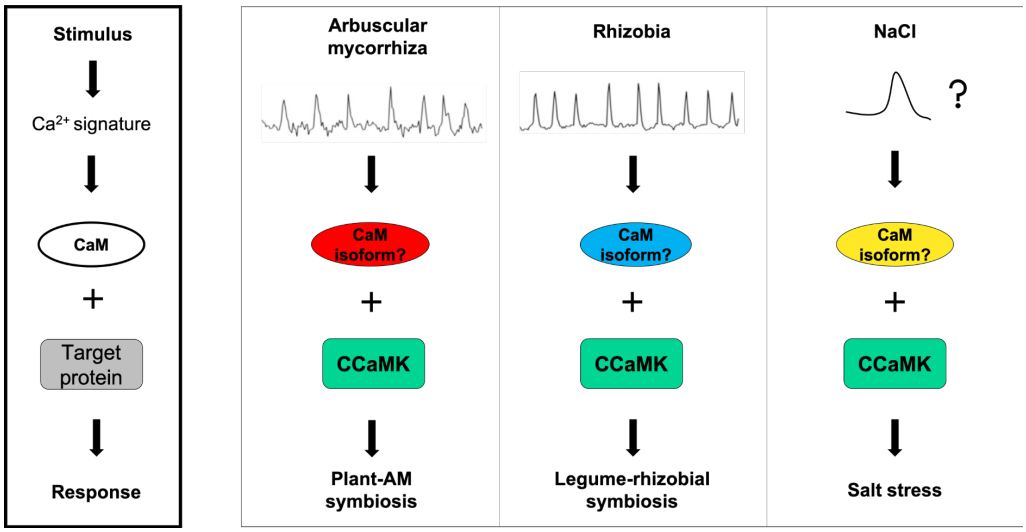

Figure 6. 3. Different CaM isoforms might be responsible for the ability of CCaMK to respond to the Ca^{2+} spiking and salt stress Ca^{2+} signal.

CCaMK is able to respond to both rhizobia and AM induced Ca^{2+} spiking and activate the specific downstream signalling components. Consistent with the results obtained in Chapter Five of this thesis, CCaMK might be able to respond to the salt-stress Ca^{2+} signal. Since the mechanism of activation of CCaMK requires the binding of CaM, and different CaM isoforms can be found in plants, it is possible that CaM isoforms might be activated differently in response to each of these Ca^{2+} signals. This would result in differences in the activation of CCaMK and therefore, the specific response to the stimulus is induced.

The CCaMK swaps showed altered abilities to allow nodulation and/or spontaneous gene expression in the absence of rhizobia (Chapter Three). As described in the previous section of this chapter, the changes in the EF-hand motif primary sequences could be responsible for providing different Ca^{2+}-binding affinities, structural arrangements and/or hydrophobic exposure abilities to the EF-hand motifs of CCaMK. In addition, the results presented in Chapter Five suggest that CCaMK might be responsible for conferring salt sensitivity to *Medicago truncatula* (Figure 5.4). Since the Ca^{2+} binding properties of the EF-hand motifs of the CCaMK swaps are different from those of the native CCaMK EF-hand motifs, it is possible that these CCaMK swaps could also have different activities than CCaMK WT during salt stress. It would be interesting to test whether those CCaMK swaps that allowed full or partial complementation of the

ccamk mutant (Figure 3.) would be less sensitive to salt. This could possibly lead to the identification of CCaMK swap variants with retained nodulation ability but potentially less ability to respond to the salt-induced Ca^{2+} signal, which would ultimately contribute to confer salt tolerance to *Medicago truncatula*. This would be of high interest in agriculture, as it would help to increase crop yields in high salinity soils.

3. Does the putative salt-induced Ca^{2+} signal occur in the cell nucleus in *Medicago truncatula*?

CCaMK conveniently localises to the nucleus of root hair cells for the decoding of Ca^{2+} spiking which also originates in the nucleus upon perception of the Nod and Myc factors at the plasma membrane (Kelner et al., 2018; Yano et al., 2008; Charpentier and Oldroyd, 2013). The generation of Ca^{2+} signals in the cell nucleus has been widely reported in response to biotic and abiotic stresses (Charpentier, 2018). These signals have been shown to be specifically generated in the cell nucleus, as during symbiosis, and not by diffusion from the cytoplasm (Charpentier, 2018; Kelner et al., 2018).

Osmotic and salt stresses have been shown to induce increases in both cytosolic $[Ca^{2+}]$ ($[Ca^{2+}]_c$) and nuclear $[Ca^{2+}]$ ($[Ca^{2+}]_n$) in *Arabidopsis* root cells and that these two Ca^{2+} signals are generated independently of each other (Huang et al., 2017; Kelner et al., 2018). Furthermore, these cytosolic and nuclear Ca^{2+} signals induced by salt stress were both shown to mediate the root growth inhibition in *Arabidopsis* usually caused by salt stress (Huang et al., 2017). In addition, these two Ca^{2+} signals are of distinct patterns as the shape of the salt-induced Ca^{2+} signature consisted of a single transient peak (monophasic) in both the cytoplasm and nucleus of the root cells in *Arabidopsis* but their amplitudes were different (Kelner et al., 2018). However, the salt-stress induced cytosolic and nuclear Ca^{2+} signals were found to be functionally independent such that the blocking of one of these signals would not have an effect on the other (Huang et al., 2017). Consistently, these two signals led to the transcriptional activation of different stress-related plant genes (Huang et al., 2017; Kelner et al., 2018). Similarly, a single increase in the $[Ca^{2+}]$ was observed in roots of *Medicago truncatula* upon treatment with NaCl (Miller, personal communication), although it is not known

whether this transient peak occurs in the cytoplasm and/or the nucleus. The fact that salt stress has been shown to induce both $[Ca^{2+}]_c$) and $[Ca^{2+}]_n$ increases in roots of *Arabidopsis* matches with the potential role of CCaMK as a decoder of the salt-induced $[Ca^{2+}]_n$ suggested by the results obtained in Chapter Five.

4. Overlapping signalling pathways between the salt-stress response and the CSSP in *Medicago truncatula*

The results presented in Chapter Five revealed that certain members of the CSSP might have an additional role during the salt-stress response in *Medicago truncatula*. As explained in section 2 of this chapter, CCaMK (DMI3), which decodes the symbiotic Ca^{2+} spiking, is one of these members that was found to be involved during salt stress. In addition, the LRR-RLK named DMI2 and the GRAS transcription factor NSP2 were also identified as potentially being involved during the salt stress response (Chapter Five). In fact, these three signalling components confer sensitivity to salt stress in *Medicago truncatula* based on the results obtained from the assessment of root growth of the *dmi3-1*, *dmi2-1* and *nsp2-2* mutants (Figure 5.4). These results suggest a potential crosstalk between the signalling pathways activated in response to salt-stress and the symbionts AM and rhizobia.

Plants in their natural habitats have to face many environmental stress factors such as high salinity, drought, high and low temperatures, nutrient deficiency and pathogen attacks that often lead to physiological damage and to the reduction of crop productivity (Pandey et al., 2015). However, plants are not usually exposed to a single environmental stress factor but instead, biotic or abiotic stresses occur either in a simultaneous or sequential manner. This requires the tight coordination of the signalling events activated by each type of stress factors. Consistently, there are many published reports addressing the signalling crosstalk in the signalling cascades induced by biotic and abiotic stresses. For instance, biotic and abiotic stress activate the signalling mediated by Ca^{2+}, the phytohormones ABA, salicylic acid (SA) and ethylene, reactive oxygen species (ROS), Mitogen-Activated Protein Kinase (MAPK) and GTP-binding proteins (G-proteins). The crosstalk between the aforementioned signalling cascades during biotic and abiotic stress have been extensively reviewed (Gupta et al., 2016; Fujita et al.,

2006; Saúl Fraire-Velázquez, 2011; Rejeb et al., 2014; Sharma et al., 2013; Ku et al., 2018). However, the underlying molecular mechanisms driving this signalling convergence among stress responses remains yet unclear.

Interestingly, it has been reported that plants are capable of developing resistance to certain stress factors upon facing a particular stress during the simultaneous exposure to different environmental stress conditions. For instance, the salt-tolerance of tomato plants was increased after wounding (Capiati et al., 2006). Another example is that the stomatal closure to stop pathogen entry also helps the plant to reduce water loss which enhances the plant resistance to drought (Goel et al., 2008). This is called cross-tolerance and requires the crosstalk among the different signalling pathways activated in response to multiple stresses in order for the plant to adapt to the changing environments (Bowler and Fluhr, 2000). For example, the crosstalk between Ca^{2+} signalling and reactive oxygen species (ROS) signalling have been reported during the response to abiotic and biotic stresses (Gilroy et al., 2016; Suzuki and Katano, 2018).

The use of the AM and rhizobial symbioses for alleviating the adverse effects of biotic and abiotic stresses on plants is growing rapidly in modern agriculture as a sustainable way to provide global food security (Duhamel and Vandenkoornhuyse, 2013; Dimkpa et al., 2009; López-Ráez, 2016; Staudinger et al., 2016; Kumar et al., 2015). The AM symbiosis provides the plant an increased water and nutrient uptake due to the fungal arbuscules formed in the plant roots (Chapter One, Section 4.2) and has been shown to induce salt tolerance in plants (Evelin et al., 2019). On the other hand, the rhizobial symbiosis provides legumes with a continuous source of nitrogen due to the ability of these bacteria to fix atmospheric nitrogen inside the plant root nodules (Chapter One, Section 4.1) and was reported to provide drought tolerance in *Medicago truncatula* (Staudinger et al., 2016). CCaMK, DMI2 and NSP2, which are members of the CSSP for establishing the rhizobial and AM symbioses, have been found to be involved during salt stress in *Medicago truncatula* (Chapter Five). However, their roles in the signalling crosstalk between symbiosis and abiotic stress needs to be further clarified. The understanding of these symbiotic interactions at the molecular level and their signalling crosstalk with biotic and abiotic stress

signalling responses may enable genetic engineering and the creation of stress-tolerant crop varieties to improve agricultural productivity.

List of references

Aboul-Soud, M.A.M., Aboul-Enein, A.M., and Loake, G.J. (2009). Nitric oxide triggers specific and dose-dependent cytosolic calcium transients in Arabidopsis. Plant Signal. Behav. **4**: 191–196.

Ahmed, N., Chachar, S., Chachar, Q., I Keerio, M., Shereen, A., and H Chachar, M. (2014). Screening for salt tolerant rice (Oryza sativa L.) genotypes at early seedling stage.

Akiyama, K., Matsuzaki, K., and Hayashi, H. (2005). Plant sesquiterpenes induce hyphal branching in arbuscular mycorrhizal fungi. Nature **435**: 824–827.

Amann, E., Ochs, B., and Abel, K.-J. (1988). Tightly regulated tac promoter vectors useful for the expression of unfused and fused proteins in Escherichia coli. Gene **69**: 301–315.

Amor, B.B., Shaw, S.L., Oldroyd, G.E.D., Maillet, F., Penmetsa, R.V., Cook, D., Long, S.R., Dénarié, J., and Gough, C. (2003). The NFP locus of Medicago truncatula controls an early step of Nod factor signal transduction upstream of a rapid calcium flux and root hair deformation. Plant J. **34**: 495–506.

Amtmann, A., Gobert, A., Sanders, D., Maathuis, F.J.M., and Park, G. (2006). Arabidopsis thaliana Cyclic Nucleotide Gated Channel 3 forms a non-selective ion transporter involved in germination and cation transport. J. Exp. Bot. **57**: 791–800.

Andersson, A., Forsen, S., Thulin, E., and Vogel, J.J. (1983). Cadmium-113 nuclear magnetic resonance studies of proteolytic fragments of calmodulin: assignment of strong and weak cation binding sites. Biochemistry **22**: 2309–2313.

Andriankaja, A., Boisson-Dernier, A., Frances, L., Sauviac, L., Jauneau, A., Barker, D.G., and de Carvalho-Niebel, F. (2007). AP2-ERF Transcription Factors Mediate Nod Factor–Dependent Mt ENOD11 Activation in Root Hairs via a Novel cis-Regulatory Motif. Plant Cell **19**: 2866–2885.

Ané, J.-M. et al. (2004). Medicago truncatula DMI1 Required for Bacterial and Fungal Symbioses in Legumes. Science **303**: 1364–1367.

Antolín-Llovera, M., Ried, M.K., and Parniske, M. (2014). Cleavage of the SYMBIOSIS RECEPTOR-LIKE KINASE Ectodomain Promotes Complex Formation with Nod Factor Receptor 5. Curr. Biol. **24**: 422–427.

Arrighi, J.-F. et al. (2006). The Medicago truncatula Lysine Motif-Receptor-Like Kinase Gene Family Includes NFP and New Nodule-Expressed Genes. Plant Physiol. **142**: 265.

Arshad, M.S., Farooq, M., Asch, F., Krishna, J.S.V., Prasad, P.V.V., and Siddique, K.H.M. (2017). Thermal stress impacts reproductive development and grain yield in rice. Plant Physiol. Biochem. **115**: 57–72.

Atlung, T., Christensen, B.B., and Hansen, F.G. (1999). Role of the Rom Protein in Copy Number Control of Plasmid pBR322 at Different Growth Rates inEscherichia coliK-12. Plasmid **41**: 110–119.

Aydın Akbudak, M. and Srivastava, V. (2017). Effect of gene order in DNA constructs on gene expression upon integration into plant genome. 3 Biotech **7**: 94–94.

Babu, Y.S., Bugg, C.E., and Cook, W.J. (1988). Structure of calmodulin refined at 2.2 Å resolution. J. Mol. Biol. **204**: 191–204.

Barker, D.G. et al. (1990). Medicago truncatula, a model plant for studying the molecular genetics of theRhizobium-legume symbiosis. Plant Mol. Biol. Report. **8**: 40–49.

Bender, K.W., Blackburn, R.K., Monaghan, J., Derbyshire, P., Menke, F.L.H., Zipfel, C., Goshe, M.B., Zielinski, R.E., and Huber, S.C. (2017). Autophosphorylation-based Calcium (Ca2+) Sensitivity Priming and Ca^{2+}/Calmodulin Inhibition of Arabidopsis thaliana Ca^{2+}-dependent Protein Kinase 28 (CPK28). J. Biol. Chem. **292**: 3988–4002.

Benedito, V.A. et al. (2008). A gene expression atlas of the model legume Medicago truncatula. Plant J. **55**: 504–513.

Berridge, M.J., Bootman, M.D., and Roderick, H.L. (2003). Calcium signalling: dynamics, homeostasis and remodelling. Nat Rev Mol Cell Biol **4**: 517–529.

Birnbaum, S. and Bailey, J.E. (1991). Plasmid presence changes the relative levels of many host cell proteins and ribosome components in recombinant Escherichia coli. Biotechnol. Bioeng. **37**: 736–745.

de Boer, H.A., Comstock, L.J., and Vasser, M. (1983). The tac promoter: a functional hybrid derived from the trp and lac promoters. Proc. Natl. Acad. Sci. **80**: 21.

Boisson-Dernier, A. (2001). Agrobacterium rhizogenes-transformed roots of Medicago truncatula for the study of nitrogen-fixing and endomycorrhizal symbiotic associations. Mol Plant Microbe Interact **14**: 695–700.

Borisov, A.Y., Madsen, L.H., Tsyganov, V.E., Umehara, Y., Voroshilova, V.A., Batagov, A.O., Sandal, N., Mortensen, A., Schauser, L., Ellis, N., Tikhonovich, I.A., and Stougaard, J. (2003). The Sym35 Gene Required for Root Nodule Development in Pea Is an Ortholog of Nin from Lotus japonicus. Plant Physiol. **131**: 1009–1017.

Boscari, A., Del Giudice, J., Ferrarini, A., Venturini, L., Zaffini, A.-L., Delledonne, M., and Puppo, A. (2013). Expression dynamics of the Medicago truncatula transcriptome during the symbiotic interaction with

Sinorhizobium meliloti: which role for nitric oxide? Plant Physiol. **161**: 425–439.

Bowler, C. and Fluhr, R. (2000). The role of calcium and activated oxygens as signals for controlling cross-tolerance. Trends Plant Sci. **5**: 241–246.

Brundrett, M.C. (2002). Coevolution of roots and mycorrhizas of land plants. New Phytol. **154**: 275–304.

Cabeza, R.A., Liese, R., Lingner, A., von Stieglitz, I., Neumann, J., Salinas-Riester, G., Pommerenke, C., Dittert, K., and Schulze, J. (2014). RNA-seq transcriptome profiling reveals that Medicago truncatula nodules acclimate N_2 fixation before emerging P deficiency reaches the nodules. J. Exp. Bot. **65**: 6035–6048.

Cao, X.-Q., Jiang, Z.-H., Yi, Y.-Y., Yang, Y., Ke, L.-P., Pei, Z.-M., and Zhu, S. (2017). Biotic and Abiotic Stresses Activate Different Ca^{2+} Permeable Channels in Arabidopsis. Front. Plant Sci. **8**: 83.

Capiati, D.A., País, S.M., and Téllez-Iñón, M.T. (2006). Wounding increases salt tolerance in tomato plants: evidence on the participation of calmodulin-like activities in cross-tolerance signalling. J. Exp. Bot. **57**: 2391–2400.

Capoen, W., Sun, J., Wysham, D., Otegui, M.S., Venkateshwaran, M., Hirsch, S., Miwa, H., Downie, J.A., Morris, R.J., Ané, J.-M., and Oldroyd, G.E.D. (2011). Nuclear membranes control symbiotic calcium signaling of legumes. Proc. Natl. Acad. Sci. U. S. A. **108**: 14348–14353.

Carrera, A.C., Alexandrov, K., and Roberts, T.M. (1993). The conserved lysine of the catalytic domain of protein kinases is actively involved in the phosphotransfer reaction and not required for anchoring ATP. Proc. Natl. Acad. Sci. U. S. A. **90**: 442–446.

Catoira, R. (2000). Four genes of Medicago truncatula controlling components of a Nod factor transduction pathway. Plant Cell **12**: 1647–1665.

Cerri, M.R., Frances, L., Laloum, T., Auriac, M.-C., Niebel, A., Oldroyd, G.E.D., Barker, D.G., Fournier, J., and de Carvalho-Niebel, F. (2012). Medicago truncatula ERN Transcription Factors: Regulatory Interplay with NSP1/NSP2 GRAS Factors and Expression Dynamics throughout Rhizobial Infection. Plant Physiol. **160**: 2155–2172.

Chabaud, M., Genre, A., Sieberer, B.J., Faccio, A., Fournier, J., Novero, M., Barker, D.G., and Bonfante, P. (2011). Arbuscular mycorrhizal hyphopodia and germinated spore exudates trigger Ca2+ spiking in the legume and nonlegume root epidermis. New Phytol. **189**: 347–355.

Chabaud, M., Venard, C., Defaux-Petras, A., Bécard, G., and Barker, D.G. (2002). Targeted inoculation of Medicago truncatula in vitro root cultures reveals MtENOD11 expression during early stages of infection by arbuscular mycorrhizal fungi. New Phytol. **156**: 265–273.

Charpentier, M. (2018). Calcium signals in the plant nucleus: origin and function. J. Exp. Bot. **69**: 4165–4173.

Charpentier, M. and Oldroyd, G.E.D. (2013). Nuclear Calcium Signaling in Plants. Plant Physiol. **163**: 496–503.

Charpentier, M., Sun, J., Martins, T.V., Radhakrishnan, G.V., Findlay, K., Soumpourou, E., Thouin, J., Véry, A.-A., Sanders, D., Morris, R.J., and Oldroyd, G.E.D. (2016). Nuclear-localized cyclic nucleotide–gated channels mediate symbiotic calcium oscillations. Science **352**: 1102–1105.

Charpentier, M., Vaz Martins, T., Granqvist, E., Oldroyd, G.E.D., and Morris, R.J. (2013). The role of DMI1 in establishing Ca($^{2+}$) oscillations in legume symbioses. Plant Signal. Behav. **8**: e22894.

Charron, D., Pingret, J.-L., Chabaud, M., Journet, E.-P., and Barker, D.G. (2004). Pharmacological Evidence That Multiple Phospholipid Signaling Pathways Link Rhizobium Nodulation Factor Perception in Medicago truncatula Root Hairs to Intracellular Responses, Including Ca($^{2+}$) Spiking and Specific ENOD Gene Expression. Plant Physiol. **136**: 3582–3593.

Chaudhuri, S., Seal, A., and Gupta, M. (1999). Autophosphorylation-dependent activation of a calcium-dependent protein kinase from groundnut. Plant Physiol. **120**: 859–866.

Chen, T., Zhu, H., Ke, D., Cai, K., Wang, C., Gou, H., Hong, Z., and Zhang, Z. (2012). A MAP Kinase Kinase Interacts with SymRK and Regulates Nodule Organogenesis in Lotus japonicus. Plant Cell **24**: 823.

Chin, D. and Means, A.R. (2000). Calmodulin: a prototypical calcium sensor. Trends Cell Biol. **10**: 322–328.

Choi, H., Hong, J., Ha, J., Kang, J., and Kim, S.Y. (2000). ABFs, a Family of ABA-responsive Element Binding Factors. J. Biol. Chem. **275**: 1723–1730.

Choi, W.-G., Toyota, M., Kim, S.-H., Hilleary, R., and Gilroy, S. (2014). Salt stress-induced Ca^{2+} waves are associated with rapid, long-distance root-to-shoot signaling in plants. Proc. Natl. Acad. Sci. **111**: 6497.

Costa, A., Navazio, L., and Szabo, I. (2018). The contribution of organelles to plant intracellular calcium signalling. J. Exp. Bot. **69**: 4175–4193.

Costa-Silva, J., Domingues, D., and Lopes, F.M. (2017). RNA-Seq differential expression analysis: An extended review and a software tool. PLOS ONE **12**: e0190152.

Cutler, S.R., Rodriguez, P.L., Finkelstein, R.R., and Abrams, S.R. (2010). Abscisic Acid: Emergence of a Core Signaling Network. Annu. Rev. Plant Biol. **61**: 651–679.

Czaja, L.F., Hogekamp, C., Lamm, P., Maillet, F., Martinez, E.A., Samain, E., Dénarié, J., Küster, H., and Hohnjec, N. (2012). Transcriptional Responses toward Diffusible Signals from Symbiotic Microbes Reveal MtNFP- and MtDMI3-Dependent Reprogramming of Host Gene Expression by Arbuscular Mycorrhizal Fungal Lipochitooligosaccharides. Plant Physiol. **159**: 1671–1685.

Damiani, I. et al. (2016). Nod Factor Effects on Root Hair-Specific Transcriptome of Medicago truncatula: Focus on Plasma Membrane Transport Systems and Reactive Oxygen Species Networks. Front. Plant Sci. **7**: 794.

De Koninck, P. and Schulman, H. (1998). Sensitivity of CaM Kinase II to the Frequency of Ca2+ Oscillations. Science **279**: 227–230.

DeFalco, T.A., Bender, K.W., and Snedden, W.A. (2010). Breaking the code: Ca^{2+} sensors in plant signalling. Biochem. J. **425**: 27–40.

Delaux, P.-M. et al. (2015). Algal ancestor of land plants was preadapted for symbiosis. Proc. Natl. Acad. Sci. **112**: 13390.

Delaux, P.-M., Séjalon-Delmas, N., Bécard, G., and Ané, J.-M. (2013). Evolution of the plant–microbe symbiotic 'toolkit.' Trends Plant Sci. **18**: 298–304.

Demidchik, V., Shabala, S., Isayenkov, S., Cuin, T.A., and Pottosin, I. (2018). Calcium transport across plant membranes: mechanisms and functions. New Phytol. **220**: 49–69.

DIMKPA, C., WEINAND, T., and ASCH, F. (2009). Plant–rhizobacteria interactions alleviate abiotic stress conditions. Plant Cell Environ. **32**: 1682–1694.

Dodd, A.N., Kudla, J., and Sanders, D. (2010). The Language of Calcium Signaling. Annu. Rev. Plant Biol. **61**: 593–620.

Dolmetsch, R.E., Xu, K., and Lewis, R.S. (1998). Calcium oscillations increase the efficiency and specificity of gene expression. Nature **392**: 933–936.

Drake, S.K. and Falke, J.J. (1996). Kinetic Tuning of the EF-Hand Calcium Binding Motif: The Gateway Residue Independently Adjusts (i) Barrier Height and (ii) Equilibrium. Biochemistry **35**: 1753–1760.

Duhamel, M. and Vandenkoornhuyse, P. (2013). Sustainable agriculture: possible trajectories from mutualistic symbiosis and plant neodomestication. Trends Plant Sci. **18**: 597–600.

Edel, K.H. and Kudla, J. (2015). Increasing complexity and versatility: How the calcium signaling toolkit was shaped during plant land colonization. Evol. Calcium Signal. **57**: 231–246.

Edel, K.H. and Kudla, J. (2016). Integration of calcium and ABA signaling. SI 33 Cell Signal. Gene Regul. 2016 **33**: 83–91.

Edel, K.H., Marchadier, E., Brownlee, C., Kudla, J., and Hetherington, A.M. (2017). The Evolution of Calcium-Based Signalling in Plants. Curr. Biol. **27**: R667–R679.

Ehrhardt, D.W., Wais, R., and Long, S.R. (1996a). Calcium Spiking in Plant Root Hairs Responding to Rhizobium Nodulation Signals. Cell **85**: 673–681.

Ehrhardt, D.W., Wais, R., and Long, S.R. (1996b). Calcium Spiking in Plant Root Hairs Responding to Rhizobium Nodulation Signals. Cell **85**: 673–681.

Endre, G., Kereszt, A., Kevei, Z., Mihacea, S., Kalo, P., and Kiss, G.B. (2002). A receptor kinase gene regulating symbiotic nodule development. Nature **417**: 962–966.

Evelin, H., Devi, T.S., Gupta, S., and Kapoor, R. (2019). Mitigation of Salinity Stress in Plants by Arbuscular Mycorrhizal Symbiosis: Current Understanding and New Challenges. Front. Plant Sci. **10**: 470.

Farooq, M., Gogoi, N., Hussain, M., Barthakur, S., Paul, S., Bharadwaj, N., Migdadi, H.M., Alghamdi, S.S., and Siddique, K.H.M. (2017). Effects, tolerance mechanisms and management of salt stress in grain legumes. Plant Physiol. Biochem. **118**: 199–217.

Forde, B.G. and Roberts, M.R. (2014). Glutamate receptor-like channels in plants: a role as amino acid sensors in plant defence? F1000prime Rep. **6**: 37–37.

Fujita, M., Fujita, Y., Noutoshi, Y., Takahashi, F., Narusaka, Y., Yamaguchi-Shinozaki, K., and Shinozaki, K. (2006). Crosstalk between abiotic and biotic stress responses: a current view from the points of convergence in the stress signaling networks. Biot. Interact. Ed. Anne Osbourn Sheng Yang He **9**: 436–442.

Gangopadhyay, J.P. and Ikemoto, N. (2008). Interaction of the Lys^{3614}–Asn^{3643} calmodulin-binding domain with the Cys^{4114}-Asn^{4142} region of the type 1 ryanodine receptor is involved in the mechanism of Ca^{2+}/agonist-induced channel activation. Biochem. J. **411**: 415.

Garcia, K., Chasman, D., Roy, S., and Ané, J.-M. (2017). Physiological Responses and Gene Co-Expression Network of Mycorrhizal Roots under K+ Deprivation. Plant Physiol. **173**: 1811–1823.

Genre, A., Chabaud, M., Balzergue, C., Puech-Pagès, V., Novero, M., Rey, T., Fournier, J., Rochange, S., Bécard, G., Bonfante, P., and Barker, D.G. (2013). Short-chain chitin oligomers from arbuscular mycorrhizal fungi trigger nuclear Ca2+ spiking in Medicago truncatula roots and their production is enhanced by strigolactone. New Phytol. **198**: 190–202.

Gentry, H.R., Singer, A.U., Betts, L., Yang, C., Ferrara, J.D., Sondek, J., and Parise, L.V. (2005). Structural and Biochemical Characterization of CIB1 Delineates a New Family of EF-hand-containing Proteins. J. Biol. Chem. **280**: 8407–8415.

George, S.E., Su, Z., Fan, D., and Means, A.R. (1993). Calmodulin-cardiac troponin C chimeras. Effects of domain exchange on calcium binding and enzyme activation. J. Biol. Chem. **268**: 25213–25220.

Gherbi, H., Markmann, K., Svistoonoff, S., Estevan, J., Autran, D., Giczey, G., Auguy, F., Péret, B., Laplaze, L., Franche, C., Parniske, M., and Bogusz, D. (2008). SymRK defines a common genetic basis for plant root endosymbioses with arbuscular mycorrhiza fungi, rhizobia, and Frankiabacteria. Proc. Natl. Acad. Sci. **105**: 4928–4932.

Gifford, J.L., Walsh, M.P., and Vogel, H.J. (2007). Structures and metal-ion-binding properties of the Ca^{2+}-binding helix–loop–helix EF-hand motifs. Biochem. J. **405**: 199–221.

Gilroy, S., Białasek, M., Suzuki, N., Górecka, M., Devireddy, A.R., Karpiński, S., and Mittler, R. (2016). ROS, Calcium, and Electric Signals: Key Mediators of Rapid Systemic Signaling in Plants. Plant Physiol. **171**: 1606.

Gleason, C., Chaudhuri, S., Yang, T., Munoz, A., Poovaiah, B.W., and Oldroyd, G.E.D. (2006). Nodulation independent of rhizobia induced by a calcium-activated kinase lacking autoinhibition. Nature **441**: 1149–1152.

Gobbato, E. et al. (2012). A GRAS-Type Transcription Factor with a Specific Function in Mycorrhizal Signaling. Curr. Biol. **22**: 2236–2241.

Gobbato, E., Wang, E., Higgins, G., Bano, S.A., Henry, C., Schultze, M., and Oldroyd, G.E.D. (2013). RAM1 and RAM2 function and expression during Arbuscular Mycorrhizal Symbiosis and Aphanomyces euteiches colonization. Plant Signal. Behav. **8**: e26049.

Goel, A.K., Lundberg, D., Torres, M.A., Matthews, R., Akimoto-Tomiyama, C., Farmer, L., Dangl, J.L., and Grant, S.R. (2008). The Pseudomonas syringae Type III Effector HopAM1 Enhances Virulence on Water-Stressed Plants. Mol. Plant. Microbe Interact. **21**: 361–370.

Gronenborn, B. (1976). Overproduction of phage Lambda repressor under control of the lac promotor of Escherichia coli. Mol. Gen. Genet. MGG **148**: 243–250.

Gruber, V., Blanchet, S., Diet, A., Zahaf, O., Boualem, A., Kakar, K., Alunni, B., Udvardi, M., Frugier, F., and Crespi, M. (2009). Identification of transcription factors involved in root apex responses to salt stress in Medicago truncatula. Mol. Genet. Genomics MGG **281**: 55–66.

Guillotin, B., Couzigou, J.-M., and Combier, J.-P. (2016). NIN Is Involved in the Regulation of Arbuscular Mycorrhizal Symbiosis. Front. Plant Sci. **7**: 1704.

Guo, K.-M., Babourina, O., Christopher, D.A., Borsics, T., and Rengel, Z. (2008). The cyclic nucleotide-gated channel, AtCNGC10, influences salt tolerance in Arabidopsis. Physiol. Plant. **134**: 499–507.

Gupta, P., Sharma, R., Sharma, M.K., Sharma, M.P., Satpute, G.K., Garg, S., Singla-Pareek, S.L., and Pareek, A. (2016). 2 - Signaling cross talk between biotic and abiotic stress responses in soybean. In Abiotic and Biotic Stresses in Soybean Production, M. Miransari, ed (Academic Press: San Diego), pp. 27–52.

Halling, D.B., Aracena-Parks, P., and Hamilton, S.L. (2005). Regulation of Voltage-Gated Ca^{2+} Channels by Calmodulin. Sci. STKE **2005**: re15.

Hanks, S., Quinn, A., and Hunter, T. (1988). The protein kinase family: conserved features and deduced phylogeny of the catalytic domains. Science **241**: 42.

Hayashi, T., Banba, M., Shimoda, Y., Kouchi, H., Hayashi, M., and Imaizumi-Anraku, H. (2010). A dominant function of CCaMK in intracellular accommodation of bacterial and fungal endosymbionts. Plant J **63**: 141–54.

Hayashi, T., Shimoda, Y., Sato, S., Tabata, S., Imaizumi-Anraku, H., and Hayashi, M. (2014). Rhizobial infection does not require cortical expression of upstream common symbiosis genes responsible for the induction of Ca^{2+} spiking. Plant J. **77**: 146–159.

Head, J.F., Inouye, S., Teranishi, K., and Shimomura, O. (2000). The crystal structure of the photoprotein aequorin at 2.3 Å resolution. Nature **405**: 372–376.

Hedrich, R. (2012). Ion Channels in Plants. Physiol. Rev. **92**: 1777–1811.

Herzberg, O. and James, M.N.G. (1988). Refined crystal structure of troponin C from turkey skeletal muscle at 2·0 Å resolution. J. Mol. Biol. **203**: 761–779.

Hiroaki Ishida and Hans J. Vogel (2006). Protein-Peptide Interaction Studies Demonstrate the Versatility of Calmodulin Target Protein Binding. Protein Pept. Lett. **13**: 455–465.

Hirsch, S., Kim, J., Muñoz, A., Heckmann, A.B., Downie, J.A., and Oldroyd, G.E.D. (2009). GRAS Proteins Form a DNA Binding Complex to Induce Gene Expression during Nodulation Signaling in Medicago truncatula. Plant Cell **21**: 545–557.

Ho, S.N., Hunt, H.D., Horton, R.M., Pullen, J.K., and Pease, L.R. (1989). Site-directed mutagenesis by overlap extension using the polymerase chain reaction. Gene **77**: 51–59.

Horváth, B. et al. (2011). Medicago truncatula IPD3 Is a Member of the Common Symbiotic Signaling Pathway Required for Rhizobial and Mycorrhizal Symbioses. Mol. Plant. Microbe Interact. **24**: 1345–1358.

Hou, C., Tian, W., Kleist, T., He, K., Garcia, V., Bai, F., Hao, Y., Luan, S., and Li, L. (2014). DUF221 proteins are a family of osmosensitive calcium-permeable cation channels conserved across eukaryotes. Cell Res. **24**: 632.

Huang, F., Luo, J., Ning, T., Cao, W., Jin, X., Zhao, H., Wang, Y., and Han, S. (2017a). Cytosolic and Nucleosolic Calcium Signaling in Response to Osmotic and Salt Stresses Are Independent of Each Other in Roots of Arabidopsis Seedlings. Front. Plant Sci. **8**: 1648.

Huang, F., Luo, J., Ning, T., Cao, W., Jin, X., Zhao, H., Wang, Y., and Han, S. (2017b). Cytosolic and Nucleosolic Calcium Signaling in Response to Osmotic and Salt Stresses Are Independent of Each Other in Roots of Arabidopsis Seedlings. Front. Plant Sci. **8**: 1648–1648.

Iliuk, A.B. and Tao, W.A. (2015). Universal non-antibody detection of protein phosphorylation using pIMAGO. Curr. Protoc. Chem. Biol. **7**: 17–25.

Inouye, S. and Sahara-Miura, Y. (2016). Expression and characterization of EF-hand I loop mutants of aequorin replaced with other loop sequences of Ca 2+ -binding proteins: an approach to studying the EF-hand motif of proteins †. J. Biochem. (Tokyo) **160**: 59–68.

Ismail, A., Takeda, S., and Nick, P. (2014). Life and death under salt stress: same players, different timing? J. Exp. Bot. **65**: 2963–2979.

Jach, G., Binot, E., Frings, S., Luxa, K., and Schell, J. (2001). Use of red fluorescent protein from Discosoma sp. (dsRED) as a reporter for plant gene expression. Plant J. **28**: 483–491.

Jauregui, E., Du, L., Gleason, C., and Poovaiah, B.W. (2017). Autophosphorylation of calcium/calmodulin-dependent protein kinase (CCaMK) at S343 or S344 generates an intramolecular interaction blocking the CaM-binding. Plant Signal. Behav. **12**: e1343779–e1343779.

Jefferson, R.A., Kavanagh, T.A., and Bevan, M.W. (1987). GUS fusions: beta-glucuronidase as a sensitive and versatile gene fusion marker in higher plants. EMBO J. **6**: 3901–3907.

Jensen, D., Reynolds, N., Yang, Y.-P., Shakya, S., Wang, Z.-Q., Stuehr, D.J., and Wei, C.-C. (2015). The exchanged EF-hands in calmodulin and troponin C chimeras impair the Ca2+-induced hydrophobicity and alter the interaction with Orai1: a spectroscopic, thermodynamic and kinetic study. BMC Biochem. **16**: 6.

Jiang, Z., Zhu, S., Ye, R., Xue, Y., Chen, A., An, L., and Pei, Z.-M. (2013). Relationship between NaCl- and H2O2-induced cytosolic Ca2+

increases in response to stress in Arabidopsis. PloS One **8**: e76130–e76130.

Jin, Y., Chen, Z., Yang, J., Mysore, K.S., Wen, J., Huang, J., Yu, N., and Wang, E. (2018). IPD3 and IPD3L Function Redundantly in Rhizobial and Mycorrhizal Symbioses. Front. Plant Sci. **9**: 267.

Jin, Y., Jing, W., Zhang, Q., and Zhang, W. (2015). Cyclic nucleotide gated channel 10 negatively regulates salt tolerance by mediating Na+ transport in Arabidopsis. J. Plant Res. **128**: 211–220.

Jin, Y., Liu, H., Luo, D., Yu, N., Dong, W., Wang, C., Zhang, X., Dai, H., Yang, J., and Wang, E. (2016). DELLA proteins are common components of symbiotic rhizobial and mycorrhizal signalling pathways. Nat Commun **7**.

Johnson, J.D., Snyder, C., Walsh, M., and Flynn, M. (1996). Effects of Myosin Light Chain Kinase and Peptides on Ca2+ Exchange with the N- and C-terminal Ca2+ Binding Sites of Calmodulin. J. Biol. Chem. **271**: 761–767.

Jonasson, P., Liljeqvist, S., Nygren, P.-A., and Ståhl, S. (2002). Genetic design for facilitated production and recovery of recombinant proteins in Escherichia coli. Biotechnol. Appl. Biochem. **35**: 91–105.

Journet, E.P. (2001). Medicago truncatula ENOD11: a novel RPRP-encoding early nodulin gene expressed during mycorrhization in arbuscule-containing cells. Mol Plant Microbe Interact **14**: 737–748.

Kalo, P. (2005). Nodulation signaling in legumes requires NSP2, a member of the GRAS family of transcriptional regulators. Science **308**: 1786–1789.

Kang, H., Zhu, H., Chu, X., Yang, Z., Yuan, S., Yu, D., Wang, C., Hong, Z., and Zhang, Z. (2011). A novel interaction between CCaMK and a protein containing the Scythe_N ubiquitin-like domain in Lotus japonicus. Plant Physiol. **155**: 1312–1324.

Kapust, R.B. and Waugh, D.S. (1999). Escherichia coli maltose-binding protein is uncommonly effective at promoting the solubility of polypeptides to which it is fused. Protein Sci. **8**: 1668–1674.

Kelner, A., Leitão, N., Chabaud, M., Charpentier, M., and de Carvalho-Niebel, F. (2018). Dual Color Sensors for Simultaneous Analysis of Calcium Signal Dynamics in the Nuclear and Cytoplasmic Compartments of Plant Cells. Front. Plant Sci. **9**: 245.

Kevei, Z. et al. (2007). 3-Hydroxy-3-Methylglutaryl Coenzyme A Reductase1 Interacts with NORK and Is Crucial for Nodulation in Medicago truncatula. Plant Cell **19**: 3974–3989.

Khan, M., Mehtab, U., Ullah, M., and Adnan, M. (2016). IN VITRO AND GREENHOUSE RESPONSE OF DIFFERENT WHEAT LINES AGAINST SALINITY STRESS.

Kistner, C. and Parniske, M. (2002). Evolution of signal transduction in intracellular symbiosis. Trends Plant Sci. **7**: 511–518.

Kosuta, S., Chabaud, M., Lougnon, G., Gough, C., Dénarié, J., Barker, D.G., and Bécard, G. (2003). A Diffusible Factor from Arbuscular Mycorrhizal Fungi Induces Symbiosis-Specific MtENOD11 Expression in Roots of Medicago truncatula. Plant Physiol. **131**: 952–962.

Kosuta, S., Hazledine, S., Sun, J., Miwa, H., Morris, R.J., Downie, J.A., and Oldroyd, G.E.D. (2008). Differential and chaotic calcium signatures in the symbiosis signaling pathway of legumes. Proc. Natl. Acad. Sci. U. S. A. **105**: 9823–9828.

Kragelund, B.B., Jönsson, M., Bifulco, G., Chazin, W.J., Nilsson, H., Finn, B.E., and Linse, S. (1998). Hydrophobic Core Substitutions in Calbindin D9k: Effects on Ca2+ Binding and Dissociation. Biochemistry **37**: 8926–8937.

Ku, Y.-S., Sintaha, M., Cheung, M.-Y., and Lam, H.-M. (2018). Plant Hormone Signaling Crosstalks between Biotic and Abiotic Stress Responses. Int. J. Mol. Sci. **19**: 3206.

Kudla, J., Batistič, O., and Hashimoto, K. (2010). Calcium Signals: The Lead Currency of Plant Information Processing. Plant Cell **22**: 541–563.

Kuhn, H., Küster, H., and Requena, N. (2010). Membrane steroid-binding protein 1 induced by a diffusible fungal signal is critical for mycorrhization in Medicago truncatula. New Phytol. **185**: 716–733.

Kumar, A., Dames, J.F., Gupta, A., Sharma, S., Gilbert, J.A., and Ahmad, P. (2015). Current developments in arbuscular mycorrhizal fungi research and its role in salinity stress alleviation: a biotechnological perspective. Crit. Rev. Biotechnol. **35**: 461–474.

LAREBEKE, N.V., ENGLER, G., HOLSTERS, M., DEN ELSACKER, S.V., ZAENEN, I., SCHILPEROORT, R.A., and SCHELL, J. (1974). Large plasmid in Agrobacterium tumefaciens essential for crown gall-inducing ability. Nature **252**: 169–170.

Lee, S.H. et al. (1999). Competitive binding of calmodulin isoforms to calmodulin-binding proteins: implication for the function of calmodulin isoforms in plants. Biochim. Biophys. Acta BBA - Protein Struct. Mol. Enzymol. **1433**: 56–67.

Lee, S.H., Johnson, J.D., Walsh, M.P., Van Lierop, J.E., Sutherland, C., Xu, A., Snedden, W.A., Kosk-Kosicka, D., Fromm, H., Narayanan, N., and Cho, M.J. (2000). Differential regulation of Ca2+/calmodulin-dependent enzymes by plant calmodulin isoforms and free Ca2+ concentration. Biochem. J. **350**: 299–306.

Lenton, T.M., Dahl, T.W., Daines, S.J., Mills, B.J.W., Ozaki, K., Saltzman, M.R., and Porada, P. (2016). Earliest land plants created modern levels of atmospheric oxygen. Proc. Natl. Acad. Sci. **113**: 9704.

Levy, J. (2004). A putative Ca2+ and calmodulin-dependent protein kinase required for bacterial and fungal symbioses. Science **303**: 1361–1364.

Li, D., Su, Z., Dong, J., and Wang, T. (2009). An expression database for roots of the model legume Medicago truncatula under salt stress. BMC Genomics **10**: 517–517.

Li, D., Zhang, Y., Hu, X., Shen, X., Ma, L., Su, Z., Wang, T., and Dong, J. (2011). Transcriptional profiling of Medicago truncatula under salt stress identified a novel CBF transcription factor MtCBF4 that plays an important role in abiotic stress responses. BMC Plant Biol. **11**: 109.

Li, P., Zhang, B., Su, T., Li, P., Xin, X., Wang, W., Zhao, X., Yu, Y., Zhang, D., Yu, S., and Zhang, F. (2018). BrLAS, a GRAS Transcription Factor From Brassica rapa, Is Involved in Drought Stress Tolerance in Transgenic Arabidopsis. Front. Plant Sci. **9**: 1792.

Liao, J., Singh, S., Hossain, M.S., Andersen, S.U., Ross, L., Bonetta, D., Zhou, Y., Sato, S., Tabata, S., Stougaard, J., Szczyglowski, K., and Parniske, M. (2012). Negative regulation of CCaMK is essential for symbiotic infection. Plant J. **72**: 572–584.

Limpens, E., Mirabella, R., Fedorova, E., Franken, C., Franssen, H., Bisseling, T., and Geurts, R. (2005). Formation of organelle-like N_2-fixing symbiosomes in legume root nodules is controlled by DMI2. Proc. Natl. Acad. Sci. U. S. A. **102**: 10375.

Lin-Chao, S., Chen, W.-T., and Wong, T.-T. (1992). High copy number of the pUC plasmid results from a Rom/Rop-suppressible point mutation in RNA II. Mol. Microbiol. **6**: 3385–3393.

Liu, J., Rutten, L., Limpens, E., van der Molen, T., van Velzen, R., Chen, R., Chen, Y., Geurts, R., Kohlen, W., Kulikova, O., and Bisseling, T. (2019). A Remote cis-Regulatory Region Is Required for NIN Expression in the Pericycle to Initiate Nodule Primordium Formation in Medicago truncatula. Plant Cell **31**: 68.

Liu, W. et al. (2011). Strigolactone Biosynthesis in Medicago truncatula and Rice Requires the Symbiotic GRAS-Type Transcription Factors NSP1 and NSP2. Plant Cell **23**: 3853–3865.

López-Ráez, J.A. (2016). How drought and salinity affect arbuscular mycorrhizal symbiosis and strigolactone biosynthesis? Planta **243**: 1375–1385.

de Lorenzo, L., Merchan, F., Blanchet, S., Megías, M., Frugier, F., Crespi, M., and Sousa, C. (2007). Differential expression of the TFIIIA regulatory pathway in response to salt stress between Medicago truncatula genotypes. Plant Physiol. **145**: 1521–1532.

de Lorenzo, L., Merchan, F., Laporte, P., Thompson, R., Clarke, J., Sousa, C., and Crespi, M. (2009). A Novel Plant Leucine-Rich Repeat Receptor

Kinase Regulates the Response of Medicago truncatula Roots to Salt Stress. Plant Cell **21**: 668.

Luehrsen, K.R., de Wet, J.R., and Walbot, V. (1992). [35] Transient expression analysis in plants using firefly luciferase reporter gene. In Methods in Enzymology (Academic Press), pp. 397–414.

Ma, F., Lu, R., Liu, H., Shi, B., Zhang, J., Tan, M., Zhang, A., and Jiang, M. (2012). Nitric oxide-activated calcium/calmodulin-dependent protein kinase regulates the abscisic acid-induced antioxidant defence in maize. J. Exp. Bot. **63**: 4835–4847.

Ma, H.-S., Liang, D., Shuai, P., Xia, X.-L., and Yin, W.-L. (2010). The salt- and drought-inducible poplar GRAS protein SCL7 confers salt and drought tolerance in Arabidopsis thaliana. J. Exp. Bot. **61**: 4011–4019.

Madsen, L.H., Tirichine, L., Jurkiewicz, A., Sullivan, J.T., Heckmann, A.B., Bek, A.S., Ronson, C.W., James, E.K., and Stougaard, J. (2010). The molecular network governing nodule organogenesis and infection in the model legume Lotus japonicus. Nat. Commun. **1**: 1–12.

Maillet, F. et al. (2011). Fungal lipochitooligosaccharide symbiotic signals in arbuscular mycorrhiza. Nature **469**: 58–63.

Marsh, J.F., Rakocevic, A., Mitra, R.M., Brocard, L., Sun, J., Eschstruth, A., Long, S.R., Schultze, M., Ratet, P., and Oldroyd, G.E.D. (2007). Medicago truncatula NIN Is Essential for Rhizobial-Independent Nodule Organogenesis Induced by Autoactive Calcium/Calmodulin-Dependent Protein Kinase. Plant Physiol. **144**: 324–335.

Matsuo, N., MINAMI, M., MAEDA, T., and HIRATSUKA, K. (2001). Dual Luciferase Assay for Monitoring Transient Gene Expression in Higher Plants. Plant Biotechnol. **18**: 71–75.

Mazumder, M., Padhan, N., Bhattacharya, A., and Gourinath, S. (2014). Prediction and Analysis of Canonical EF Hand Loop and Qualitative Estimation of Ca2+ Binding Affinity. PLOS ONE **9**: e96202.

Mbengue, M., Camut, S., de Carvalho-Niebel, F., Deslandes, L., Froidure, S., Klaus-Heisen, D., Moreau, S., Rivas, S., Timmers, T., Hervé, C., Cullimore, J., and Lefebvre, B. (2010). The Medicago truncatula E3 Ubiquitin Ligase PUB1 Interacts with the LYK3 Symbiotic Receptor and Negatively Regulates Infection and Nodulation. Plant Cell **22**: 3474.

McAinsh, M.R. and Pittman, J.K. (2009). Shaping the calcium signature. New Phytol. **181**: 275–294.

Meador, W., Means, A., and Quiocho, F. (1993). Modulation of calmodulin plasticity in molecular recognition on the basis of x-ray structures. Science **262**: 1718.

Meador, W., Means, A., and Quiocho, F. (1992). Target enzyme recognition by calmodulin: 2.4 A structure of a calmodulin-peptide complex. Science **257**: 1251.

Mhadhbi, H., Fotopoulos, V., Mylona, P.V., Jebara, M., Aouani, M.E., and Polidoros, A.N. (2013). Alternative oxidase 1 (Aox1) gene expression in roots of Medicago truncatula is a genotype-specific component of salt stress tolerance. J. Plant Physiol. **170**: 111–114.

Mhadhbi, H., Fotopoulos, V., Mylona, P.V., Jebara, M., Elarbi Aouani, M., and Polidoros, A.N. (2011). Antioxidant gene–enzyme responses in Medicago truncatula genotypes with different degree of sensitivity to salinity. Physiol. Plant. **141**: 201–214.

Millar, A.J., Short, S.R., Hiratsuka, K., Chua, N.-H., and Kay, S.A. (1992). Firefly luciferase as a reporter of regulated gene expression in higher plants. Plant Mol. Biol. Report. **10**: 324–337.

Miller, J.B., Pratap, A., Miyahara, A., Zhou, L., Bornemann, S., Morris, R.J., and Oldroyd, G.E.D. (2013). Calcium/Calmodulin-Dependent Protein Kinase Is Negatively and Positively Regulated by Calcium, Providing a Mechanism for Decoding Calcium Responses during Symbiosis Signaling. Plant Cell **25**: 5053–5066.

Minton, N.P. (1984). Improved plasmid vectors for the isolation of translational lac gene fusions. Gene **31**: 269–273.

Misawa, N., Nakagawa, M., Kobayashi, K., Yamano, S., Izawa, Y., Nakamura, K., and Harashima, K. (1990). Elucidation of the Erwinia uredovora carotenoid biosynthetic pathway by functional analysis of gene products expressed in Escherichia coli. J. Bacteriol. **172**: 6704–6712.

Misawa, N., Satomi, Y., Kondo, K., Yokoyama, A., Kajiwara, S., Saito, T., Ohtani, T., and Miki, W. (1995). Structure and functional analysis of a marine bacterial carotenoid biosynthesis gene cluster and astaxanthin biosynthetic pathway proposed at the gene level. J. Bacteriol. **177**: 6575–6584.

Mitra, R.M. (2004). A Ca2+/calmodulin-dependent protein kinase required for symbiotic nodule development: Gene identification by transcript-based cloning. Proc Natl Acad Sci USA **101**: 4701–4705.

Miura, K. and Furumoto, T. (2013). Cold signaling and cold response in plants. Int. J. Mol. Sci. **14**: 5312–5337.

Miwa, H., Sun, J., Oldroyd, G.E.D., and Downie, J.A. (2006). Analysis of Nod-Factor-Induced Calcium Signaling in Root Hairs of Symbiotically Defective Mutants of Lotus japonicus. Mol. Plant. Microbe Interact. **19**: 914–923.

Monshausen, G.B., Bibikova, T.N., Messerli, M.A., Shi, C., and Gilroy, S. (2007). Oscillations in extracellular pH and reactive oxygen species

modulate tip growth of Arabidopsis root hairs. Proc. Natl. Acad. Sci. **104**: 20996–21001.

Monshausen, G.B., Bibikova, T.N., Weisenseel, M.H., and Gilroy, S. (2009). Ca^{2+} Regulates Reactive Oxygen Species Production and pH during Mechanosensing in Arabidopsis Roots. Plant Cell **21**: 2341–2356.

Munns, R. (2002). Comparative physiology of salt and water stress. Plant Cell Environ. **25**: 239–250.

Murata, Y., Pei, Z.-M., Mori, I.C., and Schroeder, J. (2001). Abscisic Acid Activation of Plasma Membrane Ca2+ Channels in Guard Cells Requires Cytosolic NAD(P)H and Is Differentially Disrupted Upstream and Downstream of Reactive Oxygen Species Production in abi1-1 and abi2-1 Protein Phosphatase 2C Mutants. Plant Cell **13**: 2513–2523.

Nagae, M., Nozawa, A., Koizumi, N., Sano, H., Hashimoto, H., Sato, M., and Shimizu, T. (2003). The Crystal Structure of the Novel Calcium-binding Protein AtCBL2 from Arabidopsis thaliana. J. Biol. Chem. **278**: 42240–42246.

Ni, L. et al. (2019). Abscisic Acid Inhibits Rice Protein Phosphatase PP45 via H_2O_2 and Relieves Repression of the Ca^{2+}/CaM-Dependent Protein Kinase DMI3. Plant Cell **31**: 128.

Oh, M.-H., Wu, X., Kim, H.S., Harper, J.F., Zielinski, R.E., Clouse, S.D., and Huber, S.C. (2012). CDPKs are dual-specificity protein kinases and tyrosine autophosphorylation attenuates kinase activity. FEBS Lett. **586**: 4070–4075.

Oldroyd, G.E.D. (2013). Speak, friend, and enter: signalling systems that promote beneficial symbiotic associations in plants. Nat. Rev. Microbiol. **11**: 252.

Ouyang, S.-Q., Liu, Y.-F., Liu, P., Lei, G., He, S.-J., Ma, B., Zhang, W.-K., Zhang, J.-S., and Chen, S.-Y. (2010). Receptor-like kinase OsSIK1 improves drought and salt stress tolerance in rice (Oryza sativa) plants. Plant J. **62**: 316–329.

Ow, D.W., DE WET, J.R., HELINSKI, D.R., HOWELL, S.H., WOOD, K.V., and DELUCA, M. (1986). Transient and Stable Expression of the Firefly Luciferase Gene in Plant Cells and Transgenic Plants. Science **234**: 856.

P Barletta, J., Angella, G., C Balch, K., G Dimova, H., A Stern, G., Moser, M., van Setten, G., and Schultz, G. (1996). Inhibition of pseudomonal ulceration in rabbit corneas by a synthetic matrix metalloprotease inhibitor.

Pandey, P., Ramegowda, V., and Senthil-Kumar, M. (2015). Shared and unique responses of plants to multiple individual stresses and stress combinations: physiological and molecular mechanisms. Front. Plant Sci. **6**: 723–723.

Pandey, S., Tiwari, S.B., Tyagi, W., Reddy, M.K., Upadhyaya, K.C., and Sopory, S.K. (2002). A Ca2+/CaM-dependent kinase from pea is stress regulated and in vitro phosphorylates a protein that binds to AtCaM5 promoter. Eur. J. Biochem. **269**: 3193–3204.

Parniske, M. (2000). Intracellular accommodation of microbes by plants: a common developmental program for symbiosis and disease? Curr. Opin. Plant Biol. **3**: 320–328.

Patil, S., Takezawa, D., and Poovaiah, B.W. (1995). Chimeric plant calcium/calmodulin-dependent protein kinase gene with a neural visinin-like calcium-binding domain. Proc Natl Acad Sci USA **92**: 4897–4901.

Pei, Z.-M., Murata, Y., Benning, G., Thomine, S., Klusener, B., Allen, G.J., Grill, E., and Schroeder, J.I. (2000). Calcium channels activated by hydrogen peroxide mediate abscisic acid signalling in guard cells. Nature **406**: 731–734.

Piazza, M., Taiakina, V., Dieckmann, T., and Guillemette, J.G. (2017). Structural Consequences of Calmodulin EF Hand Mutations. Biochemistry **56**: 944–956.

Pimprikar, P., Carbonnel, S., Paries, M., Katzer, K., Klingl, V., Bohmer, M.J., Karl, L., Floss, D.S., Harrison, M.J., Parniske, M., and Gutjahr, C. (2016). A CCaMK-CYCLOPS-DELLA Complex Activates Transcription of RAM1 to Regulate Arbuscule Branching. Curr. Biol.

Popescu, S.C., Popescu, G.V., Bachan, S., Zhang, Z., Seay, M., Gerstein, M., Snyder, M., and Dinesh-Kumar, S.P. (2007). Differential binding of calmodulin-related proteins to their targets revealed through high-density Arabidopsis protein microarrays. Proc. Natl. Acad. Sci. U. S. A. **104**: 4730–4735.

Price, M., Jelesko, J., and Okumoto, S. (2012). Glutamate Receptor Homologs in Plants: Functions and Evolutionary Origins. Front. Plant Sci. **3**: 235.

Putkey, J.A., Sweeney, H.L., and Campbell, S.T. (1989). Site-directed mutation of the trigger calcium-binding sites in cardiac troponin C. J. Biol. Chem. **264**: 12370–12378.

Raghavendra, A.S., Gonugunta, V.K., Christmann, A., and Grill, E. (2010). ABA perception and signalling. Trends Plant Sci. **15**: 395–401.

Ramachandiran, S., Takezawa, D., Wang, W., and Poovaiah, B.W. (1997). Functional domains of plant chimeric calcium/calmodulin-dependent protein kinase: regulation by autoinhibitory and visinin-like domains. J Biochem **121**: 984–990.

Redecker, D., Kodner, R., and Graham, L.E. (2000). Glomalean Fungi from the Ordovician. Science **289**: 1920.

Rejeb, I.B., Pastor, V., and Mauch-Mani, B. (2014). Plant Responses to Simultaneous Biotic and Abiotic Stress: Molecular Mechanisms. Plants Basel Switz. **3**: 458–475.

Rewald, B., Shelef, O., Ephrath, J.E., and Rachmilevitch, S. (2013). Adaptive Plasticity of Salt-Stressed Root Systems. In Ecophysiology and Responses of Plants under Salt Stress, P. Ahmad, M.M. Azooz, and M.N.V. Prasad, eds (Springer New York: New York, NY), pp. 169–201.

Rigden, D.J. and Galperin, M.Y. (2004). The DxDxDG Motif for Calcium Binding: Multiple Structural Contexts and Implications for Evolution. J. Mol. Biol. **343**: 971–984.

Rosano, G.L. and Ceccarelli, E.A. (2014). Recombinant protein expression in Escherichia coli: advances and challenges. Front. Microbiol. **5**: 172–172.

Rose, R.J. (2008). Medicago truncatula as a model for understanding plant interactions with other organisms, plant development and stress biology: past, present and future. Funct. Plant Biol. **35**: 253–264.

Routray, P., Miller, J.B., Du, L., Oldroyd, G., and Poovaiah, B.W. (2013). Phosphorylation of S344 in the calmodulin-binding domain negatively affects CCaMK function during bacterial and fungal symbioses. Plant J. **76**: 287–296.

Saha, P. and Singh, M. (1995). Characterization of a winged bean (Psophocarpus tetragonolobus) protein kinase with calmodulin-like domain: regulation by autophosphorylation. Biochem. J. **305 (Pt 1)**: 205–210.

Samanta, K. and Parekh, A.B. (2017). Spatial Ca(2+) profiling: decrypting the universal cytosolic Ca(2+) oscillation. J. Physiol. **595**: 3053–3062.

Sanders, D., Brownlee, C., and Harper, J.F. (1999). Communicating with Calcium. Plant Cell **11**: 691–706.

Sang, J.-R., Jiang, M., Lin, F., Li, J., and Xu, S.-C. (2008). Role of nitric oxide in abscisic acid-induced subcellular antioxidant defense of maize leaves.

Sathyanarayanan, P.V., Cremo, C.R., and Poovaiah, B.W. (2000). Plant chimeric Ca2+/calmodulin-dependent protein kinase. Role of the neural visinin-like domain in regulating autophosphorylation and calmodulin affinity. J Biol Chem **275**: 30417–30422.

Sathyanarayanan, P.V., Siems, W.F., Jones, J.P., and Poovaiah, B.W. (2001). Calcium-stimulated autophosphorylation site of plant chimeric calcium/calmodulin-dependent protein kinase. J Biol Chem **276**: 32940–32947.

Saúl Fraire-Velázquez (2011). Abiotic and Biotic Stress Response Crosstalk in Plants. In Abiotic Stress Response in Plants, Raúl Rodríguez-Guerra, ed (IntechOpen: Rijeka), p. Ch. 1.

Schauser, L., Roussis, A., Stiller, J., and Stougaard, J. (1999). A plant regulator controlling development of symbiotic root nodules. Nature **402**: 191–195.

Schein, C.H. (1989). Production of Soluble Recombinant Proteins in Bacteria. Bio/Technology **7**: 1141–1149.

Schulze, C., Sticht, H., Meyerhoff, P., and Dietrich, P. (2011). Differential contribution of EF-hands to the Ca2+-dependent activation in the plant two-pore channel TPC1. Plant J. **68**: 424–432.

Schulz-Lessdorf, B. and Hedrich, R. (1995). Protons and calcium modulate SV-type channels in the vacuolar-lysosomal compartment — channel interaction with calmodulin inhibitors. Planta **197**: 655–671.

Sehgal, A., Sita, K., Siddique, K.H.M., Kumar, R., Bhogireddy, S., Varshney, R.K., HanumanthaRao, B., Nair, R.M., Prasad, P.V.V., and Nayyar, H. (2018). Drought or/and Heat-Stress Effects on Seed Filling in Food Crops: Impacts on Functional Biochemistry, Seed Yields, and Nutritional Quality. Front. Plant Sci. **9**: 1705–1705.

Selosse, M.-A., Strullu-Derrien, C., Martin, F.M., Kamoun, S., and Kenrick, P. (2015). Plants, fungi and oomycetes: a 400-million year affair that shapes the biosphere. New Phytol. **206**: 501–506.

Sharma, R., De Vleesschauwer, D., Sharma, M.K., and Ronald, P.C. (2013). Recent Advances in Dissecting Stress-Regulatory Crosstalk in Rice. Mol. Plant **6**: 250–260.

Shaw, G.S., Hodges, R.S., and Sykes, B.D. (1991). Probing the relationship between .alpha.-helix formation and calcium affinity in troponin C: proton NMR studies of calcium binding to synthetic and variant site III helix-loop-helix peptides. Biochemistry **30**: 8339–8347.

Shi, B., NI, L., LIU, Y., ZHANG, A., TAN, M., and JIANG, M. (2014). OsDMI3-mediated activation of OsMPK1 regulates the activities of antioxidant enzymes in abscisic acid signalling in rice. Plant Cell Environ. **37**: 341–352.

Shi, B., Ni, L., Zhang, A., Cao, J., Zhang, H., Qin, T., Tan, M., Zhang, J., and Jiang, M. (2012). OsDMI3 Is a Novel Component of Abscisic Acid Signaling in the Induction of Antioxidant Defense in Leaves of Rice. Mol. Plant **5**: 1359–1374.

Shimoda, Y., Han, L., Yamazaki, T., Suzuki, R., Hayashi, M., and Imaizumi-Anraku, H. (2012). Rhizobial and Fungal Symbioses Show Different Requirements for Calmodulin Binding to Calcium Calmodulin–Dependent Protein Kinase in Lotus japonicus. Plant Cell **24**: 304–321.

Shimomura, O., Johnson, F.H., and Saiga, Y. (1962). Extraction, Purification and Properties of Aequorin, a Bioluminescent Protein from the Luminous Hydromedusan, Aequorea. J. Cell. Comp. Physiol. **59**: 223–239.

Sieberer, B.J., Chabaud, M., Fournier, J., Timmers, A.C.J., and Barker, D.G. (2012). A switch in Ca^{2+} spiking signature is concomitant with endosymbiotic microbe entry into cortical root cells of Medicago truncatula. Plant J. **69**: 822–830.

Sieberer, B.J., Chabaud, M., Timmers, A.C., Monin, A., Fournier, J., and Barker, D.G. (2009). A Nuclear-Targeted Cameleon Demonstrates Intranuclear Ca2+ Spiking in Medicago truncatula Root Hairs in Response to Rhizobial Nodulation Factors. Plant Physiol. **151**: 1197–1206.

Singh, R.P., Hodson, D.P., Huerta-Espino, J., Jin, Y., Bhavani, S., Njau, P., Herrera-Foessel, S., Singh, P.K., Singh, S., and Govindan, V. (2011). The Emergence of Ug99 Races of the Stem Rust Fungus is a Threat to World Wheat Production. Annu. Rev. Phytopathol. **49**: 465–481.

Singh, S., Katzer, K., Lambert, J., Cerri, M., and Parniske, M. (2014). CYCLOPS, A DNA-Binding Transcriptional Activator, Orchestrates Symbiotic Root Nodule Development. Cell Host Microbe **15**: 139–152.

Singh, S. and Parniske, M. (2012). Activation of calcium- and calmodulin-dependent protein kinase (CCaMK), the central regulator of plant root endosymbiosis. Curr. Opin. Plant Biol. **15**: 444–453.

Smedler, E. and Uhlén, P. (2014). Frequency decoding of calcium oscillations. Biochim. Biophys. Acta BBA - Gen. Subj. **1840**: 964–969.

Smékal, F. (1973). Lysis of lyophilizedEscherichia coli cells with egg-white lysozyme without ethylenediaminetetraacetic acid. Folia Microbiol. (Praha) **18**: 146–148.

Smit, P. (2005). NSP1 of the GRAS protein family is essential for rhizobial Nod factor-induced transcription. Science **308**: 1789–1791.

Song, J., Mo, X., Yang, H., Yue, L., Song, J., and Mo, B. (2017). The U-box family genes in Medicago truncatula: Key elements in response to salt, cold, and drought stresses. PloS One **12**: e0182402–e0182402.

Soyano, T., Kouchi, H., Hirota, A., and Hayashi, M. (2013). NODULE INCEPTION Directly Targets NF-Y Subunit Genes to Regulate Essential Processes of Root Nodule Development in Lotus japonicus. PLoS Genet. **9**: e1003352.

Staudinger, C., Mehmeti-Tershani, V., Gil-Quintana, E., Gonzalez, E.M., Hofhansl, F., Bachmann, G., and Wienkoop, S. (2016). Evidence for a rhizobia-induced drought stress response strategy in Medicago truncatula. J. Proteomics **136**: 202–213.

Stougaard, J., Abildsten, D., and Marcker, K.A. (1987). The Agrobacterium rhizogenes pRi TL-DNA segment as a gene vector system for transformation of plants. Mol. Gen. Genet. MGG **207**: 251–255.

Stracke, S., Kistner, C., Yoshida, S., Mulder, L., Sato, S., Kaneko, T., Tabata, S., Sandal, N., Stougaard, J., Szczyglowski, K., and Parniske, M. (2002). A plant receptor-like kinase required for both bacterial and fungal symbiosis. Nature **417**: 959–962.

Structural Genomics Consortium et al. (2008). Protein production and purification. Nat. Methods **5**: 135–146.

Strynadka, N.C.J. and and James, M.N.G. (1989). Crystal Structures of the Helix-Loop-Helix Calcium-Binding Proteins. Annu. Rev. Biochem. **58**: 951–999.

Sun, J. et al. (2015a). Activation of Symbiosis Signaling by Arbuscular Mycorrhizal Fungi in Legumes and Rice. Plant Cell **27**: 823–838.

Sun, J. et al. (2015b). Activation of Symbiosis Signaling by Arbuscular Mycorrhizal Fungi in Legumes and Rice. Plant Cell **27**: 823–838.

Suzuki, N. and Katano, K. (2018). Coordination Between ROS Regulatory Systems and Other Pathways Under Heat Stress and Pathogen Attack. Front. Plant Sci. **9**: 490.

Suzuki, N., Rivero, R.M., Shulaev, V., Blumwald, E., and Mittler, R. (2014). Abiotic and biotic stress combinations. New Phytol. **203**: 32–43.

Swainsbury, D.J.K., Zhou, L., Oldroyd, G.E.D., and Bornemann, S. (2012). Calcium Ion Binding Properties of Medicago truncatula Calcium/Calmodulin-Dependent Protein Kinase. Biochemistry **51**: 6895–6907.

Swatek, K.N., Wilson, R.S., Ahsan, N., Tritz, R.L., and Thelen, J.J. (2014). Multisite phosphorylation of 14-3-3 proteins by calcium-dependent protein kinases. Biochem. J. **459**: 15–25.

Takeda, N., Maekawa, T., and Hayashi, M. (2012). Nuclear-Localized and Deregulated Calcium- and Calmodulin-Dependent Protein Kinase Activates Rhizobial and Mycorrhizal Responses in Lotus japonicus. Plant Cell **24**: 810–822.

Takezawa, D., Ramachandiran, S., Paranjape, V., and Poovaiah, B.W. (1996). Dual regulation of a chimeric plant serine/threonine kinase by calcium and calcium/calmodulin. J Biol Chem **271**: 8126–8132.

Taylor, T.N., Remy, W., Hass, H., and Kerp, H. (1995). Fossil Arbuscular Mycorrhizae from the Early Devonian. Mycologia **87**: 560–573.

Tirichine, L. et al. (2006). Deregulation of a Ca^{2+}/calmodulin-dependent kinase leads to spontaneous nodule development. Nature **441**: 1153–1156.

Tirichine, L., Sandal, N., Madsen, L.H., Radutoiu, S., Albrektsen, A.S., Sato, S., Asamizu, E., Tabata, S., and Stougaard, J. (2007). A Gain-of-Function Mutation in a Cytokinin Receptor Triggers Spontaneous Root Nodule Organogenesis. Science **315**: 104–107.

Töpfer, R., Pröls, M., Schell, J., and Steinbiß, H.-H. (1988). Transient gene expression in tobacco protoplasts: II. Comparison of the reporter gene systems for CAT, NPT II, and GUS. Plant Cell Rep. **7**: 225–228.

TRACY, F.E., GILLIHAM, M., DODD, A.N., WEBB, A.A.R., and TESTER, M. (2008). NaCl-induced changes in cytosolic free Ca2+ in Arabidopsis thaliana are heterogeneous and modified by external ionic composition. Plant Cell Environ. **31**: 1063–1073.

Uno, Y., Furihata, T., Abe, H., Yoshida, R., Shinozaki, K., and Yamaguchi-Shinozaki, K. (2000). Arabidopsis basic leucine zipper transcription factors involved in an abscisic acid-dependent signal transduction pathway under drought and high-salinity conditions. Proc. Natl. Acad. Sci. U. S. A. **97**: 11632–11637.

VanGuilder, H.D., Vrana, K.E., and Freeman, W.M. (2008). Twenty-five years of quantitative PCR for gene expression analysis. BioTechniques **44**: 619–626.

Venkateshwaran, M., Jayaraman, D., Chabaud, M., Genre, A., Balloon, A.J., Maeda, J., Forshey, K., den Os, D., Kwiecien, N.W., Coon, J.J., Barker, D.G., and Ané, J.-M. (2015). A role for the mevalonate pathway in early plant symbiotic signaling. Proc. Natl. Acad. Sci. **112**: 9781–9786.

Vera, A., González-Montalbán, N., Arís, A., and Villaverde, A. (2007). The conformational quality of insoluble recombinant proteins is enhanced at low growth temperatures. Biotechnol. Bioeng. **96**: 1101–1106.

Vernié, T. et al. (2016). PUB1 Interacts with the Receptor Kinase DMI2 and Negatively Regulates Rhizobial and Arbuscular Mycorrhizal Symbioses through Its Ubiquitination Activity in Medicago truncatula. Plant Physiol. **170**: 2312–2324.

Vernié, T., Kim, J., Frances, L., Ding, Y., Sun, J., Guan, D., Niebel, A., Gifford, M.L., de Carvalho-Niebel, F., and Oldroyd, G.E.D. (2015). The NIN Transcription Factor Coordinates Diverse Nodulation Programs in Different Tissues of the Medicago truncatula Root. Plant Cell **27**: 3410–3424.

Villarroel, A., Taglialatela, M., Bernardo-Seisdedos, G., Alaimo, A., Agirre, J., Alberdi, A., Gomis-Perez, C., Soldovieri, M.V., Ambrosino, P., Malo, C., and Areso, P. (2014). The Ever Changing Moods of Calmodulin: How Structural Plasticity Entails Transductional Adaptability. J. Mol. Biol. **426**: 2717–2735.

Vishwakarma, K., Upadhyay, N., Kumar, N., Yadav, G., Singh, J., Mishra, R.K., Kumar, V., Verma, R., Upadhyay, R.G., Pandey, M., and Sharma, S. (2017). Abscisic Acid Signaling and Abiotic Stress Tolerance in Plants: A Review on Current Knowledge and Future Prospects. Front. Plant Sci. **8**: 161–161.

Walton, S.D., Chakravarthy, H., Shettigar, V., O'Neil, A.J., Siddiqui, J.K., Jones, B.R., Tikunova, S.B., and Davis, J.P. (2017). Divergent

Soybean Calmodulins Respond Similarly to Calcium Transients: Insight into Differential Target Regulation. Front. Plant Sci. **8**: 208–208.

Wang, S., George, S.E., Davis, J.P., and Johnson, J.D. (1998). Structural Determinants of Ca2+ Exchange and Affinity in the C Terminal of Cardiac Troponin C. Biochemistry **37**: 14539–14544.

Ward, J.M., Mäser, P., and Schroeder, J.I. (2009). Plant ion channels: gene families, physiology, and functional genomics analyses. Annu. Rev. Physiol. **71**: 59–82.

Weber, E., Engler, C., Gruetzner, R., Werner, S., and Marillonnet, S. (2011). A Modular Cloning System for Standardized Assembly of Multigene Constructs. PLoS ONE **6**: e16765.

Werner, G.D.A., Cornwell, W.K., Sprent, J.I., Kattge, J., and Kiers, E.T. (2014). A single evolutionary innovation drives the deep evolution of symbiotic N2-fixation in angiosperms. Nat. Commun. **5**: 4087.

Wernimont, A.K. et al. (2010). Structures of apicomplexan calcium-dependent protein kinases reveal mechanism of activation by calcium. Nat Struct Mol Biol **17**: 596–601.

Whalley, H.J. and Knight, M.R. (2013). Calcium signatures are decoded by plants to give specific gene responses. New Phytol. **197**: 690–693.

Wodniok, S., Brinkmann, H., Glöckner, G., Heidel, A.J., Philippe, H., Melkonian, M., and Becker, B. (2011). Origin of land plants: Do conjugating green algae hold the key? BMC Evol. Biol. **11**: 104.

Xiong, L., Zhang, J.-Z., He, R., and Hamilton, S.L. (2006). A Ca2+-Binding Domain in RyR1 that Interacts with the Calmodulin Binding Site and Modulates Channel Activity. Biophys. J. **90**: 173–182.

Xu, K., Chen, S., Li, T., Ma, X., Liang, X., Ding, X., Liu, H., and Luo, L. (2015). OsGRAS23, a rice GRAS transcription factor gene, is involved in drought stress response through regulating expression of stress-responsive genes. BMC Plant Biol. **15**: 141–141.

Xu, L., Gomez, A.C., Pasek, D.A., Meissner, G., and Yamaguchi, N. (2017). Two EF-hand motifs in ryanodine receptor calcium release channels contribute to isoform-specific regulation by calmodulin. Cell Calcium **66**: 62–70.

Xu, Z., Ali, Z., Xu, L., He, X., Huang, Y., Yi, J., Shao, H., Ma, H., and Zhang, D. (2016). The nuclear protein GmbZIP110 has transcription activation activity and plays important roles in the response to salinity stress in soybean. Sci. Rep. **6**: 20366–20366.

Yadav, A.K., Jha, S.K., Sanyal, S.K., Luan, S., and Pandey, G.K. (2018). Arabidopsis calcineurin B-like proteins differentially regulate phosphorylation activity of CBL-interacting protein kinase 9. Biochem. J. **475**: 2621.

Yamaguchi, N., Xu, L., Pasek, D.A., Evans, K.E., and Meissner, G. (2003). Molecular Basis of Calmodulin Binding to Cardiac Muscle Ca2+ Release Channel (Ryanodine Receptor). J. Biol. Chem. **278**: 23480–23486.

Yang, C., Li, A., Zhao, Y., Zhang, Z., Zhu, Y., Tan, X., Geng, S., Guo, H., Zhang, X., Kang, Z., and Mao, L. (2011). Overexpression of a Wheat CCaMK Gene Reduces ABA Sensitivity of Arabidopsis thaliana During Seed Germination and Seedling Growth. Plant Mol. Biol. Report. **29**: 681–692.

Yang, L. and Liu, Z.-R. (2004). Bacterially expressed recombinant p68 RNA helicase is phosphorylated on serine, threonine, and tyrosine residues. Protein Expr. Purif. **35**: 327–333.

Yano, K. et al. (2008). CYCLOPS, a mediator of symbiotic intracellular accommodation. Proc. Natl. Acad. Sci. **105**: 20540–20545.

Ye, Y., Ding, Y., Jiang, Q., Wang, F., Sun, J., and Zhu, C. (2017). The role of receptor-like protein kinases (RLKs) in abiotic stress response in plants. Plant Cell Rep. **36**: 235–242.

Yoshida, T., Mogami, J., and Yamaguchi-Shinozaki, K. (2014). ABA-dependent and ABA-independent signaling in response to osmotic stress in plants. SI Cell Signal. Gene Regul. **21**: 133–139.

Yuan, F. et al. (2014). OSCA1 mediates osmotic-stress-evoked Ca2+ increases vital for osmosensing in Arabidopsis. Nature **514**: 367.

Zahaf, O. et al. (2012). Comparative Transcriptomic Analysis of Salt Adaptation in Roots of Contrasting Medicago truncatula Genotypes. Mol. Plant **5**: 1068–1081.

Zhang, A., Jiang, M., Zhang, J., Ding, H., Xu, S., Hu, X., and Tan, M. (2007). Nitric oxide induced by hydrogen peroxide mediates abscisic acid-induced activation of the mitogen-activated protein kinase cascade involved in antioxidant defense in maize leaves. New Phytol. **175**: 36–50.

Zhang, H., Ni, L., Liu, Y., Wang, Y., Zhang, A., Tan, M., and Jiang, M. (2012). The C2H2-type Zinc Finger Protein ZFP182 is Involved in Abscisic Acid-Induced Antioxidant Defense in RiceF. J. Integr. Plant Biol. **54**: 500–510.

ZHANG, J.-Y., CRUZ DE CARVALHO, M.H., TORRES-JEREZ, I., KANG, Y., ALLEN, S.N., HUHMAN, D.V., TANG, Y., MURRAY, J., SUMNER, L.W., and UDVARDI, M.K. (2014). Global reprogramming of transcription and metabolism in Medicago truncatula during progressive drought and after rewatering. Plant Cell Environ. **37**: 2553–2576.

Zhu, J.-K. (2002). SALT AND DROUGHT STRESS SIGNAL TRANSDUCTION IN PLANTS. Annu. Rev. Plant Biol. **53**: 247–273.

Zhu, Y., Yan, J., Liu, W., Liu, L., Sheng, Y., Sun, Y., Li, Y., Scheller, H.V., Jiang, M., Hou, X., Ni, L., and Zhang, A. (2016a). Phosphorylation of a NAC Transcription Factor by a Calcium/Calmodulin-Dependent Protein

Kinase Regulates Abscisic Acid-Induced Antioxidant Defense in Maize. Plant Physiol. **171**: 1651.

Zhu, Y., Yan, J., Liu, W., Liu, L., Sheng, Y., Sun, Y., Li, Y., Scheller, H.V., Jiang, M., Hou, X., Ni, L., and Zhang, A. (2016b). Phosphorylation of a NAC Transcription Factor by a Calcium/Calmodulin-Dependent Protein Kinase Regulates Abscisic Acid-Induced Antioxidant Defense in Maize. Plant Physiol. **171**: 1651.

Zörb, C., Herbst, R., Forreiter, C., and Schubert, S. (2009). Short-term effects of salt exposure on the maize chloroplast protein pattern. PROTEOMICS **9**: 4209–4220.

Appendix 1 - Level 2 constructs generated in this thesis

Construct number	Construct elements
1	GUS-dsRED-pRAM1RLUC-pNINFLUC-MtCCaMK(WT)
2	GUS-dsRED-pRAM1RLUC-pNINFLUC-MtCCaMK(311)
3	GUS-dsRED-pRAM1RLUC-pNINFLUC-MtCCaMK(T271A)
4	GUS-dsRED-pRAM1RLUC-pNINFLUC-MtCCaMK(K47E)
5	GUS-dsRED-pRAM1RLUC-pENOD11FLUC-MtCCaMK(WT)
6	GUS-dsRED-pRAM1RLUC-pENOD11FLUC-MtCCaMK(311)
7	GUS-dsRED-pRAM1RLUC-pENOD11FLUC-MtCCaMK(T271A)
8	GUS-dsRED-pRAM1RLUC-pENOD11FLUC-MtCCaMK(K47E)
9	GUS-dsRED-pMSBP1RLUC-pNINFLUC-MtCCaMK(WT)
10	GUS-dsRED-pMSBP1RLUC-pNINFLUC-MtCCaMK(311)
11	GUS-dsRED-pMSBP1RLUC-pNINFLUC-MtCCaMK(T271A)
12	GUS-dsRED-pMSBP1RLUC-pNINFLUC-MtCCaMK(K47E)
13	GUS-dsRED-pMSBP1RLUC-pENOD11FLUC-MtCCaMK(WT)
14	GUS-dsRED-pMSBP1RLUC-pENOD11FLUC-MtCCaMK(311)
15	GUS-dsRED-pMSBP1RLUC-pENOD11FLUC-MtCCaMK(T271A)
16	GUS-dsRED-pMSBP1RLUC-pENOD11FLUC-MtCCaMK(K47E)
17	dsRed-p35SRLUC-pENOD11FLUC
18	dsRed-p35SRLUC-pENOD11FLUC-MtCCaMK 1-402
19	dsRed-p35SRLUC-pENOD11FLUC-MtCCaMK 1-391
20	dsRed-p35SRLUC-pENOD11FLUC-MtCCaMK 1-477
21	dsRed-p35SRLUC-pENOD11FLUC-MtCCaMK 1-435
22	dsRed-p35SRLUC-pENOD11FLUC-MtCCaMK 1-346
23	dsRed-p35SRLUC-pENOD11FLUC-MtCCaMK K47E
24	dsRed-p35SRLUC-pENOD11FLUC-MtCCaMK D413A
25	dsRed-p35SRLUC-pENOD11FLUC-MtCCaMK D449A
26	dsRed-p35SRLUC-pENOD11FLUC-MtCCaMK D491A
27	dsRed-p35SRLUC-pENOD11FLUC-MtCCaMK D413A D449A
28	dsRed-p35SRLUC-pENOD11FLUC-MtCCaMK D449A D491A
29	dsRed-p35SRLUC-pENOD11FLUC-MtCCaMK D413A D491A
30	dsRed-p35SRLUC-pENOD11FLUC-MtCCaMK D413A D449A D491A
31	dsRed-p35SRLUC-pENOD11FLUC-MtCCaMK EF1-EF3-EF2-EF4
32	dsRed-p35SRLUC-pENOD11FLUC-MtCCaMK EF1-EF2-EF4-EF3
33	dsRed-p35SRLUC-pENOD11FLUC-MtCCaMK EF1-EF4-EF3-EF2
34	dsRed-p35SRLUC-pENOD11FLUC-MtCCaMK EF1-EF3-EF4-EF2
35	dsRed-p35SRLUC-pENOD11FLUC-MtCCaMK EF1-EF4-EF2-EF3
36	dsRed-p35SRLUC-pENOD11FLUC-MtCCaMK EF2-EF1-EF3-EF4

37	dsRed-p35SRLUC-pENOD11FLUC-MtCCaMK EF2-EF1-EF4-EF3
38	dsRed-p35SRLUC-pENOD11FLUC-MtCCaMK EF2-EF3-EF4-EF1
39	dsRed-p35SRLUC-pENOD11FLUC-MtCCaMK EF2-EF4-EF3-EF1
40	dsRed-p35SRLUC-pENOD11FLUC-MtCCaMK EF2-EF3-EF1-EF4
41	dsRed-p35SRLUC-pENOD11FLUC-MtCCaMK EF2-EF4-EF1-EF3
42	dsRed-p35SRLUC-pENOD11FLUC-MtCCaMK EF3-EF1-EF2-EF4
43	dsRed-p35SRLUC-pENOD11FLUC-MtCCaMK EF3-EF2-EF1-EF4
44	dsRed-p35SRLUC-pENOD11FLUC-MtCCaMK EF3-EF1-EF4-EF2
45	dsRed-p35SRLUC-pENOD11FLUC-MtCCaMK EF3-EF2-EF4-EF1
46	dsRed-p35SRLUC-pENOD11FLUC-MtCCaMK EF3-EF4-EF1-EF2
47	dsRed-p35SRLUC-pENOD11FLUC-MtCCaMK EF3-EF4-EF2-EF1
48	dsRed-p35SRLUC-pENOD11FLUC-MtCCaMK EF4-EF1-EF2-EF3
49	dsRed-p35SRLUC-pENOD11FLUC-MtCCaMK EF4-EF2-EF3-EF1
50	dsRed-p35SRLUC-pENOD11FLUC-MtCCaMK EF4-EF3-EF2-EF1
51	dsRed-p35SRLUC-pENOD11FLUC-MtCCaMK EF4-EF1-EF3-EF2
52	dsRed-p35SRLUC-pENOD11FLUC-MtCCaMK EF4-EF3-EF1-EF2
53	dsRed-p35SRLUC-pENOD11FLUC-MtCCaMK EF4-EF2-EF1-EF3
54	dsRed-p35SRLUC-pENOD11FLUC-MtCCaMK 1-311
55	dsRed-p35SRLUC-pENOD11FLUC-MtCCaMK T271A
56	dsRed-p35SRLUC-pENOD11FLUC-MtCCaMK(no SapI)
57	IPD3-pNINGUS-CCaMKWT
58	IPD3-pNINGUS-CCaMKT271A
59	dsRed-pNINGUS-CCaMKWT
60	dsRed-pNINGUS-CCaMKT271A
61	dsRed-pNINGUS-CCaMK 1-311
62	dsRed-pNINGUS-CCaMKK47E
63	dsRed-pNINGUS-CCaMK D413A
64	dsRed-pNINGUS-CCaMKD449A
65	dsRed-pNINGUS-CCaMKD491A
66	dsRed-pNINGUS-CCaMKD413A D449A
67	dsRed-pNINGUS-CCaMK D449A D491A
68	dsRed-pNINGUS-CCaMKD413A D491A
69	dsRed-pNINGUS-CCaMK D413A D449A D491A
70	dsRed-pNINGUS-CCaMK 1-402
71	dsRed-pNINGUS-CCaMK 1-391
72	dsRed-pNINGUS-CCaMK 1-477
73	dsRed-pNINGUS-CCaMK 1-435
74	dsRed-pNINGUS-CCaMK 1-346
75	dsRed-pNINGUS-CCaMK EF1-EF3-EF2-EF4
76	dsRed-pNINGUS-CCaMK EF1-EF2-EF4-EF3

77	dsRed-pNINGUS-CCaMK EF1-EF4-EF3-EF2
78	dsRed-pNINGUS-CCaMK EF1-EF3-EF4-EF2
79	dsRed-pNINGUS-CCaMK EF1-EF4-EF2-EF3
80	dsRed-pNINGUS-CCaMK EF2-EF1-EF3-EF4
81	dsRed-pNINGUS-CCaMK EF2-EF1-EF4-EF3
82	dsRed-pNINGUS-CCaMK EF2-EF3-EF4-EF1
83	dsRed-pNINGUS-CCaMK EF2-EF4-EF3-EF1
84	dsRed-pNINGUS-CCaMK EF2-EF3-EF1-EF4
85	dsRed-pNINGUS-CCaMK EF2-EF4-EF1-EF3
86	dsRed-pNINGUS-CCaMK EF3-EF1-EF2-EF4
87	dsRed-pNINGUS-CCaMK EF3-EF2-EF1-EF4
88	dsRed-pNINGUS-CCaMK EF3-EF1-EF4-EF2
89	dsRed-pNINGUS-CCaMK EF3-EF2-EF4-EF1
90	dsRed-pNINGUS-CCaMK EF3-EF4-EF1-EF2
91	dsRed-pNINGUS-CCaMK EF3-EF4-EF2-EF1
92	dsRed-pNINGUS-CCaMK EF4-EF1-EF2-EF3
93	dsRed-pNINGUS-CCaMK EF4-EF2-EF3-EF1
94	dsRed-pNINGUS-CCaMK EF4-EF3-EF2-EF1
95	dsRed-pNINGUS-CCaMK EF4-EF1-EF3-EF2
96	dsRed-pNINGUS-CCaMK EF4-EF3-EF1-EF2
97	dsRed-pNINGUS-CCaMK EF4-EF2-EF1-EF3

Appendix 2 – Different nodulation capabilities of CCaMK swaps (full number of plants tested)

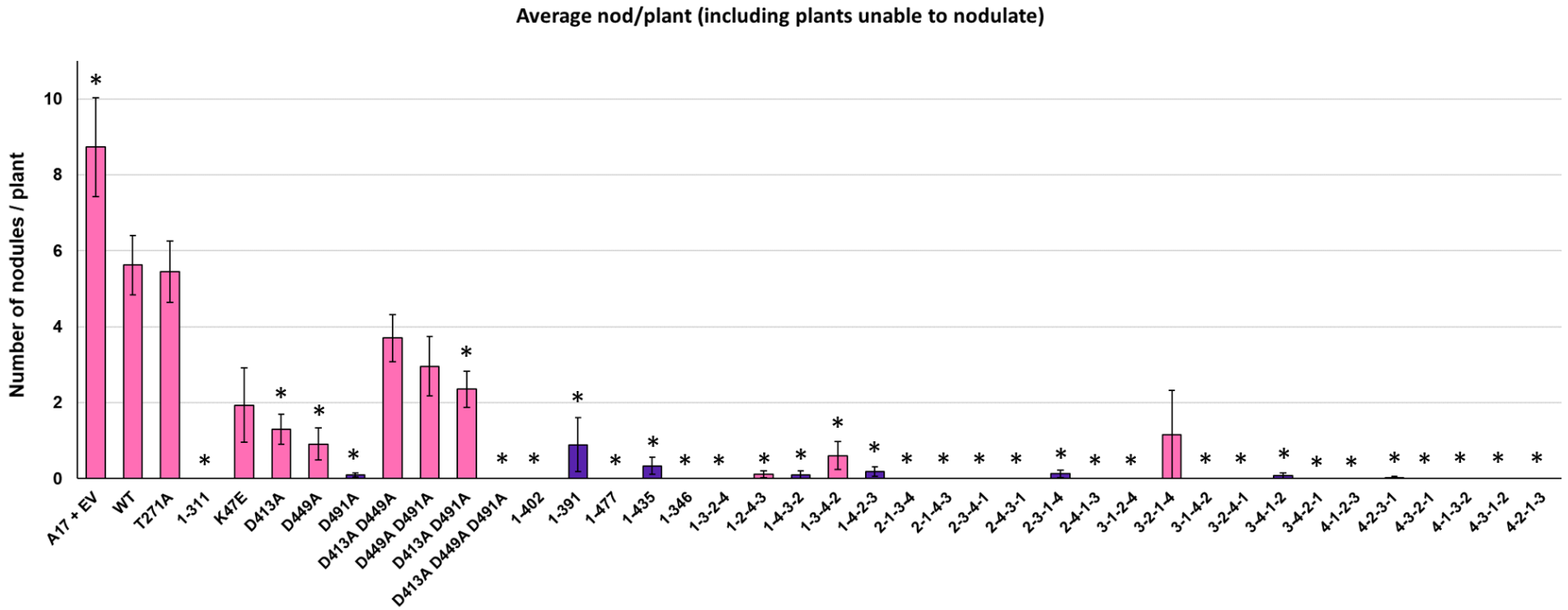

Appendix 2 Figure. Analysis of the nodulation capability of CCaMK swaps (including all plants regardless of nodule production).

Nodules were obtained from a low number of CCaMK swaps. Bars represent average number of nodules of plants assessed in at least three technical replicates comprising at least 6-10 plants per replicate. Each bar of the graph includes all plants tested regardless of whether they gave rise to either

spontaneous and / or mature nodules or no nodules at all. The nodulation capability of certain CCaMK variants was very rare and was only observed in one or two plants of the total number of plants tested across all technical replicates and therefore, a statistical analysis was not possible to perform on these variants (the analysis including only plants that produced nodules can be found in Figure 3.14 and Table 3.2). However, the data analysis that excludes plants with zero nodules still revealed the nodulation capability of the CCaMK variants and was chosen for inclusion in the body of the thesis for a better visual representation of the results. Pink bars correspond to CCaMK variants which were able to produce mature nodules and purple bars correspond to CCaMK variants which produced white nodules, potentially spontaneous. Asterisk denote statistically significant increase or decrease of nodule number induced by the total number of plants tested for each CCaMK mutant compared to CCaMK WT in a pairwaise two-tailed student t-test ($p<0.05$). Error bars represent S.E.